INFORMATION TO USERS

This material was produced from a microfilm copy of the original document. While the most advanced technological means to photograph and reproduce this document have been used, the quality is heavily dependent upon the quality of the original submitted.

The following explanation of techniques is provided to help you understand markings or patterns which may appear on this reproduction.

1. The sign or "target" for pages apparently lacking from the document photographed is "Missing Page(s)". If it was possible to obtain the missing page(s) or section, they are spliced into the film along with adjacent pages. This may have necessitated cutting thru an image and duplicating adjacent pages to insure you complete continuity.

2. When an image on the film is obliterated with a large round black mark, it is an indication that the photographer suspected that the copy may have moved during exposure and thus cause a blurred image. You will find a good image of the page in the adjacent frame.

3. When a map, drawing or chart, etc., was part of the material being photographed the photographer followed a definite method in "sectioning" the material. It is customary to begin photoing at the upper left hand corner of a large sheet and to continue photoing from left to right in equal sections with a small overlap. If necessary, sectioning is continued again – beginning below the first row and continuing on until complete.

4. The majority of users indicate that the textual content is of greatest value, however, a somewhat higher quality reproduction could be made from "photographs" if essential to the understanding of the dissertation. Silver prints of "photographs" may be ordered at additional charge by writing the Order Department, giving the catalog number, title, author and specific pages you wish reproduced.

5. PLEASE NOTE: Some pages may have indistinct print. Filmed as received.

University Microfilms International
300 North Zeeb Road
Ann Arbor, Michigan 48106 USA
St. John's Road, Tyler's Green
High Wycombe, Bucks, England HP10 8HR

78-5760

BREZINSKY, Kenneth, 1948-
MOLECULAR ORIENTATIONAL MOTION AS DETERMINED FROM CORRELATION FUNCTIONS AND BAND SHAPES OF LIQUID CRYSTALS.

City University of New York,
Ph.D., 1978
Chemistry, physical

University Microfilms International, Ann Arbor, Michigan 48106

MOLECULAR ORIENTATIONAL MOTION AS DETERMINED FROM CORRELATION FUNCTIONS AND BAND SHAPES OF LIQUID CRYSTALS

by

KENNETH BREZINSKY

A dissertation submitted to the Graduate Faculty in Chemistry in partial fulfillment of the requirements for the degree of Doctor of Philosophy, The City University of New York.

1977

This manuscript has been read and accepted for the Graduate Faculty in Chemistry in satisfaction of the dissertation requirement for the degree of Doctor of Philosophy.

10/11/77
date

Chairman of Examining Committee

10/11/77
date

Executive Officer

Supervisory Committee

David L. Beveridge
A. M. Ronn

The City University of New York

ABSTRACT

Correlation functions obtained from the Raman spectra of liquid crystals were examined in order to determine if they would reveal differences in tumbling motion in the aligned smectic, aligned nematic and isotropic phases of the mesogen, 4-Octyloxy-4'-cyanobiphenyl. The C≡N symmetric stretching band at approximately 2225 cm^{-1} was used in this study. Correlation functions calculated from I_{VH} spectra of this band were shown to be entirely reflective of vibrational relaxation processes. Correlation functions calculated from spectra of the C≡N band of the mesogen dissolved in benzene, carbon tetrachloride, chloroform and methyl thiocyanate suggested that "vibrational dephasing" was responsible for the band width and shape in the liquid crystal phases, in the isotropic phase and in the solutions. The solution studies suggested the presence of a wide distribution of local environments in the mesomorphic and isotropic phases of the mesogen and in certain solvents, $CHCl_3$ and CH_3SCN. These environments averaged out to a more narrow distribution, "motional narrowing," in C_6H_6 and CCl_4.

A study was made of the theoretical framework required for the application of correlation functions to the anisotropic molecular environment of liquid crystals. A study was also made of the errors in correlation functions that result from variations in the spectral bandshapes. In addition, a Nova computer assembly language program for calculating correlation functions by computing the Discrete Fourier Transform of a band was written. The program was based on an algorithm developed to allow moderately fast calculation, with interpolation of points, of the correlation function.

To my father, Philip, and especially to my late mother, Sylvia.

ACKNOWLEDGEMENT

I thank my advisor, Professor B. J. Bulkin, for his guidance and support during the research for and the writing of this dissertation. I also thank the members of my advisory committee, Professor D. L. Beveridge and Professor A. M. Ronn for their guidance and their confidence in me. The stimulating conversations with Dr. K. Krishnan are gratefully acknowledged. I would like to also express my thanks to the faculty and staff of the Chemistry Department of Hunter College of CUNY for their support in this research and to Mary Eschwei of the Thin Films Laboratory of Polytechnic Institute of New York for her patient help with the SiO coatings.

There are also many friends who helped me, each in his or her own way, to produce this dissertation, and I thank them all. Some of them are Kimxuan Huynh, Bob Marder, Helene Brezinsky, Ellen Resch, Gabos Flow, S. Swaminathan, Freda Moss, Paul Tergis, Arthur Noguerola and Nehama Yellin.

TABLE OF CONTENTS

LIST OF TABLES

LIST OF FIGURES

CHAPTER I

INTRODUCTION

Liquid crystals are substances which exhibit properties of liquids, such as flow, and properties of solids, such as optical anisotropy. These properties are present only in certain phases which are called mesophases or liquid crystal phases. Thermotropic liquid crystals are those that form mesophases at distinct temperatures and lyotropic liquid crystals are those which form such phases when added in the right amount to an appropriate solvent. The work in this thesis involves thermotropic liquid crystals.

On a molecular level, liquid crystals are organic compounds, often containing parasubstituted benzene rings. They are generally of an elongated structure. The various mesophases that have been observed can be readily described in terms of the orientation of the long axis of the elongated structure. In Fig. 1, three different types of mesophases are depicted with the individual molecules being represented by straight lines.

In the nematic liquid crystal phase, the long axes of the molecules all have the same preferred direction. This preferred direction is called the director. Other than this order, nematic phases show no spatial order. Smectic phases, on the other hand, do. In addition to the molecules having a preferred orientation of their

FIG. 1. Three types of thermotropic liquid crystal phases.

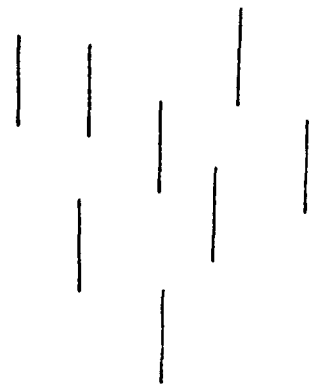

NEMATIC

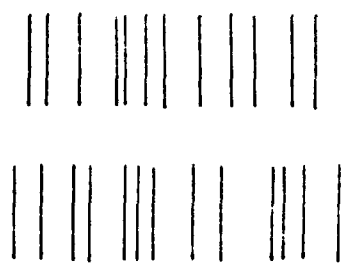

SMECTIC

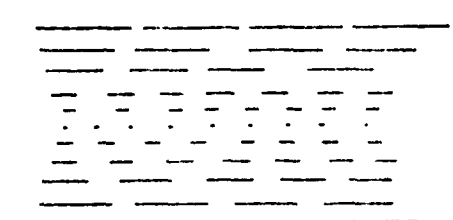

CHOLESTERIC

long axes, they have their centers of gravity located in a plane. The smectic phase drawn above is called a smectic A phase because the molecular long axes are perpendicular to the smectic plane. In other smectic phases, for example the smectic C phase, the long axes are at some angle to the smectic plane. The smectic A phase shows no spatial order among the molecules within the layer containing the smectic plane. There are phases, e.g., smectic B, which do show an orderly arrangement within the layer. In this work, only the smectic A phase will be considered. Details of the other types of smectic phases will be supplied as they are necessary to understanding the smectic A phase.

The cholesteric phase, which will not be studied in this work, is mentioned here for completeness. It can be thought of as a twisted nematic phase. The diagram shows this twist in the form of the decreased projection of the molecular long axes on the paper as an axis perpendicular to the long molecular axis is traversed.

This work is concerned with liquid crystal compounds that on heating exhibit the following series of transitions:

crystal ——— nematic ——— isotropic

crystal ——— smectic ——— nematic —— isotropic

Note that the isotropic phase is the common liquid phase and it is called isotropic because its optical and other properties are the same in all directions. In the crystal and isotropic phases of liquid crystals, molecular motion generally conforms to the types well documented for these phases. It is molecular motion in the smectic and

nematic phases that is of primary interest. By considering the representation of phases in Fig. 1, different types of motion can be imagined:

a. Rotation around the long molecular axis (spinning);

b. Rotation about an axis perpendicular to the long axis (tumbling);

c. Translation in the direction of the long axis and perpendicular to it.

Some experimental work involving a variety of techniques has been done by a number of groups in order to try to answer the questions about the nature of rotational motion in the liquid crystal phases. The conclusions have not been definitive and the following will be a sampling of them.

The X-ray diffraction studies of De Vries[1] lead him to conclude that there is no room for a more or less free rotation of the molecules around their long axis in the smectic A phase, nematic phase and just into the isotropic phase. Such tight packing also rules out any room for tumbling motion. De Vries suggests that the differences in phases results from differences in longitudinal position, with free translation along the direction of the long molecular axis only appearing in the isotropic phase.

By contrast, the electron spin resonance work of Luckhurst, Setaka and Zannoni[2] suggest to them that motion around the molecular axis is unhindered in a smectic A phase. Similarly, Luz and Meiboom[3] conclude that relative to a time scale of 10^{-6} seconds rapid rotational and translational diffusion takes place in a smectic A phase.

The far infrared investigation of the librational motion of a

nematic phase by Evans, Davies and Larkin[4] has led them to conclude that the only possible libration with a relatively small though considerable barrier to rotation would be around the long axis of the molecule. Thus, they indicate a hindered rotation around the long axis is probable. On the other hand, Amer and Shen[5] attribute peak broadening in the Raman spectra of nematic phases to the freedom of translation and more or less free rotation around the long axis that is possible in the nematic phase.

Carlile and Krebs[6] conclude from their quasielastic neutron scattering studies that in the nematic phase the liquid crystal molecules are performing a small step rotation around their long axis. In the smectic A phase the molecules are also rotating around the long axis but only at the higher temperature end of the smectic phase. The rotation is of a coupled, collective nature. The authors also suggest that tumbling motion possibly does not occur until the isotropic phase.

The question of tumbling motion has been addressed directly by a number of workers using a dielectric relaxation technique. Both Schadt[7] and Agarwal and Price[8] agree that rotation in the nematic phase about an axis perpendicular to the long molecular axis does occur and is strongly hindered. Rondelez and Mircea-Roussel[9], however, suggest that this motion measured by dielectric relaxation can best be described as rotational diffusion and as such is probably not reflective of individual molecular motion but of cooperative rotation.

Samulski, Dubowski and Wade[10] also dealt with the tumbling motion in nematics. They conclude from their NMR studies that tumbling takes place by jumps through angles greater than 60 degrees. This type of behavior implies a period of free rotation during the jump.

In addition, the authors suggest that the tumbling motion is strongly coupled to the translational motion of the molecules.

Some of the differences in conclusions about molecular motion in liquid crystal phases can be attributed to the different time scales involved in some of the experimental techniques mentioned above. However, there are also differences in results from experiments involving the same time scale. Clearly, there is room for more work in this area. Such work would be helpful if from it not only conclusions about the types of molecular motion could be drawn, but also estimates made of the time scale on which such motions are important. Vibrational spectroscopy potentially can contribute much in this area.

Both infrared and Raman spectroscopy probe vibrations that take place on the picosecond time scale. The nature of orientational motion can be inferred from its effect on such vibrations and will therefore be measured on a picosecond time scale as well. Both infrared and Raman spectroscopy lend themselves to the correlation function approach and as will be shown later, this approach allows the discrimination between motions taking place at different times.

Raman spectroscopy has a number of advantages over infrared spectroscopy. The two general methods of taking infrared spectra are by the use of a dispersive grating spectrometer or a Fourier transform interferometer. In the use of the latter instrument the mathematical operations of data manipulation distort in a complicated way the band shape of the absorption peak. Since, as we will see, orientational motion broadens and modifies the vibrational line shape, such distortion in the shape would greatly influence conclusions about the molecular motion. Dispersion spectrometers, though giving a faithful

lineshape, take an extremely long time to give peaks with the high signal to noise ratios needed for lineshape work. The Raman spectrometer used in this work is equipped with a photon counting system. Such a set up allows for a relatively rapid accumulation of data at a high signal to noise ratio. Furthermore, photon counting lends itself to the output of data in digital form, thus making the spectral results amenable to the types of computer computations that will be shown later to be necessary for the correlation function approach. Distortions of the line shape due to instrumental factors are well documented for Raman spectrometers and can be readily accounted for. In addition, Raman spectroscopy permits a clearly defined scattering geometry the knowledge of which is important in the interpretation of the correlation functions. For these reasons, this work involves the use of Raman spectroscopy.

Raman spectroscopy has been used to investigate liquid crystals by workers other than Amer and Shen[5]. For a review, see Reference 11. Some examples of these investigations follow. Bulkin and Prochaska[12] looked at the lattice mode Raman spectra of the solid phase of a liquid crystal as it approached, on heating, the nematic phase. Jen, Clark, Pershan and Priestly[13] used the depolarization ratios obtained from Raman spectra to investigate molecular order. Schnur[14] deduced from the changes in the spectrum of a liquid crystal in different phases information about different alkoxy tail conformations of the molecules. Fontana and Bini[15] drew conclusions about molecular motion in the crystalline phase of a liquid crystal from measurements of the half width of a low frequency peak that changes width when the monocrystal is heated.

The approach of Fontana and Bini, that is of measuring the change in half widths with temperature, is one often used with liquids[16]. However, orientational broadening will manifest itself throughout the peak, especially in the wings. Consequently, by measuring only the half width important information can be missed. In addition, half width measurements can only suggest types of motion possible but in the case of different types occurring at different times, can not help in sorting the motions out. Only when a well defined, analytic form band shape is obtained and only when the half width changes with temperature can such measurements be useful.

Correlation functions obtained from Raman and infrared spectroscopy[17] have provided an alternative to the study of half widths and bandshapes. Correlation functions have been used to reveal details about rotational motion in liquids through their variation in form and decay with time[18, 19]. It is their ability to reveal different types of rotational motion and the relative time importance of the motion that makes correlation functions a powerful tool.

Lugomer[20] computed correlation functions from the infrared spectrum of the smectic, nematic and isotropic phases of heptyloxyazoxybenzene. From the correlation functions, he calculated correlation times which he then compared to correlation times obtained from NMR studies. The comparison allowed him to conclude that the benzene rings that were a structural part of the liquid crystal molecule, rotated faster than the whole molecule and through angles of 30, 60 and greater than 60° for the smectic, nematic and isotropic phases respectively. These results did not lead to any conclusions about the importance of molecular rotation in each phase. Lugomer used a formalism for his

work that is strictly applicable to molecules in an isotropic environment. The applicability of such a formalism to the anisotropic molecular environment of the mesomorphic phases was not discussed.

Evans[21] obtained a correlation function from the far infrared spectrum of N-4-methoxybenzylidene-4'-n-butylaniline (MBBA) for use in his comparison of various models of molecular motion; however, he did not draw any detailed conclusions about the molecular motion of MBBA.

Correlation functions have not been used in conjunction with the Raman spectroscopy of liquid crystals. It is the aim of this thesis work to determine if correlation functions obtained from Raman spectroscopy, when adapted for the anisotropic environment of liquid crystals, will reveal the nature of rotational motion in the smectic, nematic and isotropic phases. The details of achieving this aim will follow in succeeding chapters.

CHAPTER II

BACKGROUND THEORY

Correlation functions can be developed from the theoretical formulation of the Raman effect; the development is shown in this chapter. In addition, this chapter will contain the definition of correlation functions as well as their significance. Their connection with liquid crystal systems will also be stressed and their connection with regular liquids. A discussion of the use of bandwidths for determining orientational motion is included at the end.

A. The Scattering Formulation and Its Connection With Correlation Functions

Liquid crystals can be aligned, that is, on the average the molecules in a macroscopic sample can be oriented in a direction. Such aligned molecules offer the advantage of a known molecular geometry relative to the laboratory. A scattering formulation of the Raman effect that clearly takes into account the molecular orientation as well as the electric vector orientation of the interacting light would obviously be of great value when working with aligned samples, as we do. Such a formulation for the intensity is given by Born and Huang[22] and further clarified by Maradudin[23] and Callender and Pershan.[24] The following discussion follows Callender and Pershan and will first out-

line the theory of the Raman effect and then lead into correlation functions.

The intensity of scattered light per solid angle for linearly polarized incident light, ignoring the finite nature of the incident wavelength, is[24]

$$I(\omega) = \frac{\eta(\omega_o+\omega)^4}{2\pi c^3} \sum_{ijkl} \hat{n}_i \hat{n}_j I^{\nu}_{ik,jl}(\omega) E^-_k E^+_l \qquad (2\text{-}1)$$

where

η = total number of scattering molecules

ω_o = laser angular frequency

ω = total angular frequency shift due to scattering and equals $\omega_{\text{scattered}} - \omega_o$

C = speed of light

i,j,k,l = the cartesian coordinates X, Y, Z in the laboratory framework

$\hat{n}_i, \hat{n}_j$ = components of a unit vector in the direction of the electric field vector of the scattered light

E^-_k, E^+_l = components of the electric field vector of the incident light when the electric field vector is expressed as

$$E(t) = E^- \exp(-i\omega t) + E^+ \exp(i\omega t)$$

In 2-1 the $I^{\nu}_{ik,jl}$ are elements of a fourth rank tensor and are expressed as

$$I^{\nu}_{ik,jl}(\omega) = \sum_{\xi\xi'} (Z'Z_{int.})^{-1} \exp(-E_{\xi}/kT) \langle \xi' | a^{\nu}_{ik} | \xi \rangle \times \langle \xi | a^{\nu}_{jl} | \xi' \rangle \delta(-\omega - \omega_{\nu} - \hbar^{-1}(-E_{\xi} + E_{\xi'})) \quad (2\text{-}2)$$

where

ξ, ξ' = the eigenstates, excluding those for the molecular internal vibrational modes, of the Hamiltonian of the scattering molecule and its surroundings

δ = delta function which here expresses the conservation of energy

$E_{\xi}, E_{\xi'}$ = the energy of the eigenstates ξ and ξ'

k = Boltzman's constant

T = temperature

Z' = the partition function for the eigenstates ξ' and ξ

$Z_{int.}$ = the partition function for the internal molecular vibrational eigenstates

$\hbar$ = Planck's constant divided by 2π

ω_{ν} = angular frequency of the ν vibrational mode

a^{ν}_{ik} , a^{ν}_{jl} = the components of the second rank tensor $a^{\nu}(MF)$ after it has been adjusted for rotation into the laboratory frame and where

$a^{\nu}_{ij}(MF) \equiv \int \psi^{v=0} a^{\nu}_{ij} \psi^{v=1} d\tau$ is the ij component of the tensor and where the ψ are the simple harmonic oscillator wave functions for the internal molecular modes and ij are the cartesian coordinates in the molecular framework,

$a^{\nu}_{ij} \equiv \left(\frac{\partial a_{ij}}{\partial Q^{\nu}}\right)_{Q^{\nu}=0} Q^{\nu}$ where Q^{ν} is the ν internal coordinate, and ij refer to the cartesian coordinates of the molecular framework

and

a_{ij} = the elements of the polarizability tensor in the molecular framework.

For 2-1 and 2-2 the Born-Oppenheimer separation of the vibrational wavefunction from the rotational-translational wavefunction is assumed. The vibrational wavefunctions are approximated by the orthogonal harmonic oscillator wavefunctions therefore leading to the uncoupling of the vibrations of neighboring molecules. Thus the equations apply to a large number of individual molecular scatterers. It is the uncoupling of the vibrational modes that allows the formulae to be applied to crystals and liquid crystals.

The various α terms that are associated with equation 2-2 require closer examination of their meaning since, as will be seen, they are important in the determination of molecular motion. The

α_{ij} are the elements of the polarizability tensor in terms of a coordinate system fixed at the molecular center of mass, rotating and translating with the molecule. The polarizability tensor in its classical sense is a 3x3 matrix which when premultiplying the components of the amplitude of the electric field vector in the form of a column vector will lead to the components of the induced dipole:

$$\begin{vmatrix} \mu_x \\ \mu_y \\ \mu_z \end{vmatrix} = \begin{vmatrix} \alpha_{xx} & \alpha_{xy} & \alpha_{xz} \\ \alpha_{yx} & \alpha_{yy} & \alpha_{yz} \\ \alpha_{zx} & \alpha_{zy} & \alpha_{zz} \end{vmatrix} \begin{vmatrix} E_x \\ E_y \\ E_z \end{vmatrix}$$

Note that it is radiation emitted from an induced oscillating dipole that comprises the Raman effect as well as Rayleigh scattering.

A more quantum mechanical approach to the Raman effect using the Placzek approximation[25] requires that the elements of the polarizability tensor be of the form $\int \psi_o \alpha_{ij} \psi_k \, d\tau$, where $i = x, y, z$ and $j = x, y, z$. The tensor elements defined this way are called transition polarizability elements. In the usual case, the Raman effect involves a transition to a final vibrational state from the ground vibrational state. Then, ψ_o will belong to the totally symmetric representation of the molecule's point group and ψ_k will belong to one of the representations, including the totally symmetric one. The α_{ij} are then, in the Placzek quantum mechanical approach, the elements of a second order tensor and are written semiclassically in terms of the dipole moment operator and the electronic eigenstates. The α_{ij} can also be formulated using a completely quantum mechanical approach.[26]

By considering the transformation properties of the α_{ij} and using projection operator techniques, the tensor comprised of the α_{ij} can be broken up into other second order tensors for which the tensor elements are zero for certain species while for other species these elements exist, transforming according to that species. Then the integrals, $\int \psi_o \alpha_{ij} \psi_k \, d\tau$, can be formed for ψ_k belonging to different symmetry species. As a result the tensor comprised of the matrix elements can be separated into tensors whose elements transform as a specific representation.[27,28] However, the form of the polarizability tensor as determined this way from symmetry considerations in the molecular framework is not of immediate use to us since we are more concerned with the direct connection between the molecular and laboratory coordinate system. This connection will be clearer as we proceed.

In the course of a molecular vibration the polarizability tensor elements change and for small displacements of the nuclei from their equilibrium positions a Taylor expansion of the elements can be made:

$$\alpha_{ij} = \alpha^{o}_{ij} + \sum_{\nu=1} \left(\frac{\partial \alpha_{ij}}{\partial Q^{\nu}} \right)_{Q^{\nu}=0} Q^{\nu} \quad ,$$

where Q^{ν} is the normal coordinate for the ν normal mode. The α^{o}_{ij} term does not depend on the vibrational mode and is responsible for Rayleigh scattering. The individual terms of the sum are dependent on the normal mode of vibration and are therefore important in the vibrational Raman effect. The terms can be rewritten for convenience as α^{ν}_{ij} so that

$$\alpha_{ij}^{\nu} \equiv \left(\frac{\partial \alpha_{ij}}{\partial Q^{\nu}}\right)_{Q^{\nu}=0} Q^{\nu} \quad .$$

Vibrational transitions involving normal modes for which the vibrational quantum number changes by one, the allowed value, are studied in our work. Using the Taylor expanded form of the polarizability tensor elements, the matrix elements for the Raman effect for a transition from the ground state of the ν normal mode to the final harmonic oscillator eigenstate can be written

$$\int \psi_{\nu}^{\upsilon=0} \left(\frac{\partial \alpha_{ij}}{\partial Q^{\nu}}\right)_{Q^{\upsilon}=0} Q^{\nu} \; \psi_{\nu}^{\upsilon=1} \; d\tau$$

Using simpler notation

$$\alpha_{ij}^{\nu}(MF) \equiv \int \psi_{\nu}^{\upsilon=0} \alpha_{ij}^{\nu} \psi_{\nu}^{\upsilon=1} \, d\tau$$

For molecules for which the molecular fixed axis does not coincide with the laboratory axis, the $\alpha_{ij}^{\nu}(MF)$ must be adjusted before they can be used in equation 2-2. This adjustment can be made by first recalling that within the Placzek polarizability approximation the relationship between the induced dipole and the incident electric field can be expressed in matrix form as

$$\overline{\mu} = \overline{\alpha}\,\overline{E}$$

where $\overline{\mu}$ and $\overline{E}$ are column matrices and $\overline{\alpha}$ is the matrix of the transition polarizability elements which are, in the case under consideration, the $\alpha_{ij}^{\nu}(MF)$. By considering that the labora-

tory coordinate system (LF) and the molecular coordinate system can be related through a transformation matrix, $\overline{R}$, then

$$\overline{\mu}(LF) = \overline{R}\,\overline{\mu}(MF)$$

$$\overline{E}(LF) = \overline{R}\,\overline{E}(MF) \quad .$$

From these relationships the transition polarizability matrix in the laboratory frame is[29]

$$\overline{a^{\nu}}(LF) = \overline{R}\,\overline{a^{\nu}}(MF)\,\overline{R^{-1}}$$

The elements of $\overline{a^{\nu}}(LF)$ must be the ones used in equation 2-2. Note, importantly, that when the molecular coordinate system differs from the laboratory reference frame only by rotations through the Euler angles (α, β, γ) that connect the systems, then the R matrices will be functions of these angles and

$$\overline{a^{\nu}}(LF) = \overline{R}(\alpha\beta\gamma)\,\overline{a^{\nu}}(MF)\,\overline{R^{-1}}(\alpha\beta\gamma)$$

The above few paragraphs give some idea of the importance of the α terms as constituent parts of equation 2-2 and therefore 2-1. Looking now at these equations from an overall view, it can be seen that they express the frequency dependence of the intensity of Raman scattering in the Schrodinger representation, that is, they define the Raman effect in terms of transitions between stationary states. The Schrodinger picture has its limitations,[30] the chief one being that for liquids and solids the lines corresponding to various rotational transitions are so close together that they form continuous bands which are difficult to interpret in terms of transitions.

A picture of spectroscopic results that involves the time development of the system would facilitate the visualization and interpretation of the orientational motion of the molecules in liquids and solids. The Heisenberg representation offers such a picture. We see now how the Schrodinger representation of Raman spectroscopy can be converted to the Heisenberg representation with the consequent formation of a correlation function.

A delta function can be written as

$$\delta(\omega) = \frac{1}{2\pi} \int_{-\infty}^{\infty} \exp(i\omega t)\, dt$$

Therefore the delta function appearing in equation 2-2 can be rewritten and the equation becomes

$$I^{\nu}_{ik,jl}(\omega) = \sum_{\xi\xi'} (Z'Z_{int})^{-1} \exp(-E_{\xi}/kT) \langle \xi' | a^{\nu}_{ik} | \xi \rangle \langle \xi | a^{\nu}_{jl} | \xi' \rangle$$

$$\times \int_{-\infty}^{\infty} \exp\left[-i(\omega+\omega_{\nu})t\right] \exp(iE_{\xi}t/\hbar) \exp(-iE_{\xi'}t/\hbar)\, dt$$

By bringing some of the exponential terms within the matrix elements and changing their order of multiplication we have

$$I^{\nu}_{ik,jl}(\omega) = \int_{-\infty}^{\infty} \Big[\sum_{\xi\xi'} (Z'Z_{int})^{-1} \exp(-E_{\xi}/kT)$$

$$\times \langle \xi \exp(iE_{\xi}t/\hbar) | a^{\nu}_{jl} | \exp(-iE_{\xi'}t/\hbar) \xi' \rangle \langle \xi' | a^{\nu}_{ik} | \xi \rangle$$

$$\times \exp\left[-i(\omega+\omega_{\nu})t\right] \Big]\, dt$$

By considering that any exponential can be expanded as

$$\exp(a) = \sum_{n=0}^{\infty} \frac{1}{N!} a^{n}$$

we see that, for example, the following substitution can be made:

$$\exp(-iE_{\xi'}t/\hbar)\times\xi' = \xi' - (it E_{\xi'}/\hbar)\xi' + \frac{1}{2}(it E_{\xi'}/\hbar)^2\xi' + \cdots$$

$$= \xi' - (itH'/\hbar)\xi' + \frac{1}{2}(itH'/\hbar)^2\xi' + \cdots$$

$$= \exp(-iH't/\hbar)\times\xi'$$

Substituting for the exponential terms and summing over the complete set of final states ξ' we have

$$I^{\nu}_{ik,jl}(\omega) = \int_{-\infty}^{\infty}\left[\sum_{\xi}(Z'Z_{int})^{-1}\exp(-E_{\xi}/kT)\ \times\right.$$

$$\left.<\xi|\exp\left(\frac{iHt}{\hbar}\right)a^{\nu}_{jl}\exp\left(\frac{-iH't}{\hbar}\right)a^{\nu}_{ik}|\xi>\exp\left[-i(\omega+\omega_{\nu})t\right]\right]dt$$

If we assume that the Hamiltonian for the excited states does not differ greatly from that in the ground state then we can replace H' with H. As a consequence, the a^{ν}_{jl} term is now in the form to fulfill Heisenberg's equations of motion in which operators are time dependent,[31] that is

$$a^{\nu}_{jl}(t) = \exp(iHt/\hbar)a^{\nu}_{jl}\exp(-iHt/\hbar)$$

Note that a^{ν}_{ik} is in the form

$$a^{\nu}_{ik}(t) = \exp(iH0/\hbar)a^{\nu}_{ik}\exp(-iH0/\hbar) = a^{\nu}_{ik}(0)$$

Note also that the sum over ξ including the partition function and $\exp(-E_{\xi}/kT)$ leads to an ensemble average and therefore

$$I^{\nu}_{ik,jl}(\omega) = \int_{-\infty}^{\infty} \langle a^{\nu}_{jl}(t) a^{\nu}_{ik}(0) \rangle_{av.} \exp\left[-i(\omega+\omega_{\nu})t\right] dt$$

(2-3)

Equation 2-3 shows that the frequency dependent part of the scattering intensity can be expressed as the Fourier transform of a time dependent part. This is a direct result of converting to the Heisenberg form of operators evolving in time. The ensemble average term in angle brackets is a correlation function. Its specific significance for interpretation of spectral results which follows from its time dependence will be seen in Section C of this chapter; its general significance will be discussed in Section B. Note for future reference that part of the argument of the exponential, $\omega+\omega_{\nu}$, is the frequency displacement from the band center.

Equation 2-3 can be inserted into 2-1; if we then construct our laboratory set up so that the E vector of linearly polarized incident light and the E vectors of the scattered light are coincident with the laboratory axes it follows that i=j, k=l and further choosing only one value of i and k the resultant equation is

$$I_{l=j,k=l}(\omega) = \frac{\eta(\omega_o+\omega)^4}{2\pi c^3} \hat{n}_i \hat{n}_i E^-_k E^+_k \int_{-\infty}^{\infty} \langle a^{\nu}_{ik}(t) a^{\nu}_{ik}(0) \rangle \times \exp\left[-i(\omega+\omega_{\nu})t\right] dt$$

This equation can now be inverse Fourier transformed to give

$$\langle a^{\nu}_{ik}(t) a^{\nu}_{ik}(0) \rangle = \frac{2\pi c^3}{\eta E^-_k E^+_k \omega_o^4} \int_{-\infty}^{\infty} I(\omega) \exp\left[+i(\omega+\omega_{\nu})t\right] d\omega$$

(2-4)

where the small contribution of ω to ω_o has been ignored. Equation 2-4 can be normalized by dividing through by the t=0 value, which, as we will see in the next section, is the maximum value, and therefore

$$\frac{\langle \alpha^{\nu}_{ik}(t)\alpha^{\nu}_{ik}(0)\rangle}{\langle \alpha^{\nu}_{ik}(0)\alpha^{\nu}_{ik}(0)\rangle} \equiv \overline{\langle \alpha^{\nu}_{ik}(t)\alpha^{\nu}_{ik}(0)\rangle} = \frac{\int_{-\infty}^{\infty} I(\omega)\exp\left[+i(\omega+\omega_{\nu})t\right]d\omega}{\int_{-\infty}^{\infty} I(\omega)\,d\omega}$$

Similar but more complicated and less useful results can be obtained for other laboratory goemetries.

We now see that a correlation function can be isolated by computing the Fourier transform of the experimentally obtained scattering intensity. Since the time dependence of the α terms in the correlation function results from the time dependence of the transformation matrices R, that is $\overline{\alpha^{\nu}_{LF}(t)} = \overline{R(t)}\;\overline{\alpha^{\nu}(MF)}\;\overline{R^{-1}(t)}$, we now have a way of getting information about the time evolution, i.e., rotation, and/or translation, of the molecular frame with respect to the laboratory frame, from spectroscopic results.

B. The Definition and Significance of Correlation Functions

Correlation functions have been used regularly in statistical mechanics[32,33] and more recently in nuclear magnetic resonance spectroscopy.[34] The form of definition commonly used in statistical mechanics will be followed here.

Consider, for example, two cases in which a property of the system fluctuates around its average value of zero but in one case the frequency and form of fluctuation differs from the other; see Figs. 2a and 2b. Intuitively it is recognized that in 2b the value of V at some time t, and the value a short time later, $t+\tau$, are more closely related than in 2a. How can one quantitatively determine the degree to which $V(t+\tau)$ depends on $V(t)$ so that the two cases above can be quantitatively distinguished? A correlation function is designed to give the answer.

To form a correlation function, one first forms the product $V(t)V(t+\tau)$, for any variable fluctuating around its mean, for some choice of t and τ. Then the product is formed again for a new t; the process is repeated. In the limit of choosing the values very close together the time average can be formed:

$$\overline{V(t)V(t+\tau)} = \lim_{t'\to\infty} \frac{1}{t'} \int_0^{t'} V(t)V(t+\tau)\,dt$$

This time average, also called $C(\tau)$, is the correlation function. Note that the integration over t leaves the correlation function as a function of τ only.

The definition of the correlation function can be broadened by using the postulate of statistical mechanics that an average over the members of an ensemble can be used for the time average of a single system. Therefore, one first forms a canonical ensemble of systems identical to the one that exhibited the property V. For each member of the ensemble the product $V(t)V(t+\tau)$ is produced.

FIG. 2. Two cases ideally suited for the application of correlation functions.

a) rapidly fluctuating variable

b) slowly fluctuating variable.

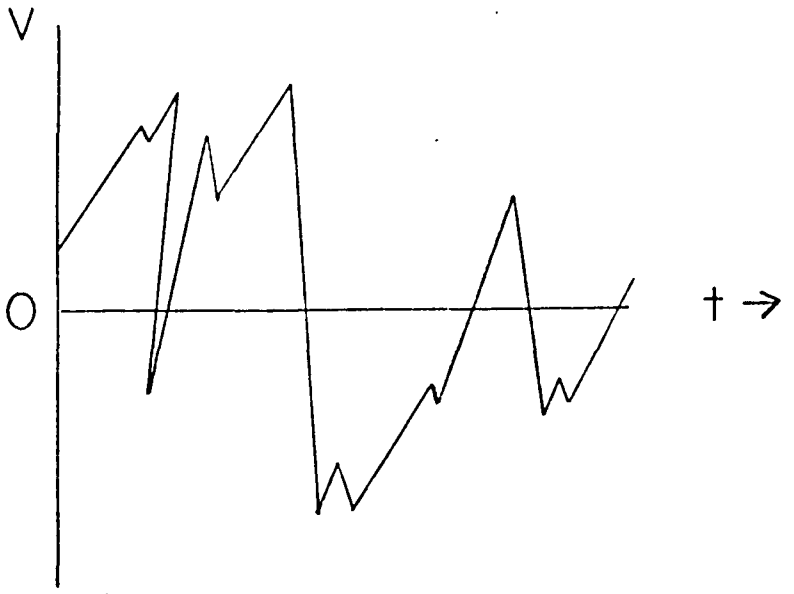

a

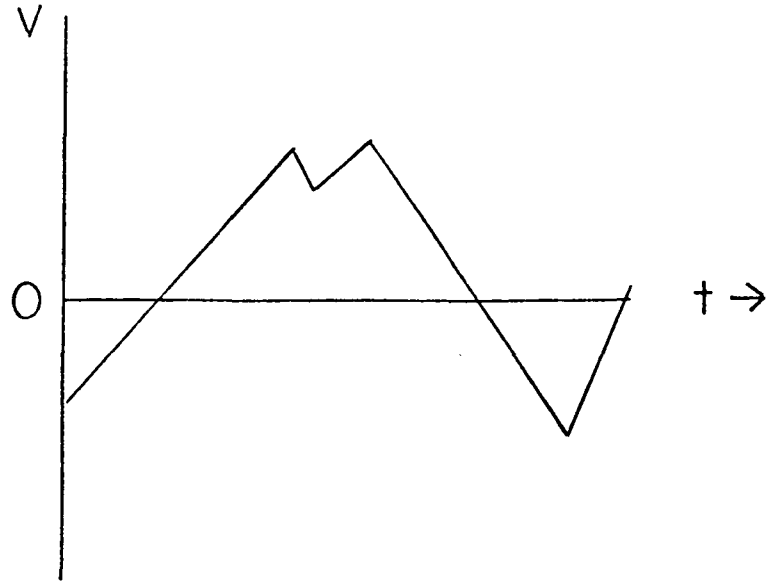

b

Then the ensemble average is created, $\langle V(\dagger)V(\dagger+\tau)\rangle$. Within the limitations of the above postulate which holds for systems in which the causesof the fluctuations do not change with time[35] the following can then be written

$$C(\tau) \equiv \overline{V(\dagger)V(\dagger+\tau)} = \langle V(\dagger)V(\dagger+\tau)\rangle$$

Setting the ensemble average equal to the time average is often the most convenient way of finding the time average, but it is particularly useful in the case of dynamical properties, that is, properties that depend on the quantum state of the system. Since for such properties the time dependent wavefunction is usually not known, the integral over time cannot be formed and the ensemble average approach is the only practical way to calculate the time average. Thus for a dynamical property X the following can be written

$$C(\tau) \equiv \overline{X(\dagger)X(\dagger+\tau)} = \langle X(\dagger)X(\dagger+\tau)\rangle$$

Note that only a single time, $\dagger$, need be chosen for the members of the ensemble when forming the ensemble average since at $\dagger$ the members of the ensemble will be exhibiting the variety of values of V (or X) that would be exhibited by a single system at different $\dagger$ values. By the same reasoning, it can be set equal to zero and therefore

$$C(\tau) = \langle V(\dagger)V(\dagger+\tau)\rangle = \langle V(0)V(\tau)\rangle$$

By examining now the two cases introduced earlier, it can be seen what information a correlation function can yield, keeping in mind that the following arguments apply equally well to correlation

functions of dynamical properties, X. For small τ the product $V(0)V(\tau)$ would in general be large and therefore the average, $\langle V(0)V(\tau)\rangle$, would be large. However, for the case in Fig. 2a the range of τ values for which the average remains relatively large will be much smaller than for the case in Fig. 2b. Similarly, for large τ the positive and negative fluctuations will cause $\langle V(0)V(\tau)\rangle$ to approach zero. In the case of Fig. 2a the value of τ for which this occurs will be smaller than for the case in Fig. 2b. In addition, in either case if the factors that influence the correlation between $V(\tau)$ and $V(0)$ change in importance with the change in time interval, then the variation of $\langle V(0)V(\tau)\rangle$ with τ will change in form. Thus by obtaining the value of $\langle V(0)V(\tau)\rangle$ as a function of τ one has both an average measure of the frequency and the form of fluctuations.

Note that the two limiting cases for $C(\tau)$ are

a) $\lim_{\tau \to 0} C(\tau) = \langle V(0)V(0)\rangle$ = maximum value

b) $\lim_{\tau \to \infty} C(\tau) = 0$ (when the mean equals zero)

Note also that $C(\tau)$ can be normalized

$$C'(\tau) = \frac{\langle V(0)V(\tau)\rangle}{\langle V(0)V(0)\rangle}$$

and therefore

$$\lim_{\tau \to 0} C'(\tau) = 1$$

C. The Connection of Correlation Functions To the Spectra of Liquid Crystals

For liquid crystals, the use of correlation functions is particularly apt; liquid crystal molecules in a macroscopic domain are, on the average, aligned in a given direction about which they fluctuate. (Note that though correlation functions are most often used for systems that are best described as randomly fluctuating ones, their use need not be limited to such situations;[17] indeed, for the case of molecular spectroscopy, there is some time interval for which the molecular motion is not best described as random and can be described by an analytic expression, albeit an unknown one.) The intermolecular forces which cause the fluctuations are varied and influence the motion over varied time intervals. As a result, the overall orientational motion is a composite of various types of motion. Correlations functions are designed to sort out in time the variations within a fluctuating quantity. Since for the high frequency vibrations that will be examined the vibrations of neighboring molecules will be uncoupled, the correlation function will perform such sorting out as if only the average behavior of one molecule under the influence of its surroundings was being considered. Thus a clear physical situation can be visualized.

More precise information can be extracted from correlation functions obtained from Raman spectra by further consideration of the transition polarizability terms. Any second rank tensor can be separated into an isotropic part and anisotropic part, that is, a part invariant to a unitary transformation and a part that is not.

For the matrix of the transition polarizability elements in the molecular framework, this separation is written

$$\overline{\alpha^{\nu}(MF)} = \alpha_c^{\nu}\overline{I} + \overline{\beta^{\nu}(MF)}$$

where $\alpha_c^{\nu} = \frac{1}{3}\,\text{Trace}\,\overline{\alpha^{\nu}(MF)}$ and is a constant, $\overline{\beta^{\nu}(MF)} = \overline{\alpha^{\nu}} - \alpha_c^{\nu}\overline{I}$ and is traceless, and I is the identity matrix. In the Heisenberg representation where α evolves in time the separation can be written

$$\overline{\alpha^{\nu}(t)} = \alpha_c^{\nu}\overline{I} + \overline{\beta^{\nu}(t)}$$

where

$$\overline{\beta^{\nu}(t)} = \overline{R(t)}\ \overline{\beta^{\nu}(MF)}\ \overline{R^{-1}(t)} \quad .$$

Note that there is no time dependence in the first part of the separation, $\alpha_c^{\nu}\overline{I}$, since the trace of a matrix is invariant under any unitary transformation such as the one resulting from the application of the $R(t)$ matrices.

The individual elements of the transition polarizability tensor can also be written in terms of their isotropic and anisotropic parts and consequently the correlation function described earlier, equation 2-3, can now be written

$$\langle \alpha_{jl}^{\nu}(t)\alpha_{ik}^{\nu}(0)\rangle = (\alpha_c^{\nu})^2\delta_{jl}\delta_{ik} + (\alpha_c^{\nu})\delta_{ik}\langle\beta_{jl}^{\nu}(t)\rangle + (\alpha_c^{\nu})\delta_{jl}\langle\beta_{ik}^{\nu}(0)\rangle + \langle\beta_{jl}^{\nu}(t)\beta_{ik}^{\nu}(0)\rangle \qquad (2\text{-}5)$$

The α_c^{ν} terms have been brought out of the ensemble average

because as constant, orientationally independent terms they are unaffected by the average over all rotation-translation states.

The right hand side of the above equation, 2-5, is the decomposition of the correlation function into parts that transform as a scalar, as the ensemble average of the elements of a second rank tensor, and as the ensemble average of the elements of a fourth rank tensor. Under conditions of thermal equilibrium, molecules occupying sites of O_h symmetry in a cubic crystal will have no non zero elements transforming as the ensemble average of second rank tensor elements and the above decomposition becomes[24]

$$\langle \alpha^{\nu}_{jl}(t)\alpha^{\nu}_{ik}(0)\rangle = (\alpha^{\nu}_{c})^2 \delta_{jl}\delta_{ik} + \langle \beta^{\nu}_{jl}(t)\beta^{\nu}_{ik}(0)\rangle .$$

The O_h site symmetry puts further constraints on the terms appearing as the ensemble average of fourth rank tensor elements. However, for liquid crystals there is some X-ray evidence[1] that indicates the molecules have site symmetry of D_{6h} or one of its subgroups. In such a case, the only β terms that will transform as the ensemble average of second rank tensor will be diagonal ones,[36] and the correlation function decomposition is written as

$$\langle \alpha^{\nu}_{jl}(t)\alpha^{\nu}_{ik}(0)\rangle = (\alpha^{\nu}_{c})^2 \delta_{jl}\delta_{ik} + (\alpha^{\nu}_{c})\delta_{ik}\langle \beta^{\nu}_{jl}(t)\rangle \delta_{jl}$$

$$+(\alpha^{\nu}_{c})\delta_{jl}\langle \beta^{\nu}_{ik}(0)\rangle \delta_{ik} + \langle \beta^{\nu}_{jl}(t)\beta^{\nu}_{ik}(0)\rangle$$

In order to keep the discussion general and to avoid at this time the assumption of D_{6h} site symmetry for liquid crystal molecules, the decomposition of the correlation function into its parts as first written in equation 2-5 will continue to be used. By con-

sidering the right hand side of 2-5 and the laboratory situation mentioned earlier, the E vector of the polarized incident light and the E vector of the collected scattered light are coincident with the laboratory axis, Table 1 can be drawn up.

Incident E Vector Coincident With Axis:	Scattered E Vector coincident With Axis:	i=j=	k=l=	$(\alpha_c^\nu)^2\delta_{ik}\delta_{ik}+(\alpha_c^\nu)\delta_{ik}\langle\beta_{ik}^\nu(t)\rangle$ $+(\alpha_c^\nu)\delta_{ik}\langle\beta_{ik}^\nu(0)\rangle+\langle\beta_{ik}^\nu(t)\beta_{ik}^\nu(0)\rangle$
X	X	X	X	$(\alpha_c^\nu)^2+\alpha_c^\nu\langle\beta_{XX}^\nu(t)\rangle+\alpha_c^\nu\langle\beta_{XX}^\nu(0)\rangle$ $+\langle\beta_{XX}^\nu(t)\beta_{XX}^\nu(0)\rangle$
X	Y	Y	X	$\langle\beta_{YX}^\nu(t)\beta_{YX}^\nu(0)\rangle$
X	Z	Z	X	$\langle\beta_{ZX}^\nu(t)\beta_{ZX}^\nu(0)\rangle$
Y	X	X	Y	$\langle\beta_{XY}^\nu(t)\beta_{XY}^\nu(0)\rangle$
Y	Y	Y	Y	$(\alpha_c^\nu)^2+\alpha_c^\nu\langle\beta_{YY}^\nu(t)\rangle+\alpha_c^\nu\langle\beta_{YY}^\nu(0)\rangle$ $+\langle\beta_{YY}^\nu(t)\beta_{YY}^\nu(0)\rangle$
Y	Z	Z	Y	$\langle\beta_{ZY}^\nu(t)\beta_{ZY}^\nu(0)\rangle$
Z	X	X	Z	$\langle\beta_{XZ}^\nu(t)\beta_{XZ}^\nu(0)\rangle$
Z	Y	Y	Z	$\langle\beta_{YZ}^\nu(t)\beta_{YZ}^\nu(0)\rangle$
Z	Z	Z	Z	$(\alpha_c^\nu)^2+\alpha_c^\nu\langle\beta_{ZZ}^\nu(t)\rangle+\alpha_c^\nu\langle\beta_{ZZ}^\nu(0)\rangle$ $+\langle\beta_{ZZ}^\nu(t)\beta_{ZZ}^\nu(0)\rangle$

Table 1

It can be seen in this Table that only when the E vector of the collected scattered light is perpendicular to the E vector of the incident light does the correlation function reduce to one involving only β terms. As was mentioned, the β terms are the ones sensitive to molecular motion. Thus, a correlation function computed from a Raman band obtained when the E vector of the incident light and the E vector of the scattered light are parallel will also contain information on the molecular motion, but this information will be obscured by the presence of the non correlation function terms in the decomposition. We note that since the transition polarizability tensor is a symmetric one, the following equalities can be written:

$$\langle \beta^{\nu}_{YX}(t)\,\beta^{\nu}_{YX}(0)\rangle = \langle \beta^{\nu}_{XY}(t)\,\beta^{\nu}_{XY}(0)\rangle$$

$$\langle \beta^{\nu}_{ZX}(t)\,\beta^{\nu}_{ZX}(0)\rangle = \langle \beta^{\nu}_{XZ}(t)\,\beta^{\nu}_{XZ}(0)\rangle$$

$$\langle \beta^{\nu}_{ZY}(t)\,\beta^{\nu}_{ZY}(0)\rangle = \langle \beta^{\nu}_{YZ}(t)\,\beta^{\nu}_{YZ}(0)\rangle$$

From these equalities it can be seen that at most only three perpendicular E vector laboratory situations need be considered. We also note for completeness that when thinking of the intensity of a Raman band as the Fourier transform of the correlation function (See Section A of this chapter), the β terms as they appear for any configuration of E vectors are responsible for the orientational broadening of the intensity peak obtained under that laboratory situation.

It still remains to be shown how the specific E vector configurations, the particular liquid crystal alignment directions, and the various possible orientational motions, are related. This area is postponed until the discussion of experimental results.

D. Correlation Functions and Liquids

The molecules composing the scattering volume of a liquid are randomly oriented with respect to each other as well as to the incident and scattered polarization directions. Consequently, it is possible to average over all orientations of the molecules and get a simplified form for the correlation functions. After using such an averaging procedure and after separating the transition polarizability matrix into its isotropic and anisotropic parts, Nafie and Peticolas[26] find for the intensities that

$$I_{\parallel}(\omega) = \frac{A}{2\pi}(\omega_1 - \Omega_\nu)^4 \int_{-\infty}^{\infty} \left\langle (\alpha^\nu)^2 + \frac{2}{15} \mathrm{Tr}\left[\beta^\nu(0)\cdot\beta^\nu(t)\right]\right\rangle \left\langle Q^\nu(0) Q^\nu(t)\right\rangle_{vib} \times \exp(i\omega t)\, dt$$

$$I_{\perp}(\omega) = \frac{A}{2\pi}(\omega_1 - \Omega_\nu)^4 \int_{-\infty}^{\infty} \left\langle \frac{1}{10} \mathrm{Tr}\left[\beta^\nu(0)\cdot\beta^\nu(t)\right]\right\rangle_{tr} \left\langle Q^\nu(0) Q^\nu(t)\right\rangle_{vib} \exp(i\omega t)\, dt$$

In their notation some symbols are new and these are defined as

$I_{\parallel}$ = intensity when incident and scattered polarization directions are $\parallel$

$I_{\perp}$ = intensity when incident and scattered polarization directions are $\perp$

ω_1 = angular frequency of the incident light

Ω_ν = angular frequency of the ν normal mode

$\omega = \omega_2 - \omega_1 + \Omega_\nu$ where ω_2 is the circular frequency of the scattered light

A = a constant

Tr = operation of taking the trace of a matrix

$\dagger r$ = symbolizes translation-rotation part

vib = symbolizes the vibrational part.

In their formulation, it can be noticed that a correlation function, $<Q^{\nu}(0)\, Q^{\nu}(t)>_{vib}$, identified with only vibrational motion appears. This results from the introduction into the Hamiltonian of the system of an operator, V^{ν}, which accounts for the various mechanisms of vibrational relaxation. This operator perturbs the vibrational energy levels and through a consideration of the conservation of energy and use of the mathematical operations outlined in Section A a correlation function reflecting vibrational relaxation occurs.[26] Note that a part, $Tr\left[\beta^{\nu}(0)\,\beta^{\nu}(t)\right]$, sensitive to translational and rotational motion is, of course, also present.

The introduction into the Hamiltonian of an operator to reflect vibrational relaxation is not limited to liquids. The same technique can be used with liquid crystals with the formalism outlined in Sections A and C of this chapter. First, it should be noted that the β terms in the correlations function derived earlier, $<\beta_{ik}^{\nu}(t)\,\beta_{ik}^{\nu}(0)>$, are actually of the form $\left(\frac{\partial \beta_{ik}}{\partial Q^{\nu}}\right)_{Q^{\nu}=0} Q^{\nu}$. Thus when the operator V^{ν} is introduced and its attendant consequences taken into account the correlation function can be factored as

$$\langle \beta_{ik}^{\nu}(t)\beta_{ik}^{\nu}(0)\rangle = \left\langle \left(\frac{\partial \beta_{ik}^{\nu}(t)}{\partial Q^{\nu}}\right)\left(\frac{\partial \beta_{ik}^{\nu}(0)}{\partial Q^{\nu}}\right)\right\rangle \langle Q^{\nu}(0)Q^{\nu}(t)\rangle$$

$$\equiv \langle \underline{\beta_{ik}^{\nu}(t)}\ \underline{\beta_{ik}^{\nu}(0)}\rangle \langle Q^{\nu}(0)Q^{\nu}(t)\rangle .$$

Here, just as for the Nafie and Peticolas formalism, the $\langle Q^{\nu}(0)Q^{\nu}(t)\rangle$ term is sensitive to vibrational relaxation and the $\langle \underline{\beta_{ik}^{\nu}(t)}\ \underline{\beta_{ik}^{\nu}(0)}\rangle$ term is sensitive to only the translational-rotational motion. This means that all the correlation functions obtained for liquid crystals when the incident and scattered polarization directions are perpendicular to each other (See Section C) will be the product of a vibrational part and a translational-rotational part.

The formalism used for crystals and liquid crystals does not, however, permit the averaging over all orientation angles that can be done for liquids. In this regard, liquids offer an advantage; the averaging procedure for liquids allows the relatively easy removal of the vibrational part of the correlation function. Following once again the formalism of Nafie and Peticolas, it can be seen that the Fourier transform of the normalized vibrational correlation function can be obtained from the following:

$$\hat{I}_{vib}(\omega) = I_{\parallel}(\omega) - 4/3\, I_{\perp}(\omega) \Big/ \int_{-\infty}^{\infty} \left[I_{\parallel}(\omega) - 4/3\, I_{\perp}(\omega)\right] d\omega$$

and therefore

$$\hat{I}_{vib}(\omega) = (2\pi)^{-1} \int_{-\infty}^{\infty} \overline{\langle Q^{\nu}(0)Q^{\nu}(t)\rangle}_{vib} \exp(i\omega t)\, dt \quad ,$$

where $\hat{I}_{vib}(\omega)$ is the normalized pure vibrational lineshape. Performing the inverse Fourier transform on the above equation isolates the vibrational correlation function:

$$\overline{\langle Q^{\nu}(0)\, Q^{\nu}(t)\rangle}_{vib} = \int_{-\infty}^{\infty} \hat{I}_{vib}(\omega) \exp(-i\omega t)\, d\omega$$

Similarly, the inverse Fourier transform of the normalized $I_{\perp}(\omega)$ lineshape gives

$$\overline{\langle \mathrm{Tr}\left[\beta^{\nu}(0)\beta^{\nu}(t)\right]\rangle}_{tr}\,\overline{\langle Q^{\nu}(0)\, Q^{\nu}(t)\rangle}_{vib} = \int_{-\infty}^{\infty} \hat{I}_{\perp}(\omega) \exp(-i\omega t)\, d\omega$$

A simple quotient of these results removes the vibrational correlation function and isolates the orientational one:

$$\frac{\overline{\langle \mathrm{Tr}\left[\beta^{\nu}(0)\beta^{\nu}(t)\right]\rangle}_{tr}\,\overline{\langle Q^{\nu}(0)\, Q^{\nu}(t)\rangle}_{vib}}{\overline{\langle Q^{\nu}(0)\, Q^{\nu}(t)\rangle}_{vib}} = \overline{\langle \mathrm{Tr}\left[\beta^{\nu}(0)\beta^{\nu}(t)\right]\rangle}_{tr}$$

$$= \int_{-\infty}^{\infty} \hat{I}_{\perp}(\omega) \exp(-i\omega t)\, d\omega \Big/ \int_{-\infty}^{\infty} \hat{I}_{vib}(\omega) \exp(-i\omega t)\, d\omega$$

Since it is information on orientational motion that is desired, this result is an important one.

It should be emphasized once again that the isolation of $\overline{\langle \mathrm{Tr}\left[\beta^{\nu}(0)\,\beta^{\nu}(t)\right]\rangle}_{tr}$ as outlined above is possible only because averaging of all molecular orientations simplifies $I_{\parallel}$ and $I_{\perp}$. The above procedure is applicable to mesogens only when they are in the isotropic phase (random orientation) and when they are dissolved in solvents. (The term mesogen refers to a compound that is

capable of forming liquid crystal phases.)

E. Bandwidths and Orientational Motion

The use of bandwidths to yield information on orientational motion is most completely described by Bartoli and Litowitz.[16] They outline two methods for obtaining the orientational part of the half width at half height (HWHH). The first method involves calculating the I_{vib} spectrum as outlined in the previous section:

$$I_{vib}(\omega) = I_{\parallel}(\omega) - 4/3 I_{\perp}(\omega)$$

By convolving an assumed Lorentzian lineshape with I_{vib}, the experimentally obtained peak, $I_{\perp}$ can be generated. The Lorentzian band that successfully leads to the experimental peak is then used as the orientationally dependent part of the experimental peak. From this band an orientational HWHH is measured, ω_{OR} .

The second method they outline, essentially an extension of Rakov's method,[37] involves measuring the temperature dependence of the HWHH. At low enough temperature, the HWHH becomes temperature independent. This HWHH is approximately equal to the intrinsic width, ω_{vib} . If both the intrinsic lineshape, I_{vib}, and the orientational lineshape, I_{OR}, are Lorentzian, then the HWHH of the experimentally obtained spectrum is the sum of the HWHH of the intrinsic and orientational parts:

$$\omega_{exp} = \omega_{vib} + \omega_{OR}$$

Once ω_{vib} is known from the temperature studies, then ω_{OR}

can be calculated, for any temperature, by subtracting ω_{vib} from the experimentally obtained HWHH at that temperature.

In both of these methods, I_{OR} is a Lorentzian. For Lorentzian lineshapes ω_{OR} (in units of cm^{-1}) can be related to a reorientational time:

$$\tau_{OR} = \frac{1}{2\pi c \omega_{OR}}$$

These τ_{OR} can be compared with reorientational times obtained from other techniques such as Rayleigh scattering and various orientational models. From the comparison conclusions can be drawn about the mechanisms of reorientation in liquids.[16]

Kirov and Simova[38] use Rakov's method, the second method of Bartoli and Litowitz, to determine the potential barrier to molecular reorientation in liquid crystals. (Note that since Rakov's method does not depend on averaging over all molecular orientations, it can be used for the anisotropic environment of liquid crystals.) This can be done by first considering ω_{OR} to have an Arrhenius temperature dependence:

$$\omega_{OR} = A \exp(-U_{OR}/kT)$$

where A is constant and U_{OR} is the reorientation barrier. Then by determining ω_{exp} at a number of temperatures, U_{OR} can be isolated.

The use of the HWHH to yield reorientational times of potentials depends on I_{vib} and I_{OR} having a Lorentzian shape. To a good approximation they do.[16] However, it is the deviation of I_{OR} from

the Lorentzian shape, especially in the band wings, that contains additional information about orientational motion. Since it is diffusion processes that lead to a Lorentzian bandshape, non diffusional processes are excluded by using the Lorentzian lineshape. Essentially, this means that the information gained by the HWHH approach using Lorentzian bandshapes pertains to the long time molecular orientational relaxation processes to the exclusion of the short time ones.[39]

CHAPTER III

EXPERIMENTAL

Experimental work has essentially consisted of taking Raman spectra of aligned liquid crystal samples and solutions of the mesogen. In this Chapter, the methods of sample preparation will be described, as well as the spectroscopic techniques.

A. Sample preparation.

1. Aligned liquid crystals.

The liquid crystal used in this study was 4-n-Octyloxy 4'-cyanobiphenyl:

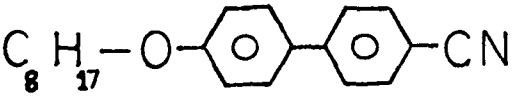

This substance has the following transition temperatures: crystal to smectic, 54.5; smectic to nematic, 67; nematic to isotropic, 80.[40] The liquid crystal was prepared by BDH Chemicals Ltd. of England and was purchased in this country from Gallard and Schlesinger Chemical Manufacturing Corporation. The manufacturer guaranteed a minimum of 99.5% purity and the liquid crystal was used without further purification.

The liquid crystal was aligned on 3-inch x 1-inch Thomas Pre-Cleaned Microslides by two techniques. To produce alignment with the

long molecular axes of the liquid crystal in the plane of the surface of the glass slides, a silicon monoxide coating was first put on the glass slides following the method of Janning[41] and Urbach, Boix and Guyon[42]. The slides were carefully cleaned with Bon Ami detergent, distilled water, and distilled acetone to remove grease and particles. They were then placed in a standard bell jar apparatus used for high vacuum thin film deposition work. The slides were at least ten inches away from a silicon monoxide source. In order to get eventual alignment of the liquid crystal long axes parallel to the short side of the slide[42], the slides were positioned so that the short side was pointed down in the bell jar and the whole slide tilted at an angle of about 65 degrees from the horizontal, see Fig. 3.

To get eventual alignment of the liquid crystal with the long axes parallel to the long side of the slide, the same slide placement was made, except that the long side of the slide faced downward. The silicon monoxide source was heated and deposition took place at approximately 5×10^{-6} torr, the pressure range not being crucial as long as it was below 10^{-5} torr.[41] The film thickness was monitored by the use of a quartz crystal placed at about the midpoint of the glass slide with the flat face of the crystal making a zero degree angle with the horizontal. This crystal was wired to a frequency monitor which measured the change in the frequency of oscillation of the crystal as a film formed on its surface. The thickness of the film on the crystal could be calculated, for silicon monoxide, from the change in frequency from the following equation supplied by the manufacturer: $\Delta f = A^{\circ} \times \frac{2.1}{2}$, where Δf is the change in frequency, A° is the thickness of the deposited film and 2.1 is the density of silicon monoxide.

FIG. 3. Position of the microscope slide for coating with SiO so that planar S alignment of the liquid crystal is achieved. Note that the slide edge (heavy black line) is pictured coming out of the plane of the paper.

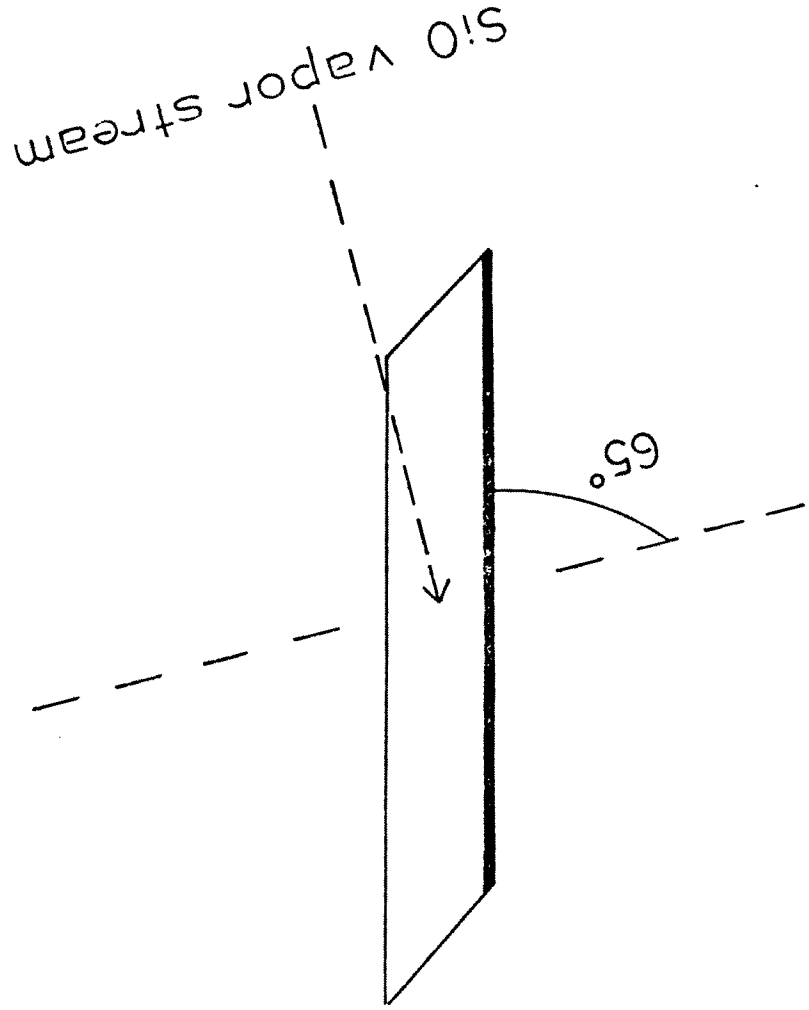
SiO vapor stream
65°

From the film thickness on the reference quartz crystal, the film thickness on the glass slide could be calculated from an equation due to Janning:

$$Ta = \cos \emptyset \ A°$$

where Ta is the thickness on the slide and $\emptyset$ is the angle the slide made with the horizontal. Film thickness on the slides was generally about 200 A°, however, thickness was not crucial since alignment has been reported using films ranging in thickness from 50 to 1000 A°.[42] The slides were stored in a glass container until use with the liquid crystal. For a discussion of the microscopic nature of the silicon monoxide surface and its role in aligning the liquid crystal, see the article by Dixon, Brody and Hester.[43]

In order to achieve the eventual alignment of the liquid crystal molecular axes perpendicular to the glass slide surface, the slides were first coated with a surfactant using the method of Proust, Ter-Minassion-Saraga and Guyon.[44] Hexadecyltrimethylammonium bromide (HTAB), the surfactant, was obtained from Professor Horst Hoyer of the Chemistry Department of Hunter College. The HTAB showed a melting range of 186-202°C when tested in a Mel-Temp apparatus. This temperature range was considerably below the 232-247°C range given in the Fisher Catalogue for practical grade material, though the magnitude of the range was about the same. This material did, nevertheless, give alignment of the liquid crystal and was used without further purification. The HTAB was dissolved in water to form two solutions of approximately 3.0×10^{-5}M and 6.0×10^{-5}M. Both solutions led

to the alignment of the liquid crystal. Solutions ranging in concentration from 8.10×10^{-6} to 6.10×10^{-5}M have been reported as giving alignment.[44] The slides were coated with the HTAB by withdrawing them by hand at a rate of 1 - 1.5cm/min from a beaker containing the solutions, with the direction of withdrawal being perpendicular to the liquid surface. The reported range of allowable withdrawal rates is 0.5 to 1.5cm/min.

The procedure for adding the liquid crystal to the coated microscope slides was the same for either type of coating. First, mylar spacers, 25mm by 25mm, were prepared. These spacers could be selected from a variety of thickness ranging from 25μ to 250μ. Most of the samples have been prepared with either a double layer of 75μ spacers leading to samples that were 150μ thick or a single layer of 250μ spacers. The mylar spacers were placed on the coated side of one slide towards each of the ends of the slide. Since a 3-inch by 1-inch slide is approximately 75mm by 25mm, this left a clear area of approximately 25mm by 25mm in the center, see Fig. 4. The second slide was then placed on the mylar spacers with the coated side touching the spacer; thus, the coated sides were facing each other. The two slides were then clamped together with common tension clamps used for a large sheaf of papers. Care was taken to not allow the short ends of the slides to touch the clamps, since when the slides contained the liquid crystal in the isotropic phase, capillary action would pull the substance out from between the slides and onto the clamps, see Fig. 4.

The two slides clamped in this manner formed an empty sample cell. The cell was placed on the surface of a hot plate so that the

FIG. 4. Sample cell for the aligned liquid crystal.

I Front View

a) sample region

b) mylar spacer

c) spring clamp

II Top View

a) sample region

b) mylar spacer

c) spring clamp

d) edge of glass slide

e) empty space.

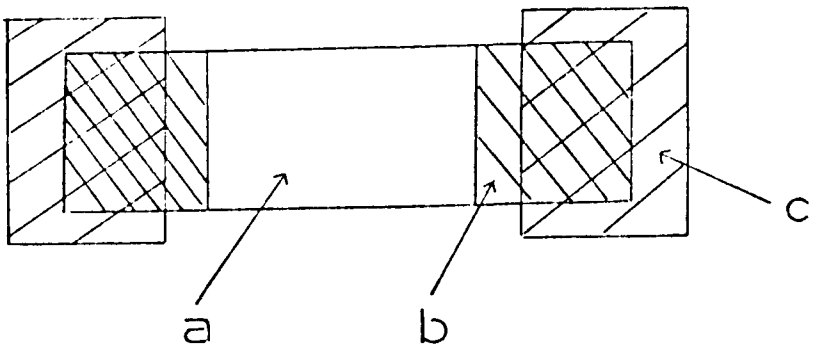

I

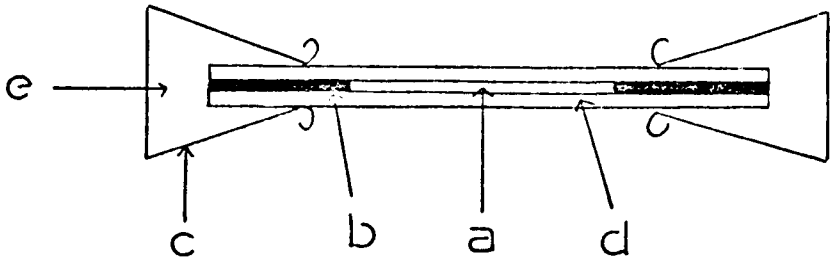

II

flat sides of the slides were in a plane perpendicular to the plane of the surface of the hot plate. Since the clamps extended beyond the bottom edges of the slides, the edges were kept from touching the hot plate and thus prevented the eventual loss of sample through capillary action. They were then heated to a temperature above that needed to cause the liquid crystal to undergo its transition to the isotropic phase; for the 4-n- Octyloxy-4' -cyanobiphenyl, i.e., above 80°C. Then, a 1mm inner diameter capillary tube, partially filled with isotropic phase liquid crystal that had just been withdrawn by suction from its container, was touched to the top edge of the hot slides. Capillary action pulled the molecules out of the capillary tube and into the sample cell. This procedure was repeated until the cell was filled to the desired level. Note that sample did fill in the thin regions between the mylar spacers and the glass surface. However, no problems resulted from this, except for the possibility of leakage from the ends of the slides, which, as was mentioned, was prevented by proper placement of the clamps. After being filled, the cell and its contents were allowed to cool slowly to room temperature.

Alignment of the liquid crystal was checked by taking advantage of its optical anisotropy. The liquid crystal in this study behaved optically in its smectic and nematic phases as a uniaxial crystal. The optic axis of the 4-n-Octyloxy-4'-cyanobiphenyl lay in the direction of the director, the average direction of the long molecular axes. Uniaxial crystals and liquid crystal mesophases demonstrate very characteristic patterns when viewed through a microscope equipped with crossed polarizers. When the optic axis is pointed in the direction of propagation of the incident viewing light,

light extinction is achieved for all rotation angles of the microscope stage on which the crystal is sitting. If a conoscopic image is formed by converging the incident light to a sharp focus at the crystal, then for this position of the optic axis, a black cross is obtained which remains for all rotation angles of the stage.

When the optic axis is in a plane perpendicular to the propagation direction of the incident light, extinction is achieved for every 90° rotation of the microscope stage. The conoscopic image will be a flash figure[45] every 90°, that is, a very sudden extinction every 90° rotation of the stage. Under the correct conditions of thin samples and good focusing, the flash figure can be more clearly seen as two hyperbolic dark areas moving quickly into the viewing field along a diagonal, meeting to form a cross and then exiting along the other diagonal, all as the microscope stage is turned through a small angle. The reason for these extinction patterns depend on the electric vector direction of the ordinary and extraordinary rays formed in these birefringent materials. For further discussion of these points, see the books by Wood[45] and by Hartshorne and Stuart.[46]

The liquid crystal samples used in this study were examined with a Bausch and Lomb Optical Company polarizing microscope. To get conoscopic images, a 7mm focal length lens was added to the bottom polarizing apparatus of the microscope. A simple hot stage was constructed from aluminum and heating tape to allow the viewing of the liquid crystal in its smectic and nematic phases. Note that repeated heating of the liquid crystal to bring it from its crystal phase to its mesophases did not destroy the alignment in the mesophases. The liquid crystal samples which were supposedly homeotropically aligned

were examined to see the patterns described above for crystals with the optic axis parallel to the propagation direction of the incident light. Only those samples with the correct patterns were used. The planar aligned samples, the molecules' long axes should have been in the plane of the glass slide surface, were likewise examined to see the correct images for crystals with the optic axis in a plane perpendicular to the propagation direction of the incident light. Only those samples with the correct patterns were used. Since unaligned liquid crystals do not show any of these images, those samples that did not give such images were not used. Newly prepared samples never had to be rejected. Some samples, after repeated use, lost alignment and had to be rejected.

2. Mesogen Solutions

Solutions were prepared of the 4-n-Octyloxy-4'-cyanobiphenyl in four solvents: benzene, carbon tetrachloride, chloroform and methylthiocyanate. Basically, the same preparation procedure was used for all the solutions. A quantity of the isotropic phase mesogen was drawn into a weighed, open-ended glass capillary tube of either 0.9 to 1.0 or 1.6 to 1.8 millimeter inner diameter. After the capillary tube with the mesogen was again weighed, the clean end of the capillary tube was sealed in an oxygen-gas torch. A quantity of the solvent was then introduced, by syringe, into the other end. The tube was weighed again and then carefully sealed to avoid burning any material that might be adhering to the tube sides near the opening. After the tube was sealed, the sample was heated and shaken to induce uniform mixing. From the weights of the substances, the mole fraction concentration of mesogen was calculated; with a little experience

the approximate volumes of mesogen and solvent needed to form specific mole fractions could be judged by eye, simplifying sample preparation.

The solvents were taken, without further purification, from newly opened reagent bottles. The manufacturers and quality of the solvents were:

1. benzene--Fisher, Purified
2. carbon tetrachloride--Mallinckrodt, Analytical
3. chloroform--Mallinckrodt, Nanograde
4. methylthiocyanate--Aldrich.

In the case of chloroform, where water was a possible impurity, the solvent was first dried over Davison Molecular Sieves which had an effective pore size of 4 Angstroms. Before being used, the chloroform was filtered through a Millipore filter to eliminate any particles that might have been introduced by the Molecular Sieves.

B. Spectroscopic Techniques

Most spectra were taken using a Spex model 1401, 3/4 meter Czerny-Turner double monochromator spectrometer equipped with ruled, blazed plane gratings. Detection was through the use of a ITT FW-130 phototube. Spectra could be recorded in analog or digital form. The spectrometer was under the control of a PDL 8L minicomputer. Under such computer control, a stepping drove the gratings. At each wavenumber or fraction of a wavenumber interval selected out by the gratings, the number of photons scattered were amplified, counted and displayed as either the total number of photons counted during the

collection time interval or as the counts per second. Spectra were generally taken using a $0.5cm^{-1}$ sampling interval and 60 or 30-second collection time. For samples in which peak intensity was relatively weak, less than 200 photon counts per second, a 60-second collection was used. For peaks of greater intensity, a 30-second collection time was sufficient to minimize electrical noise. To avoid truncation errors which result from the division of the number of counts by the number of total seconds of the collection period to give the counts per second, data was generally collected, for moderately weak peaks (<300cps) in the form of unaltered total counts. These data were punched in ASC II decimal form on paper tape by the paper tape punch of a model ASR-33 Teletype. The digital data were processed on a Data General Corporation Nova minicomputer which had 12 thousand words of available memory. This computer was equipped with a tape cassette reader for fast input of programs. An ASR-33 Teletype with a paper tape reader was used for the input of paper tape data and communication with the computer. Data processing details will follow in a separate chapter.

The entry and exit slits of the monochromator were set (unless otherwise noted) at 50μ and the center slit, which allowed the transfer of light from the first monochromator to the second, was set at 100μ . These slit settings allowed a spectral bandpass of $1cm^{-1}$, well below the requirement of the bandpass equalling one half the halfwidth at half height needed for these kinds of studies.[47] These slit settings were also shown to not affect the peak shape by comparing the full width at half height (FWHH) of the peak of interest at bandpasses of 0.5, 0.8, 1.0, $2.0cm^{-1}$. From the comparison, it was seen that the FWHH was the same at 0.5, 0.8 and $1.0cm^{-1}$ bandpasses. It was con-

cluded that the instrumental function made no contribution to the shape at a bandpass of $1.0cm^{-1}$ or less. The scattered light was passed through a polarization analyzer which could be fixed in two positions 90 degrees apart. The light then passed through a quartz scrambler and was focused on the slits by a f1.6 lens.

The incident light was provided by a Spectra Physics model 164 Argon ion laser powered by a model 265 exciter. The 514.5 nm line of Argon was used. In the "light mode" control of the laser, output power stability was specified by the manufacturer to be $\pm$0.5% over a 10 hour period. This was generally found to be correct. The output commonly used was 400mW accurately read from a power meter to within $\pm$5% at 514.5 nm. The light, after leaving the laser, was reflected off of two mirrors. It was then brought to a focus at the sample after first passing through a filter which, though cutting the power by about 60%, also removed the non lasing emission lines of the Argon ion plasma. If a sample showed evidence of flourescence in the form of a sloping background or more commonly as a higher intensity low frequency baseline compared to the high frequency baseline, the sample was allowed to sit in the beam for at least two hours before the taking of a spectra.

The glass slides containing the liquid crystal were positioned in the sample compartment of the Spex 1401 to permit the scattering geometries and liquid crystal alignments shown in Fig. 5. Incident light was propagated in the Z direction and was polarized in the Y direction. It entered between the glass slides hitting the liquid crystal sample. The bottom edges of the glass slides were coated with an opaque silver coating to reflect those parts of the incident

FIG. 5. Various scattering geometries and liquid crystal alignments.

I_{VH} refers to the intensity obtained when the incident polarization is along Y and the scattered polarization is along Z

I_{VV} refers to the intensity obtained when the incident polarization is along Y and the scattered polarization is along Y

S refers to the alignment of the liquid crystal long molecular axes (shown as straight lines) parallel to the short side of the microscope slide, in the plane of the slide.

L refers to alignment parallel to the long side of the slide and in the plane of the slide

H refers to alignment perpendicular to the surface of the glass slide (homeotropic alignment).

$\sim\!\!\rightarrow$ indicates the propagation direction

$\longleftrightarrow$ indicates the polarization direction.

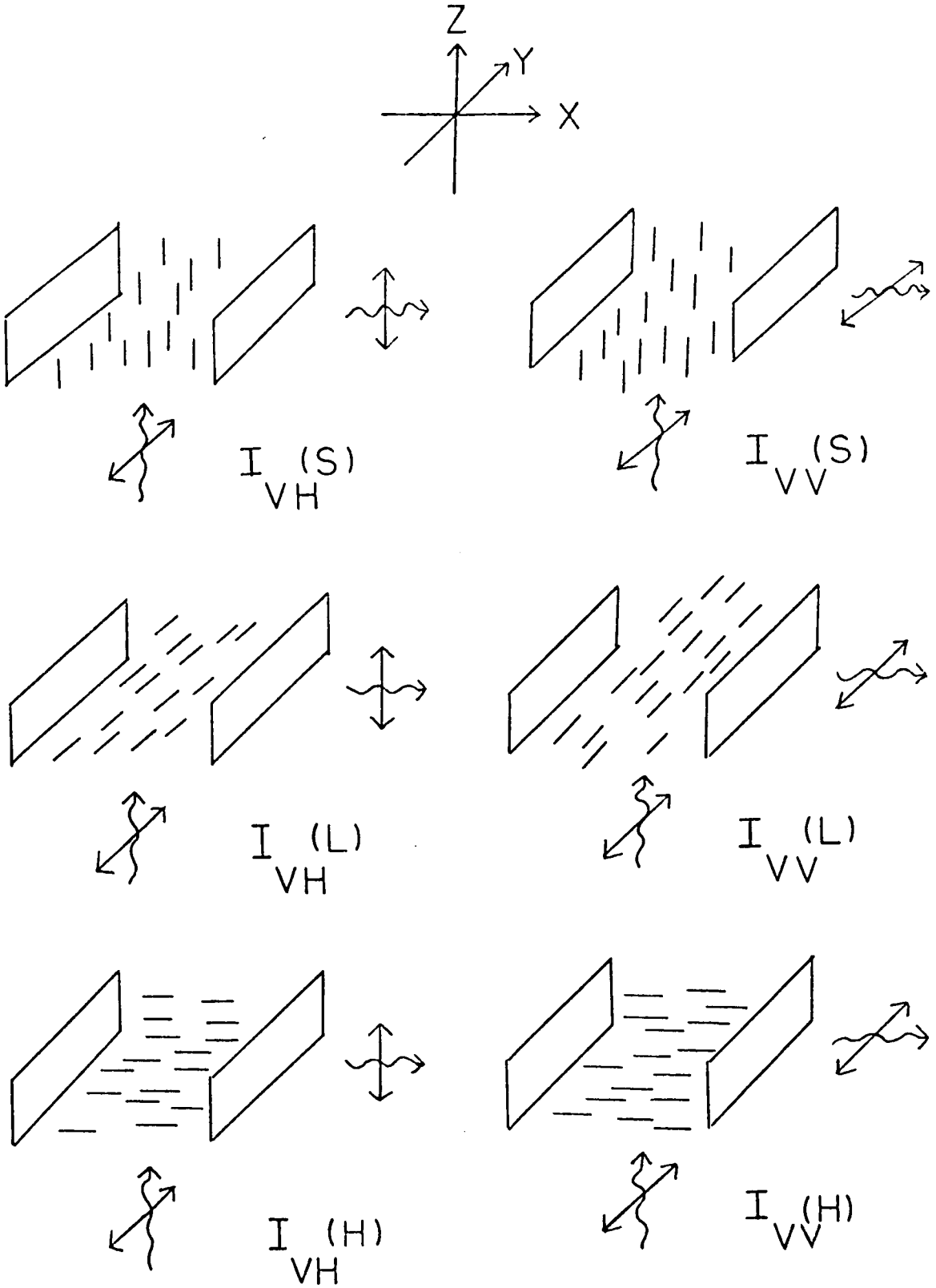
Z
Y
X
$I_{VH}^{(S)}$
$I_{VV}^{(S)}$
$I_{VH}^{(L)}$
$I_{VV}^{(L)}$
$I_{VH}^{(H)}$
$I_{VV}^{(H)}$

beam that did not pass between the glass slides and might otherwise pass into the glass through the bottom edges, causing spurious effects.

The scattered light exited from the front of the glass slides at 90° from the incident direction. The light propagating in the X direction was collected with either Z or Y polarization by using a polarization analyzer. As was mentioned in Chapter Two, the polarization configuration that would lead to information about orientational motion is YZ; this corresponds to all the I_{VH} configurations shown in Fig. 5. Generally, spectra were taken in the I_{VH} configuration. For these polarization measurements, the polarization analyzer was first fixed in its holder so that the depolarization ratio, I_{VH}/I_{VV}, of the 313 and 459cm^{-1} lines of CCl_4 matched as closely as possible to those in the literature.

A sample holder and oven were specially constructed for use with the microscope slide samples. The slides were held in position by four screws placed in four aluminium support blocks (Fig. 6). When these screws were tightened, the glass slides could be held in position 2mm above the aluminium base plate to prevent loss of the fluid phase samples due to capillary action. The aluminium base plate had a center hole which allowed the incident light to enter. The base plate was fixed to the Spex sample holder base by four screws and was held stable and level 7mm above the top of the Spex base by three aluminium blocks. This height of the plate allowed the focused beam to strike the sample at a position in line with the center of the collecting lens. The slides and sample holder were contained in an asbestos insulated aluminium housing that allowed the collecting lens to be close to the sample, (Fig. 6).

Heating of the sample was accomplished through the use of a

FIG. 6. I Sample Holder

a) screws

b) aluminum block for slide support

c) baseplate

d) baseplate support block

e) Spex base

f) heating tape

II Oven-Front View

g) aluminum housing

h) asbestos covering (over the whole housing)

i) aluminum base and side plate (asbestos covered)

j) glass window

k) exit hole for laser beam

III Oven-Top View with cutaway

l) collection lens

m) top view of sample holder with slides

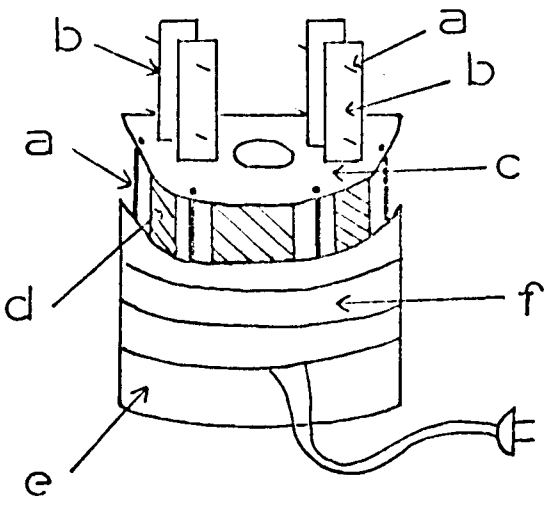

I

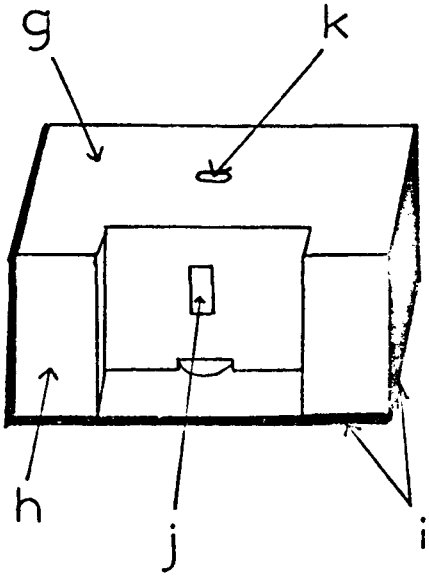

II

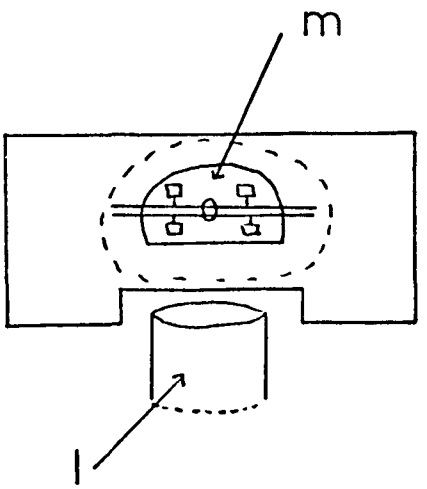

III

Brisheat flexible heating tape, available through the Arthur H. Thomas Co. This tape was 3/8 inch by 12 inches. It gave 43 watts of power at 115 volts. The tape was wrapped around the Spex sample holder base with the leads exiting from the back of the oven. Though many heating techniques were tried, the use of this heating tape led to the most uniform heating of the microscope slides. This was tested by taking millivoltage readings from a copper-Constantan thermocouple placed at various positions on the glass slides within the sample area. The thermocouple had been calibrated outside of the oven against the known melting points of napthalene (80.2°C), benzoic acid (122.4°C) and dichlorobenzene (53.1°C). The tests in the oven showed that the maximum temperature differential between the positions was 1.5°C. Considering that scattering results from a small volume of sample at the bottom of the glass slides, it can be concluded that the temperature differential within the scattering volume of sample was much less than 1.5°C.

This same copper-Constantan thermocouple was used to determine the temperature of the sample during the taking of spectra. The end of the thermocouple was taped to the back of the glass slides as close to the region of scattering as possible. The estimated inaccuracy of the temperature was about 2°C for this thermocouple position based on the fact that the laser beam will heat up a sample by 2°C. However, when the sample was observed visually as it underwent mesomorphic state transitions, it was seen that the transition temperatures based on thermocouple readings were 4°C higher than the literature values. Therefore, it can be concluded that the actual temperature is 4°C lower than that measured. Millivoltage readings were taken from a Keithley Model 160 Digital Multimeter. Millivoltages were interpreted as temp-

eratures from a conversion table based on a zero degree reference junction. Such a reference was established by the placement of a thermocouple junction in an ice-water bath contained in a Dewar flask.

In order to provide the high temperature needed, the heating tape of the oven was connected to a variable transformer; changing the voltage led to different temperatures. Such a method of regulation often led to a temperature drift of 1 to 2 degrees and required constant fine readjustment of the voltage setting to keep the drift from becoming even greater. However, with close attention, the transformer maintained adequate temperature stability.

To take spectra of the smectic and nematic phases, and in order to make sure that the solid was completely melted and had a chance to get aligned, each sample was first heated to the isotropic phase and left in that phase for about one hour. The sample was then slowly cooled, with the laser beam blocked from hitting the sample, to the appropriate phase and left for at least one hour at the temperature desired. The sample was periodically viewed through the front window of the oven using a 20mW beam as illumination. When the sample showed the uniform texture characteristic of aligned samples, the full power beam was allowed to hit the sample. The beam was then aligned and the other procedures for taking a spectrum were followed. Before taking an isotropic phase spectrum, the sample was allowed to remain at the temperature desired for at least two hours to insure high temperature stability.

When spectra were first taken of planar aligned samples, the sample thickness used was 150μ .With a few samples, it was noticed that a change in the sample had occurred where the laser beam had passed.

Examination of these samples with the polarizing microscope showed the changed region to be homeotropically aligned. When a set of such slides were washed to remove the liquid crystal contents and then reloaded with fresh liquid crystal material, a central region of homeotropic alignment returned. It was suspected that the laser beam was knocking the silicon monoxide coating off the glass slide surface and allowing raw glass surface interactions to homeotropically align the liquid crystal. Indeed, when the liquid crystal was added to a sample cell made from untreated glass slides taken from the manufacturer's box, homeotropic alignment was achieved.

In order to keep the laser beam from possibly hitting the glass slide surface, planar aligned samples were made with 250μ thick mylar spacers. Furthermore, care was taken to align the laser beam so that it could be clearly seen to go between the slides, up through the sample and out the space at top. After the taking of spectra, the samples were carefully examined in the smectic and nematic phases under the polarizing microscope to see if any homeotropic regions were present. When using the 250μ samples and the carefully aligned beam, no such homeotropic alignment was seen. The homeotropically 150μ aligned samples had shown no obvious change with the passage of the beam and consequently only a microscopic examination with polarized light was conducted to confirm alignment after the taking of spectra. However, for the planar aligned samples, some additional measures were taken to insure sample alignment. As was mentioned previously, the beam was blocked from hitting the liquid crystal during the approximately one hour needed for the molecules to completely align on the slide surface. This procedure served to prevent any possible inter-

ference from the electric vector of the intense beam during this sensitive time. Once the sample was observed to show the uniform texture of planar alignment and before a spectrum was taken, the depolarization ratio was generally obtained, that is, the ratio of the maximum intensity of the 2225^{-1} peak in the I_{VH} configuration to the maximum intensity in the I_{VV} configuration was formed. After the spectrum was taken, the depolarization ratio was again taken and compared with the pre spectrum ratio. For the 250μ samples, these ratios matched to within experimental error. Since the depolarization ratio depends on the polarizability tensor elements and since the elements are related to the sample orientation (see Chapter Two), the stability of the depolarization ratios supplementarily insured that the sample alignment had not changed during the taking of spectra. Also, since the ratios differed for the same phase in the S and L planar aligned samples, there was further indication that no change to a common alignment was occurring. The following approximate ratios were obtained:

	S aligned	L aligned
nematic	2.3	0.50
smectic	1.5	0.17

For comparison, the isotropic depolarization ratio was 0.56. The above depolarization ratios were further revealing. For unaligned samples, multiple scattering from the different alignment regions leads to a depolarization ratio of one. Since for the planar aligned samples, the ratios were different from one, there was indication that the samples were well aligned.

The taking of spectra of the solution samples was fairly rou-

tine. The sample chamber of the Spex 1401 spectrometer was equipped with a sample so that the transverse-transverse geometry shown in Fig. 7 was obtained.

The laser beam and collection optics were aligned in order to maximize the scattered intensity and the spectrum was taken in the manner described for the aligned liquid crystal samples.

For the heating of samples in a capillary tube, an oven already available in the laboratory was used. This simple oven which was constructed from an aluminium block and nichrome wire and was fitted to the Spex 1401 sample chamber, held the capillary in the same transverse-transverse geometry of Fig. 7. As for the oven used to heat the aligned samples, a variable transformer was used to control the heating with the capillary oven. An approximate measure of the temperature was obtained by placing a copper-Constantan thermocouple as close as possible to that part of the capillary tube from which scattering was taking place.

For some of the solution spectra, a J-Y Optical Systems Ramanor HG2S spectrometer was used. This machine has a better throughput than the Spex 1401. For a $1cm^{-1}$ spectral bandpass, the intensity of the C≡N stretching peak was at least three to four times greater than that obtained with the Spex 1401. The greater sensitivity of the HG2S made it very useful for obtaining spectra from the weak peak of dilute solutions. Since the signal to noise ratio, when using this machine, was quite high, shorter and more convenient collection times could be used for solutions of all concentrations. To make sure that the HG2S did not make a contribution to the correlation function through its instrumental function, a number of correlation functions were cal-

FIG. 7. Transverse scattering geometry

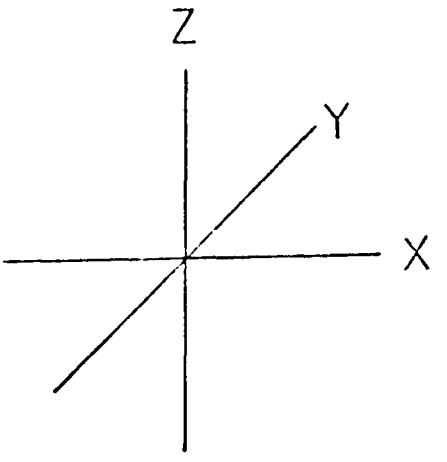
Z
Y
X

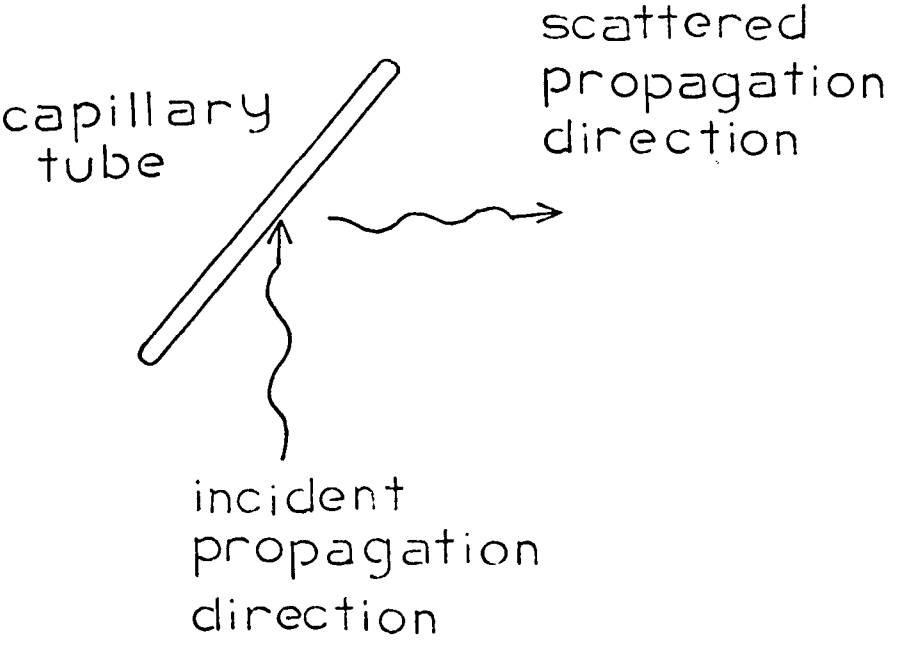
scattered
propagation
direction
capillary
tube
incident
propagation
direction

culated from spectra obtained from both the HG2S and the Spex 1401 using the same samples. The correlation functions matched each other to within experimental error. It was concluded from this comparison that correlation functions calculated from data obtained with the HG2S could be used along with those obtained from data from the Spex machine.

The Ramanor HG2S is a one meter double spectrometer equipped with concave aberration corrected holographic gratings. The spectrometer is fitted with a quartz scrambler and a polarization analyzer. Detection uses a RCA C31034A photomultiplier tube in a Products for Research tube housing for cooling. A Princeton Applied Research Corporation model 1109 photon counter is used with the photomultiplier tube. A Nova 2 minicomputer is interfaced to the spectrometer. Computer control of the spectrometer is very similar to that described for the Spex 1401. Spectra are obtained on magnetic tape in digital form. Paper tape copies for processing using the DFT system (see Appendix B) could be made from the data on magnetic tape.

CHAPTER IV

DATA PROCESSING

The Fourier transform relationship between the Raman intensity and the correlation function has been shown in Chapter Two. Since intensity data are obtained in digital form in our laboratory, a method of computing the Fourier transform of this finite range of data is required. A Fourier transform of the form

$$X(t) = \int_{-\infty}^{\infty} I(\omega) \exp(-i\omega t)\, d\omega$$

is computed by calculating

$$X(n) = \sum_{k=0}^{N-1} x(k) \exp -i2\pi \frac{nk}{N}$$

where x(k) is the k th data point, n is the index of the output point, N is the total number of input data points. This form of calculating the Fourier transform is called the Discrete Fourier Transform (DFT). For a discussion of the justification of this approach as well as its limitations, see reference 48.

By the Euler expansion of the exponential, the DFT can be rewritten as

$$X(n) = \sum_{k=0}^{N-1} x(k) \left[\cos 2\pi \frac{nk}{N} - i\sin 2\pi \frac{nk}{N}\right]$$

This form can easily be calculated using a computer by multiplying each input point by the appropriate cosine and sine value, storing the result and eventually summing all the results. This direct approach can be very time consuming since the calculation of each output point requires 2N multiplications and 2N additions. The Fast Fourier Transform (FFT) is an algorithm for rapidly computing the DFT which takes advantage of the periodic nature of the cosine and sine functions to eliminate a great number of the multiplications. (For further details on the FFT, see reference 48.) The method of sorting of input data required for the FFT limits the number of input points to 2^n, where n is an integer. This limitation prevents us from using this desirable algorithm for the calculation of the DFT since our data range must necessarily be flexible.

Our method of calculating the DFT is therefore basically the direct method of performing all the multiplications and summations. However, some time can be saved in the calculation of the cosine and sine values. Since only the real part of the correlation function has physical, interpretable meaning, the imaginary part resulting from the multiplication by sine $2\pi mk/N$ is not calculated. In addition, by taking advantage of the property of cosine values that makes the cosine multiplier of x(k) and x(N-K) the same (for further discussion of this property and its implementation see Appendices A and B), the time spent calculating the appropriate cosine value can be approximately halved.

The DFT as outlined above gives N output points for N input points. A method of interpolation has been developed which will give 2N, 3N ... output points for N input points. The details of the method and the justification for each is given in Appendix A. The method involves the insertion of an appropriate number (N, 2N ...) of zeros in

the center of the input data array. The result is a better defined correlation function. However, the addition of N zeros, for example, to N data points doubles the computation time for each point. Since there are now 2N output points to be calculated, overall computation time has increased by four times. It is apparent that time saving steps would be useful. An algorithm has been developed that simulates the addition of zeros and does not actually introduce them into the data. This keeps the multiplications and additions to N for each output point. The result is to keep calculation time down to two times instead of four for N added zeros, three times instead of nine for 2N added zeros, and four times instead of sixteen for 3N added zeros. Some details of this programming are given in Appendix B.

The entire program system for the calculation and the necessary support subroutines are written in Data General Corporation's Nova assembly language. The section specifically for calculating the DFT is written in a special form of assembly language which permits the calculation to be carried out in floating point arithmetic. This "floating point interpreter" allows the representation of numbers as a signed seven bit characteristic and a twenty-four bit mantissa instead of the usual signed fifteen bit form. The floating point form permits numbers of a wider dynamic range, substitutes the more accurate round off procedure for truncation, allows the calculation of cosine values as needed instead of choosing them from a limited table, and permits a greater number of significant figures due to the increased word size.

Before the DFT program can be applied to the spectroscopically obtained digital data, some adjustments of the data must first be made.

Consider a peak which has its center at the origin of a two dimensional coordinate system and its low and high frequency sides extending into the positive and negative regions of the abscissa respectively:

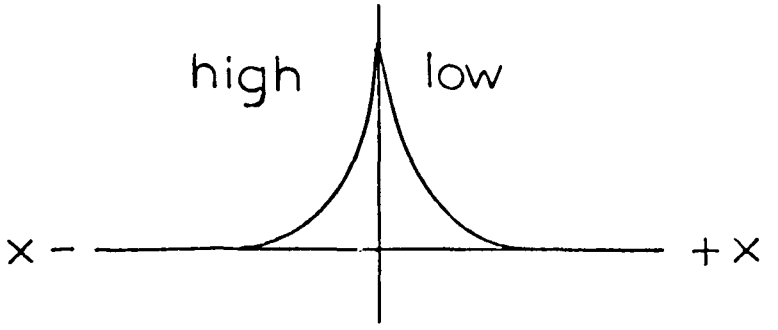

Recall that the correlation function is obtained from the Fourier transform of the peak intensity as a function of the frequency displacement from the center of the peak. In terms of the diagram above, this means calculating the Fourier transform of the data that is increasing in frequency displacement in the +x direction and the data that is increasing in frequency displacement in the -x direction. The DFT would not be capable of performing such a calculation since it considers all input data as functions of positive abscissa values.[48] Nevertheless, the DFT is capable of calculating the Fourier transform of a peak centered on the origin since it considers all input data as periodic. A peak centered at the origin is expected by the DFT to repeat itself starting at the positive abscissa value equal to one half the period. If the high frequency data is copied into the +x region as shown in the following diagram:

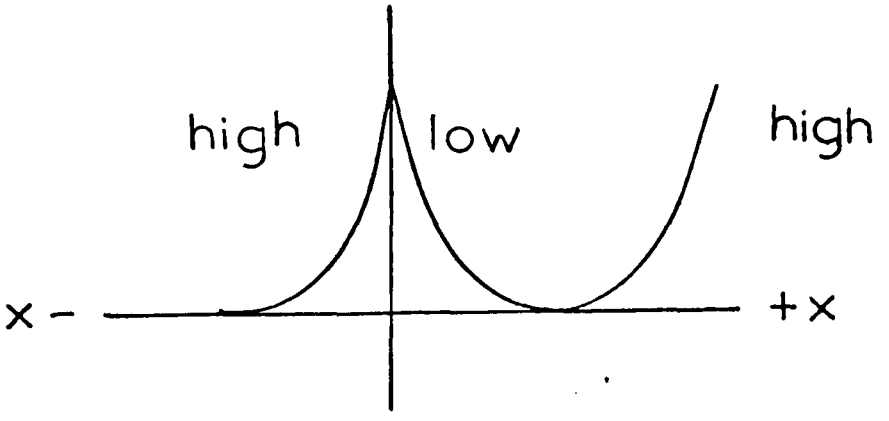

and then the DFT is used to calculate the transform of the data that is now a function of positive abscissa values, the desired transform will be obtained. Therefore, before calculating the correlation function from the experimentally obtained peak, the data is right circularly rotated to make it a function of a positive abscissa value in the form outlined above.

Some peaks must be folded before being rotated. The high frequency side is most often folded about the maximum to the low frequency side. This creates a symmetric peak. In principle, all vibrational peaks should be symmetric. Sometimes hot bands create an asymmetry on the low frequency side, or neighboring peaks interfere with some portion of the peak. Folding may remove these problems. Folding was not necessary for the symmetric peak used in our work.

In addition to the rotation adjustments, a baseline adjustment is made before the data are processed. In order to remove DC background, the minimum value of the baseline is set to zero. This is accomplished by subtracting the minimum value in the spectrum from all the data values. If it is necessary to divide one spectrum by another, then the minimum is adjusted to +1 rather than zero since this adjustment averts division by zero.

After the data have been put in the proper form, the transform is calculated. The number of points transformed is determined during the peak rotating step since during that adjustment a decision on the endpoints of the peak is made. The peaks used in our work have been chosen to include a one hundred wavenumber range sampled every one half wavenumber, leading to two hundred input points. The reasons for these choices are discussed in the error section of Chapter Five.

Either the raw or normalized transform results may be printed out on the Teletype in decimal exponential form. The normalized results are achieved by dividing all values of the output by the first value, making the first value one, and succeeding values less than one. The first point of the transform is the t=0 point. As we saw in Chapter Two, it is the maximum valued point. The output, which now consists of one point for every input point (real or zero extended), is plotted against a time scale by hand. DFT output points are evenly spaced in time with the interval determined by $T=1/N\Delta f$, where N is the number of input points and Δf is the frequency interval between them. For example, the time interval for the usual case of a peak range of 100 cm^{-1} which has been sampled every 0.5 cm^{-1} would be

$$T = 1 / (200)\ 2.99\times10^{-10}\frac{cm}{sec} \times 0.5\ cm^{-1} = 0.00334\times10^{-10}sec$$

or 0.334 picoseconds; if the data were zero extended once, the time interval would be

$$T = 1 / (400)\ 2.99\times10^{-10}\frac{cm}{sec} \times 0.5\ cm^{-1} = 0.00167\times10^{-10}sec$$

or 0.167 picoseconds. Though the results can be plotted on a linear ordinate scale, they are usually plotted on a logarithmic ordinate scale. As will be discussed in a later chapter, certain types of molecular motion lead to an exponental time decay of the correlation function; plotting on a logarithmic scale makes such decay, if it exists, obvious as a straight line.

For computing I_{vib} according to the equation

$$I_{vib}(\omega) = I_{\parallel}(\omega) - 4/3\, I_{\perp}(\omega)$$

which is described in Chapter Two, Section D, programs already available in the laboratory were used. These programs first convert data to a Basic language format and then perform the above operations in the floating point mode of Basic. The results are rounded off and a paper tape is produced. The I_{vib} peak obtained is then treated just as an experimentally obtained peak and processed in the same way to obtain its Fourier transform. Other programs were available in the laboratory that performed the calculation necessary for obtaining $I_{vib}(\omega)$ using single precision arithmetic. The correlation functions obtained from I_{vib} calculated this way, and from I_{vib} calculated using the Basic language program were compared. The comparison indicated no significant difference between the correlation functions. Consequently, the more convenient technique of single precision arithmetic was generally used.

For fitting least squares deviation straight lines to curves, a Basic language program was written and used. A copy of this program is included at the end of Appendix B.

CHAPTER V

RESULTS AND DISCUSSION

A. Introduction

The mesogen used for this study, 4-Octyloxy-4'-cyanobiphenyl (8OCB) was chosen because the -C≡N group it contains undergoes a high frequency stretching vibration at approximately 2225cm^{-1}.

The peak occurs at a frequency which suggests that the vibration is localized and is not complicated by the presence of other molecular modes of vibration.

The high frequency vibration is especially important since, as was mentioned in Chapter Two, for such a vibration a Born-Oppenheimer separation of the vibronic motions from the rotational-translational motions can be assumed.[17] The vibrational modes are represented by the harmonic oscillator wavefunctions. When the Heisenberg representation of the normal coordinate is formed using these wavefunctions and then the ensemble average is formed, $\langle Q^{\nu}(0)Q^{\nu}(t)\rangle$, the orthogonality of the normal coordinates leads to an average of zero for the same vibrational mode, ν, on two different molecules -- 1 and 2:

$$\langle Q_1^{\nu}(0)Q_2^{\nu}(t)\rangle = 0$$

By recalling from Chapter Two, Section D, that the correlation function that is obtained from experimental data is of the form

$$\langle \underline{\beta_{ik}^{\nu}(t)}\ \underline{\beta_{ik}^{\nu}(0)}\rangle\ \langle Q^{\nu}(0)Q^{\nu}(t)\rangle$$

it is then clear that non-zero correlation functions can only contain

terms pertaining to a single molecule. Thus, the correlation function calculated from a peak from the high frequency vibration can be interpreted as the average motional behavior of an individual molecule.

The C≡N symmetric stretch of the 8OCB is expected from bond angle consideration to be along the long molecular axis of the molecule. If during the course of the vibration, the molecule rotates around an axis perpendicular to the long axis (tumbling), the polarizability tensor elements in the laboratory framework would be changed by the rotation. This modulation of the tensor elements is the origin of the time dependence in the correlation function and consequently will be the source of information on tumbling motion. However, if during the course of the symmetric stretch, the molecule rotates around the long axis (spinning), or does not rotate at all, the tensor elements in the laboratory framework will not be changed. Such motion would not be detected by a correlation function.

A sense of why tumbling affects the correlation function while spinning does not can be obtained by examining how each of these motions affects the anisotropic part of the polarizability tensor. The C≡N stretch, as was mentioned, is considered to be localized. As a result, the rest of the molecule can be considered to be a rigid cylindrical body attached to the carbon, increasing its mass. Thus, the molecular situation might be approximated by a heteronuclear diatomic (or triatomic) molecule of $C_{\infty v}$ point group symmetry. The transition polarizability tensor composed of elements in the molecular framework and transforming as the species of the symmetric stretch, Σ^+, of such a diatomic is[26]

$$\begin{pmatrix} a_{xx}+a_{yy} & 0 & 0 \\ 0 & a_{xx}+a_{yy} & 0 \\ 0 & 0 & a_{zz} \end{pmatrix}$$

The anisotropic part of this tensor in the molecular framework is (26)

$$\begin{pmatrix} \frac{1}{3}(a_{xx}+a_{yy}-a_{zz}) & 0 & 0 \\ 0 & \frac{1}{3}(a_{xx}+a_{yy}-a_{zz}) & 0 \\ 0 & 0 & \frac{2}{3}(a_{zz}-a_{xx}-a_{yy}) \end{pmatrix}$$

The z axis corresponds to the long molecular axis and the x and y axes are two orthogonal axes perpendicular to z. For cylindrically symmetric molecules $a_{xx} = a_{yy}$. The anisotropic tensor must be put in terms of the laboratory framework before it can be used with the equations developed in Chapter Two. However, some simplifying geometries permit the use of the above form of the tensor to obtain an understanding of the affect of spinning and tumbling.

Consider the case where the molecule is aligned with its axes coincident with the laboratory axes. Then the molecular framework tensor elements are identical to the laboratory framework elements and the form of the anisotropic tensor given above applies in the laboratory framework:

$$\begin{pmatrix} \frac{1}{3}(\alpha_{XX} + \alpha_{YY} - \alpha_{ZZ}) & 0 & 0 \\ 0 & \frac{1}{3}(\alpha_{XX} + \alpha_{YY} - \alpha_{ZZ}) & 0 \\ 0 & 0 & \frac{2}{3}(\alpha_{ZZ} - \alpha_{XX} - \alpha_{YY}) \end{pmatrix}$$

where X, Y and Z refer to the laboratory axes. If the molecule is now rotated by 90 degrees around its z axis, i.e., it "spins" through a 90 degree angle, the α_{XX} term changes from α_{xx} to α_{yy}, the α_{YY} term changes from α_{yy} to α_{xx} and the α_{ZZ} term remains equal to α_{zz}. Since $\alpha_{xx} = \alpha_{yy}$, this interchange will have no effect on the anisotropic tensor in the laboratory framework. For other angles of rotation, linear combinations of α_{xx} and α_{yy} will result, but also leave the anisotropic tensor the same. The correlation function, which depends on the laboratory framework anisotropic tensor, will be unaffected.

Consider now a 90 degree rotation of the molecule around the x axis, tumbling. This motion changes the laboratory framework α_{ZZ} term from α_{zz} to α_{yy}, the α_{YY} from α_{yy} to α_{zz} and leaves α_{XX} unchanged. Such a change clearly affects the laboratory framework anisotropic tensor since $\alpha_{zz} \neq \alpha_{yy}$. Correlation functions which, of course, are derived from the tensor, will be affected also. This will hold true for tumbling motion through any angle since this motion will mix α_{zz} with α_{xx} or α_{yy}.

The above discussion ignores the more complicated aspects of molecular motion: other molecular alignments, rotation through angles other than 90 degrees, and the time dependence of the rotation. There

are ways of treating these situations more quantitatively.[16, 24] However, from the less quantitative discussion given above, a sense can be gotten of why tumbling motion will be detected by monitoring the C≡N stretch and spinning will not. Thus, it is seen that the liquid crystal chosen possibly provides a means of examining the individual molecular tumbling motion of the liquid crystal molecules.

Smectic and nematic mesophases of a liquid crystal show, of course, a preferred direction of their long molecular axes. Such molecular arrangement implies a barrier to tumbling motion. As the liquid crystal is heated and undergoes a transition to the next phase, it is expected that the barrier to tumbling should decrease and be much lower in the less ordered phase. The correlation function should reflect a consequent increase in tumbling motion. The C≡N group, by providing a probe of tumbling motion, permits a way of ascertaining the importance of molecular tumbling to the existence of the liquid crystal phases.

B. Results for aligned liquid crystals and discussion

As was mentioned in Chapter Three, spectra were taken of liquid crystal samples with the molecules oriented perpendicular to the glass slide surface (homeotropic alignment) and with the molecules in the plane of the slides both parallel to the short side (planar S) and parallel to the long side (planar L), see Fig. 5, Chapter Three. The purpose of this approach was to see if a particular alignment was more sensitive to changes in orientation due to molecular motion and might therefore more clearly provide information on tumbling. The reason why this sensitivity might result can be understood as follows: once

again, consider the case of the molecules being aligned so that the molecular framework axes coincide with the laboratory coordinates. If the experiment is conducted so that the incident light is polarized in the Y direction and the scattered light collected is polarized in the Z direction (see Chapter Two for the theoretical basis for this set up) then no peak should be obtained since, as was seen in the Introduction to this present Chapter, there are no off diagonal terms in the laboratory framework polarizability tensor. If, however, the molecule is slightly displaced due to the molecular motion so that the molecular fixed axes are no longer coincident with the laboratory axes, then a unitary transformation of the molecular polarizability terms must be performed in order to determine the polarizability in the laboratory coordinate system. This transformation will lead, in general, to off diagonal terms in the laboratory framework polarizability and a spectrum will be obtained. The degree to which the molecular polarizability terms, α_{xx}, α_{yy}, α_{zz}, contribute to the laboratory framework α_{YZ} term depends, of course, on the Euler angles through which the molecular framework is displaced. The relationship can be expressed quantitatively.[16, 24] By choosing different alignments of the liquid crystal molecules, different Euler angles between the molecular and laboratory framework are obtained. These Euler angles will be basically such that the molecular framework axes coincide exactly or coincide within 90° rotations with the laboratory axes. With the molecules in these positions no I_{VH} spectrum is expected; the laboratory framework tensor will be different for the different alignments, but will still be diagonal. Molecular motion will further change the Euler angles for each alignment and it is possible that for

one of the alignments, the mix of α_{xx}, α_{yy} and α_{zz} that forms α_{YZ} will be especially sensitive to changes in the Euler angles and cause large effects in the spectrum.

Spectra obtained from the smectic and nematic phases of the homeotropically aligned sample and the isotropic phase are shown in Fig. 8. The correlation functions calculated from these peaks are shown in Fig. 9. Similar spectra to those from the homeotropically aligned samples were obtained for both the planar S and the planar L aligned samples. The correlation functions calculated from them are shown in Fig. 10 and Fig. 11 respectively. Note that the homeotropic aligned samples were 150μ thick. The planar aligned samples were 250μ thick to avoid the change in alignment mentioned in Chapter Three.

Some general observations about these correlation functions can be made. They all have a value of one at the time origin as expected for a normalized correlation function. In addition, as time increases, the curves decay toward zero as is also expected. On a graph with a linear abscissa scale and a logarithmic ordinate scale, the curves do not seem to be linear, though the accumulation of errors which become significant at longer times, about which more will be said shortly, makes it hard to see if the curves are starting to become linear at longer times.

Some specific observations about these correlation functions can also be made. Significantly, for each alignment the results from the smectic and nematic phase spectra are quite close to the correlation function obtained from the isotropic phase data. A detailed discussion of the precision of these correlation functions will follow

FIG. 8. Cyano stretching peak (I_{VH}) obtained from the smectic (S), nematic (N) and isotropic (I) phase 8OCB. (Spex instrument) The absolute maximum intensities, after setting the baseline equal to zero, are

S: 145 counts per second

N: 100 counts per second

I: 295 counts per second

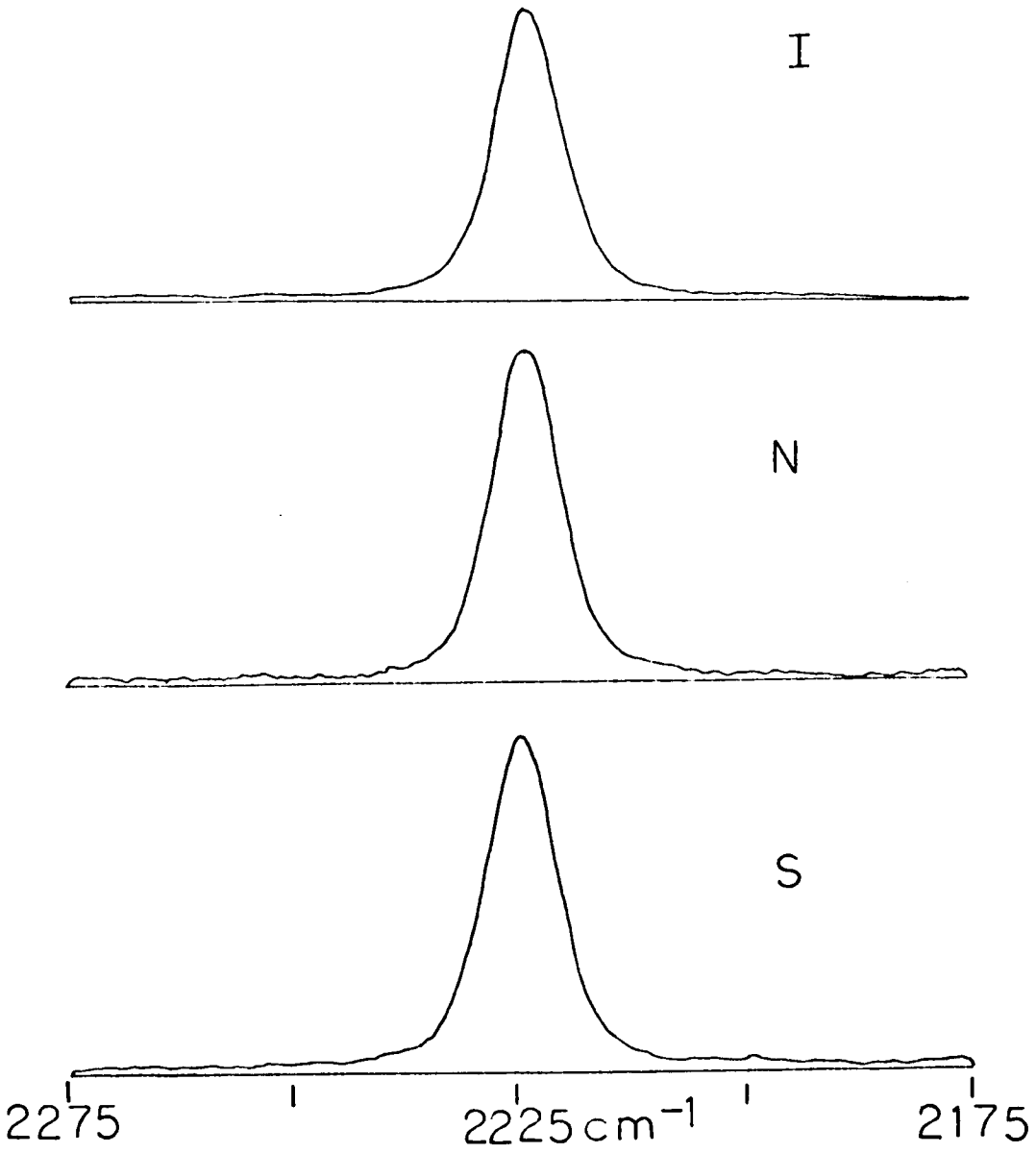
I
N
S
2275
2225 cm⁻¹
2175

FIG. 9. Correlation functions calculated from I_{VH} of the homeotropically aligned smectic (S) and nematic (N) phase 80CB and the isotropic (I) phase 80CB.

FIG. 10. Correlation functions calculated from I_{VH} of the planar S aligned smectic (S) and nematic (N) phase 80CB and the isotropic (I) phase 80CB.

FIG. 11. Correlation functions calculated from I_{VH} of the planar L aligned smectic (S) and nematic (N) phase 80CB and the isotropic (I) phase 80CB.

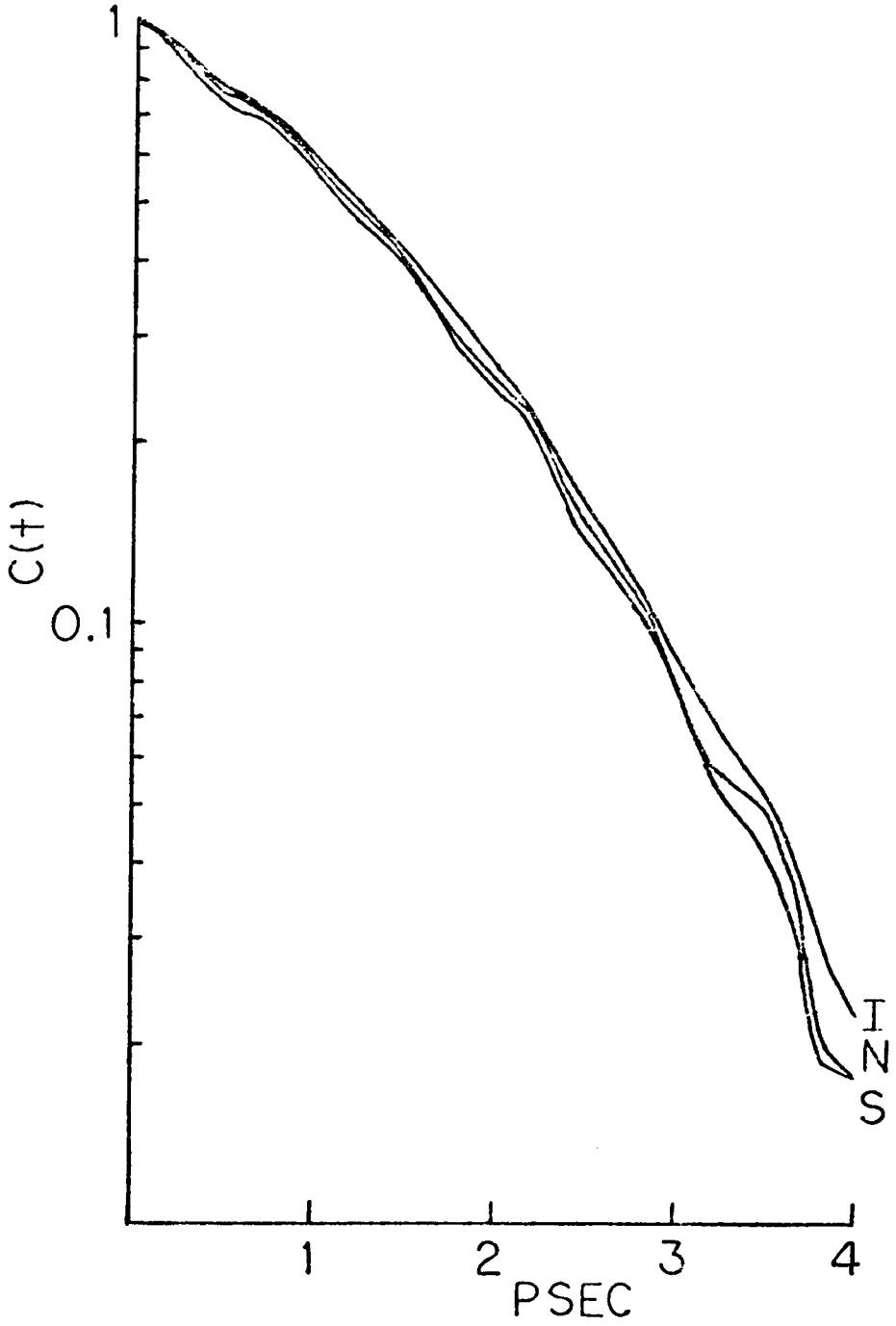
1
C(t)
0.1
I
N
S
1
2
3
4
PSEC

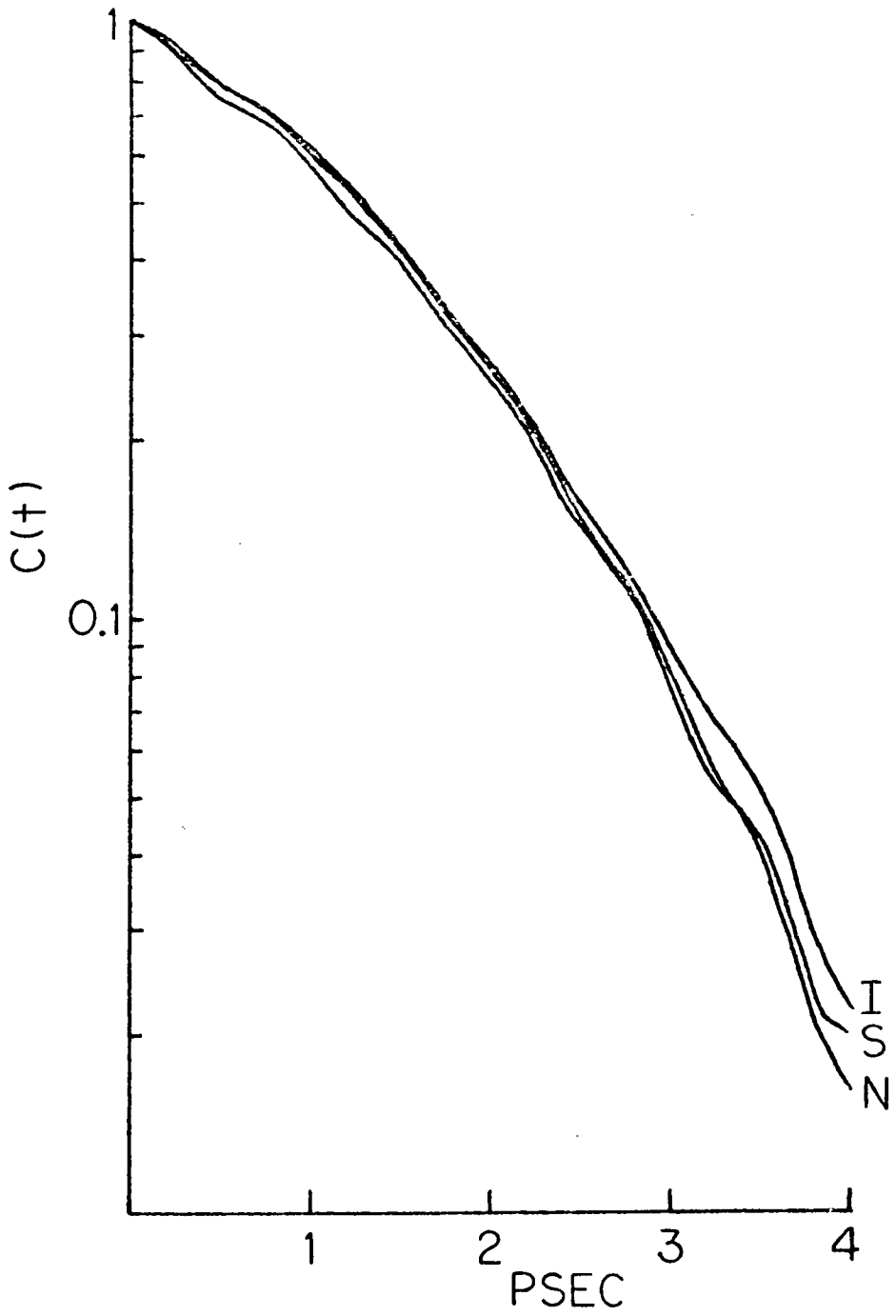
1
0.1
C(+)
1
2
3
4
PSEC
I
S
N

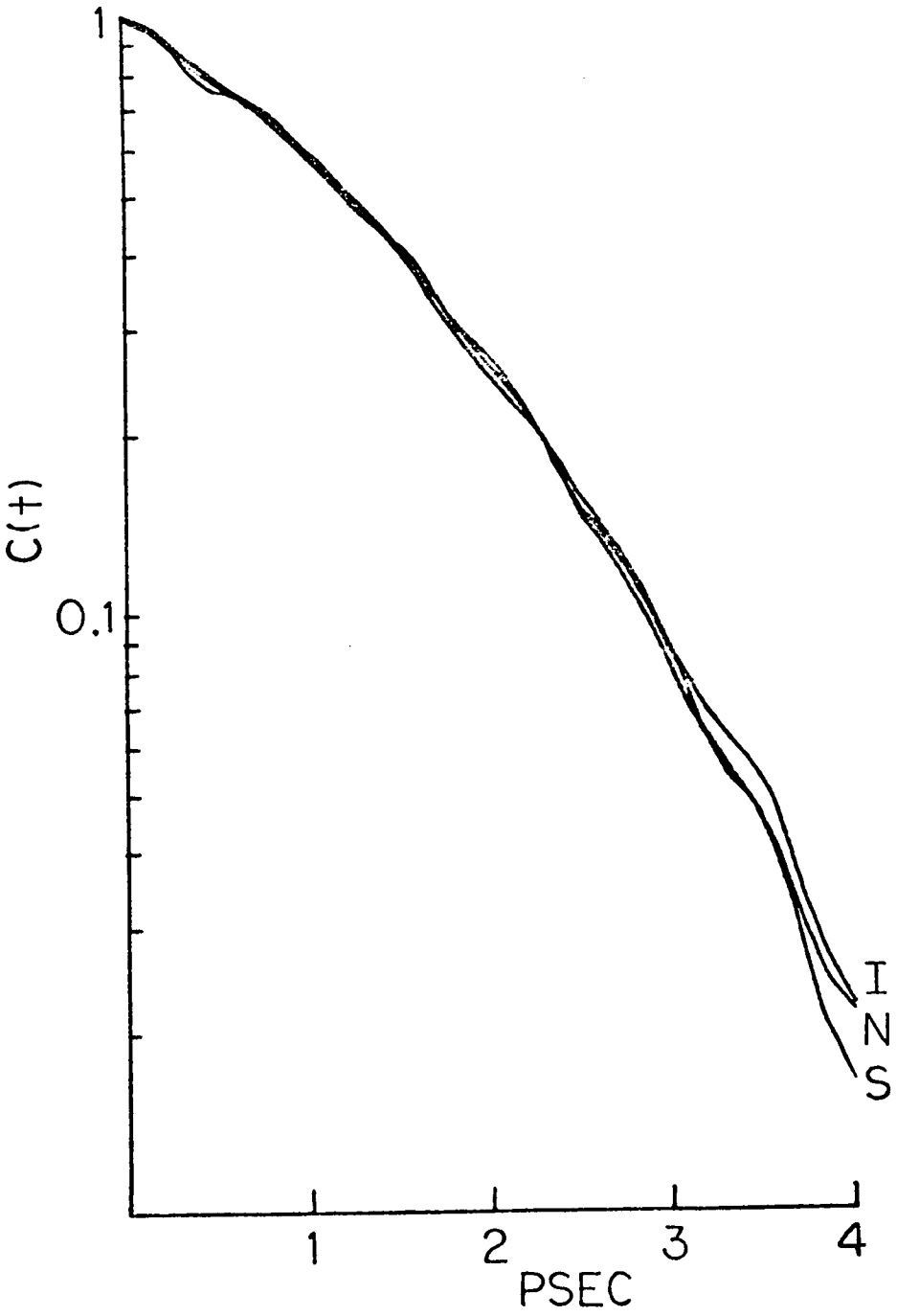
1
0.1
C(t)
1
2
3
4
PSEC
I
N
S

in the next chapter. That discussion will show that it can be concluded that within experimental error, all the correlation functions shown in the figures are identical. Note that not only are the nematic, smectic and isotropic results obtained for a given alignment identical to each other, but they are also identical to the results in the other alignments. This can be seen by comparing each curve to the common curve from the isotropic results. It also can be noticed that not only are the correlation functions showing the same decay rate but also the same form; the shape of the curves are quite similar. No particular significance is attached to the mild oscillations that appear in some of the curves or to the dip in the functions at short times. As will be discussed later, these properties of the curves can be attributed to the computational technique when experimental data of a certain quality are used for the correlation function calculation.

Some preliminary conclusions can be made from the above data. First, however, it should be remembered that since peaks are obtained under the I_{VH} condition, the liquid crystal molecules can not be perfectly aligned so that the molecular axes are coincident with the laboratory axes or coincident within a 90° rotation. The lack of alignment could, of course, result from the dynamic situation of molecular motion. That the correlation functions are all the same yields the preliminary conclusion that if tumbling molecular motion is responsible for the presence of the peaks, then the degree of tumbling is not greatly different in the smectic, nematic and isotropic phases. The lack of coincidence with the laboratory axes could result from a static cause. The mechanical processes that align the molecules could

be imperfect, leading to relatively fixed molecules forming regions with varying alignments or a large region with a continuous deflection of the director. Since the samples all showed the extinction patterns characteristic of well aligned samples, static (or dynamic), misalignment could not have been gross. On the other hand, extinction was not 100%, that is, totally dark images were not obtained, and some misalignment, static or dynamic, must have been present. It must be noted that static misalignment along is not a cause for band broadening; it only leads to the existence of an I_{VH} peak and the degree of misalignment only determines the intensity of the peak. Its presence could complicate the interpretation of the spectroscopic and correlation function results. Similarly, the presence, but not the width, of an I_{VH} peak could also result from the breakdown of the assumption that the $C\equiv N$ stretch is a localized one and could be represented by the tensor of heteronuclear diatomic. That the peaks had a full width at half height of $\sim 9cm^{-1}$ indicates that the I_{VH} peak must have been accompanied by a band broadening mechanism.

Rotational motion, tumbling being a specific type, would be a broadening mechanism. In the gas phase spectra, rotational fine structure, consisting of discrete lines, attend a vibrational line. As the gas becomes more condensed, intermolecular interactions broaden the rotational lines. In liquids, the broadening becomes so complete that a single broad contour surrounding the vibrational center results.[49] A similar situation is expected for liquid crystals because of their fluidity. It was shown in Chapter Two that Raman spectra obtained in the $I_{VH}(I_{YZ})$ configuration are most clearly influenced by the broadening of the rotational lines.

A large contribution to the bandshape due to tumbling motion becomes questionable since the correlation functions are not obviously becoming linear at longer times. Linear correlation functions are expected for random molecular reorientation motion[50, 51, 52] (and the references therein). After a certain period of time, most of the molecules in liquids would have been involved in a number of collisions with their neighbors. The accumulative effect of the collisions would be to reorient the molecules so that the rotational motions appear random. Models of random diffusion, such as Debye's theory[53] would then be appropriate for describing the molecular motion. The models predict a Lorentzian shaped peak in the frequency domain and a correlation function of the form

$$C'(t) = \exp(-Bt)$$

where $B = 2\pi cb$ and b is the half width at half height.[52] Forming the logarithm of both sides of the above equation leads to

$$\ln C'(t) = -Bt.$$

It can clearly be seen that if this logarithm of the correlation function is plotted against linear values of t, the plot would be a straight line. For small[50] and moderately sized[18] molecules, the effect of collisions on orientational motion can be seen through the appearance of a linear correlation function for times less than 1 picosecond. It seems from our results that for a larger molecule, the randomizing effect of collisions is still not manifested in the form of the correlation functions on the 4 picoseconds time scale. It is this fact which suggests that tumbling orientational motion

does not significantly contribute to the bandshape being investigated and is probably not responsible for the observed width of the peak. This conclusion must be very tentative though, since, as was mentioned, not too much weight can be given to the form of the correlation functions at longer times because of the influence of calculation errors.

There are other processes, i.e., the vibrational relaxation of the molecule, that could also lead to the broad bandshape obtained. Clearly then, the peaks must be examined further to determine if their widths, shapes and correlation functions are nevertheless resulting from tumbling motion or are resulting from some other broadening processes.

C. Vibrational Relaxation Correlation Function

The correlation function obtained experimentally from the I_{VH} spectrum (denoted $I_{\perp}$ in Chapter Two) of liquids and isotropic phase mesogens, C_{VH}, was pointed out in Section D, Chapter Two, to be the product of an orientational correlation function and a vibrational relaxation correlation function:

$$C_{VH} = \overline{\langle \mathrm{Tr}\ \beta^{\nu}(o)\ \beta^{\nu}(t) \rangle}\ \overline{\langle Q^{\nu}(o)\ Q^{\nu}(t) \rangle}$$

If the normalized orientational correlation function, $\overline{\langle \mathrm{Tr}\ \beta^{\nu}(o)\ \beta^{\nu}(t) \rangle}$ is a slowly varying function with time, then its value will be very close to 1. In such a case, the experimentally obtained correlation function would be equal to the vibrational relaxation correlation function. The vibrational correlation function, as was pointed out in

Chapter Two, can be obtained by computing the Fourier transform of I_{vib}:

$$\overline{\langle Q^{\nu}(0) Q^{\nu}(t) \rangle}_{vib} = \int_{-\infty}^{\infty} \hat{I}_{vib}(\omega) \exp(-i\omega t)\, d\omega$$

where

$$\hat{I}_{vib}(\omega) \equiv I_{VV}(\omega) - 4/3\, I_{VH}(\omega) \Big/ \int_{-\infty}^{\infty} \left[I_{VV}(\omega) - 4/3\, I_{VH}(\omega) \right] d\omega$$

Comparison of the vibrational correlation function obtained by the above calculation with the experimentally obtained C_{VH} would give a measure of the degree of contribution of the orientational correlation function and the vibrational correlation function to C_{VH}. Such a comparison is shown in Fig. 12. The curve marked C_{vib} is the vibrational correlation function and the curve marked C_{VH} is the one obtained from the I_{VH} spectrum. Within experimental error and computational capability, these curves are equal. (The slight differences and their causes will be discussed in the error chapter.) The equality of these correlation functions indicates very clearly that C_{VH} is a vibrational relaxation correlation function. The orientational correlation function makes an undetectable contribution to C_{VH}. We will speculate on the reasons for this later, after additional data are presented.

There is an additional, complementary way of looking at the contribution of the orientational correlation function to C_{VH}. The normalized correlation function obtained from the normalized I_{VV} spectrum (denoted $I_{\parallel}$ in Chapter Two, Section D) of a liquid or

FIG. 12. The correlation function, C_{VH}, calculated from isotropic phase I_{VH} spectra compared with the vibrational relaxation correlation function, C_{vib}, obtained from isotropic phase I_{VH} and I_{VV} spectra.

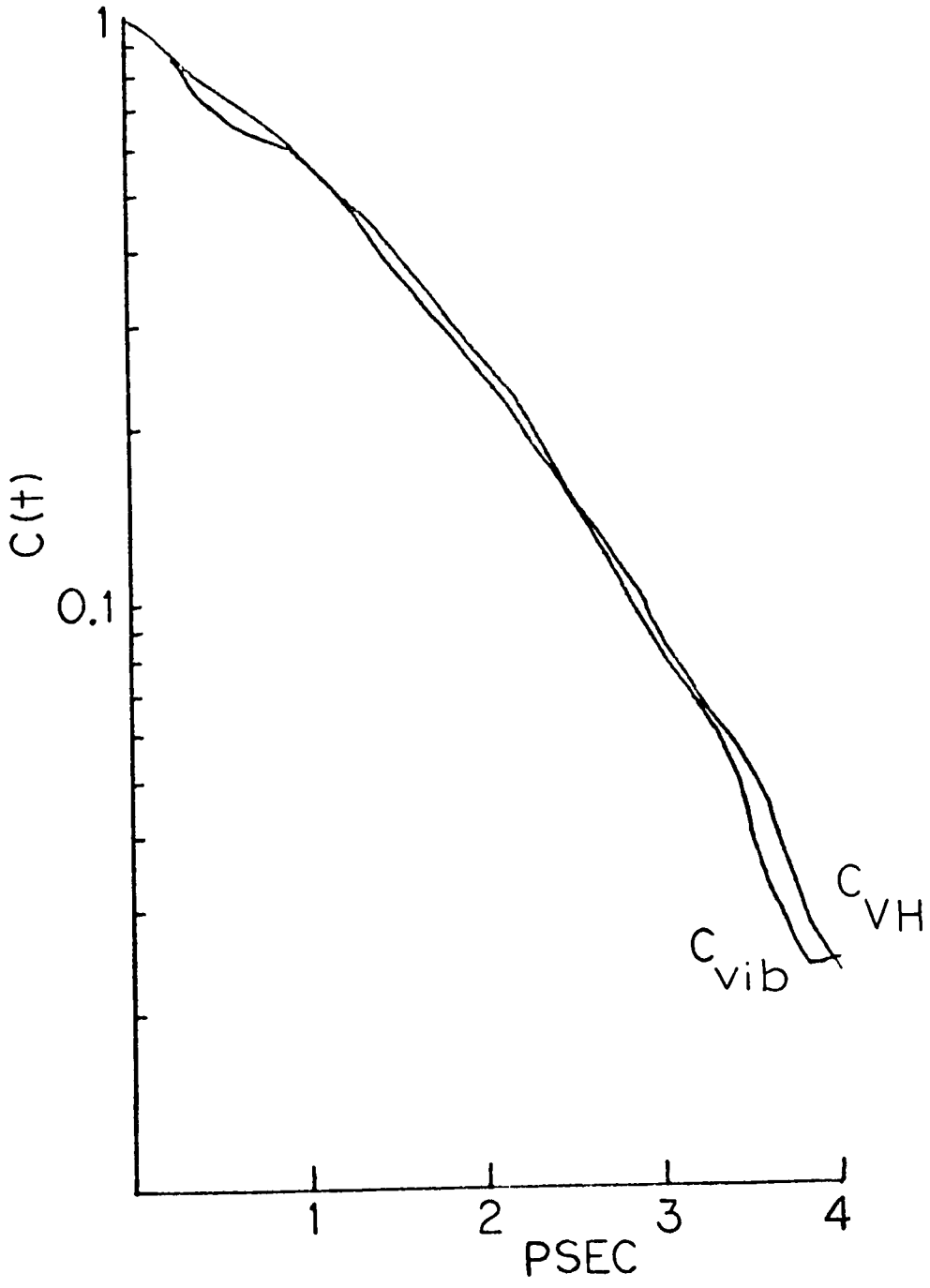
1
0.1
C(t)
1
2
3
4
PSEC
C_{VH}
C_{vib}

isotropic phase mesogen is

$$\frac{\langle a^2 + \frac{2}{15} \mathrm{Tr}\, \beta^{\nu}(0)\beta^{\nu}(t)\rangle \langle Q^{\nu}(0)\, Q^{\nu}(t)\rangle}{\langle a^2 + \frac{2}{15} \mathrm{Tr}\, \beta^{\nu}(0)\beta^{\nu}(0)\rangle \langle Q^{\nu}(0)\, Q^{\nu}(0)\rangle}$$

$$= \frac{\int_{-\infty}^{\infty} I_{VV}(\omega) \exp(-i\omega t)\, d\omega}{\int_{-\infty}^{\infty} I_{VV}(\omega)\, d\omega}$$

If $\mathrm{Tr}\beta^{\nu}(0)\beta^{\nu}(t)$ is slowly varying, in that it equals $\mathrm{Tr}\beta^{\nu}(0)\beta^{\nu}(0)$, then the above equation becomes

$$\frac{\langle Q^{\nu}(0)\, Q^{\nu}(t)\rangle}{\langle Q^{\nu}(0)\, Q^{\nu}(0)\rangle} \equiv \overline{\langle Q^{\nu}(0)\, Q^{\nu}(t)\rangle}$$

$$= \frac{\int_{-\infty}^{\infty} I_{VV}(\omega) \exp(-i\omega t)\, d\omega}{\int_{-\infty}^{\infty} I_{VV}(\omega)\, d\omega}$$

The normalized correlation function obtained from the I_{VH} spectrum is (see Chapter Two)

$$\frac{\langle \mathrm{Tr}\, \beta^{\nu}(0)\beta^{\nu}(t)\rangle \langle Q^{\nu}(0)\, Q^{\nu}(t)\rangle}{\langle \mathrm{Tr}\, \beta^{\nu}(0)\beta^{\nu}(0)\rangle \langle Q^{\nu}(0)\, Q^{\nu}(0)\rangle} = \frac{\int_{-\infty}^{\infty} I_{VH}(\omega) \exp(-i\omega t)\, d\omega}{\int_{-\infty}^{\infty} I_{VH}(\omega)\, d\omega}$$

If once again $\mathrm{Tr}\beta^{\nu}(0)\beta^{\nu}(t)$ is considered to be slowly varying with time, the above equation reduces to

$$\langle \overline{Q^{\nu}(0)\, Q^{\nu}(t)} \rangle = \frac{\int_{-\infty}^{\infty} I_{VH}(\omega) \exp(-i\omega t)\, d\omega}{\int_{-\infty}^{\infty} I_{VH}(\omega)\, d\omega}$$

Thus, it can be seen that if the orientational correlation function makes no contribution to C_{VH} because it varies slowly, then the correlation function calculated from the I_{VV} spectrum, denoted C_{VV}, will be equal to C_{VH}. In Fig. 13 are shown C_{VH} and C_{VV} obtained from one of the sets of data that were used for obtaining C_{vib}. Clearly C_{VH} and C_{VV} are equal.

The implications of the results shown in Figs. 12 and 13 are as follows. The clearest implication is that the correlation function from the I_{VH} spectrum of the isotropic 8OCB is a measure of the vibrational relaxation of the molecule. The term vibrational relaxation is used broadly here to mean any process that is reflected by the decay of $\overline{\langle Q^{\nu}(o) Q^{\nu}(t) \rangle}$. Specific processes will be discussed shortly. That C_{VH} and C_{VV} for the isotropic phase results are equal implies, by their Fourier transform relationship, that the normalized I_{VH} and I_{VV} would be equal both in intensity and bandshape. The unnormalized spectra differ only by a scaling factor. Therefore, it would be expected that the FWHH of the unnormalized I_{VH} peak would equal the FWHH of the unnormalized I_{VV} peak. This was found to be true within experimental error (approximately $\pm$ 0.25 cm^{-1}).

That the correlation functions obtained from the I_{VH} spectra

FIG. 13. The comparison between C_{VH} and C_{VV} obtained from isotropic phase I_{VH} and I_{VV} spectra. Note that these correlation functions have no oscillations because of the greater intensity of the I_{VH} and I_{VV} spectra of the isotropic phase.

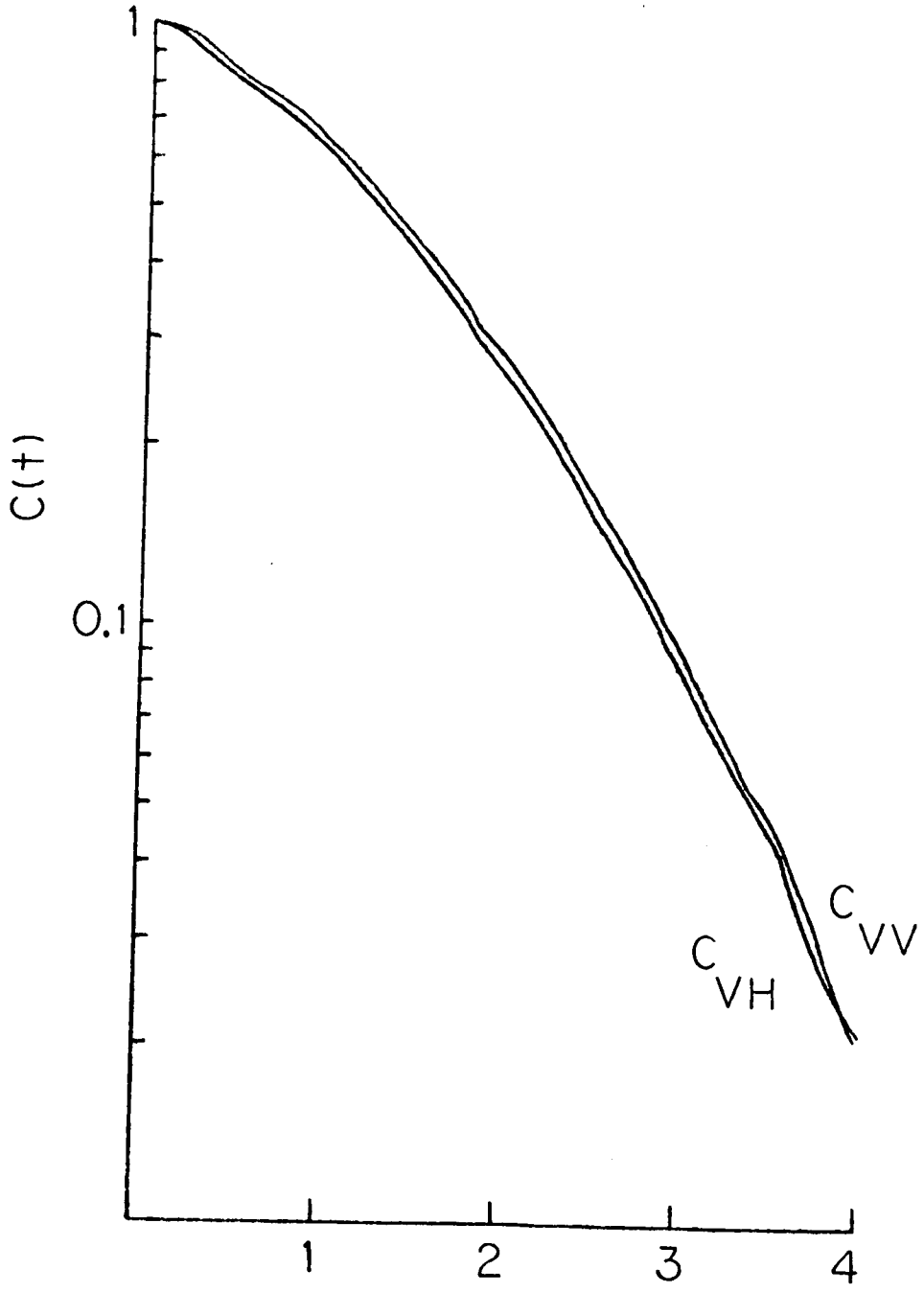
1
0.1
C(τ)
1
2
3
4
C VV
C VH

of the smectic and nematic phase liquid crystal were equal to the one from the isotropic results implies that these correlation functions are also reflective of vibrational relaxation processes. Two other possible situations could lead to this equality of correlation functions, but their influence can be ruled out. First, it is possible that the vibrational relaxation processes are less efficient in the mesomorphic phases. This would lead to a slower decay of the vibrational correlation function. If the orientational motion were more rapid in the mesomorphic phases, leading to a more rapid decay of the orientational correlation function, then the product of the two correlation functions might result in a cancellation of effects; the net correlation function would then be equal to that from the isotropic results. However, it is highly unlikely that more rotational motion would be possible in the more ordered liquid crystal phases. This first possibility seems unlikely. Secondly, it is possible that vibrational relaxation is more rapid in the mesomorphic phases and that rotational motion is slower, leading to a slower decaying orientational correlation function. Then once again the counterbalance of effects in the product of the correlation functions is possible. This is a reasonable possibility from the physical point of view. However, it has just been shown that the C_{VH} is insensitive to the presumably rapid orientational motion in the isotropic phase liquid crystal. Since the orientational correlation function for an isotropic environment is not inherently less sensitive than the one for a less symmetric environment, it is highly unlikely that the correlation function would now be more sensitive to this possible case of slower rotational motion. It can be concluded with some certainty that the correlation functions

obtained from the smectic and nematic phase spectra are vibrational correlation functions. Note that the FWHH for the smectic, nematic and isotropic spectra were all equal within experimental error.

D. Solution Studies

It has just been shown that C_{VH} obtained for the 8OCB in its isotropic and mesomorphic phases reflects vibrational relaxation processes. The question arises as to whether or not this fact results from a unique liquid crystal environment which is maintained in the isotropic phase. It might be expected that when the 8OCB molecules are introduced into the more fluid environment of relatively small molecule solvents that rotational motion would increase. Under such circumstances, the peak would be expected to broaden. The correlation function would then increase in its rate of decay, possibly change in form and not equal C_{vib}. To examine such a possibility, the 8OCB was dissolved, in varying concentrations, in four solvents: benzene, carbon tetrachloride, chloroform and methylthiocyanate.

The correlation functions calculated from the I_{VH} spectra of the benzene and carbon tetrachloride solutions are shown in Fig. 14 and Fig. 15. C_{VH} from the isotropic results is also included. Immediately, it is noticed that the rate of decay decreases with increasing dilution. The change in rate is not quite as large for the CCl_4 solutions as for the C_6H_6 ones. As will be pointed out in the error chapter, these shifts in the average values of the correlation functions far exceed the uncertainty in the average values of the correlation functions that were plotted. That these shifts with dilution are real is further supported

FIG. 14. C_{VH} calculated from spectra of 8OCB dissolved in benzene in mole fractions of 0.51, 0.14 and 0.04. Also included are the C_{VH} from spectra of the isotropic (I) phase and the polycrystalline (cry.) solid.

FIG. 15. C_{VH} calculated from spectra of 8OCB dissolved in carbon tetrachloride in mole fractions of 0.32, 0.12 and 0.03 and also from spectra of the isotropic (I) phase.

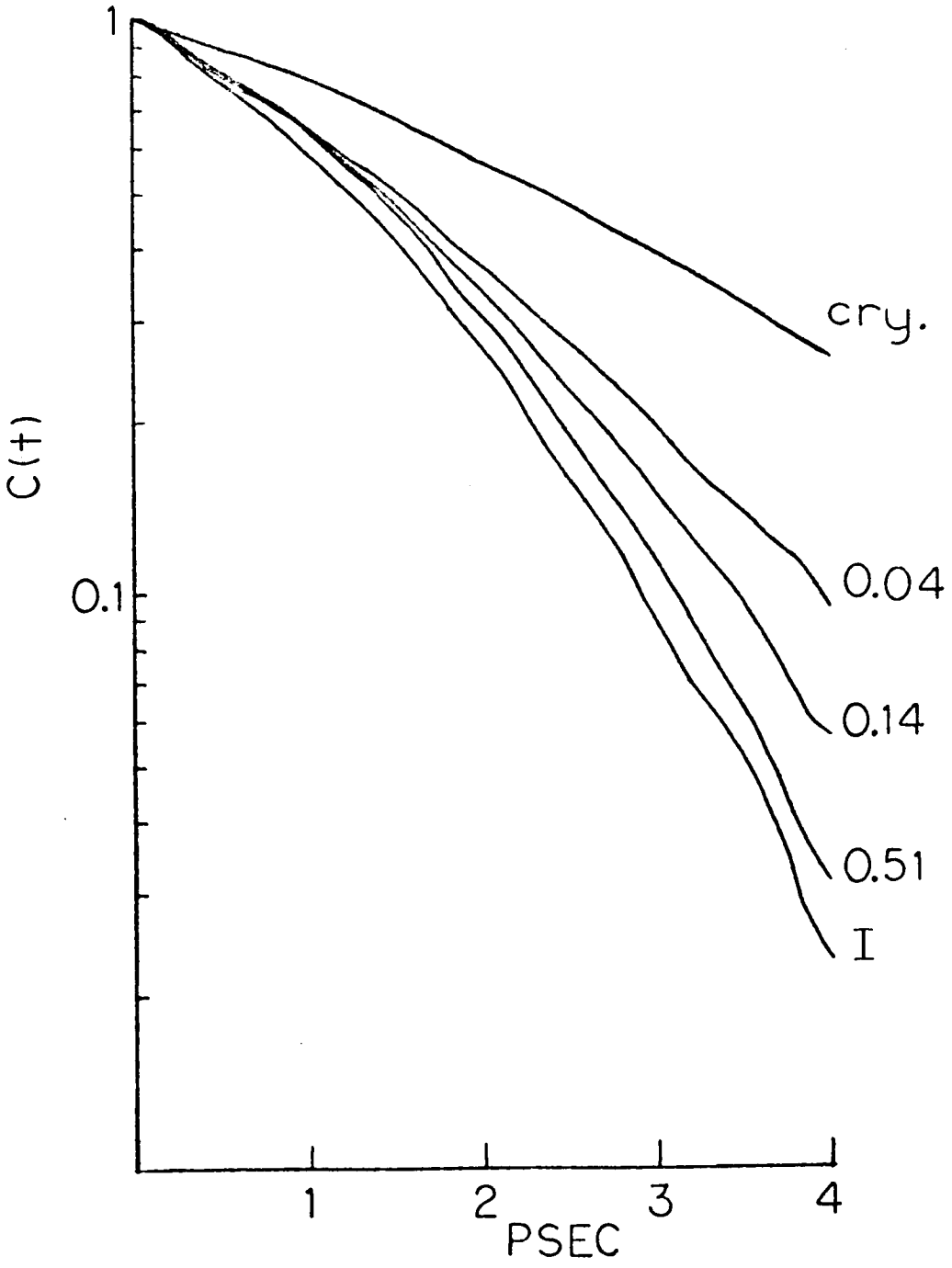
1
0.1
C(t)
cry.
0.04
0.14
0.51
I
1
2
3
4
PSEC

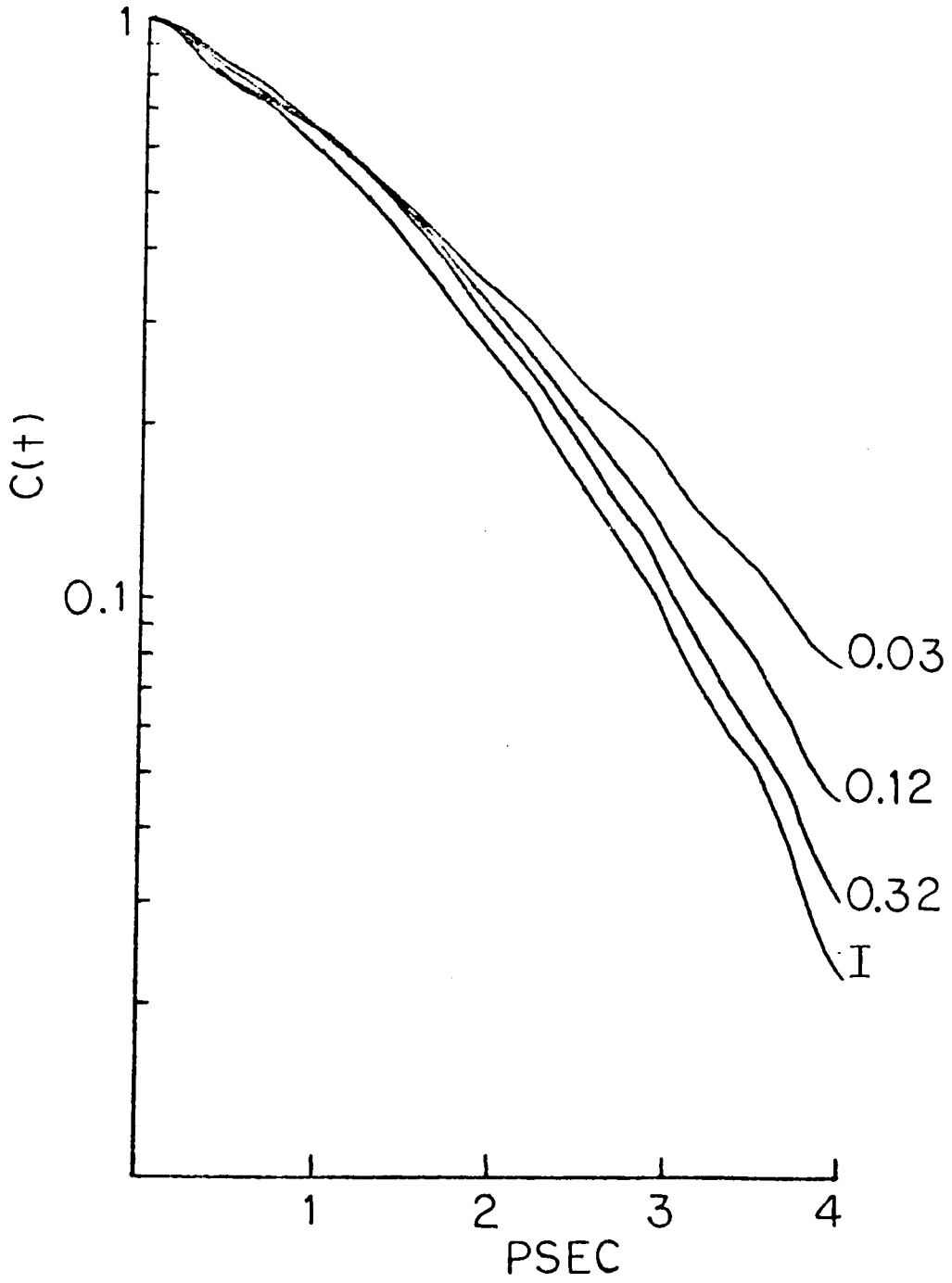
1
0.1
C(t)
0.03
0.12
0.32
I
1
2
3
4
PSEC

by the fact that the FWHH decreases as dilution increases. For example, the 0.51 mole fraction C_6H_6 solution gave a peak with a FWHH of 8.5 cm^{-1}. The 0.04 mole fraction C_6H_6 solution gave a peak with a FWHH of 6.4 cm^{-1}. Also included in Fig. 14 for comparison and future reference, is the correlation function calculated from the spectrum of the polycrystalline solid that had been taken shortly after the sample had solidified. (Samples that were left for at least a day in the solid phase showed a distinct shoulder on the main peak. These crystal spectra will be discussed further at the end of this chapter.) The peak from the solid sample had a FWHH of 4.3 cm^{-1}. Notice that the corresponding correlation function shows the slowest rate of decay. The results from the three different concentrations of solution for each solvent also seem to be equal at the 1 picosecond mark. It is after this time that they gradually separate. Since, as will be discussed in the error chapter, no special significance can be attributed to the dips in the functions between 0-1 picoseconds, the equality of the correlation functions at 1 picosecond suggests that the short time behavior of the molecules in the different concentration solutions is the same.

Another fact about the solution C_{VH} is revealed by attempting to fit each curve in the 2-4 picosecond range with a least squares deviation straight line. In Fig. 16 and Fig. 17 are shown the results of this fit for the solution C_{VH} and the isotropic C_{VH}. Note that the functions are not plotted on a semi logarithmic graph as were the ones shown in Fig. 14 and Fig. 15. In order to calculate the least squares fit, the values of the points defining the correlation functions were first converted to their logarithmic values. The result of this conversion and the least squares straight lines are plotted against linear ordinate and abscissa

FIG. 16. Least squares straight line fit to benzene solution C_{VH}. See explanation on page 112.

FIG. 17. Least squares straight line fit to carbon tetrachloride solution C_{VH}. See explanation on page 112.

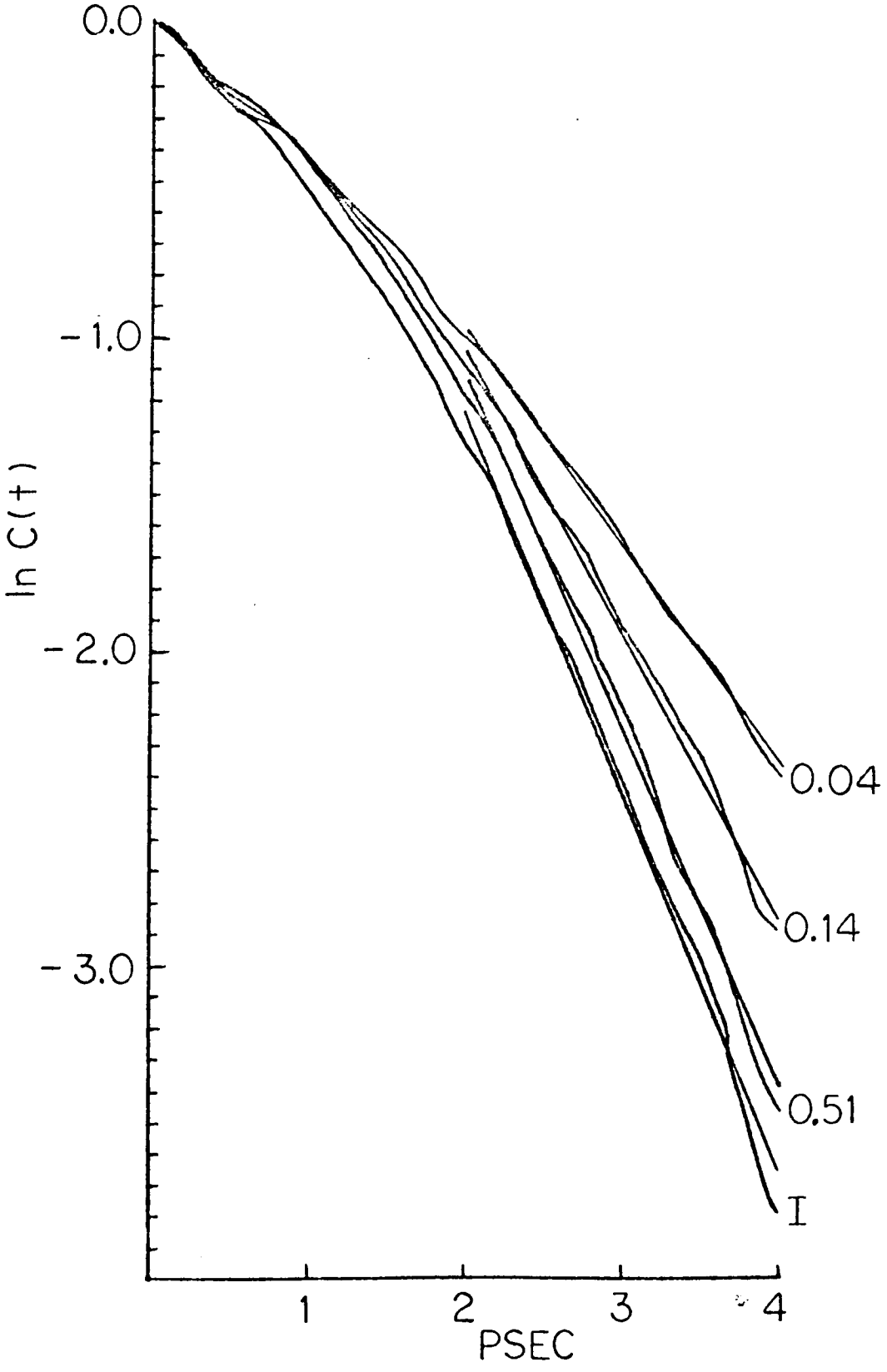
0.0
-1.0
-2.0
-3.0
ln C(t)
1
2
3
4
PSEC
0.04
0.14
0.51
I

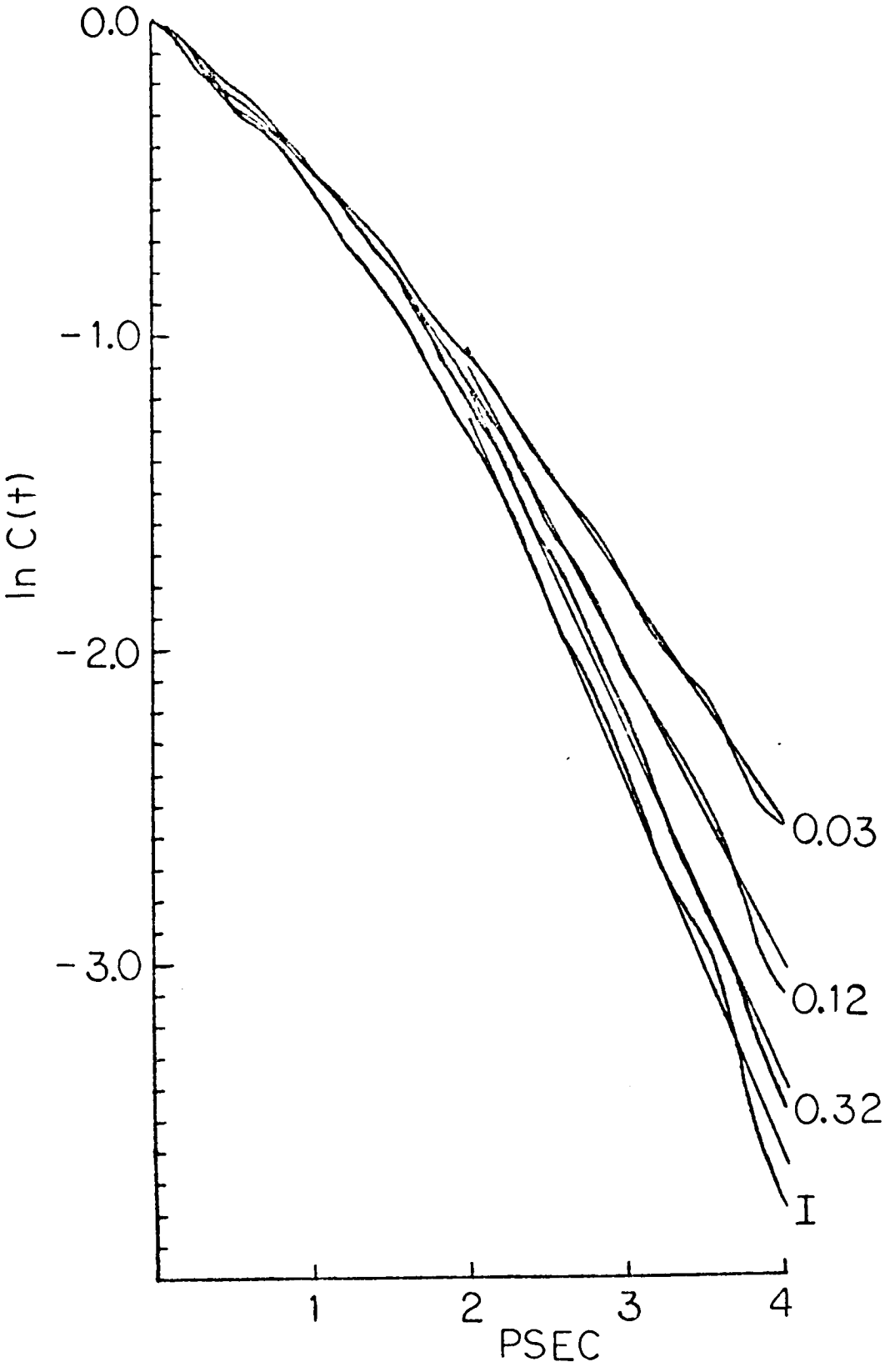
0.0
-1.0
-2.0
-3.0
ln C(t)
0.03
0.12
0.32
I
1
2
3
4
PSEC

scales in Fig. 16 and Fig. 17.

Though the least squares fit appears good for all concentrations of the 8OCB, close examination of the fit to the higher concentration C_{VH} and the isotropic C_{VH} indicates that the fit looks like

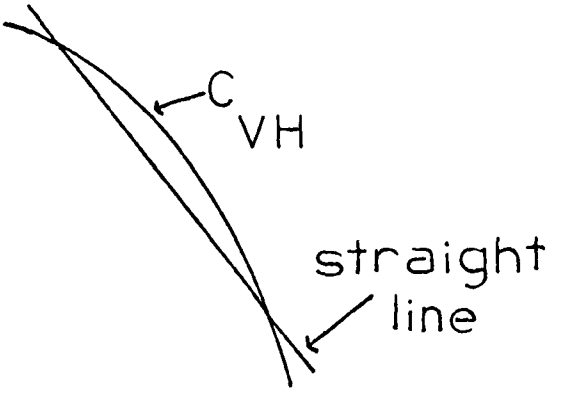

This suggests that the C_{VH} have not become completely linear at these longer times and some curvature is still present. The straight line fit to the 0.04 mole fraction C_6H_6 solution and the 0.03 mole fraction CCl_4 solution is good. The C_{VH} show small positive and negative oscillations around the line suggestive of a strong tendency toward linearity.

It was pointed out earlier in this chapter, that molecular rotational motion interrupted frequently by collisions would lead to linearity in C_{VH} at longer times. Since the dilute solutions afford the 8OCB molecules the most freedom of rotation as well as the most possible collisional contact with the solvent, it is possible that the collision interrupted rotation explanation is an appropriate one to describe these results. To check this hypothesis, spectra were once again taken of the most dilute solutions but I_{VV} as well as I_{VH} was obtained. From spectra in these two configurations, I_{vib} can be calculated, as was described earlier for the isotropic phase results.

From I_{vib}, C_{vib} can be calculated. In Fig. 18 and Fig. 19 are shown comparisons of C_{VH} and C_{vib} for the dilute C_6H_6 and CCl_4 solutions. Once again, it is seen that C_{VH} reflects vibrational relaxation completely. Rotational motion interrupted frequently by collisions can be ruled out as a significant factor in determining the rate of decay and form of the correlation functions. Since the more concentrated solutions are less extreme cases of the effects present in the most dilute solution, it is concluded that they too are dominated by vibrational relaxation.

It seems clear that both the shift in the correlation functions on going from the 100% 80CB to increasingly dilute solutions and the onset of linearity in the most dilute solutions must be explained in terms of vibrational relaxation processes. Until this point, such processes have been essentially undefined. It is now necessary to go into greater detail about the processes that would lead to changes in $\langle Q^{\nu}(0)\ Q^{\nu}(t)\rangle$ before attempting to explain the observed correlation functions.

Three vibrational relaxation processes are important in liquids:[54] (1) dipole - dipole induced transitions; (2) resonance vibrational energy transfer; (3) vibrational dephasing. In dipole - dipole induced transitions, the excited vibrator is in an electric field created by the transition dipoles of its neighbors. The field can induce transitions in the oscillator so that it drops to a less excited vibrational state. The energy difference between states is transferred to the rotational and translational degrees of freedom of the neighboring molecules. This dissipative process shortens the vibrational lifetime and thus leads to the relaxation of the initial vibrational conditions. Valiev has des-

FIG. 18. Comparison of C_{VH} and C_{vib} obtained from spectra of the 0.04 mole fraction solution of 8OCB in benzene.

FIG. 19. Comparison of C_{VH} and C_{vib} obtained from spectra of the 0.03 mole fraction solution of 8OCB in carbon tetrachloride.

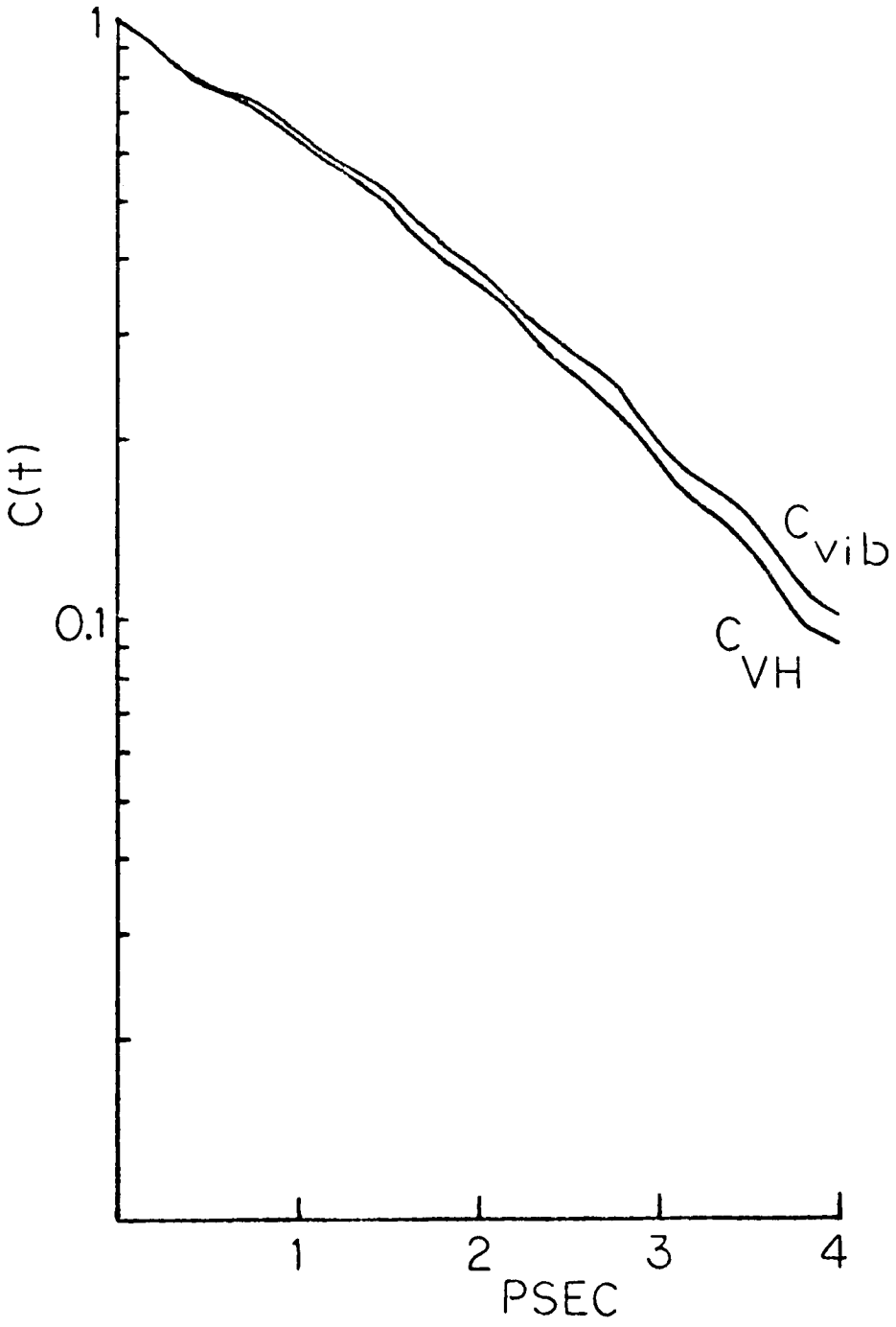
1
0.1
C(t)
C_{vib}
C_{VH}
1
2
3
4
PSEC

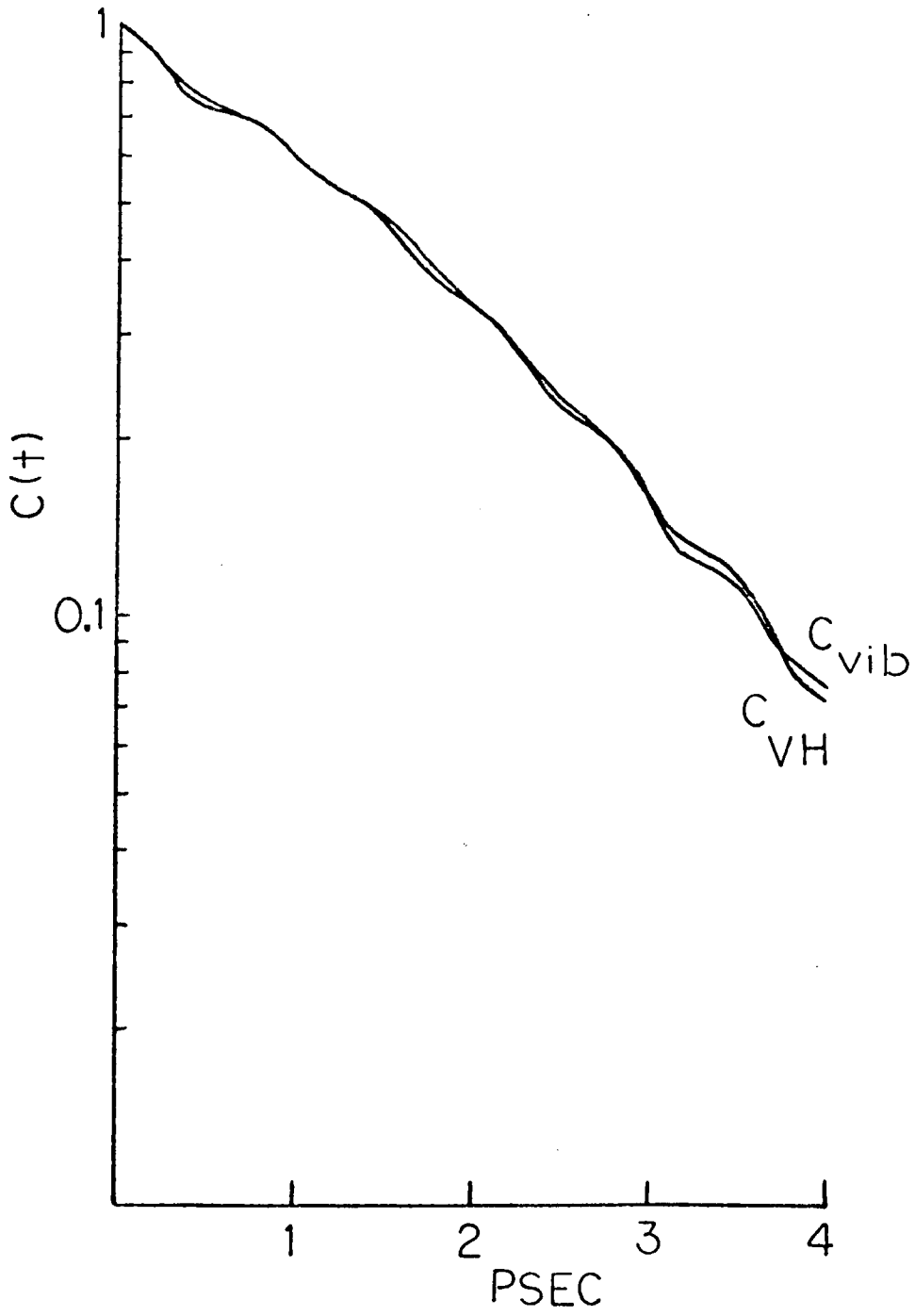
1
0.1
C(+)
C vib
C VH
1
2
3
4
PSEC

cribed quantitatively the broadening effect of such a shortened lifetime.[55] (Note that previously given arguments and examples have shown that the broadening of a peak leads to a more rapid decay of the correlation function.) Tokuhiro and Rothschild have made the reasonable argument that the dissipation of vibrational energy to the liquid "lattice" is in general inefficient because the high frequencies of vibration match poorly with the lower frequencies of rotational and translational motion.[56] Rothschild, et.al[39] have used Valiev's formulation with a small modification to calculate the dissipative broadening of the vibrational bands of chloroform. They have been able to quantitatively determine that the dissipative mechanism makes an insignificant contribution to the band widths. Following their lines of reasoning, we rule out the dissipation of vibrational energy to the surrounding molecules as an explanation for our observed results.

Resonance vibrational energy transfer describes the situation in which an excited vibrator transfers its vibrational quantum to the same mode of an unexcited neighboring molecule. Consequently, the excited molecule returns to the ground vibrational state and the neighboring molecule ends up in the excited vibrational state. The intermolecular potential responsible for this transfer can be described as due to the dipolar nature of the neighbors[55] or to a repulsive type potential.[56] This type of vibrational relaxation also leads to a shortened vibrational lifetime. A shortening of the lifetime leads to a broadening of the peak.[57] Broadening of the peak will be reflected in a change in the correlation function. Rothschild has asserted [54] (and references therein) that resonance vibrational energy transfer also makes a relatively small contribution to band

broadening. For the case of chloroform, Rothschild, et.al[39] calculated the contribution of this mechanism to the vibrational band width and found it to be small. Experimental evidence will be given that strongly suggests that in the case of our solutions, resonance vibrational energy transfer is probably not important.

The vibrational dephasing mechanism can be understood as a recent extension of some older ideas. One explanation[57] for the lineshape due to a radiating ion in a crystal is that different sets of ions are affected by different crystal fields which result from microscopic distortions of the crystal structure. The change from the ideal symmetric environment perturbs the energy levels of the radiator and the emitted light is shifted slightly from the frequency the radiator would emit in the perfect environment. A broad Gaussian shaped band results which can be thought of as being composed of a number of overlapping vibrational peaks. The same concept has been used to explain the broad Raman lineshape of the OH stretching vibration in water.[58] It was argued that each water molecule sees a different instantaneous local field and the resulting band is a superposition of the peaks from many of such molecules. Bratos, et.al.[59] recently quantified these ideas for liquids by formulating expressions for the coupling of a radiating oscillator with the stochastic potential due to the liquid environment. Bratos considered only the case of the stochastic potential being constant during the period of vibration. Then the oscillator appears to be located in an amorphous solid.[60] Rothschild, building on the work of Bratos, et.al., and Kubo,[61] generalized the concept of dephasing to include the effect of changes in the environment that take place rapidly on the time scale of a molecular vibration.[54]

Rothschild established a criterion for determining when the effects of fast and slow variations of the environment are important, namely

$$\left\langle \{\omega_1(0)\}^2 \right\rangle^{1/2} \tau_c \gtrless 1$$

where $\omega_1(0)$ is the instantaneous frequency displacement due to the environment at time = 0 and τ_c is the correlation time that measures the speed of modulation of the vibration by the environment. When the above product is greater than 1, slow modulation is in effect. This means that the instantaneous local fields exist long enough to significantly perturb the energy levels of the vibrators. The perturbation leads to a distribution of vibrational frequencies; the band becomes broader. Rothschild shows that, for such a case, the vibrational correlation function shape will be Gaussian.

When the product is <1 fast modulation of the instantaneous frequency takes place. The environment is changing very rapidly on the time scale of the molecular vibration. The molecular interaction is in form of collisions. For such a case, the perturbations due to different local environments do not last long enough to significantly change the vibrational frequency. The local environments average out. As a result, the lineshape shrinks. This has been called "motional narrowing".[61] Rothschild shows that in this case the vibrational lineshape is Lorentzian and the vibrational correlation function is exponential.

It seems obvious that for short enough times, any liquid would approach the "rigid lattice" condition of slow modulation. For longer times, it is expected that the effect of collisions would show up and

the effects of fast modulation would be obvious. For correlation functions, it is then predicted that for some short time range the correlation function will show the curvature characteristic of a Gaussian shape. For longer times it is predicted that the logarithm of the vibrational correlation function will show the linear form characteristic of the exponential that results from the Fourier transform of a Lorentzian bandshape.

The term "vibrational dephasing" though commonly used to describe the above processes is not clearly defined in the literature. In view of the physical picture presented above, we speculate on the meaning of this term. Consider the simple case of a classical one dimensional harmonic oscillation. Its displacement in the x direction is[62]

$$x = A \cos (\omega t+\delta),$$

where A is the amplitude of vibration, ω the angular frequency, t is the time and δ the phase constant. The phase constant takes into account the starting position on the cosine curve of the oscillator. Suppose now that the frequency is suddenly changed so that

$$x = A \cos ((\omega+\omega_1) t+\delta) = A \cos (\omega t + (\delta+\omega_1 t)$$

For a given time t the x displacement will be on a different part of the cosine curve than it was originally. As the last equality shows, it is as if the phase constant has changed. There is thus, a loss of phase autocorrelation;[54] the molecule gets out of phase with itself. Note, that Bratos, et.al., have argued[60] that the dephasing time reflective of the loss of phase autocorrelation measured by Raman spectro-

scopy is the same as the dephasing time reflective of the loss of phase correlation between oscillators as measured by picosecond stimulated Raman techniques.[63] It should be noted that this dephasing time is not reflective of the vibrational lifetime.

It is in the context of vibrational dephasing that our correlation function results will be discussed. Before doing so though, the correlation function results from solutions of the 8OCB in $CHCl_3$ and CH_3SCN will be presented. In Fig. 20 are shown the C_{VH} calculated from the cyano stretching vibration of the 8OCB dissolved in three concentrations of chloroform. The C_{VH} from the isotropic phase is included for comparison. The correlation functions all fall very close together. (Note that experimental conditions were such that for the weak peak from the 0.02 mole fraction solution, noisy spectra were obtained. As will be pointed out in the following chapter on errors, under such conditions no special significance should be given to the oscillations seen and the slight increase in decay rate of the correlation function.) They do not show the marked change in decay rate with dilution that the C_6H_6 and CCl_4 solution results showed. In order to check if the presence of increased rotational motion is contributing to the rapid decay in the 0.02 mole fraction solution, C_{vib} was calculated. The comparison between C_{vib} and C_{VH} for the 0.02 mole fraction solution is shown in Fig. 21. Note that C_{VH} is equal to C_{vib}. It clearly is a vibrational relaxation correlation function. Since the C_{VH} of the 8OCB in this polar solvent are close to each other and to the C_{VH} from the isotropic phase 8OCB, it is suggested that dipole interaction between the cyano group of the 8OCB and the cyano groups of other 8OCB molecules or the dipolar $CHCl_3$ molecules is important in determining the rate of decay and form of

FIG. 20. C_{VH} calculated from spectra of 8OCB dissolved in chloroform in mole fractions of 0.31, 0.16 and 0.02 and also from spectra of the isotropic (I) phase.

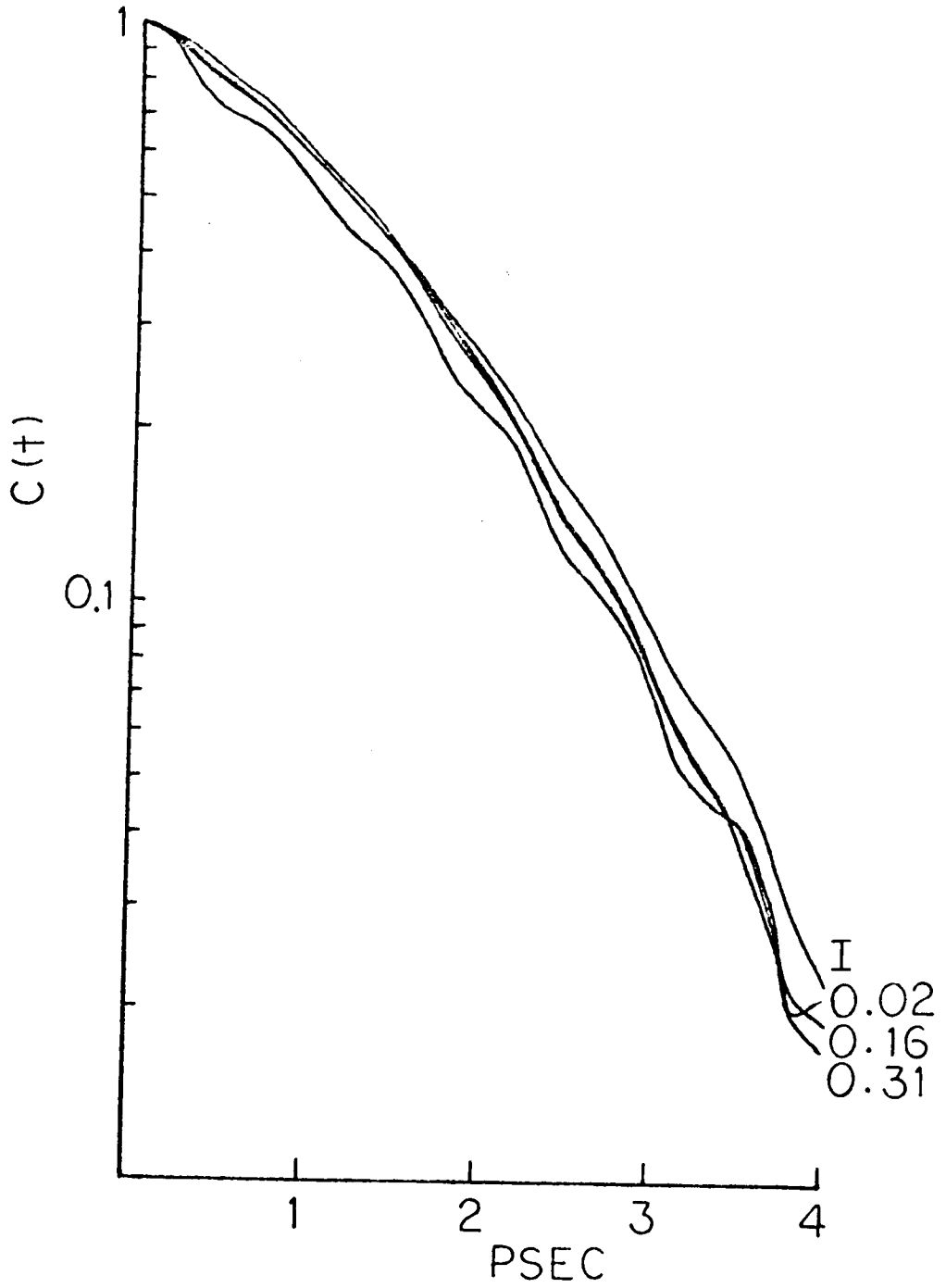
1
C(+)
0.1
I
0.02
0.16
0.31
1
2
3
4
PSEC

FIG. 21. Comparison of C_{VH} and C_{vib} obtained from spectra of the 0.02 mole fraction solution of 8OCB in chloroform.

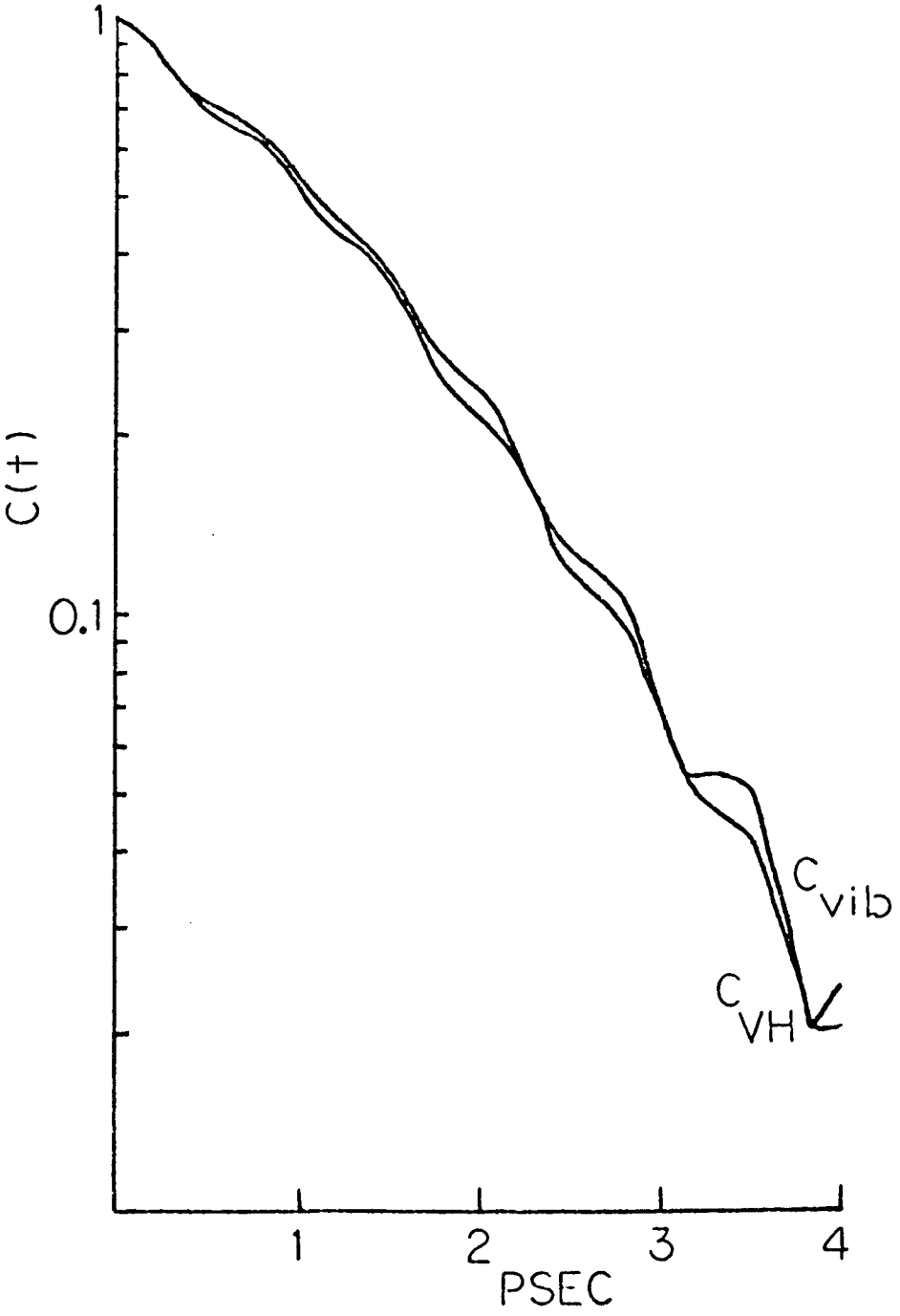
1
0.1
C(t)
1
2
3
4
PSEC
C vib
C VH

C_{VH} as well as its dominance by vibrational relaxation.

The correlation functions calculated from solutions of the 8OCB in CH_3SCN are shown in Fig. 22 with C_{VH} from the isotropic 8OCB. Here too the correlation functions are all about the same. A note about the method of calculating these correlation functions should be included since the cyano stretching band of the solvent falls roughly near that of the 8OCB. The cyano stretching band of the solvent occurs at approximately $2155cm^{-1}$ and that of the 8OCB at approximately $2225cm^{-1}$. For the 0.28 mole fraction solution the intensity of the solvent peak was quite weak and there was little interference with the 8OCB peak. For the more dilute solutions, the solvent peak was of significant intensity. The low frequency baseline region of the 8OCB peak was obviously increased in intensity by a contribution from the high frequency wing of the solvent peak. Examination of the low frequency side of the solvent peak indicated over what range the peak wings extended before meeting the baseline.

The solvent peak was assumed to be symmetric. By examining the range on the high frequency side of the solvent peak that corresponded to the range of importance of the wings on the low frequency side, it was determined that the solvent wings would only perturb the wings of the 8OCB peak. The peak center of the cyano stretch in the 8OCB fell far enough away that it was expected that its FWHH would be unaffected by the wings of the solvent peak. Therefore, for all the solution spectra, the high frequency side of the 8OCB peak was folded about the peak maximum to give a symmetric cyano stretching peak. The resultant peak was examined to make sure the FWHH was the same as before folding; this procedure rules out a spurious maximum causing a change in the FWHH, with the consequent effect on the correlation function.

FIG. 22. C_{VH} calculated from spectra of 8OCB dissolved in methyl thiocyanate in mole fractions of 0.28, 0.08 and 0.02 and also from spectra of the isotropic (I) phase.

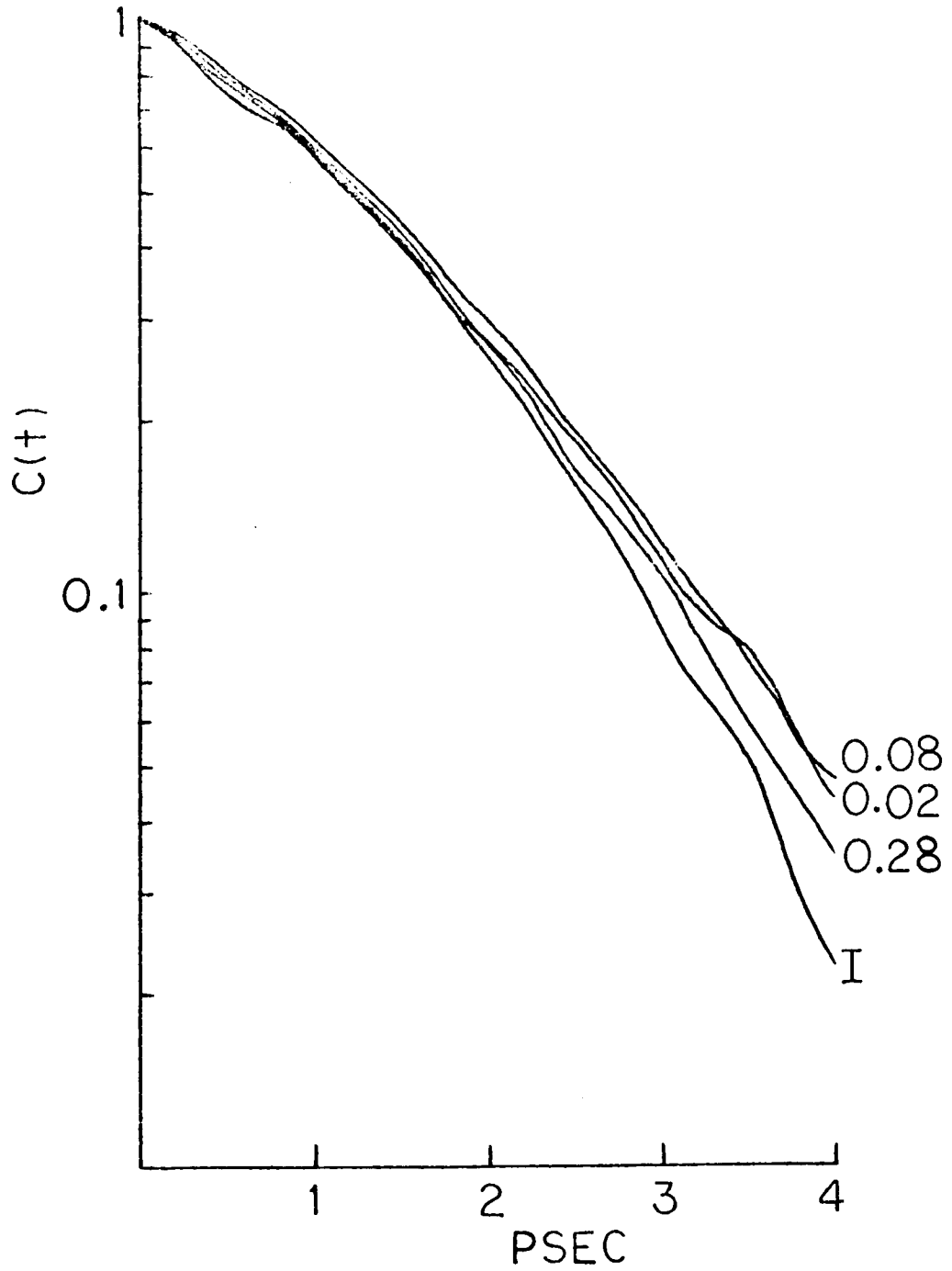
1
C(+)
0.1
0.08
0.02
0.28
I
1
2
3
4
PSEC

The correlation functions calculated from such peaks are interesting for two reasons. First, they seem to confirm the $CHCl_3$ results on the importance of dipole interactions in determining the C_{VH} since the CH_3SCN is a dipolar molecule. Secondly, they provide an argument for ruling out the importance of resonance vibrational energy transfer. Resonance vibrational energy transfer involves the transfer of a quantum of vibrational energy to the same normal mode in a neighboring molecule. It was possible in all the solvents previously discussed that the 8OCB formed clusters in solution. In such clusters resonance vibrational energy transfer could have been taking place, since the immediate neighbors were all 8OCB molecules with the same available vibrational frequency. In CH_3SCN, clusters would be less likely to exist since there is no reason that the cyano groups of the 8OCB would preferably lock together, through dipole attraction, with other 8OCB cyano groups rather than with those of the solvent. (It is possible that clusters might exist through interactions other than those involving the cyano groups of the 8OCB, but it is hard to imagine what type of interactions would be strong enough to resist solvation.) Once 8OCB molecules were completely solvated, resonance energy transfer would not be possible. The difference in vibrational frequency between the 8OCB cyano stretch and the solvent's is $70cm^{-1}$. In work on benzene where resonance vibrational energy transfer was important between modes of near frequency coincidence, a range of $30cm^{-1}$ was found to be a reasonable range where such transfer was still important.[64] The $70cm^{-1}$ difference in the present case would rule out resonance transfer. If resonance transfer was no longer important in the CH_3SCN solutions, a narrowing of the peak FWHH would

be seen, with increased narrowing with increased dilution. This would lead to a decreased rate of decay of the correlation function. No such change in the correlation functions is seen with changes in concentration, within the approximation of folding the high frequency side of the peak. (Note that though there is some decrease in decay of the C_{VH} at longer times from the solution results, this is felt to probably not be significant because of the uncertainty in the values at these times.) Therefore, resonance vibrational energy transfer can be ruled out as an important vibrational relaxation band broadening mechanisms in our experiments.

E. Conclusions

Vibrational dephasing offers a detailed framework in which to explain our experimentally obtained correlation functions. The decrease in decay of the correlation functions seen in C_6H_6 and CCl_4 solution results is consistent with motional narrowing of the Raman band. In these solutions, the 8OCB molecules are surrounded by rapidly changing environments, i.e., fast modulation. Perturbation effects are brief; the peak reflects a narrow range of frequencies. The onset of linearity in the dilute C_6H_6 and CCl_4 solutions is consistent with the prediction of the dephasing formulation that collisions would lead to a Lorentzian bandshape. In these dilute solutions, collisions between the 8OCB and the solvent molecules are more frequent. The effects of the collisions become obvious sooner and on the time scale examined become more apparent. This implies that were it possible to examine the correlation functions at longer times than 4 picoseconds, the

correlation functions from the more concentrated solutions would become linear as well. The equality of the correlation function from the C_6H_6 and CCl_4 solution spectra at 1 picosecond suggests the time range in which slow modulation, the rigid lattice approximation, is important. In the 0-1 picosecond range the environments due to the C_6H_6 and CCl_4 solvent molecules are essentially static and the same at each concentration. These rigid lattice environments of the solutions are probably different from the rigid lattice environment of the isotropic 8OCB since the three C_{VH} from each solvent are not equal to the C_{VH} from the isotropic 8OCB at the 1 picosecond mark. On the other hand, the C_{VH} from 8OCB in $CHCl_3$ and CH_3SCN approximately match the C_{VH} from the isotropic 8OCB at 1 picosecond suggesting that in these solutions the rigid lattice is roughly the same as that in the isotropic 8OCB.

That the decay of the isotropic C_{VH} is more rapid than the decay of the C_{VH} from the C_6H_6 and CCl_4 solutions, strongly suggests the presence of many significant local structures in this phase probably caused by the dipolar nature of the cyano group. These results represent a case of slow modulation in which different perturbations of the vibrator frequency are long lasting. The breadth of the band reflects these perturbations. These results also suggest the presence of some degree of order in the isotropic phase. It can also be concluded that the smectic and nematic phases of the liquid crystal have many regions of different local order caused by the cyano group. The correlation functions obtained from these mesomorphic phases showed the same decay rate and form as the C_{VH} from the isotropic phase results. This conclusion is also reasonable in view of the intermolecular forces that

must be present for maintaining the order of these phases and in view of the fluid mobility of the molecules. Many ordered structures differing slightly because of molecular motion are not unreasonable. However, it appears that changes in the local order due to molecular motion take place on a longer scale than 4 picoseconds; i.e., they represent slow modulation. It was mentioned earlier in this chapter that the presence of an I_{VH} peak in the liquid crystal spectrum might be due to the static misalignment of the molecules. Such a static misalignment would lead to band broadening if in the slightly different alignments the local environments were different. In the present context, it would be a case of slow modulation.

The C_{VH} obtained from the polar solvents $CHCl_3$ and CH_3SCN were very similar in decay rate and form to those from the isotropic 8OCB. This suggests that local structures were present in these solutions. Since little change was observed on going to the most dilute solutions, it appears that the solvent molecules are involved in the make up of the local structures. Since the significant difference between these solvent molecules and C_6H_6 and CCl_4 is the presence of a permanent dipole moment, it seems reasonable to suggest that dipole interactions are important in slow modulation of the vibration frequency. However, there is both evidence from the literature[18] and our laboratory that other factors are also important. For example, Rothschild finds no change in the correlation functions when he compares the results from a neat benzonitrile sample and 0.25 and 0.17 mole fraction solutions of benzonitrile in CCl_4.[18] Since benzonitrile is similar to the 8OCB molecule studied and CCl_4 is one of the solvents that lead to large changes in our correlation functions, his results are surprising. On the other hand,

the spectrum of a dilute solution of the 8OCB in the polar solvent acetone, taken in our laboratory, showed the motional narrowing of the peak seen with non polar solvents. Rothschild has concluded, based on theoretical considerations, that the shapes of the molecules determine the speed of the frequency modulation processes. An extensive examination of the 8OCB in solvents of different polarity and molecular shapes would have to be done before any firm conclusions about the connection between local structure and the nature of the solvent could be made.

It was shown earlier that C_{VH} obtained from all the spectra were vibrational correlation functions. We suggest that the reason that orientational motion does not influence C_{VH} is simply because rotational motion for the large 8OCB molecule is very slow. On the time scale examined, 0-4 picoseconds, the 8OCB molecules have reoriented through only a small angle. The anisotropic tensor elements are changed very slightly and the orientational correlation function involving them appears to have the value 1. Support for this conclusion is derived from a similar study on quinoline.[65] In that study, dielectric and NMR relaxation studies showing that rotational reorientation was insignificant during the first 5-10 picoseconds were confirmed by the correlation function results. The orientational correlation function from the infrared spectrum was seen to equal 1. When quinoline was dissolved in a 0.09 mole fraction solution of CS_2, the same type of decrease in decay rate that was observed for our C_6H_6 and CCl_4 solutions was seen. Vibrational dephasing was offered as the explanation of these results.[54, 65]

Returning now to the case of the solid 8OCB, the I_{VH} spectrum

of the sample taken just after cooling is shown in Fig. 23. The spectrum of the solid taken after the sample has remained in the solid phase for a few days is shown in Fig. 24. In the later spectrum, a distinct less intense peak is seen on the low frequency side of the intense peak. Note that the frequency of the peak maximum in Fig. 23 falls roughly between the frequencies of the maximum of the two peaks in Fig. 24. In Fig. 25 are shown the correlation functions calculated from the spectra. The C_{VH} from the recently crystalized sample decays much more slowly than the older sample. Though a straight line can be fit nicely through the curve in the 2-5 picosecond range, the C_{VH} from the recently cooled 80CB seems to have some curvature to it in this time range. It has been suggested that for crystals, the uniform environment and the increased rate of collisions due to the high density of the phase would lead to a situation analogous with motional narrowing in the liquid.[54, 65] However, it is not clear if a Lorentzian bandshape is expected for the solid. Therefore, it is not clear if a straight line would be expected at longer times on a semi-logarithmic plot. Five models have been suggested for the smectic phase of this liquid crystal.[66] These are pictured in Fig. 26. It is suggested that soon after cooling, the crystal exists in a densely packed state of one of these structures. Collisions are frequent and an average uniform environment leads to a narrow peak.

The double curvature and more rapid decay of C_{VH} from the aged sample suggests the following. With time, the densely packed structure reorders to a more fixed, less densely packed regular crystalline structure. Within this structure there are two conformational possibilities analogous to I and II (or any other combination) in Fig. 26. One of

FIG. 23. I_{VH} spectrum of polycrystalline solid 80CB just after cooling. (J-Y instrument, see comment on page 158.)

FIG. 24. I_{VH} spectrum of polycrystalline solid 80CB after the sample was in the solid phase for a few days. (J-Y)

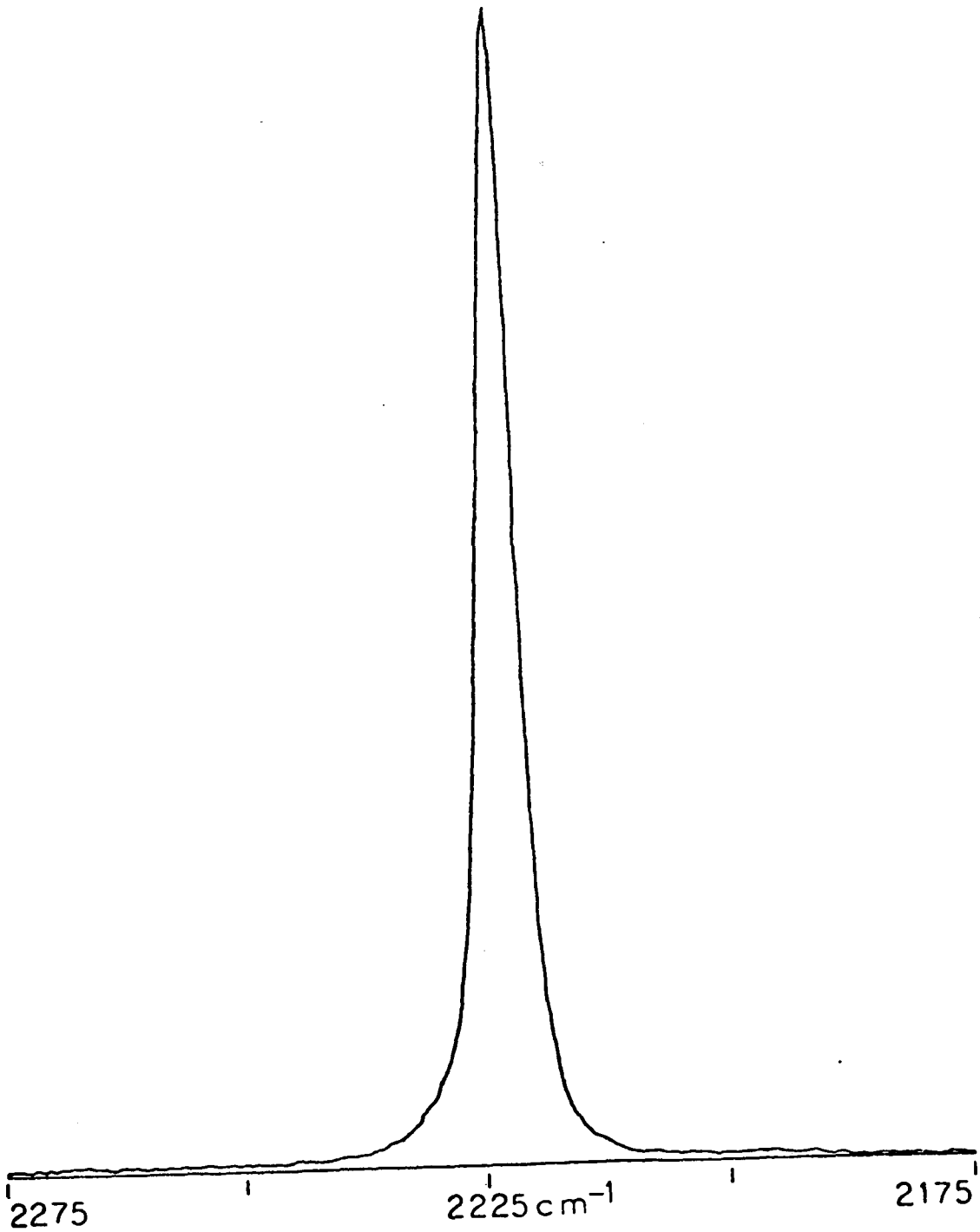
2275
2225 cm⁻¹
2175

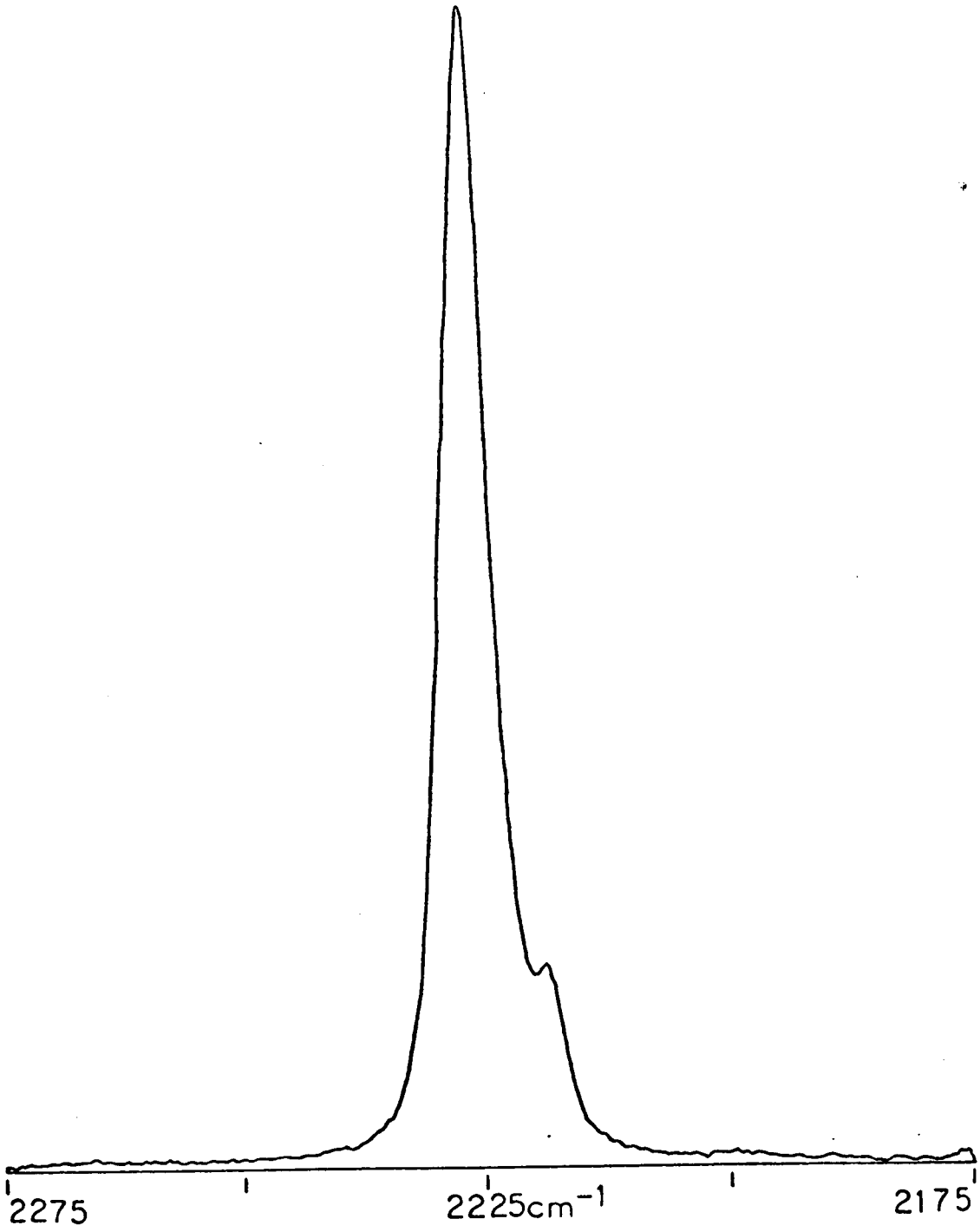
2275
2225cm⁻¹
2175

FIG. 25. C_{VH} obtained from spectra of the polycrystalline solid 8OCB just after cooling, upper curve, and from spectra of the 8OCB that had been a solid for a few days, lower curve.

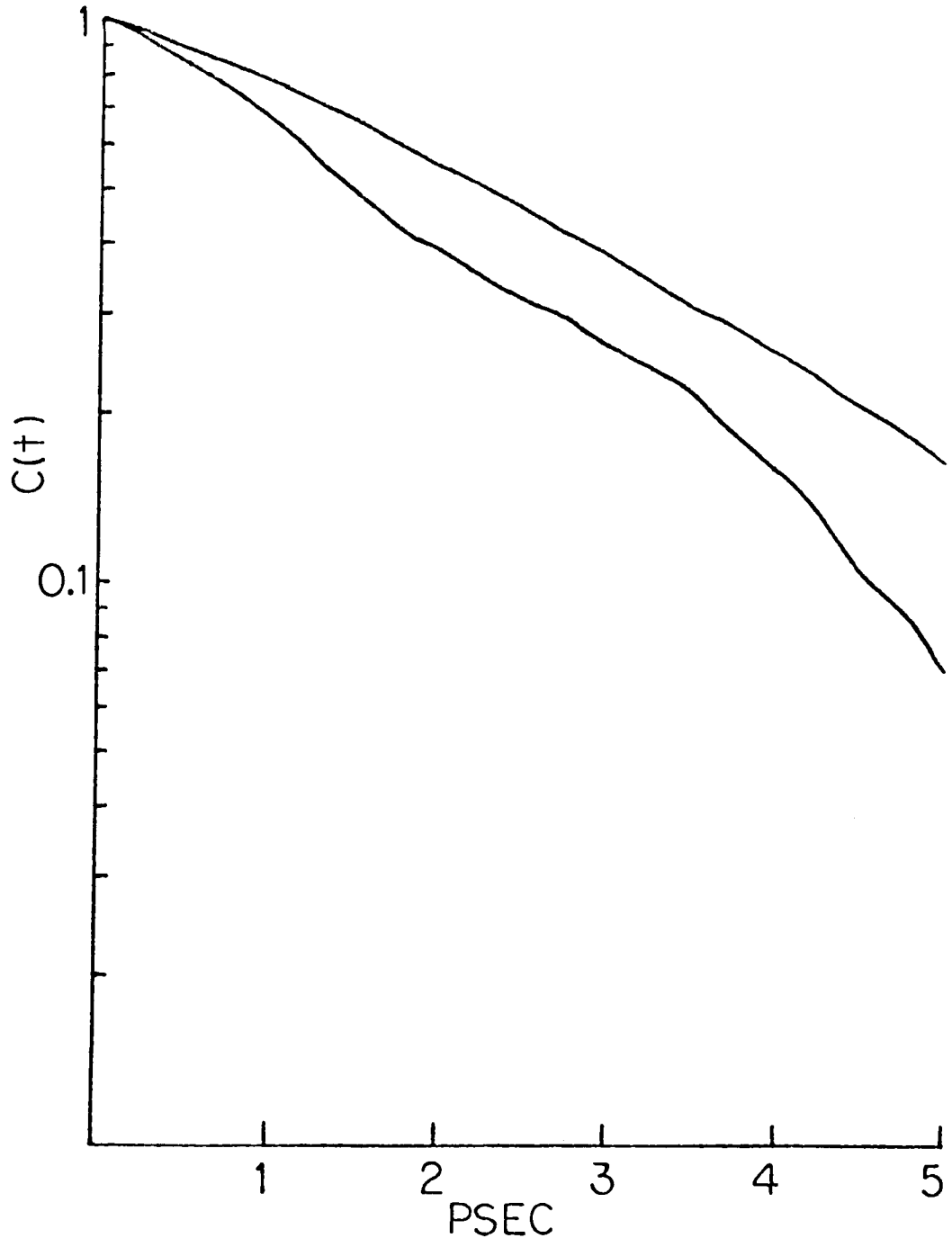
1
C(t)
0.1
1
2
3
4
5
PSEC

FIG. 26. Five models of the smectic bilayer of 8OCB. Diagram based on that of reference 66.

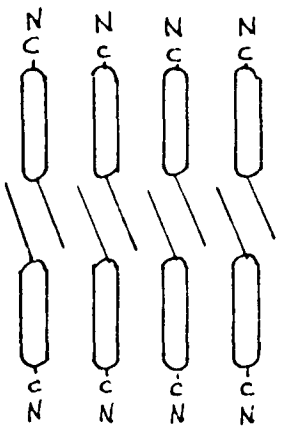

I

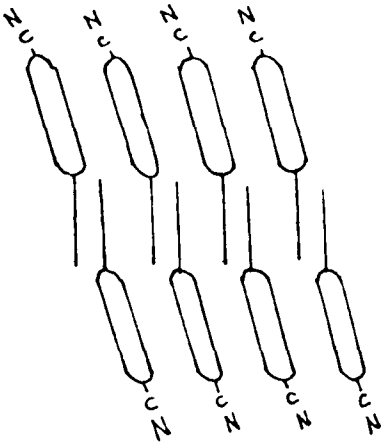

II

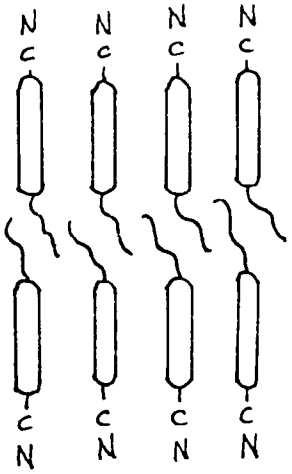

III

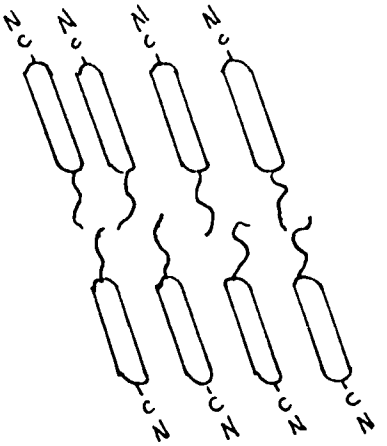

IV

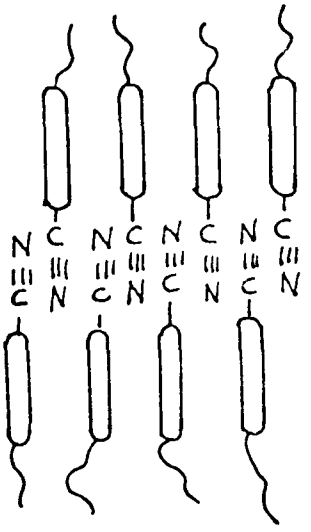

V

these conformations is less preferred than the other. In this less dense crystalline state there is a significant contribution from a distribution of environments, i.e., slow modulation, for each conformation. Thus two curved portions of the function are seen. Note though that this correlation function decays less rapidly than that from the mesomorpic and isotropic phases suggesting the still large importance of a generally uniform environment.

CHAPTER VI

ERROR APPRAISAL

The correlation functions calculated from Raman bandshapes are particularly sensitive to the variations in the wings of the band and the baseline. In the first part of this chapter, some of the major variations and their consequences on the correlation functions are discussed. In addition to the random errors from the baseline effects, there are more systematic errors resulting from the method and technique of calculating the correlation functions. These are discussed in the second part of this chapter. In the third part of the chapter, the correlation functions obtained from the aligned liquid crystal samples, the solutions, the neat liquids and from I_{vib} of various samples are discussed in view of the types of errors that could result from the baseline variations mentioned in the first part of this chapter. The baseline will be considered, in the following discussion, to be that region preceding and following the peak that has a constant average value about which the noise fluctuates. Note that because the lowest valued point in the spectrum is set equal to zero, this average value will probably not be zero. The wings of the peak will be considered the sloping parts of the peak that just meet the baseline.

A. Baseline Effects

Consider the cyano stretching peak shown in Fig. 27. The correlation function calculated from it is shown in Fig. 28. The oscillations in the correlation function are quite unusual and are not seen in correlation functions reported in the literature. Crawford and Fujiyama reported that the same type of oscillations occur when the zero intensity level of a peak is lowered below its true zero level [51] or equivalently, the peak is displaced upward from the zero level by a constant amount. However, for the peak shown this does not appear to be the case at first glance. Examination of the baseline does reveal, though, a large rise in the baseline toward the low frequency end and a slight rise toward the high frequency end. The low frequency rise either resulted from a time decreasing flourescence of the sample or a decrease in the laser power. The high frequency rise probably resulted from a laser power fluctuation. When the range of data was truncated so as to exclude these rising regions and the correlation function calculated, the result shown in Fig. 29 was obtained. Note the absence of the oscillations at the shorter times. In order to check if the rise was responsible for the oscillations, the peak in Fig. 30 was created; the blocked in areas approximate the height of the low and high frequency rises. They are inserted at the ends of the truncated data used to calculate the correlation function shown in Fig. 29. The correlation function calculated from this peak is shown in Fig. 31. The large oscillations have returned. Clearly, a situation, from the computational point of view similar to displacing the peak upwards is created. This type of baseline introduced

FIG. 27. I_{VH} of the cyano stretching peak of isotropic phase 80CB. (Spex)

FIG. 28. C_{VH} calculated from I_{VH} shown in Fig. 27. Note that all curves, such as this one, which do not have ordinate values plotted for the full range of abscissa values occur when there are ordinate values less than $1x10^{-3}$ at longer times.

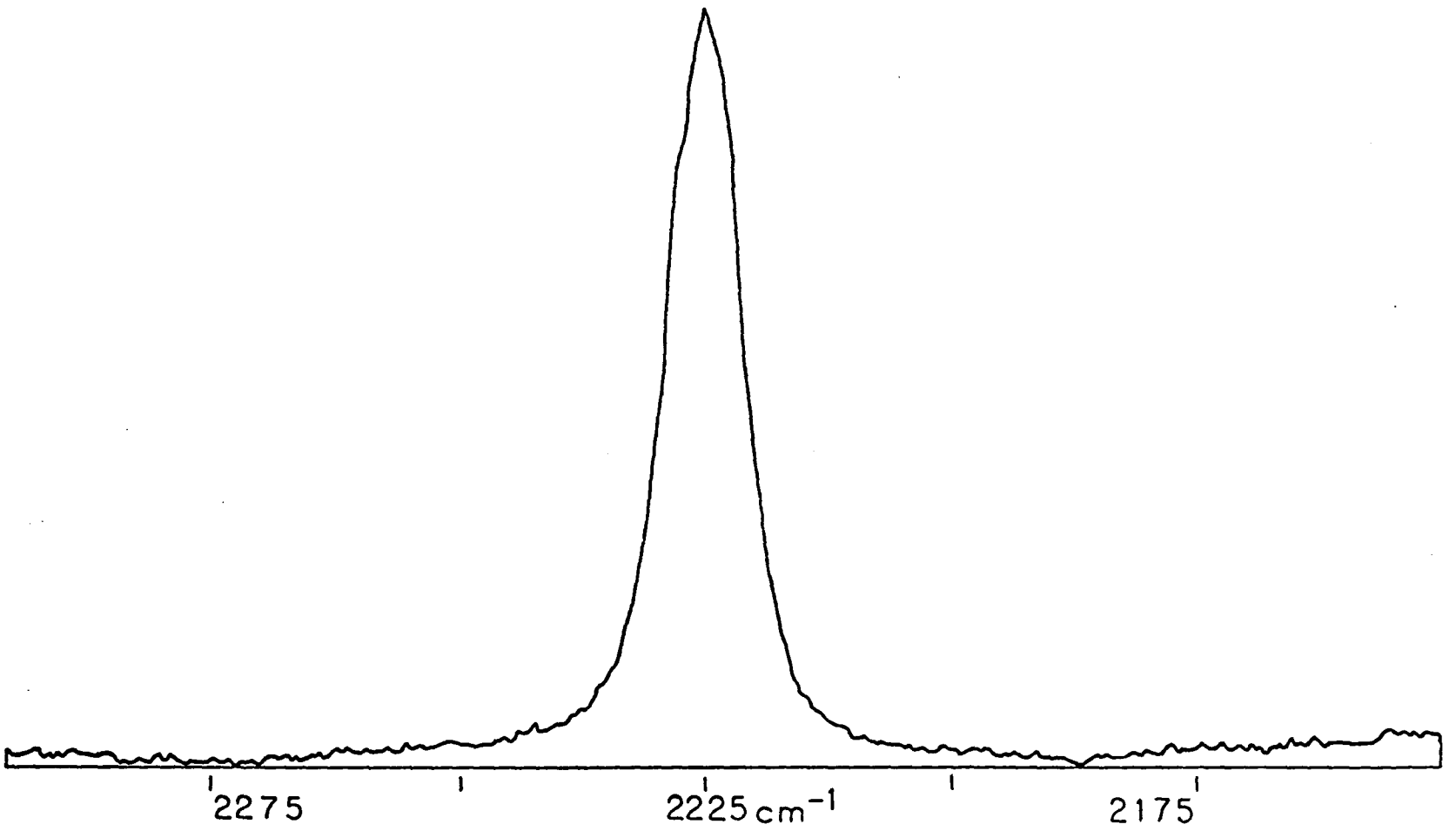
2275
2225 cm⁻¹
2175

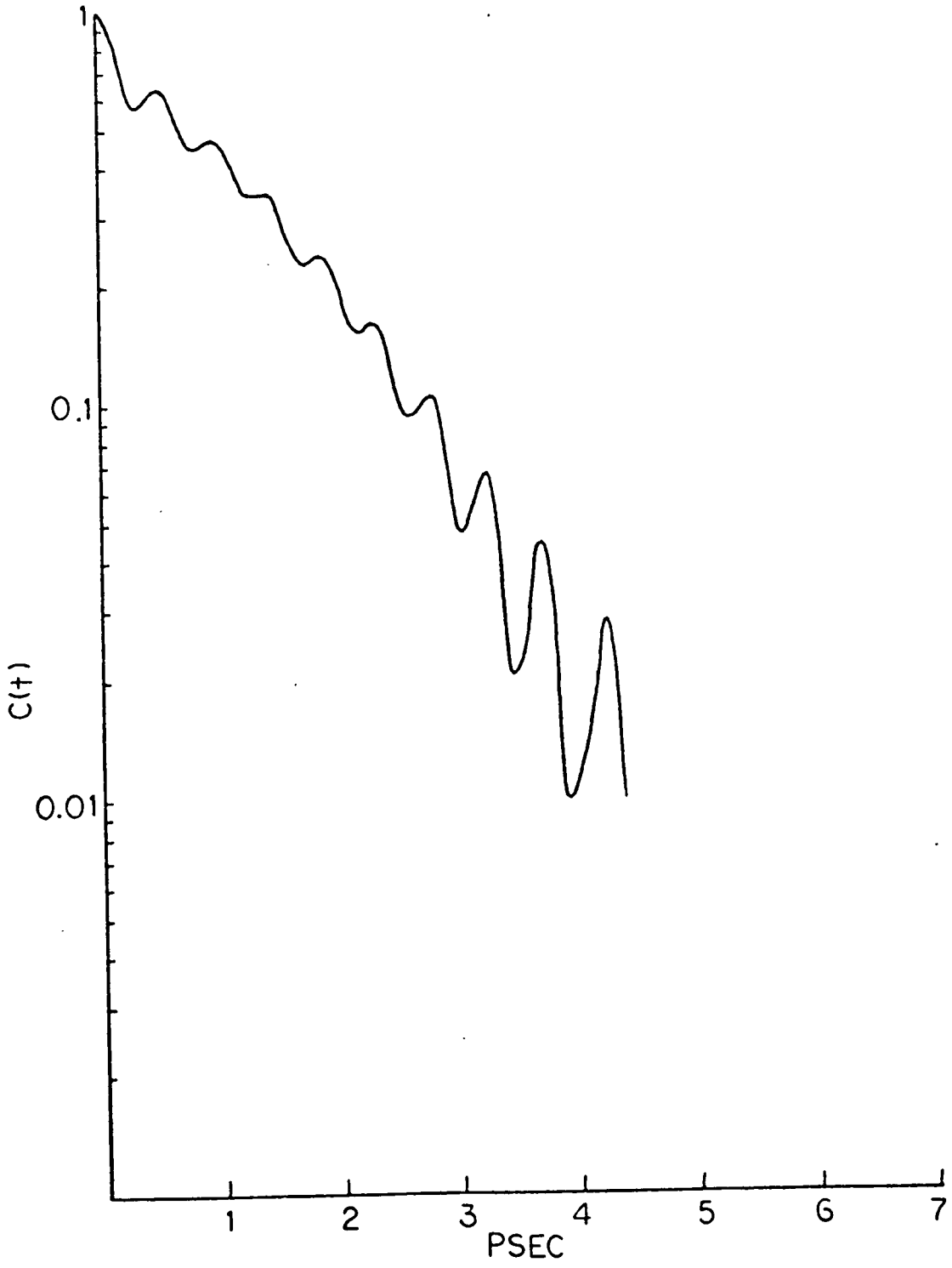
1
0.1
0.01
C(t)
1
2
3
4
5
6
7
PSEC

FIG. 29. C_{VH} calculated from the I_{VH} of Fig. 27 truncated to eliminate regions of rising baseline.

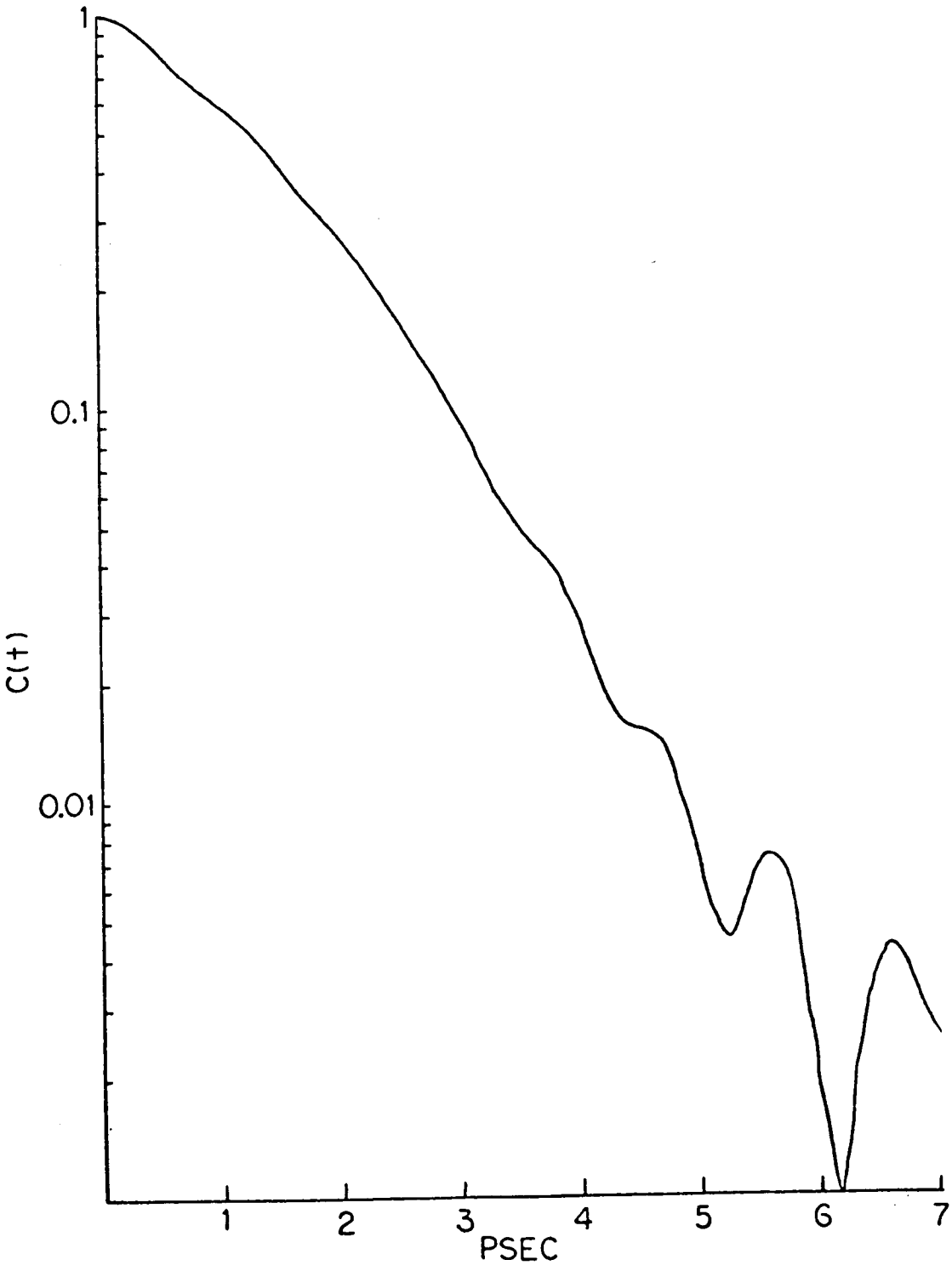
1
0.1
0.01
C(+)
1
2
3
4
5
6
7
PSEC

FIG. 30. I_{VH} of Fig. 27 with parts of the baseline blocked in to simulate the regions of baseline rise.

FIG. 31. C_{VH} calculated from the I_{VH} of Fig. 30.

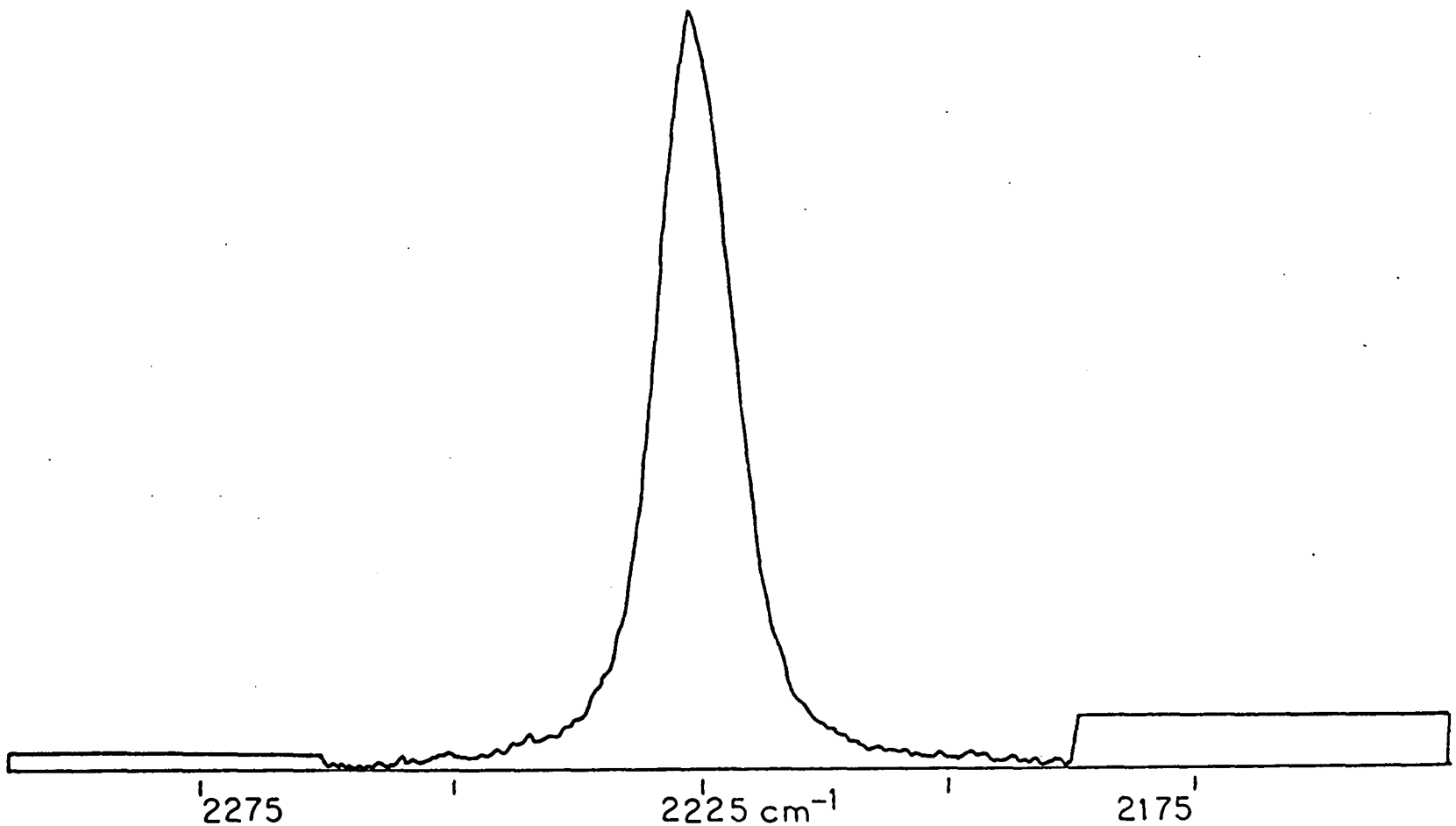
2275
2225 cm⁻¹
2175

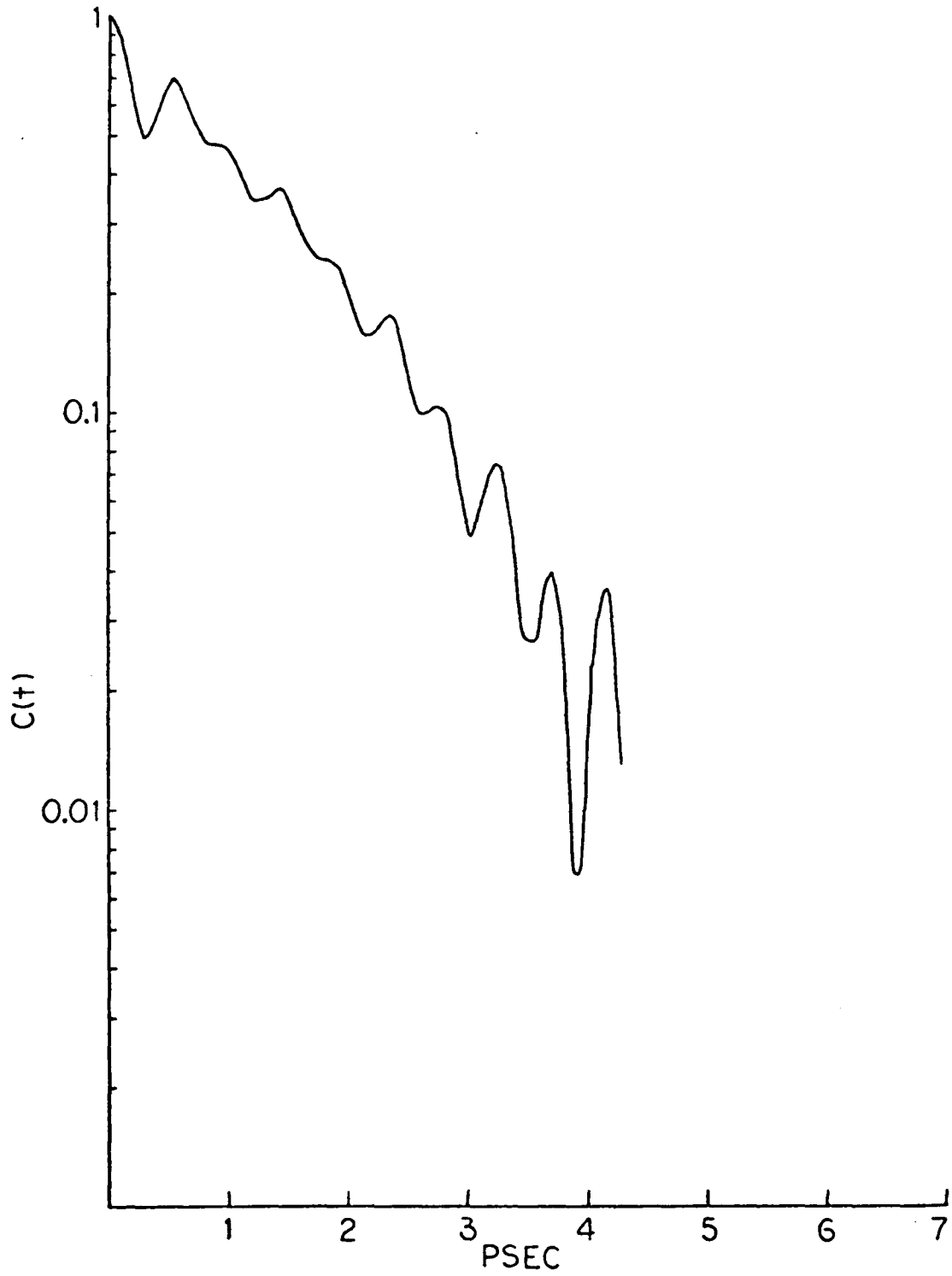
1
0.1
0.01
C(t)
1
2
3
4
5
6
7
PSEC

error can be eliminated by making sure the laser output is steady and allowing the sample to sit sufficiently long in the laser beam so that a flat baseline is obtained.

If the rise in the baseline is less intense, the oscillations occur to a lesser degree. Fig. 32 shows a peak with a low frequency baseline slightly higher than the high frequency baseline; the low frequency rise resulted from the presence of decreased, but still existent, sample flourescence after the sample had been in the beam for some time. In Fig. 33 the same peak from the same sample is shown with about the same signal to noise ratio but with the low frequency baseline level with the high frequency end; this flat baseline was achieved by allowing the sample to remain in the beam for about 2 hours. The correlation functions obtained from the peaks are shown in Fig. 34. Notice that the correlation function from the peak with the baseline rise has an initial dip during the first 0.5 picosecond, a series of mild oscillations throughout the remainder of the curve and it is shifted downwards compared to the more accurate result. The initial dip, when present without the oscillations, is usually ascribed to the presence of free rotation in a sample which has broadened or intensified the peak wings.[39] Here, though, it is clear that the dip and oscillations are vestiges of the more extreme dip and oscillations such as those shown in Fig. 28. The slight dip shown in the correlation function from the sample with the level baseline could possibly be associated with a period of free rotation, but is most probably due to a small amount of baseline noise causing the wings to be slightly displaced upwards in intensity. Once again, note that the problem described here, a slightly increased baseline,

FIG. 32. I_{VH}, with a small low frequency baseline rise, from a 0.12 mole fraction solution of 80CB in carbon tetrachloride. (J-Y) Note that the frequency range is 2170 to 2270 cm^{-1}. Spectra obtained using the J-Y instrument generally have peaks that are approximately 5 cm^{-1} lower in frequency than the peaks in spectra obtained with the Spex instrument. This is attributed to differences in the wavenumber calibration of each instrument.

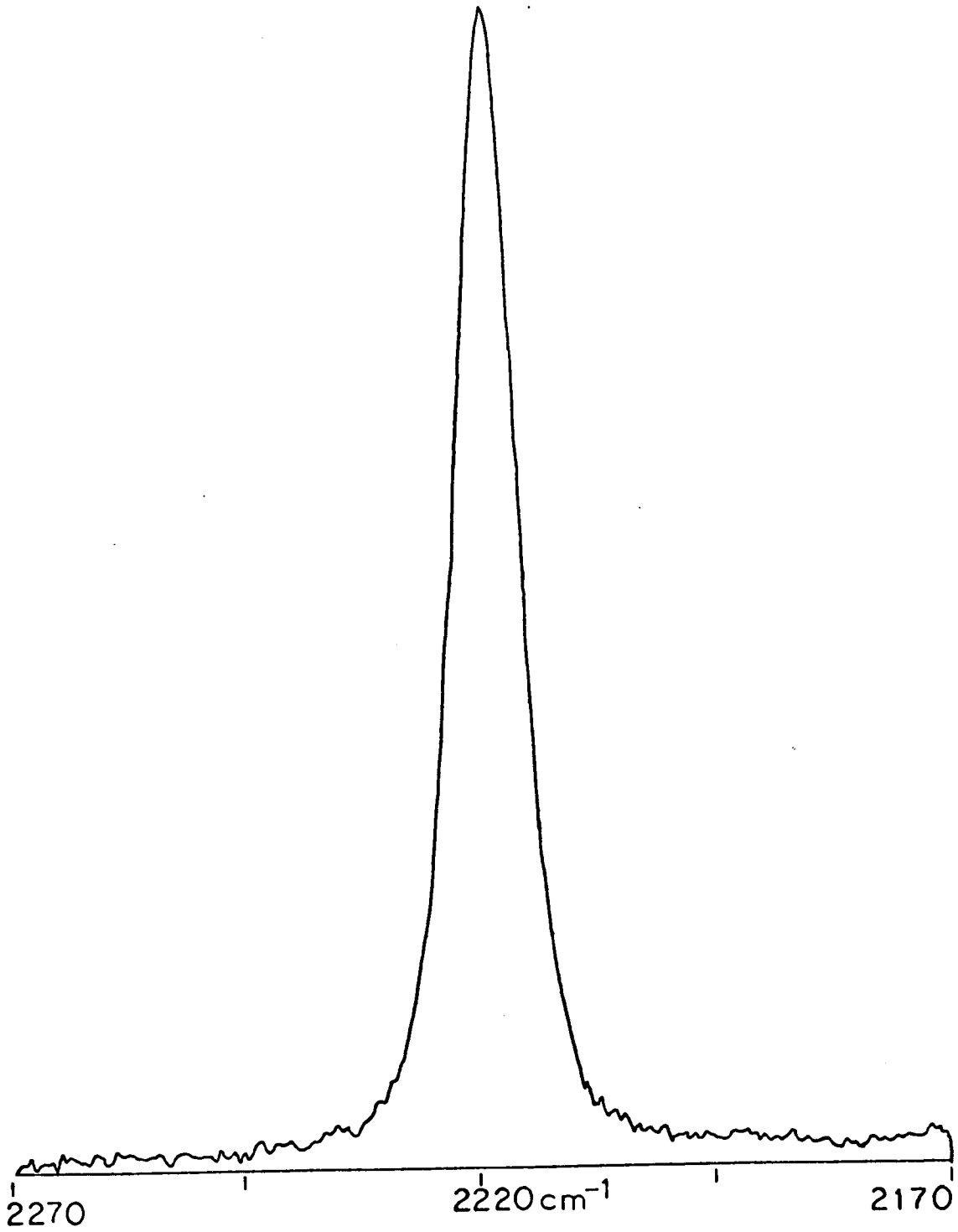
2270
2220 cm⁻¹
2170

FIG. 33. I_{VH}, with a level baseline, from a 0.12 mole fraction solution of 8OCB in carbon tetrachloride. (J-Y)

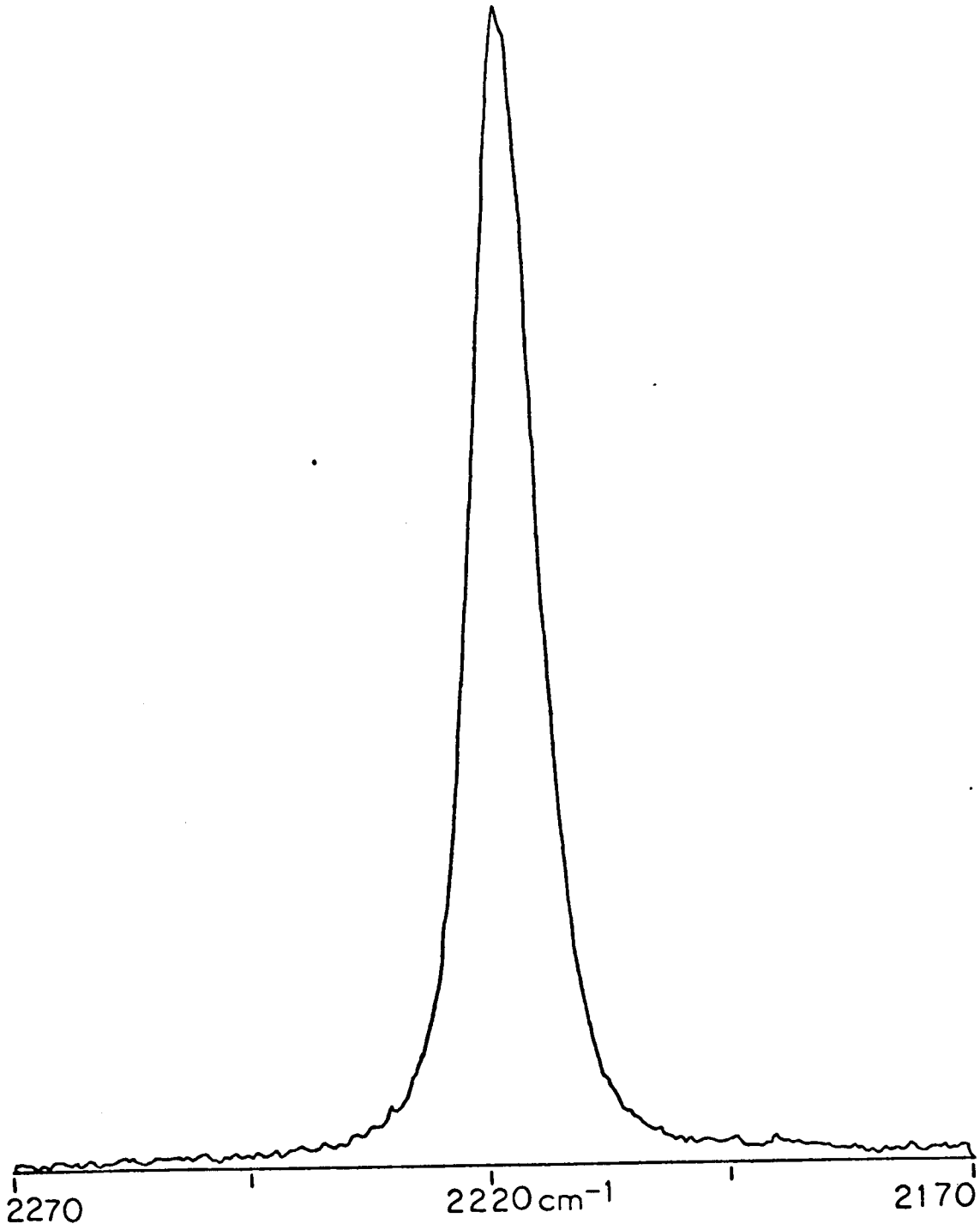
2270
2220 cm⁻¹
2170

FIG. 34. C_{VH} calculated from the I_{VH}, with the baseline rise, of Fig. 32, lower curve, and from the I_{VH} of Fig. 33, upper curve.

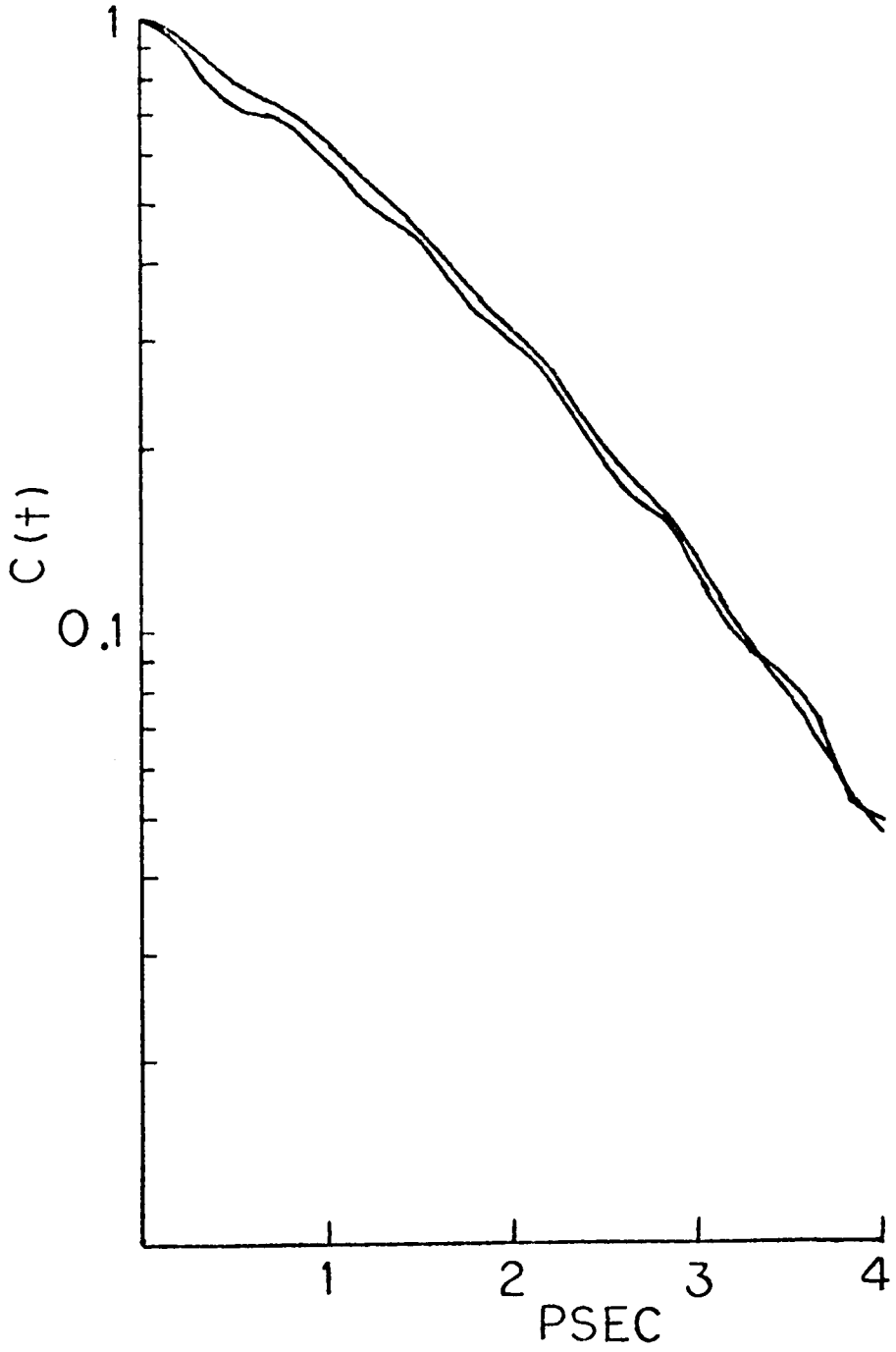
1
C(t)
0.1
1
2
3
4
PSEC

can be avoided in the same way as for the problem due to a large baseline rise--allow the sample to sit sufficiently long in the beam.

The effect of noise, that is, high frequency fluctuations, in the baseline can be dramatic. In Fig. 35 is shown a peak with a noisy baseline. In Fig. 36 the same peak from the same sample is shown but with a greatly improved signal to noise ratio. The correlation functions calculated from these peaks are shown in Fig. 37. The correlation function from the noisy data shows a large initial dip, oscillations and a large downward displacement compared to the less noisy results. This correlation function seems to be approaching the extreme shown in Fig. 28. The noise in the wings defines a baseline by its downmost fluctuation. The large number of positive fluctuations seem to add a significant weight to the wings much in the manner that the blocked in areas of Fig. 30 did. Therefore the noise leads to the initial dip and following oscillations in the correlation function. Decreasing the amount of noise leads to a lesser effect; eventually a level of noise can be reached where the dip and oscillations are almost completely eliminated.

The problem due to the noise can be partially avoided if it is first recognized that the signal to noise ratio of a peak is proportional to the square root of the total number of photon counts. To improve the ratio, the total number of counts must be increased. For a given slit setting, this can be done by aligning the sample such that the scattered intensity is maximized and/or by increasing the time spent counting the photons at any given wavenumber. For some samples, though, even the best alignment leads to a relatively low intensity peak and consequently a lower number of total counts;

FIG. 35. Noisy I_{VH} spectrum, 1 second count time, from 0.03 mole fraction solution of 80CB in carbon tetrachloride. (J-Y)

FIG. 36. I_{VH} spectrum, 30 second count time, from 0.03 mole fraction solution of 80CB in carbon tetrachloride. (J-Y)

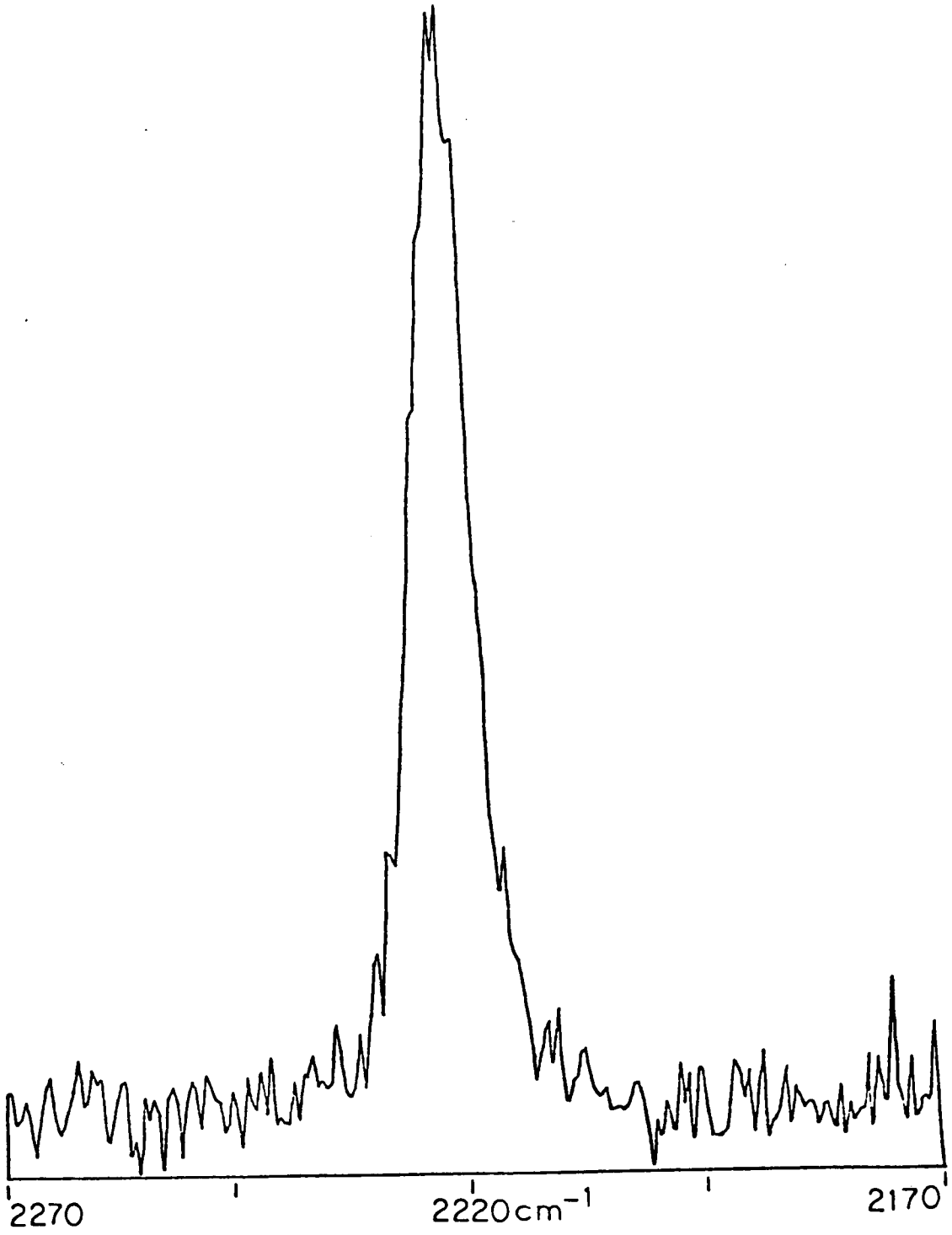
2270
2220cm⁻¹
2170

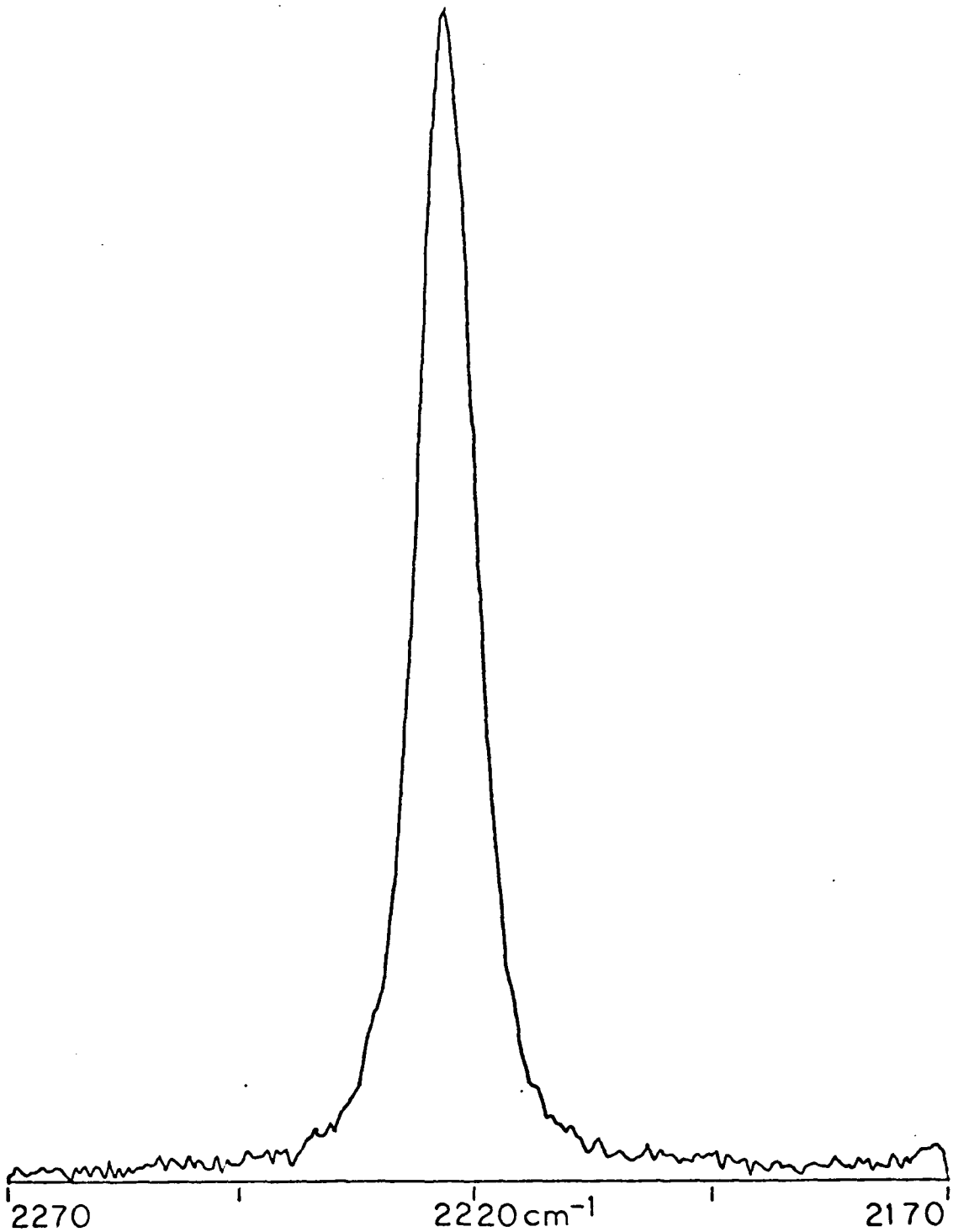
2270
2220 cm⁻¹
2170

FIG. 37. C_{VH} calculated from the noisy spectrum of Fig. 35, lower curve, and from the spectrum of Fig. 36, upper curve.

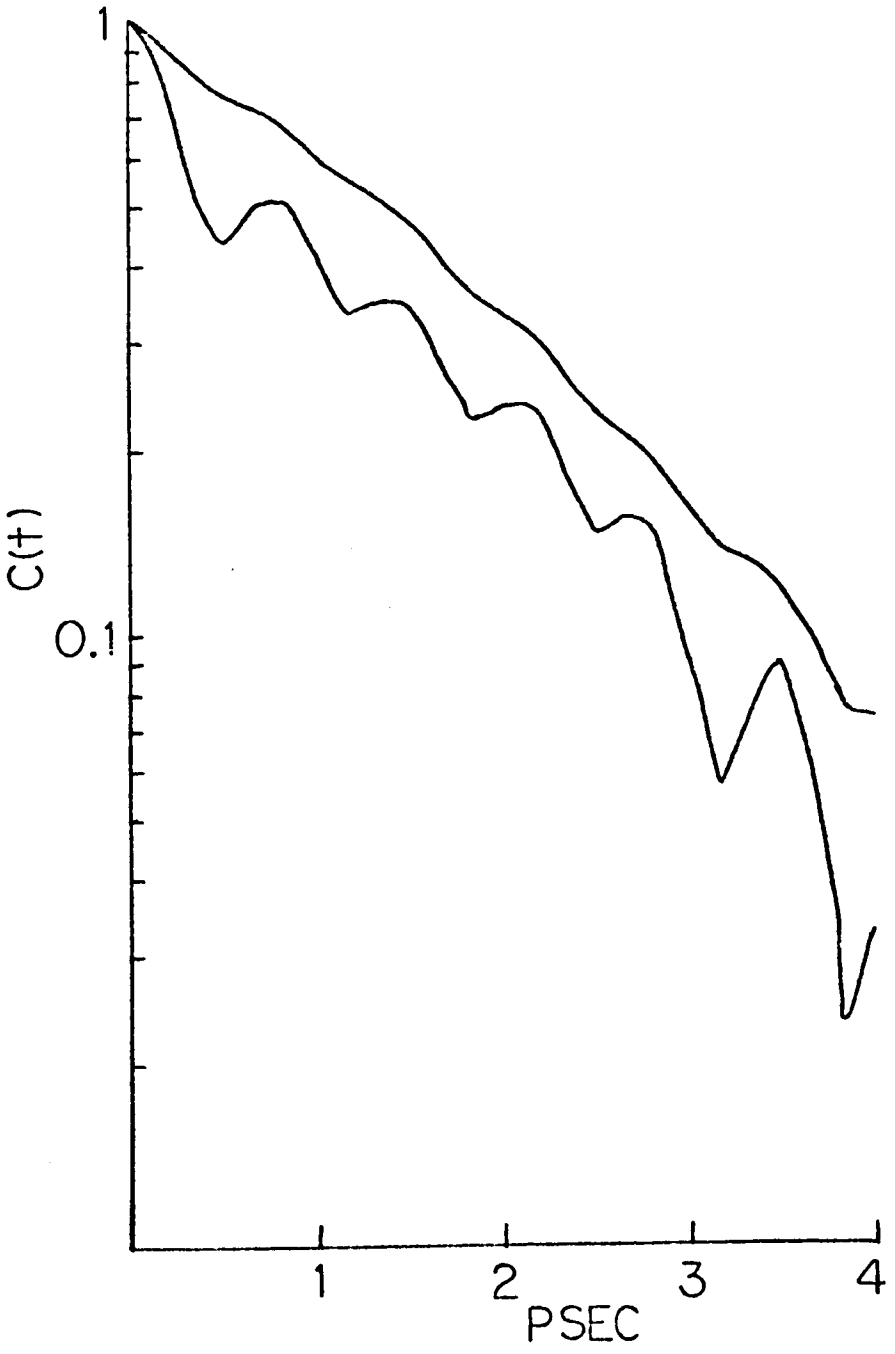
1
C(t)
0.1
1
2
3
4
PSEC

the aligned liquid crystals are this type of sample. Furthermore, there is a practical limit to the counting time; longer counting times mean longer total time for taking a spectrum and consequently a more rigorous requirement that the system be stable. Also, few spectra can be obtained in one day. It was found that the best compromise led to count times of 60 seconds when the peak maximum was between 150 and 200 counts per second. For the 200 points usually obtained in the spectrum, a 60 second count time led to a run time of 3 hours and 20 minutes. This counting time generally brought the noise fluctuations down to about 1% of the peak maximum as required to eliminate baseline effects.[51] For more intense peaks, shorter count times were used, commonly 30 or 15 seconds per point. This also kept the noise fluctuations down to approximately 1% of the peak maximum. Note however that a perfectly smooth and noiseless peak has generally not been obtained under our practical conditions and consequently some slight noise effects will almost always be present in the correlation functions.

Other workers in this field have treated baseline and wing noise differently. Rothschild, et.al.,[39] draw by hand the best curve that fits the experimentally obtained spectroscopic data. They then digitize the results and use them to calculate the correlation function. Goldberg and Pershan[19] fit a calculated spectrum to the observed spectrum; Jones, et.al.,[67] fit an exponential function with adjustable parameters to the wings. Both groups then used the analytical curves to calculate the correlation functions. These techniques, of course, have the merit of eliminating the troublesome effects. However, they do presume a shape and structure for

the band which may be unwarranted, or in other words, information can be added or lost by these techniques. Our technique of using the raw data was aimed at extracting only the information actually present in the bandshape and, in principle, is the correct approach. As can be deduced from the above discussion on noise, our technique makes it somewhat difficult to separate the meaningful results from the noise induced ones, especially in the short time range.

The frequency range over which the Fourier transform of a peak is calculated, in principle, will have an important effect on the correlation function. Ideally, the complete band should be included in the calculation since information is contained not only in the region around the peak maximum, but also in the wings. In practice, the wings are often perturbed by neighboring peaks and the band must be truncated. The effect of truncation on the Fourier transform of the peak is to convolve a function of the form $A\omega/\pi(\sin \omega t)/\omega t$ with the function that would be obtained from the whole bandshape, leading to periodic oscillations in the true function.[48] Fujiyama and Crawford studied the effect of different truncation ranges on a Lorentzian bandshape.[51] They found that the correlation function on the 0-2ps time scale was still affected by periodic oscillations when the integration range was 8 times the FWHH. It should be noted that a Lorentzian function asymptotically goes to zero over a wide frequency range. It would be expected that if a wide integration range was chosen which nevertheless still excluded part of the wings that the correlation function would be affected. If on the other hand, a wide integration range was chosen for computing the Fourier transform of a peak that quickly came down to

the baseline, then some of the baseline would be included in the calculation. This situation might occur if it was not clear where the peak ended and the baseline began. Inadvertently including baseline as part of the peak ideally should have no effect since the baseline, being essentially zero valued, would only serve to cause the interpolation of points as discussed in Appendix A.

The effect of truncation on the cyano stretching peak of the liquid crystal was examined. In Figs. 38, 39, 40 and 41 are shown peaks that are defined by 200, 167, 134 and 84 data points (one every $0.5cm^{-1}$). These numbers of points correspond respectively to integration ranges of approximately 11, 9, 7, 5 times the FWHH. The correlations functions calculated from these peaks are shown in Fig. 42. It should be noticed that the truncation to 167 and 134 points leads to virtually no change in the correlation functions. Truncation to 84 points makes a slight change especially at shorter times. Note that the dip in the 200 point transform is progressively removed by truncation. For a peak with a narrower FWHH, the same results have been obtained.

The above results clearly show that the range of integration commonly used for our calculations, $100cm^{-1}$, does not introduce truncation effects into the correlation functions. The fact that severe oscillations like the ones Fujiyama and Crawford found do not occur in the correlation function calculated from 84 points suggests that the cyano peak comes quickly down to the baseline with most of its information contained in the region around the peak maximum. The changes in the correlation functions at short times do nevertheless suggest that information (real or spurious) is contained in the wings.

FIG. 38. $200_{(10)}$ point I_{VH} spectrum, one point every 0.5 cm^{-1}, obtained from a 0.37 mole fraction solution of 80CB in benzene. (Spex)

FIG. 39. I_{VH} truncated to $167_{(10)}$ points.

FIG. 40. I_{VH} truncated to $134_{(10)}$ points.

FIG. 41. I_{VH} truncated to $84_{(10)}$ points.

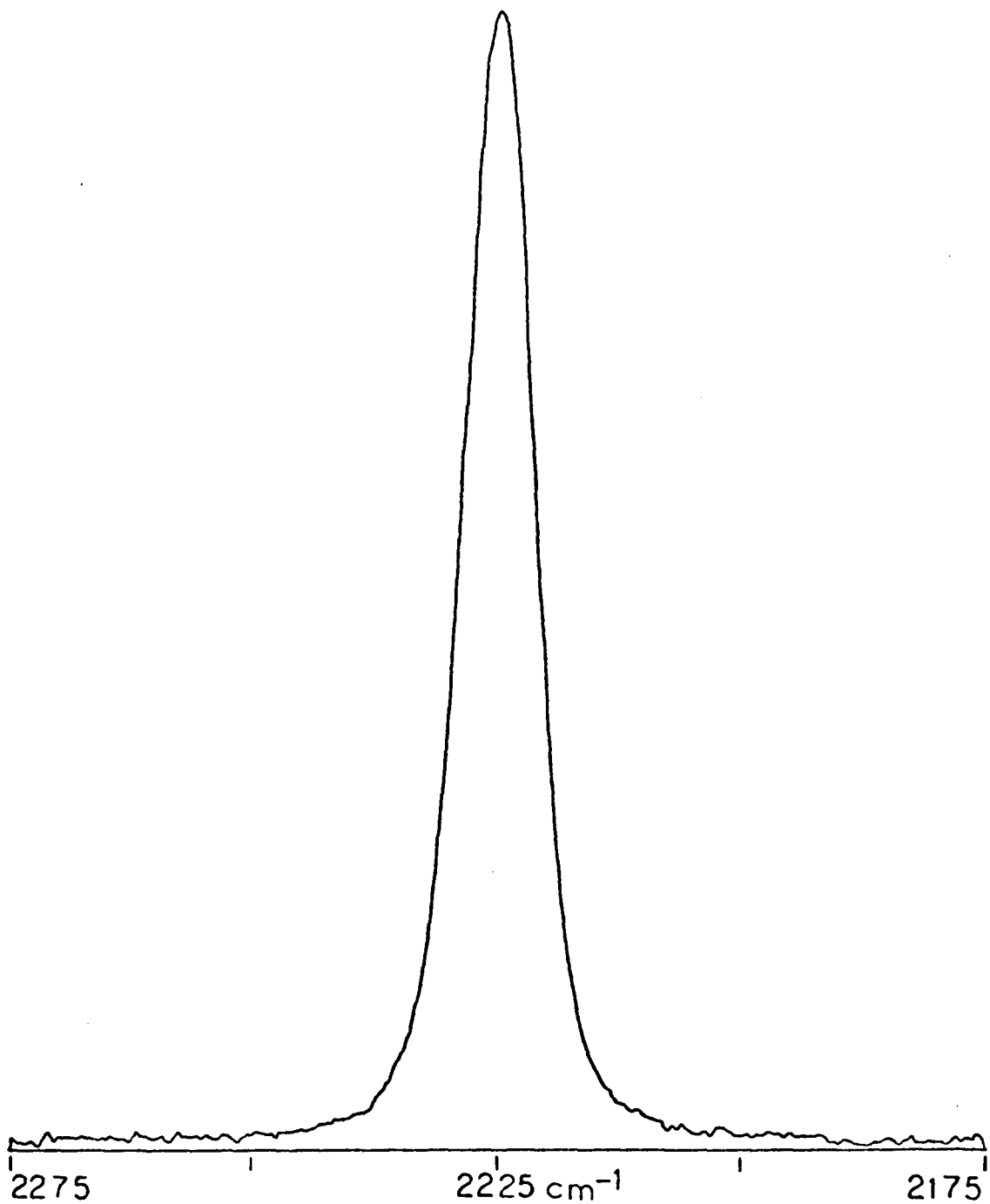
2275
2225 cm⁻¹
2175

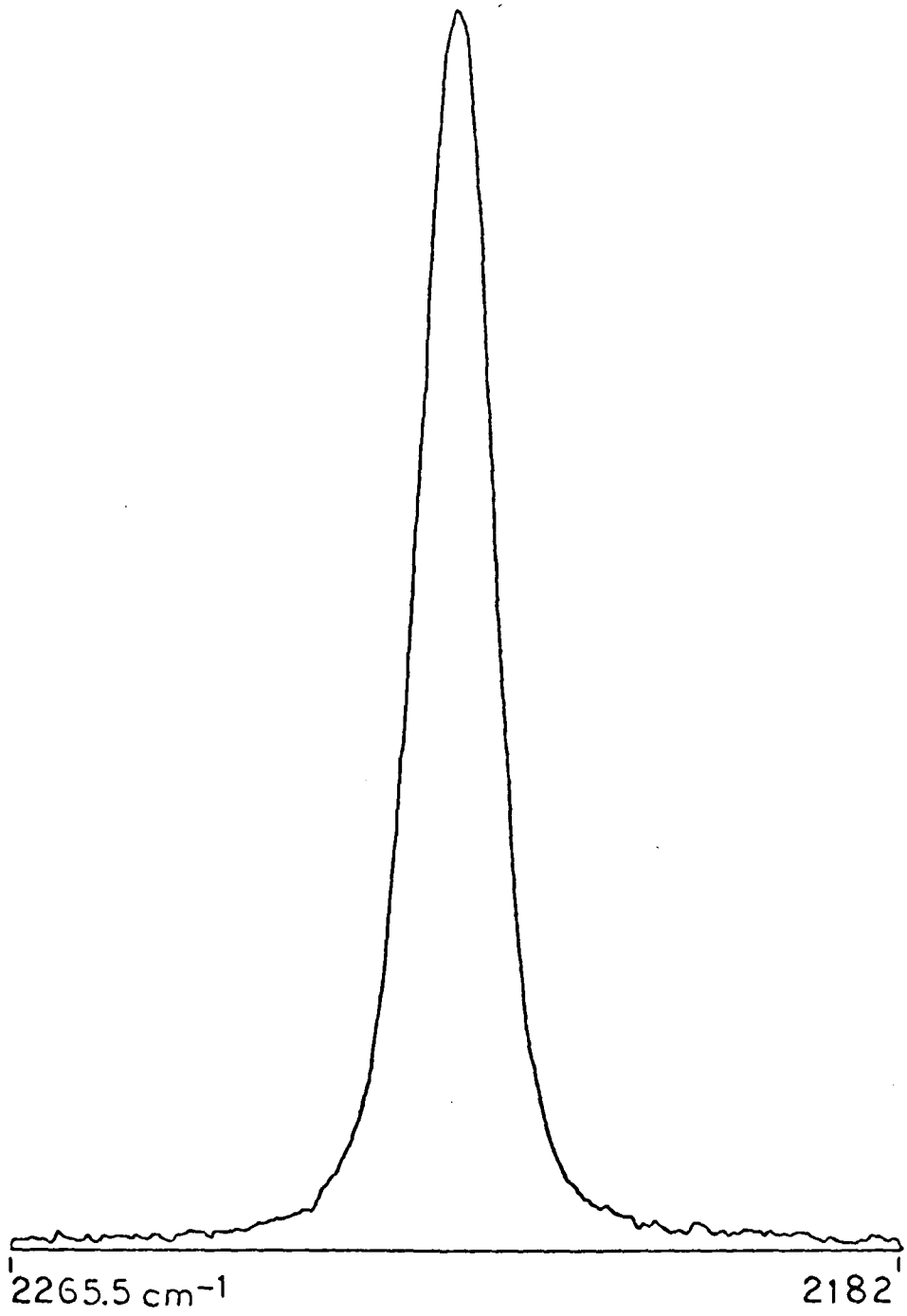
2265.5 cm⁻¹
2182

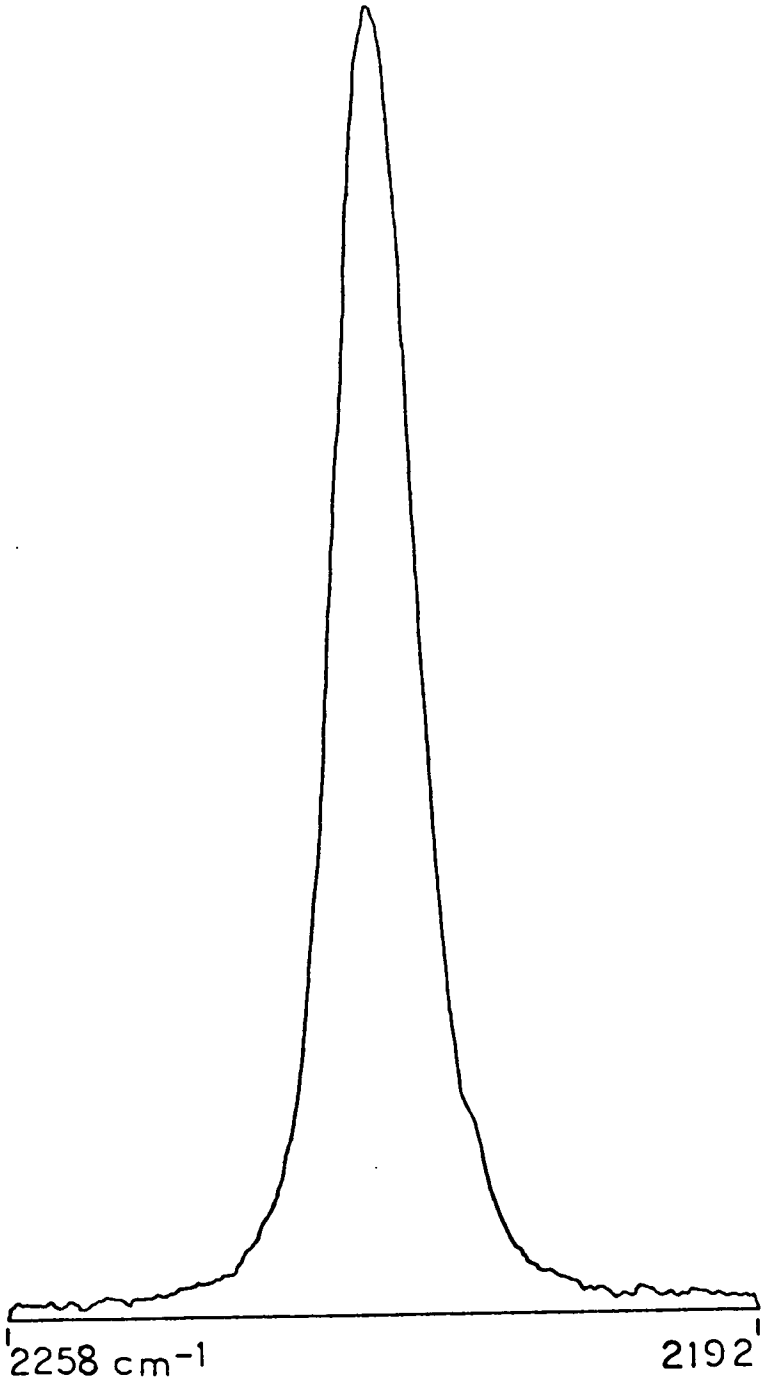
2258 cm-1
2192

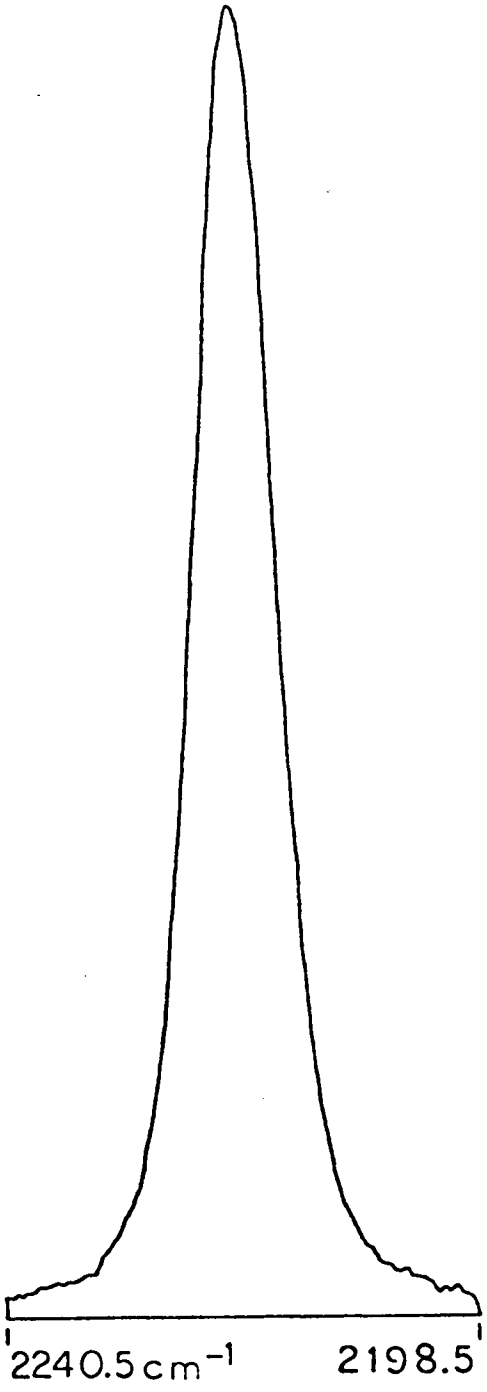
2240.5 cm⁻¹
2198.5

FIG. 42. C_{VH} calculated from the peaks shown in Figs. 38, 39, 40, 41. Note that the ordinate scale is expanded so that differences in values will be magnified.

. - C_{VH} from 200 point I_{VH}

x - C_{VH} from 167 point I_{VH}

⊙ - C_{VH} from 134 point I_{VH}

⊡ - C_{VH} from 84 point I_{VH}

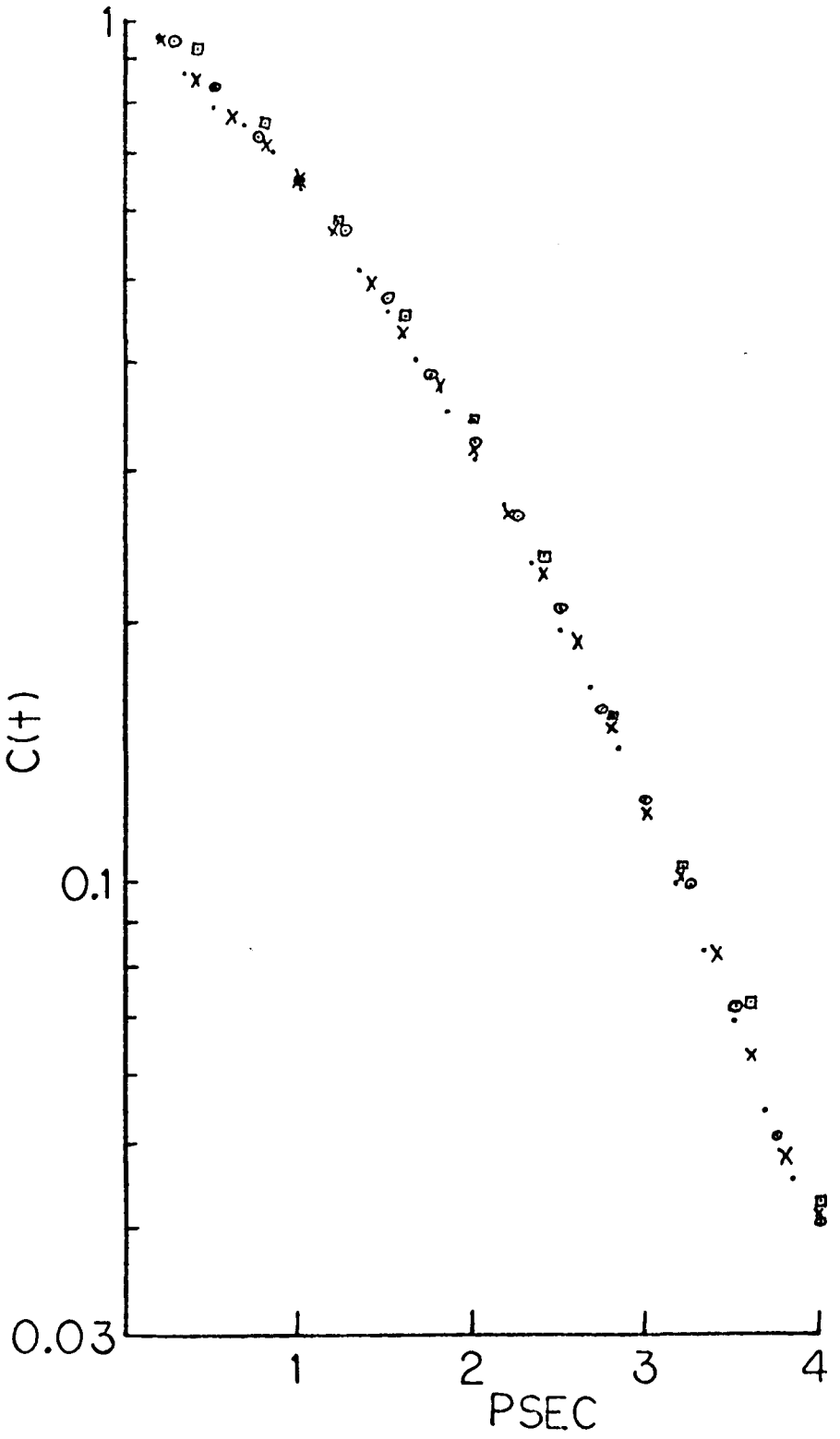
1
0.1
0.03
C(+)
1
2
3
4
PSEC

In summary, this part of the chapter on errors has given an idea of the magnitude of the effects on correlation functions that baseline and wing variations cause. Almost all the effects can be minimized in the manners mentioned. The error discussion indicates that if a correlation function obtained under the best possible experimental conditions still shows a mild initial dip followed by mild oscillations, then not much significance should be accorded to the dip. Nevertheless, significance should be given to the whole correlation function since it will be a very close approximation to the accurate function. When the initial dip appears and is not attended by oscillations, then its significance under our laboratory conditions is much harder to evaluate. Probably the best evaluation is the conservative one of not attaching much importance to it.

B. Errors from the Calculation Technique

The algorithm used for calculating the Fourier transform (discussed in detail in Chapter Four and Appendices A and B) was checked for accuracy by computing the Fourier transform of a Lorentzian bandshape. The Fourier transform of a Lorentzian is an exponential function which when plotted on semi-logarithmic graph would be a straight line. In Fig. 43 the result of this calculation is shown for a computer generated Lorentzian which has a peak maximum of 12,000 counts per second, a FWHH of $9cm^{-1}$, a data range of 450 wavenumbers and a sampling interval of $0.5cm^{-1}$. A perfect straight line is obtained confirming the inherent accuracy of the algorithm.

In our work, high peak intensities and wide data ranges were

FIG. 43. C_{VH} obtained from a computer generated Lorentzian peak of the following specifications:

peak maximum:	12,000 counts per second
FWHH:	9 cm^{-1}
range:	450 cm^{-1} (900 points)
sampling interval:	0.5 cm^{-1}

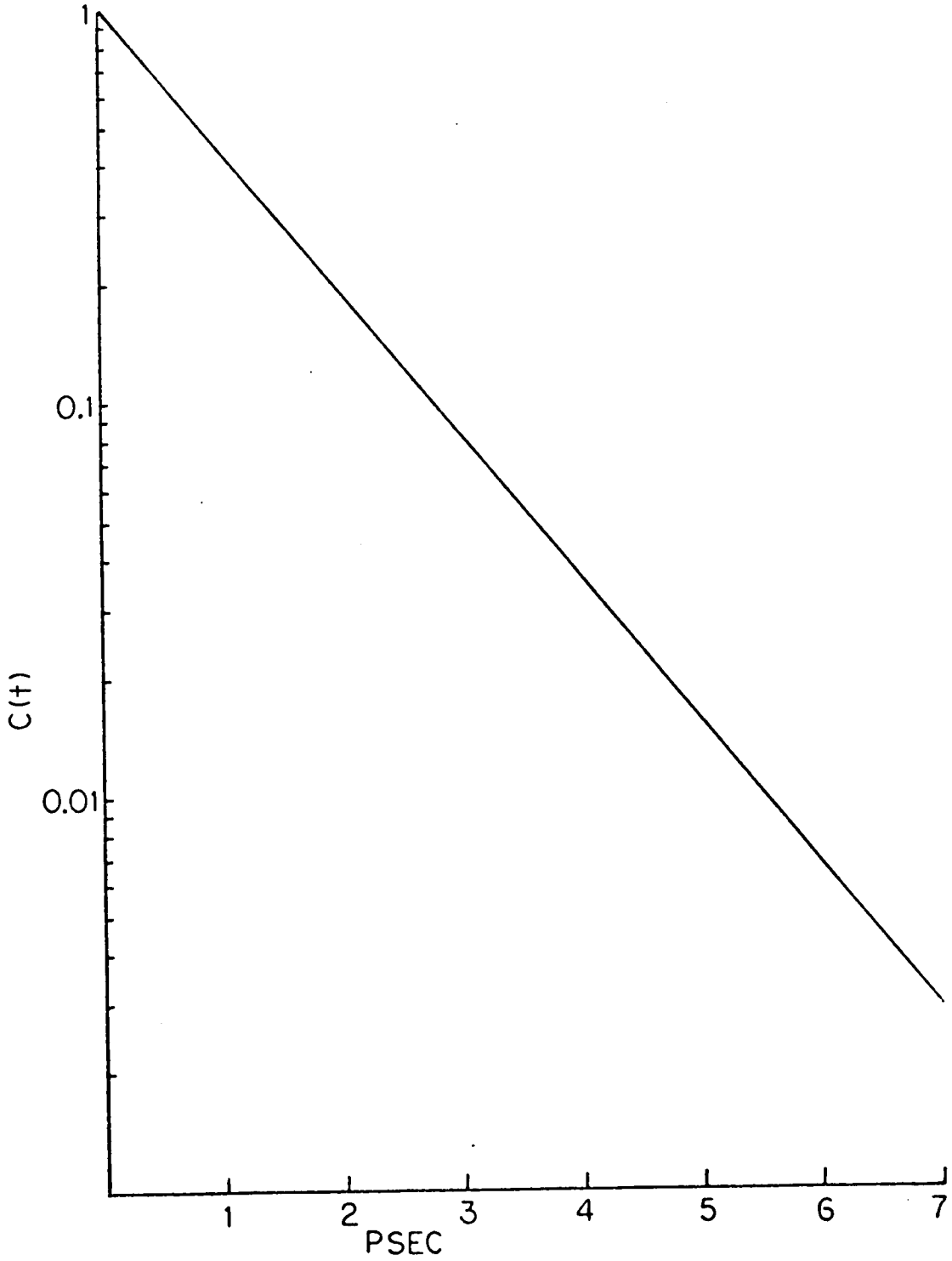
1
0.1
0.01
C(t)
1
2
3
4
5
6
7
PSEC

not possible to obtain. For the data obtained in our laboratory, the correlation functions often showed peculiarities at the longer times. In Fig. 29 was shown the correlation function calculated from the peak shown in Fig. 27. That peak had a maximum intensity of 120 cps and was truncated to 151 points (0.5 wavenumber sampling interval). The correlation function is generally smooth up to 4 picoseconds after which some larger oscillations set in. In order to see the accuracy of the algorithm under these conditions, a Lorentzian was formed with the same dimensions as the experimentally obtained peak. Truncation of the decimal parts of non integer numbers in the Lorentzian was done in order to approximate the data collection process. (Note the use of the word truncation in a different way here.) The correlation function calculated from this peak is shown in Fig. 44. Notice that though it approximates a straight line nicely at short times, it is not a perfect fit especially after 4 picoseconds. Forming a Lorentzian in which rounding off instead of truncation was used with non integer numbers did not measurably improve the fit of the correlation function to the straight line and especially did not remove the oscillations at longer times. Doubling the data range to 300 points also did not improve or remove the oscillations. However, doubling the data range and then adding the value one to every truncated data value did give the improved correlation function shown in Fig. 45. As can be seen, the fit to a straight line in the first 4 picoseconds is excellent but the long time oscillations are still present. Adding one to every point in the extended range apparently

FIG. 44. C_{VH} calculated from a computer generated Lorentzian (discussed on page 183) of the following specifications:

peak maximum: 120 counts per second

FWHH: 9 cm^{-1}

range: 75 cm^{-1} (151 points)

sampling interval: 0.5 cm^{-1}

Note that a straight line has been fit, by eye, to C_{VH} so as to best match the short time values yet still reasonably approximate the long time ones.

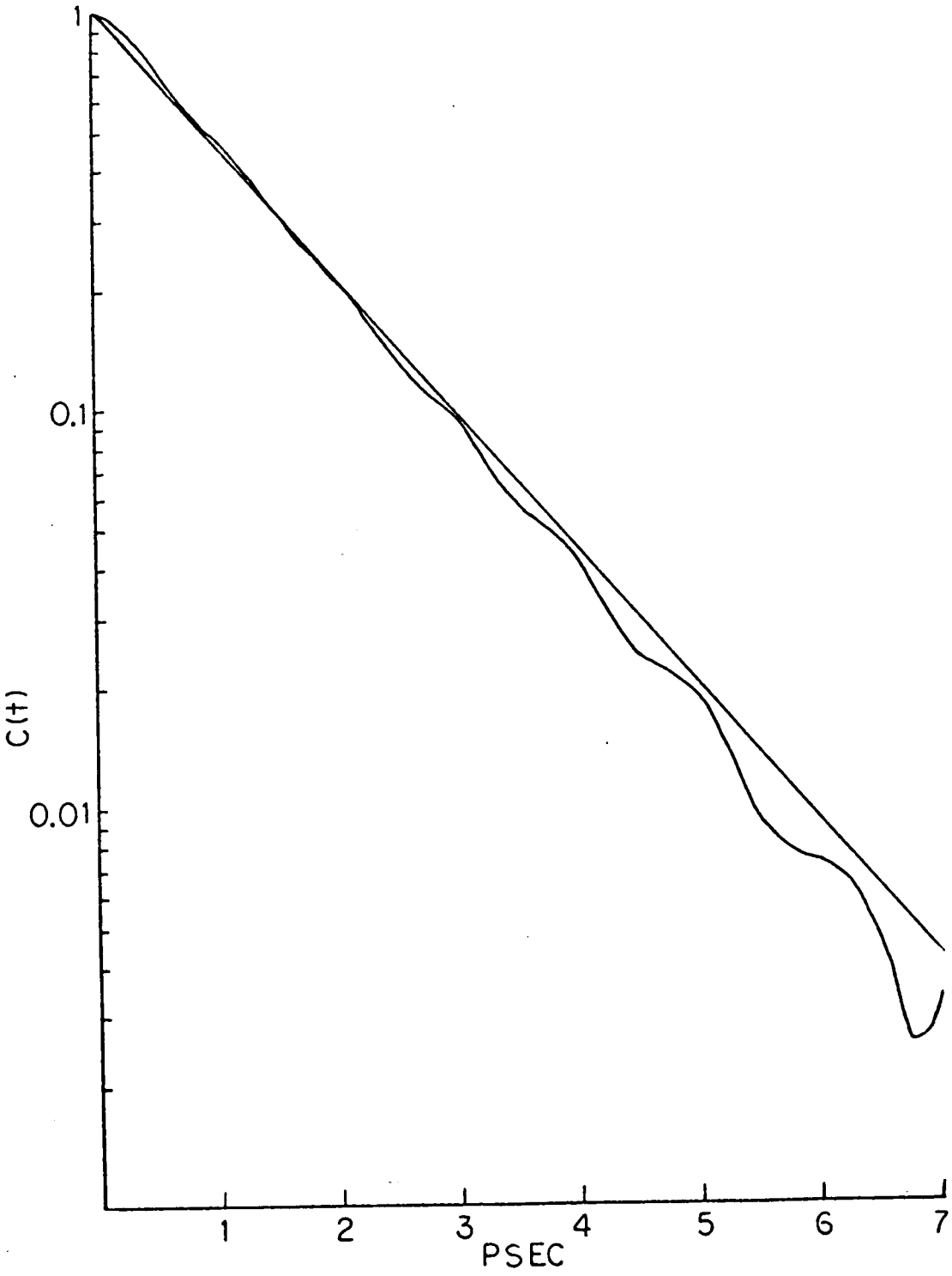
1
0.1
0.01
C(t)
1
2
3
4
5
6
7
PSEC

FIG. 45. C_{VH} calculated from a computer generated Lorentzian (discussed on page 183) of the following specifications:

peak maximum: 120 counts per second

FWHH: 9 cm^{-1}

range: 150 cm^{-1} (300 points)

sampling interval: 0.5 cm^{-1}

Also included is a straight line fit, by eye, to C_{VH}.

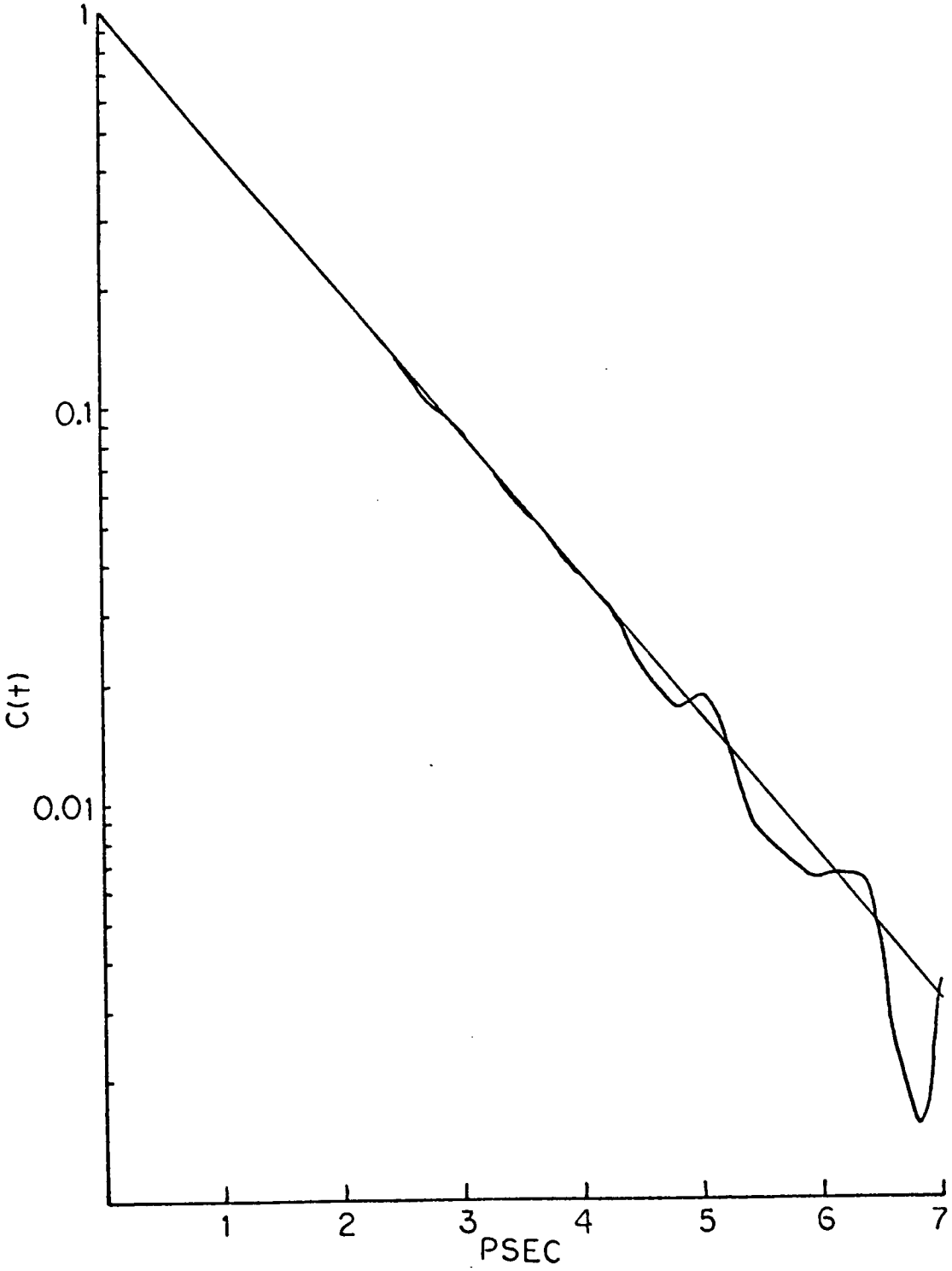
1
0.1
0.01
C(+)
1
2
3
4
5
6
7
PSEC

gives a greater weight to the wings than was obtained before and apparently was required. The long time oscillations can only be explained, as suggested by other authors,[18, 68] by the large accumulation of arithmetic and data errors starting after 4 picoseconds; even the well defined intense Lorentzian whose correlation function was shown in Fig. 43 did show slight oscillations in the correlation function after 7 picoseconds.

The above tests on Lorentzians did suggest some procedures to follow. Clearly, as much of the band as could be sampled should be (though remember the baseline considerations of part 1). In addition, the data points comprising the wing parts of a weak peak should not be truncated. This fact led to the experimental procedure for weak peaks of obtaining only the total photon counts during a collection interval, rather than dividing, with consequent truncation, the total counts by the seconds counted to get the counts per second. Lastly, it probably is best to report as reliable, correlation functions obtained from our data for only the first 4 picoseconds.

A test of the importance of the sampling interval size was also conducted. The Lorentzian closest to experimental conditions that gave the best fit to a straight line, the one with 120 counts per second maximum, 151cm^{-1} range, sampled every 0.5cm^{-1} and ones added to every point was also sampled every 0.25cm^{-1}, 1.0cm^{-1} and 2.0cm^{-1}. The correlation functions calculated from these peaks showed no measurable difference from the one calculated from the 0.5cm^{-1} sampled peak. Good linearity in the first 4 picoseconds was obtained and oscillations at the longer times were still present. Clearly, the sampling interval size is not as important as the other

factors in determining the correlation function. Our experiments were conducted with a sampling interval of $0.5cm^{-1}$ which was felt to be sufficient to adequately sample the peak, since the resolution due to the spectral bandpass was $1.0cm^{-1}$, but wide enough to avoid spending excessively long periods of time in obtaining spectra.

C. Data Precision

To plot the correlation functions shown in Fig. 9, 10 and 11 for the aligned liquid crystal samples, average values for points every 1.67 picoseconds apart were first calculated. Then the points were connected to give the continuous lines seen. The average value points were calculated from the correlation function points computed from two spectra for each alignment. In Fig. 46, 47, and 48 are shown the range of values that contributed to these averages. Since all the data points are spaced 1.67 picoseconds apart, it was necessary to displace some error bars to the left and the right of the true position so that they would not all overlap. Located at the proper positions every 1.67 picoseconds apart are the error bars for the correlation functions calculated from the isotropic phase mesogen spectra. These error bars are emphasized by horizontal bars placed on top and bottom so that they look like I. To the right of them are shown the error bars for the nematic results. To the left are shown the error bars for the smectic results.

In the first 3 picoseconds the error bars overlap closely supporting the statement that all these correlation functions are identical. The overlap of the error bars is not perfect. However,

FIG. 46. Range of values that contributed to the average values of C_{VH} plotted in Fig. 9, (homeotropic results).
See explanation of the plotting technique on page 189. Note that the ordinate scale is expanded for clarity; the lowest ordinate value is 0.015.

FIG. 47. Range of values that contributed to the average values of C_{VH} plotted in Fig. 10 (planar S results). See explanation on page 189. Note expanded ordinate scale.

FIG. 48. Range of values that contributed to the average values of C_{VH} plotted in Fig. 11 (planar L results). See explanation on page 189. Note expanded ordinate scale.

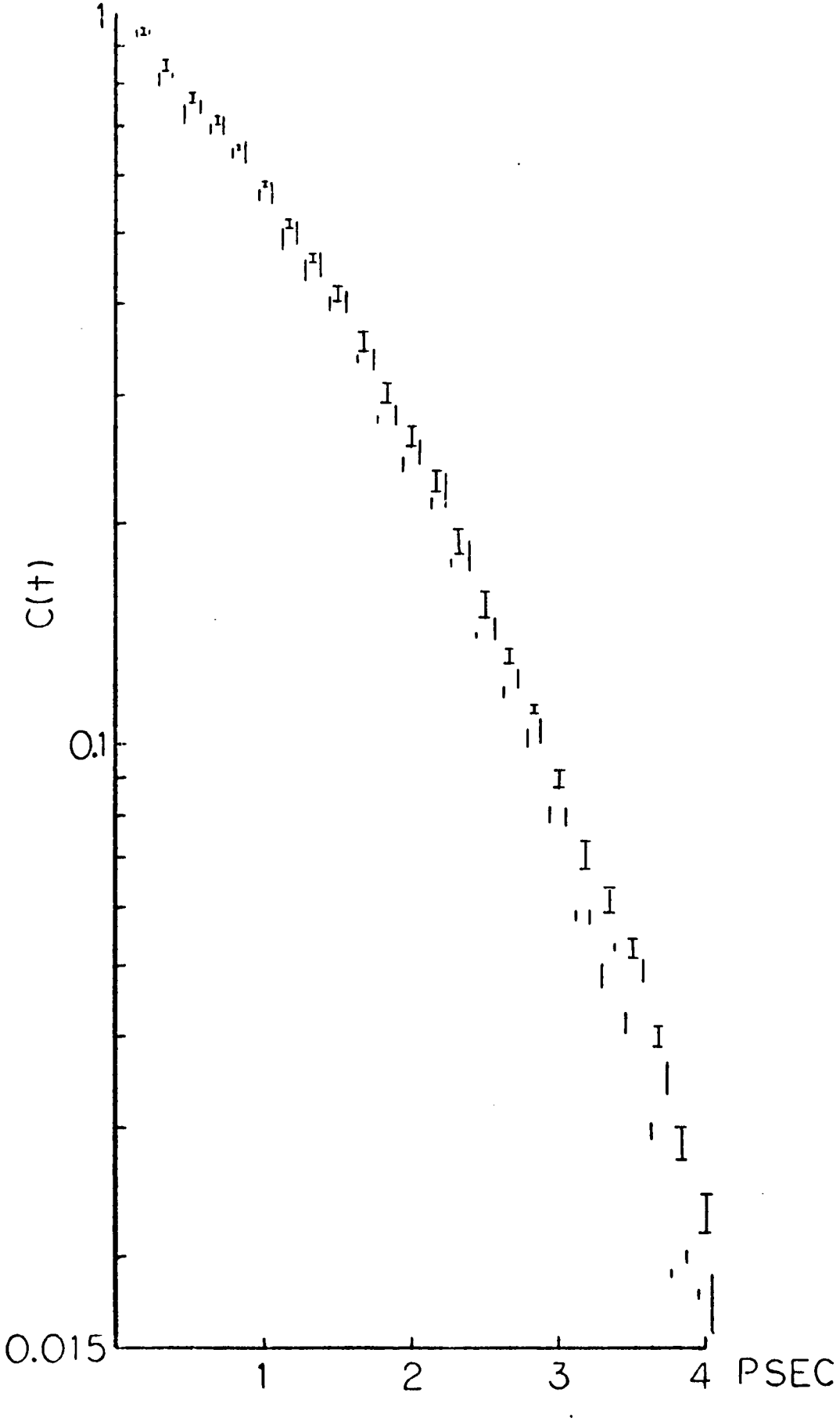
1
0.1
0.015
C(+)
1
2
3
4
PSEC

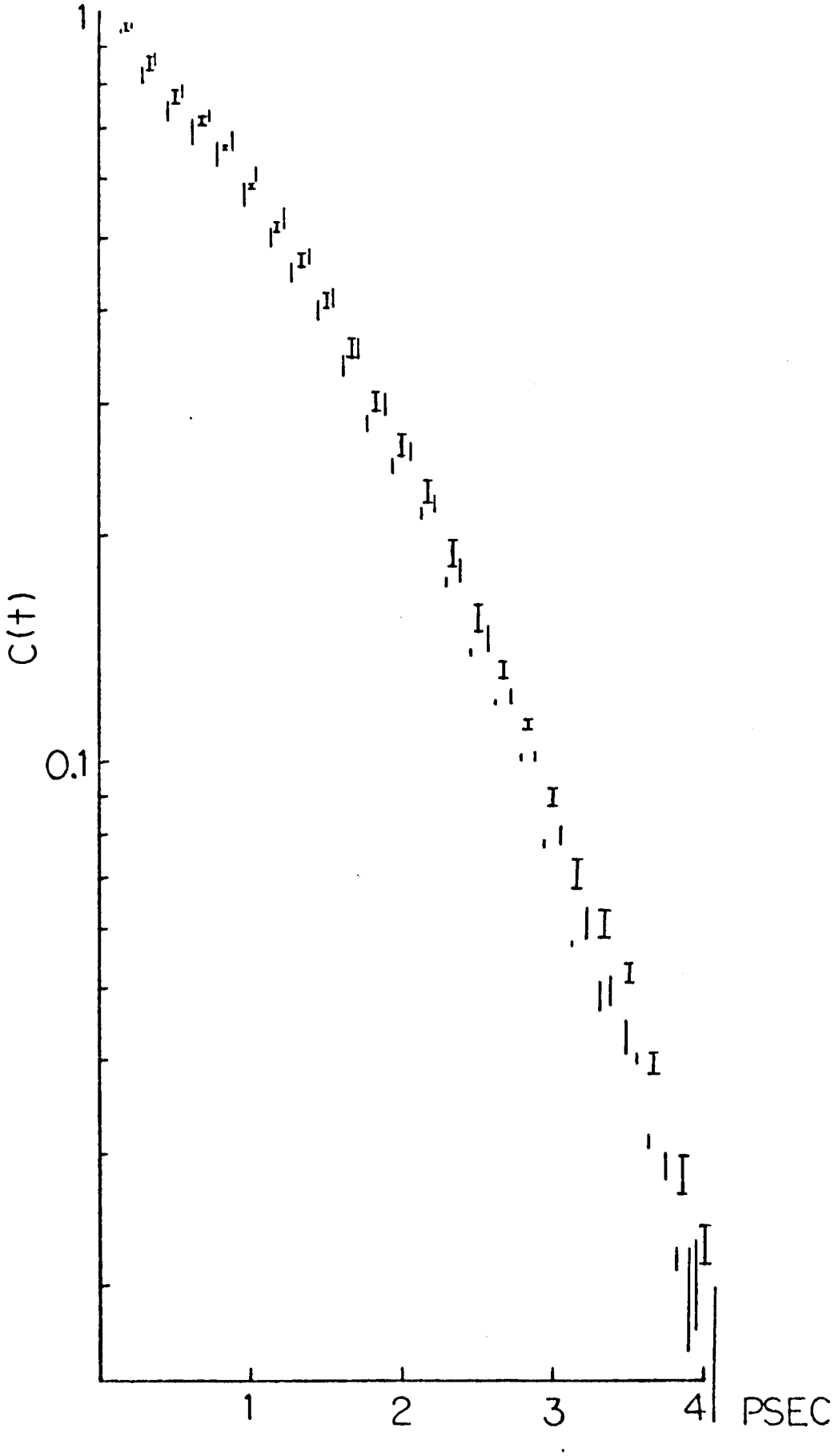
1
0.1
C(+)
1
2
3
4
PSEC

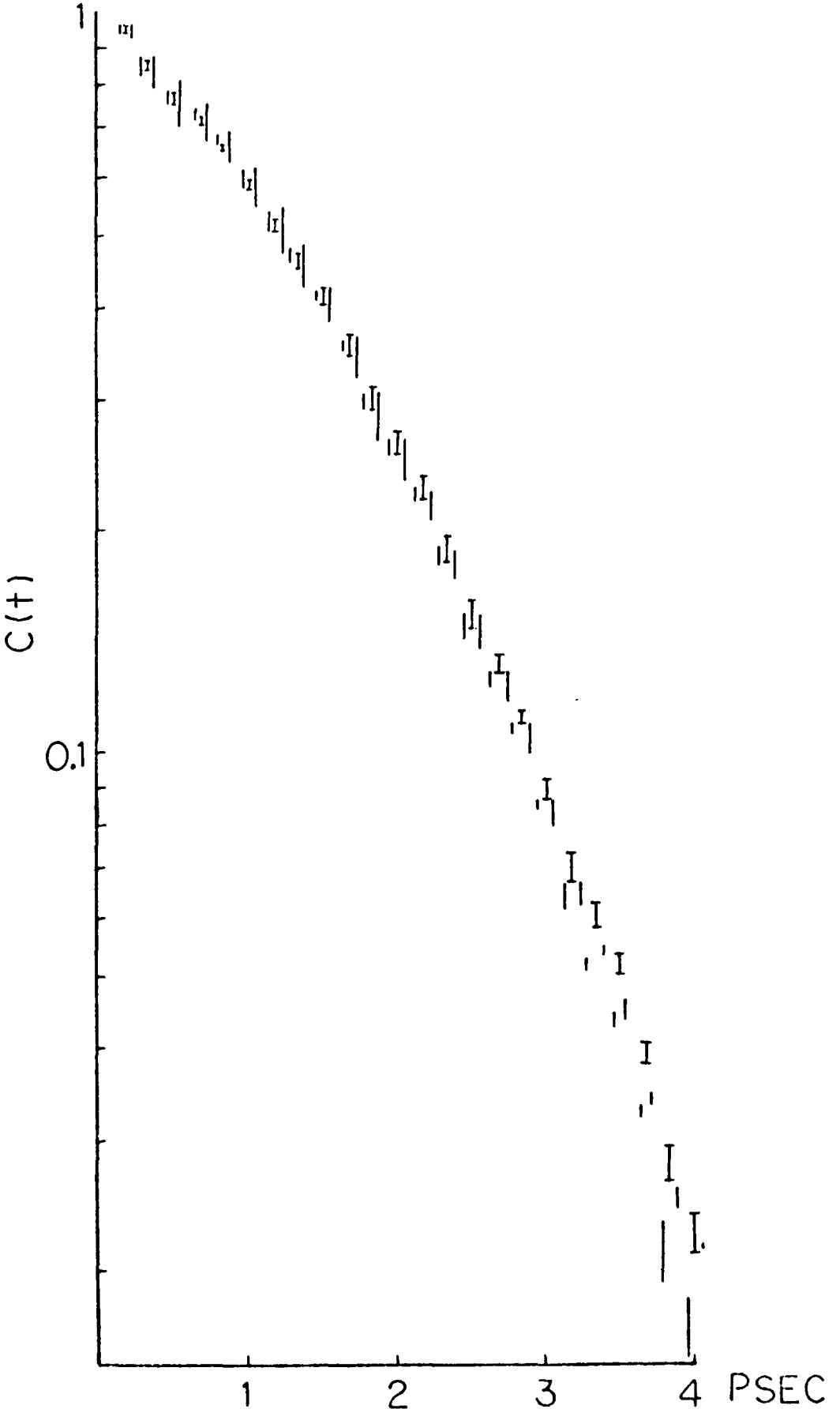
1
0.1
C(+)
1
2
3
4
PSEC

if it is recalled that the continuous line correlation functions from the smectic and nematic phase data showed the mild dips and mild oscillations characteristic of slightly perturbed and displaced correlation functions, then it is realized that the overlaps shown are indeed quite good and probably are actually better.

In the 3-4 picosecond range, the error bars grow in size and don't overlap well. Accumulation of arithmetic and data errors have begun to affect the results. This effect seems to occur to a greater degree with the less intense, more noisy peaks. The work with the Lorentzian bandshapes indicated that only when a very intense peak was used for the calculation of a correlation function could the oscillation be removed in the 4-6 picosecond range. The smectic spectra used for the calculation of the correlation functions varied from each other in intensity because of the experimental technique used; this was true for the nematic phase spectra also. Consequently, the effect of the accumulation of errors on the correlation functions calculated from these less intense spectra, though large for all of them, was larger for some than for others. Since some of the correlation functions already had a component of oscillation from noise contributions, a large range of values at approximately 4 picoseconds is not unexpected. It should be noted that the oscillations grew so large and non periodic after 4 picoseconds that the correlation functions had to be truncated at the 4 picosecond mark. Therefore, it is concluded that the differences between the correlation functions in the 3-4 picosecond range are not real. It is assumed that were better experimental results possible for these samples the

match between the correlation functions seen in the 0-3 picosecond range would be observed in the 3-4 picosecond range.

In Fig. 49 are shown the rangesof values that contributed to the average valued points for the correlation functions obtained from the spectra of the 80CB in benzene. These solution results are typical of the other solutions. For the first 2 picoseconds, the system of displaced error bars is used for the three solutions. The ranges of values for the 0.14 mole fraction results are located at the correct time positions. These ranges are shown as I. Slightly displaced from each I to the right is the error bar for each point calculated from the 0.04 mole fraction solution. To the left is the error bar for each point calculated from the 0.51 mole fraction solution. The ranges for the isotropic results are included and placed in their proper positions. Below 0.5 picoseconds, the ranges from the isotropic results begin to interfere with those from the solutions and have been left out. To see their magnitude in this range, one only has to look at Fig. 46 since the isotropic result plotted there is identical to the one plotted here. In the 2-4 picosecond range the error bars will not overlap and obscure each other. The continuous line correlation functions have been drawn. The ranges of values are placed at the proper positions on each curve. This placement of the error bars in the 2-4 picosecond range will allow it to be seen if the magnitudes of the curve differences are real.

The solution spectra were of much better quality than those from the aligned liquid crystals. Positioning of the capillary tubes, containing the samples, in the Spex 1401 sample chamber so as to achieve maximum intensity was much easier than positioning the

FIG. 49. Rangesof values that contributed to the average values of C_{VH} obtained from spectra of 80CB dissolved in benzene and also from spectra of the isotropic phase 80CB. See explanation on page 195 for plotting technique. Note expanded ordinate scale.

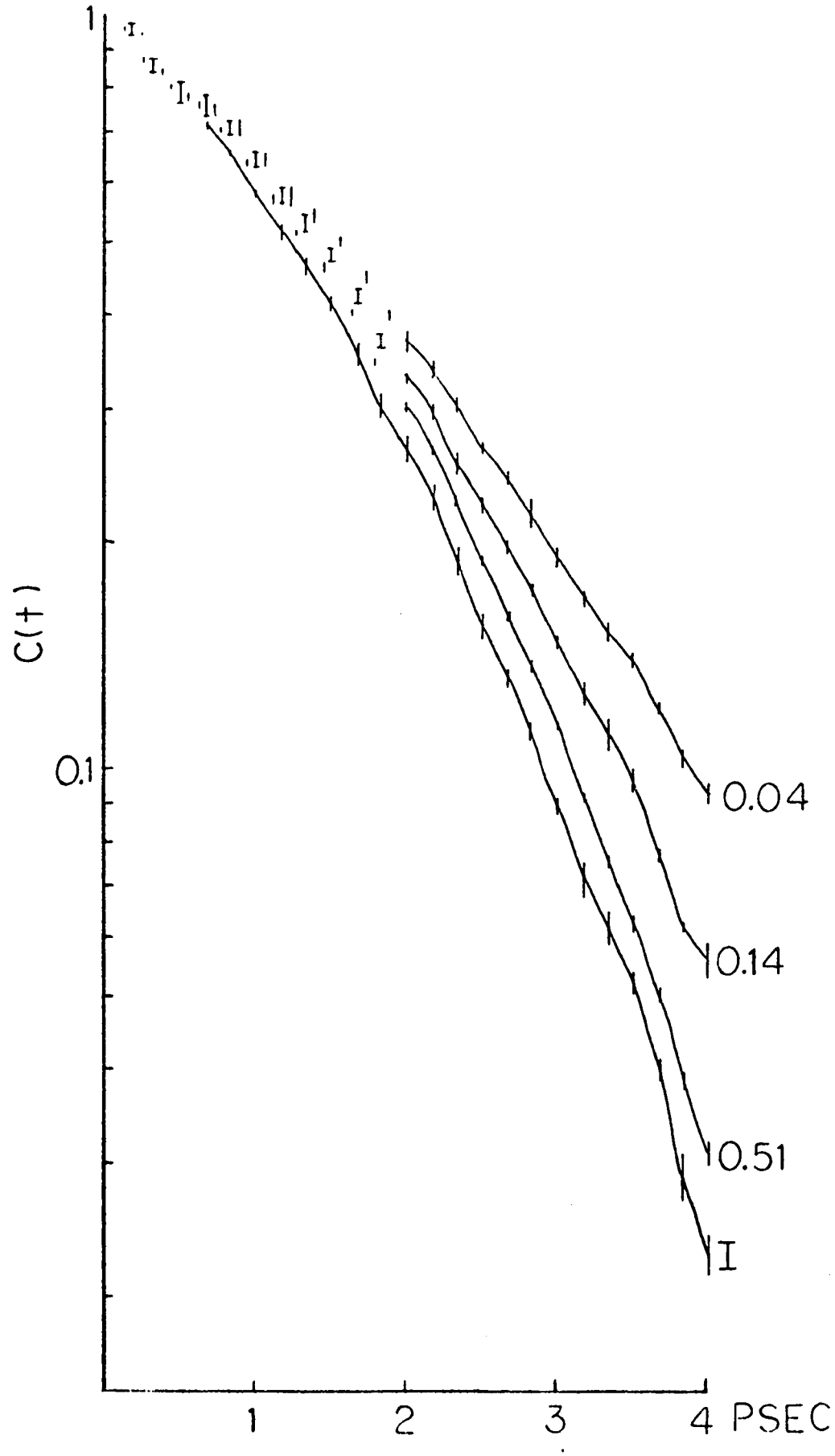
1
0.1
C(+)
0.04
0.14
0.51
I
1
2
3
4 PSEC

microscope slides which contained the aligned liquid crystals. Much greater intensity for the cyano stretching peak was obtained with the solutions than with the aligned liquid crystals. Also, the J-Y Instruments HG2S spectrometer was used with a number of samples, especially the dilute ones. As was mentioned in Chapter Three, this machine leads to intense peaks with high signal to noise ratios.

The improved intensity and signal to noise ratios of the solution spectra is reflected in the much smaller error bars shown in Fig. 49. In the 2-4 picosecond range the error bars are not nearly as large as those seen in Fig. 46, 47, and 48. Note that there are virtually no oscillations in this region as well. The evidence suggests that the influence of the accumulation of errors that was so strong for the aligned liquid crystal results is not strong here. That the error bars do not overlap in this region also strongly suggests that the differences among the curves are real. Indeed, the spectra show differences in FWHH for the solutions of different concentrations. Since, as was pointed out in Chapter Two, and in this chapter, differences in the FWHH can be related to molecular motions, it is expected that differences in the correlation functions would be seen. One reservation must be included for the correlation function obtained from the 0.51 mole fraction solution. Its displacement from the correlation function obtained from the isotropic spectra is probably significant since their error bars do not overlap at all except at very short time. In addition, the FWHH of each of the spectra used for the computations of the correlation function of the solution was $8.4cm^{-1}$ com-

pared to $9.1cm^{-1}$ for each of the isotropic spectra. It must be kept in mind, though, that the separation between these correlation functions is of the order of magnitude of the separation, at longer times, between the correlation functions calculated from the aligned liquid crystal results. For those results that separation was considered not to be important.

It should be noted that the error bars drawn in the 0-2 picosecond range once again indicate that when the continuous line correlation functions seem to be very close and virtually identical, they indeed are.

In Fig. 50 is shown the I_{vib} spectrum obtained from the isotropic phase 80CB spectra. Recall that I_{vib} is a computed spectrum that results from subtracting 4/3 the I_{VH} spectrum from the I_{VV} spectrum. The I_{VH} and I_{VV} spectra were moderately weak; the I_{VH} one had a maximum intensity of approximately 300cps and the I_{VV} spectrum had a maximum of approximately 600cps. Though long count times minimized the noise variations in the wings and baseline, the subtraction procedure apparently accentuated them. When the Fourier transform was computed from the 200 point spectrum shown, in order to get the vibrational relaxation correlation function, a large dip and large oscillations occurred. This is not surprising since the spectrum shows large noise fluctuations as well as a high frequency rise. A second I_{vib} spectrum calculated from another set of spectra showed the same features of high noise and baseline rise. In order to extract information on vibrational relaxation, two modifications of the two I_{vib} spectra were made. First, an anomalously low point appearing in the beginning of each spectrum was removed by setting

FIG. 50. I_{vib} obtained from I_{VH} and I_{VV} spectra of isotropic phase 80CB. (Spex)

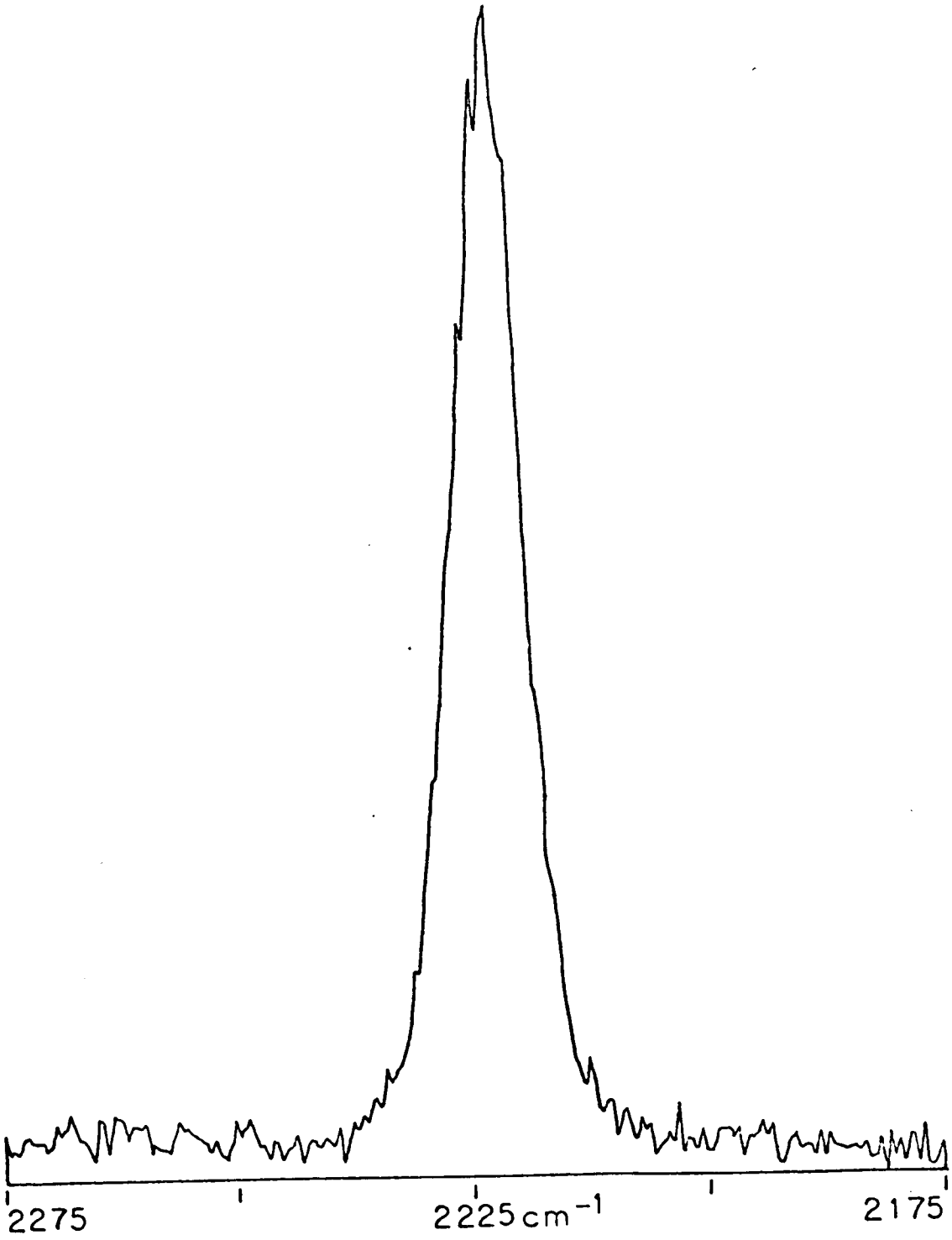
2275
2225 cm⁻¹
2175

it equal to the average of the preceding and succeeding values. Then once again the minimum value in the spectrum was set equal to zero, as described in Chapter Four. This operation had the effect of lowering the baseline somewhat. Secondly, the high frequency end of each spectrum was truncated so that the whole spectrum was defined by 167 points. The result of these modifications for one I_{vib} spectrum is shown in Fig. 51.

There are a number of justifications for the modifications made. It was shown previously that large noise fluctuations in the wing and baseline regions establish a baseline that is abnormally too high. The high baseline is caused by the downmost fluctuations defining the zero level. When a single low value point is clearly creating the same situation, it seems plausible to offset its effect by removing it and lowering the baseline values. It was also shown that truncations of the cyano stretching peaks had little effect on the correlation functions. The truncation performed on the data discussed here was done only on one side of the peak. This brings the high frequency side to an end closer to the peak center than when the truncation to 167 points was done by removing values at each end. Note, however, that this one sided truncation still does not bring the high frequency end to the point near the peak center that the truncation to 84 points did. For that extreme truncation, little significant effect was seen except in the short time scale results. Therefore, it is concluded that the truncation procedure performed on I_{vib} will not distort significantly the results of the Fourier transform calculation.

FIG. 51. I_{vib} of Fig. 50 with low point removed, minimum set equal to zero again, and high frequency baseline truncated.

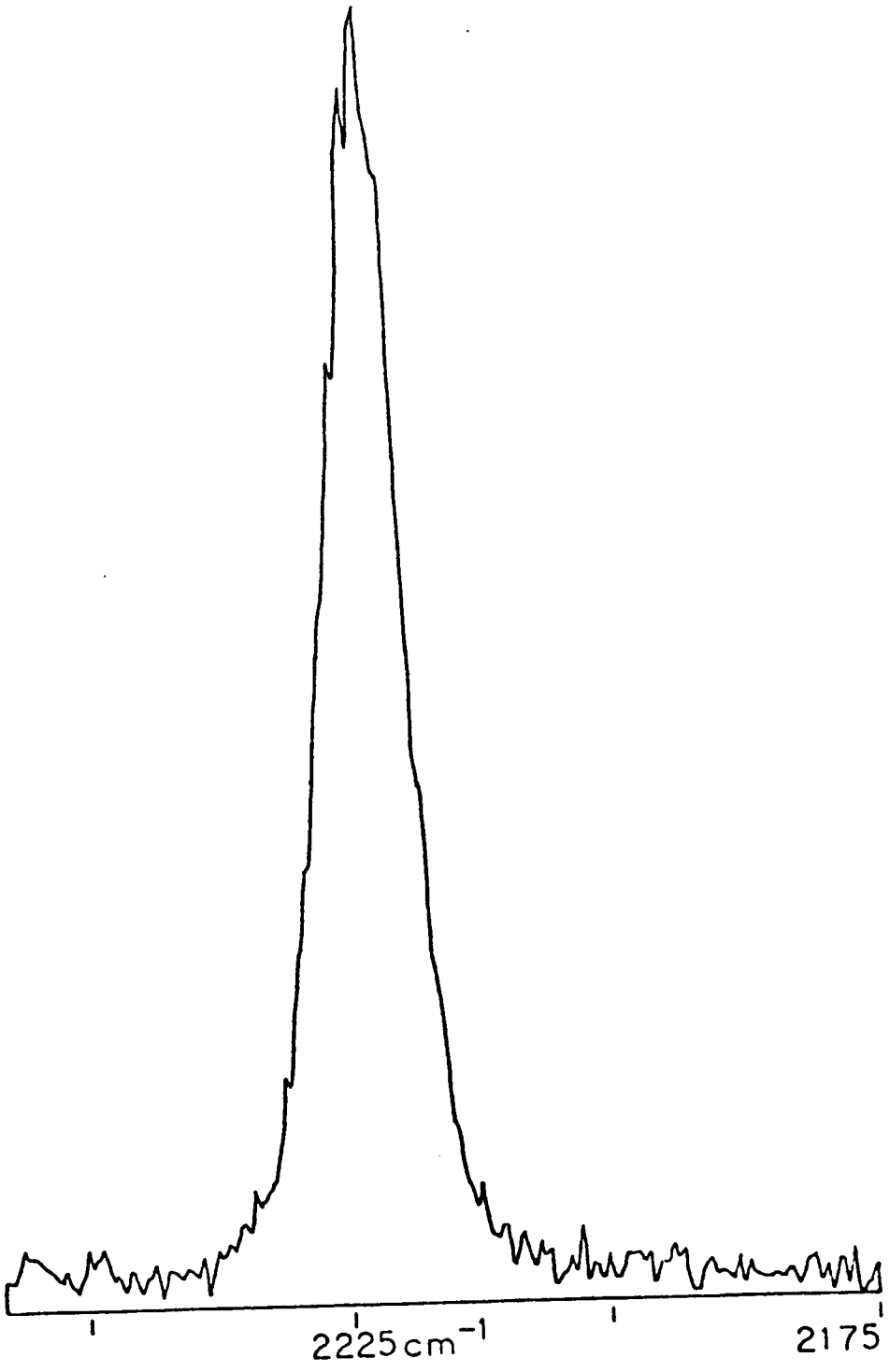
2225 cm⁻¹
2175

The ranges of values that were used for calculating the average vibration correlation function values are shown in Fig. 52. The correlation function calculated from the I_{VH} spectra of the isotropic phase 8OCB is also included. Despite the modifications in the I_{vib} spectra, the ranges are large, especially in the 3-4 picosecond range. This indicates that there are still perturbing aspects present in each I_{vib} spectrum that exist in each to different degrees. Presumably, it is mostly the noise differences. The rangesof values do, nevertheless, overlap very closely with the correlation function from the isotropic results. Examination of correlation functions, presented in the literature, [18, 39] for cases where rotational motion influences the correlation functions calculated from the I_{VH} spectra indicates that the separation between the vibrational correlation function and that from the I_{VH} spectrum is quite large, larger than the error bars shown in Fig. 52. In Fig. 53 is shown a reproduction of one such case from Rothschild's work.[39] Consequently, it is concluded that the two correlation functions shown in Fig. 52 are identical. Further support for this conclusion was given earlier in this chapter. In that discussion of these same results, it was pointed out that if the vibrational relaxation correlation function was identical to the one from the I_{VH} spectrum, then the correlation function calculated from the I_{VV} spectrum should be the same as that calculated from the I_{VH} one. This was shown to indeed be true.

In Fig. 54 is shown a vibrational relaxation correlation function with its error bars that is typical, in the range of contributing values, of the solution results. The correlation function

FIG. 52. C_{vib} calculated from I_{vib} of Fig. 51. Placed on C_{vib} are bars which indicate the range of values that contributed to the average values that are plotted as C_{vib}. Included also is C_{VH} calculated from I_{VH} spectra of the isotropic phase 8OCB.

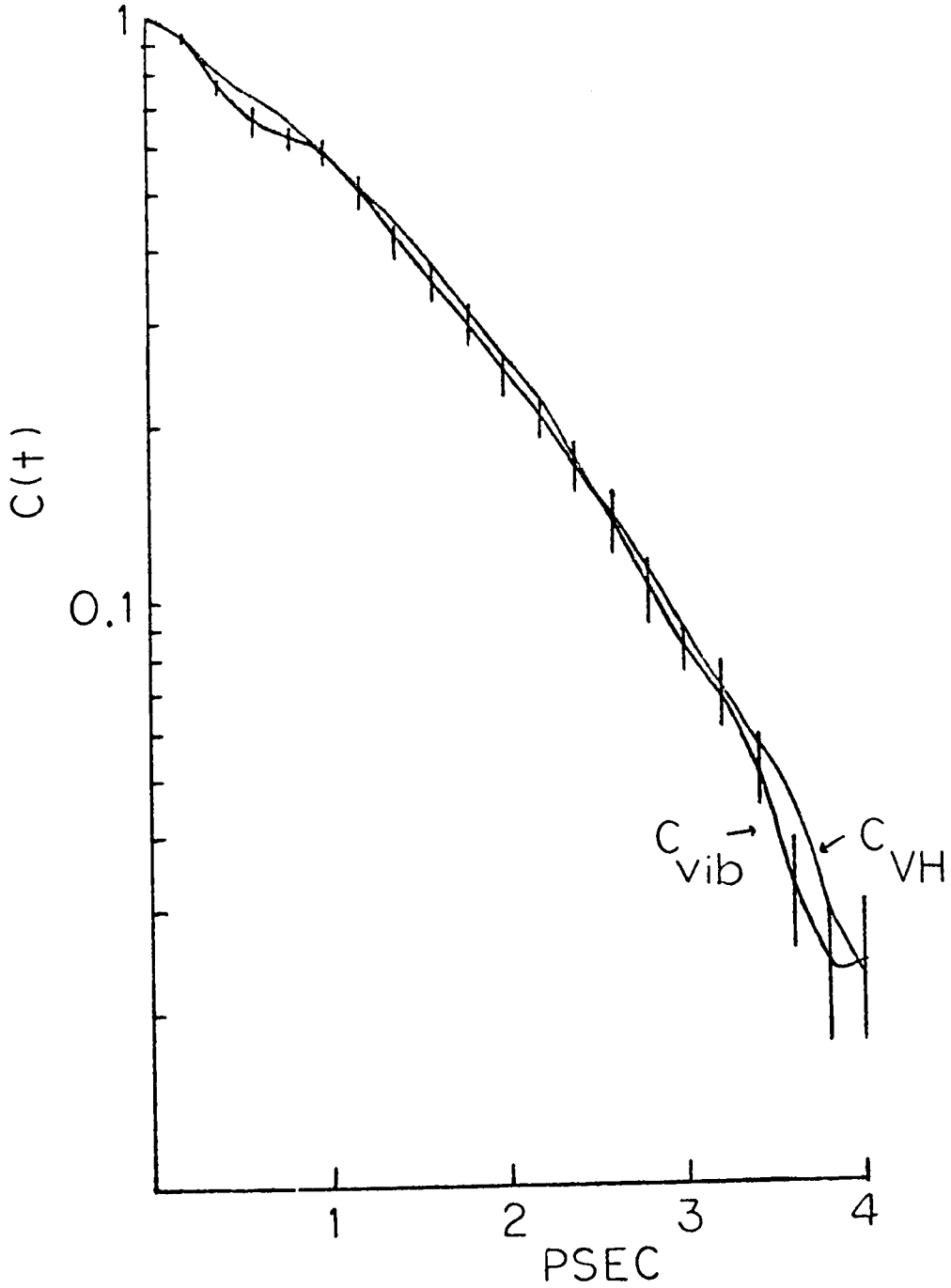
1
0.1
C(+)
C_{vib}
C_{VH}
1
2
3
4
PSEC

FIG. 53. Comparison of C_{vib} with C_{VH}, obtained from I_{VH} and I_{VV} spectra of the ν_1 band of chloroform. Diagram based on that of reference 39.

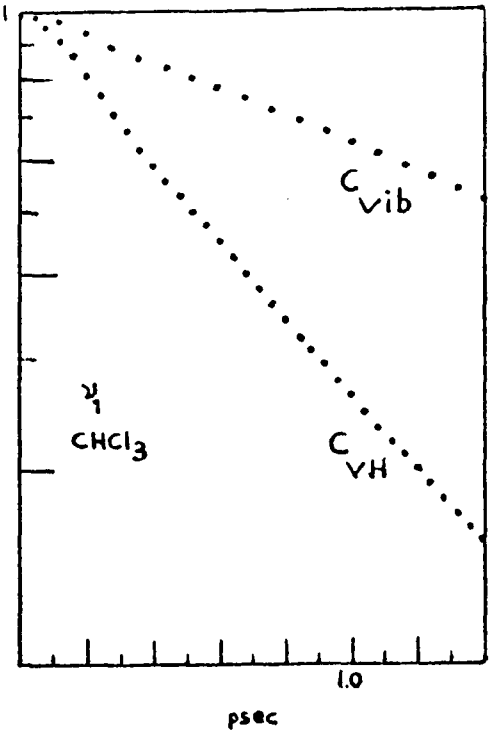
C_{vib}
ν_1
$CHCl_3$
C_{VH}
1.0
psec

FIG. 54. The ranges of values that contributed to the average values of C_{vib} plotted in Fig. 18. The C_{vib} values were calculated from I_{vib} obtained from I_{VH} and I_{VV} spectra of a 0.04 mole fraction solution of 8OCB in benzene. Also included is C_{VH} calculated from I_{VH} of the same solution.

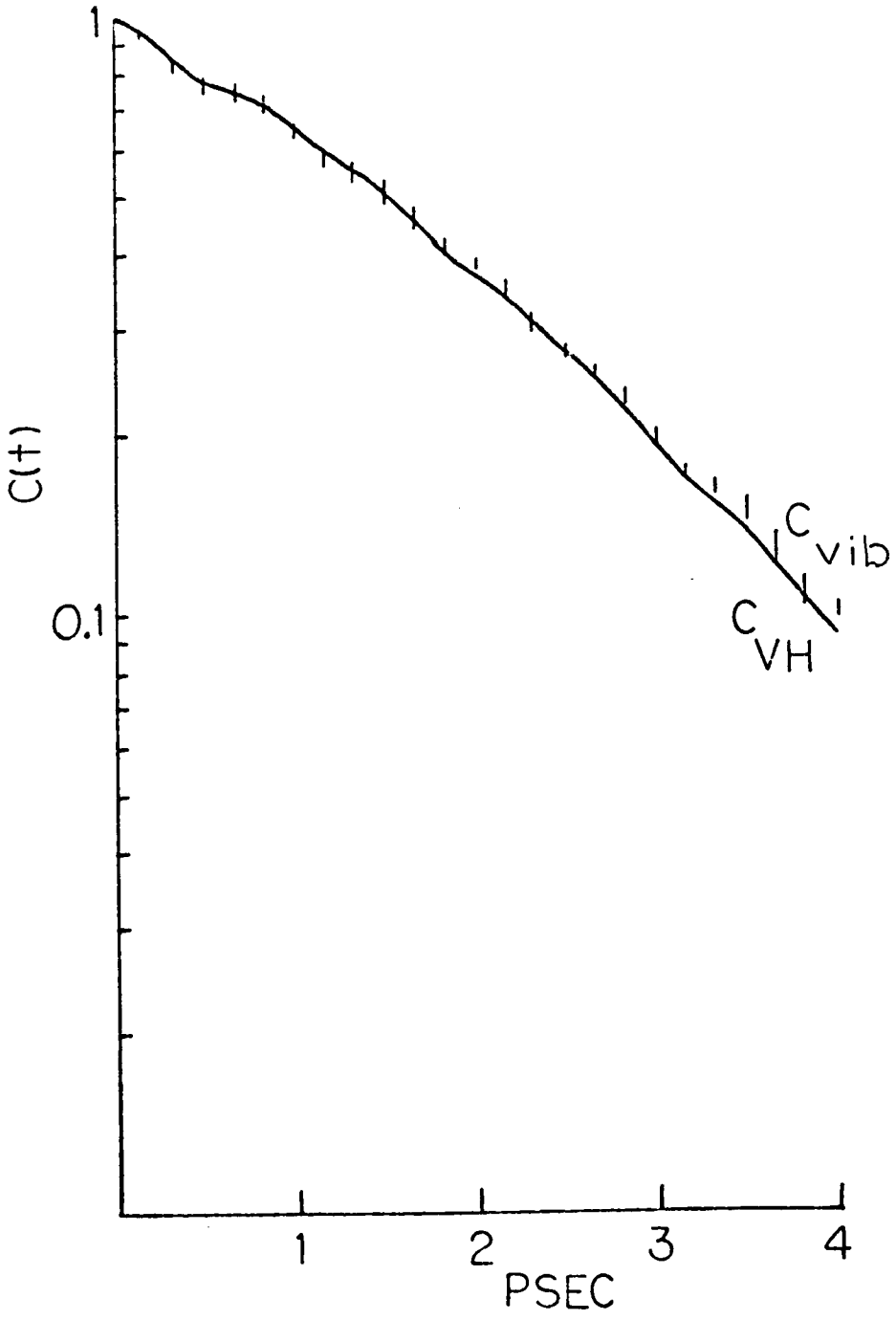
1
0.1
C(t)
C vib
C VH
1
2
3
4
PSEC

calculated from the I_{VH} spectra is also shown. As a result of improved intensity of the I_{VH} and I_{VV} spectra, none of the modifications of the I_{vib} spectra just described were necessary. Note, that the precision of the vibration relaxation correlation function results is also improved. It seems clear that the two correlation functions shown match closely.

CHAPTER VII

SUMMARY AND SUGGESTED PROJECTS

Can correlation functions be used to determine differences in rotational motion between the smectic, nematic and isotropic phases of a liquid crystal? At least for the system discussed in this thesis, the answer is no. Correlation functions did reveal significant information about the vibrational relaxation processes present in the liquid crystal samples.

Under certain conditions it might be possible to use correlation functions to examine rotational motion in liquid crystals. If the signal-to-noise ratio in the wings of a band could be greatly increased, then information in the 0-1 picosecond range of the correlation function would be revealed. In our studies this range was obscured by noise induced dips. It is in this time period that the rather small changes in rotational motions between phases, if they exist, might show up. Correlation functions would then provide useful information.

If a band more sensitive to rotational motion were examined, correlation functions might again be useful. In a recent study[69] of a liquid crystal containing a C≡C bond directed along the long molecular axis, changes in the FWHH of the stretching band were observed. Such a band would probably be amenable to a correlation function analysis. It has also been suggested[70] that certain vibrational modes of

a liquid crystal molecule might be particularly sensitive to rotations of the constituent benzene rings. Those modes could be examined using the correlation function approach.

The results presented in this thesis do not negate the intrinsic advantage of correlation functions over an analysis of peak FWHH as typified by the work of Bartoli and Litovitz. When changes in the FWHH were observed, so were changes in the correlation functions. When the FWHH remained constant for different samples, so did the correlation function. It was seen that changes in the form as well as the decay of the correlation function were revealing about molecular processes. This is the inherent advantage over the FWHH approach. Only when a FWHH examination is combined with a quantitative lineshape analysis, can such an approach be almost as revealing as the correlation function approach. It is clear from the present work that were better experimental and computational results possible, further information about molecular processes would be available from curves that were observed to merely change in FWHH.

The above comments and the experimental results obtained in this work suggest a number of research projects, some simple and some complex. Since the intensity of the vibrational peak played an important part in the accuracy of the correlation functions obtained from it, work on the present system could be repeated under conditions of improved intensity and signal to noise ratio. The intensity could be improved by using a more sensitive instrument such as the J-Y HG 2S Raman spectrometer. The intensity could further be increased using wider slits. Then a computer program could be developed to remove the instrumental function that would be convolved with the actual peak.

Increase in intensity would improve the signal-to-noise ratio in the wings where it is so badly needed. This ratio could further be improved by using even longer integration times than those used in this work, limited only by the endurance of the investigator. Since the cyano stretching band has been shown to be dominated, in the liquid crystal by vibrational relaxation, it is expected that repeating the work under better experimental conditions would not yield new information except possibly in the 0-1 picosecond range of the correlation function.

As was mentioned previously, other liquid crystal systems that have vibrational modes more sensitive to rotational motion could be studied. Along these same lines, probe molecules could be inserted in the liquid crystal. Liquid crystal molecular motion could be deduced from changes in the vibrational spectrum of the probe. Some preliminary work was done in our laboratory using CH_3SCN as a probe in the 4-Octyloxy-4'-cyanobiphenyl. This molecule did dissolve in the liquid crystal and offered the advantage of a cyano stretching peak far from the one due to the liquid crystal. The correlation functions from both peaks could be observed. Changes in each could be related to molecular changes in both the liquid crystal and the probe. Using a volatile probe like CH_3SCN requires a sealed sample cell to prevent its loss. Such a cell was not convenient to use under our experimental conditions. Furthermore, there is virtually no theoretical framework in which to explain the correlation function results obtained from the Raman spectra of a probe molecule in an anisotropic medium. Such a framework would have to be developed.

The work on solutions presented in this thesis suggests an interesting further project. The liquid crystal studied and other larger slowly rotating molecules such as quinoline could be dissolved in a variety of solvents. The connection between solvent molecular size, shape and polarity and motional narrowing could possibly be established from Raman and infrared spectroscopy. The important condition of the slow rotation of the molecules could be established by NMR and dielectric relaxation studies. The existence of slowly rotating clusters of mesogen molecules in the solvents could be examined by far infrared spectroscopy since it is in this region of long wavelengths that such rotation would be spectroscopically apparent. For those solvent systems that showed no change in the correlation functions with dilution, temperature studies could be conducted. If solvent dipoles were causing clusters, the increase in temperature should lead to spectroscopic and correlation function changes as the clusters were broken up.

Further examination of the various vibrational relaxation processes in the liquid crystal system could be pursued both on a theoretical path and an experimental one. Using the formalism of Rothschild, et.al.,[39, 56] and Valiev[55] the actual band broadening contributions of dipole-dipole energy dissipation and resonance vibrational energy transfer could be calculated. Using the dephasing formalism,[54] correlation functions could be calculated for slow and fast modulations of the vibrational frequency. Calculating the inverse Fourier transform of the correlation function would yield a predicted vibrational band. Its shape and FWHH could be compared with the experimentally obtained one[54] and provide a measure of the

accuracy of the dephasing model for the liquid crystal system studied.

Experimentally, the importance of resonance vibrational energy transfer could be further evaluated for the liquid crystal by an isotopic dilution experiment.[64] This would require the synthesis of the liquid crystal with the cyano group containing C^{13} and N^{15} atoms. The vibrational frequency of the isotope substituted liquid crystal would be shifted to a lower frequency than the 2225 cm^{-1} of the unsubstituted liquid crystal. As the concentration of the unsubstituted liquid crystal was decreased in the isotopically substituted one, the band should narrow and the correlation function change as resonance vibrational energy transfer is removed. The removal of the energy transfer is predicated, of course, on its existence and on the inability of the unsubstituted molecule to transfer vibrational energy to a mode with a different frequency. However, the change in frequency due to the isotopic substitution would be small since the changes in mass are small. It is quite possible that transfer would still be present between the unsubstituted molecules and the substituted ones. Therefore, though this experiment seems worthwhile, the prognosis for its success in revealing the degree of resonance vibrational energy transfer is not good.

A well financed investigator might consider examining the liquid crystal using picosecond stimulated Raman scattering.[71] The dephasing time could be measured directly and then compared with that from spontaneous Raman scattering experiments.[60] Such an experiment could establish the importance of the dephasing mechanism in broadening the cyano stretching peak of the liquid crystal. However, the

intensity of stimulated Raman scattering is related inversely to the band FWHH.[72] For the broad band of the cyano stretch, the gain in intensity of the stimulated Raman effect might not be large enough to make this experiment possible.

The work on the solid phase liquid crystal suggests that the examination of a single crystal of the substance would be interesting. The effects of temperature changes on the spectrum and correlation functions as the crystal is heated to just below its transition temperature might be revealing of the packing changes postulated in this thesis. A similar study was conducted on a monocrystal of the liquid crystal terephtal-bis-butyl-aniline[15] and offers a model for conducting this experiment.

REFERENCES

1 A. De Vries, Mol. Cryst. Liquid Cryst. 11, 361 (1970).

2 G. R. Luckhurst, M. Setaka, and C. Zannoni, Mol. Phys. 28, 49 (1974).

3 Z. Luz and S. Meiboom, J. Chem. Phys. 59, 275 (1973).

4 M. Evans, M. Davies, and I. Larkin, J. Chem. Soc., Faraday Trans. II 69, 1011 (1973).

5 N. M. Amer and Y. R. Shen, J. Chem Phys. 56, 2654 (1972).

6 C. J. Carlile and K. Krebs, Mol. Cryst. Liquid Cryst. 29, 43 (1974).

7 M. Schadt, J. Chem. Phys. 56, 1494 (1972).

8 V. K. Agarwal and A. H. Price, J. Chem. Soc., Far. Trans. II 70, 188 (1974).

9 F. Rondelez and A. Mircea-Roussel, Mol. Cryst. Liquid Cryst. 28, 173 (1974).

10 E. T. Samulski, C. R. Dybowski, and C. G. Wade, Phys. Rev. Lett 29, 340 (1972).

11 B. J. Bulkin, in "Advances in Liquid Crystals" (G.H.Brown, ed.), Vol. 2, pp. 199-231. Academic Press, New York, 1976.

12 B. J. Bulkin and F. T. Prochaska, J. Chem. Phys. 54, 635 (1971).

13 S. Jen, N.A. Clark, P.S. Pershan, and E. B. Priestley, Phys. Rev. Lett. 31, 1552 (1973).

14 J. M. Schnur, Phys. Rev. Lett. 29, 1141 (1972).

15 M. P. Fontana and S. Bini, Phys. Rev. A, 14, 1555 (1976).

16 F. J. Bartoli and T. A. Litovitz, J. Chem. Phys. 56, 404 and 413 (1972).

17 R. G. Gordon, Advan. Magn. Resonance 3, 1 (1968).

18 W. G. Rothschild, J. Chem. Phys. 57, 991 (1972).

19 H. S. Goldberg and P. S. Pershan, J. Chem. Phys. 58, 3816 (1973).

[20] S. Lugomer, Mol. Cryst. Liquid Cryst. 29, 141 (1974).

[21] M. Evans, J. Chem. Soc., Faraday Trans. II 71, 2051 (1975).

[22] M. Born and K. Huang, "Dynamical Theory of Crystal Lattices", Clarendon, Oxford, 1956.

[23] A. A. Maradudin, in "Solid State Physics" (F. Seitz and D. Turnbull, eds.). Vol. 19, p. 1. Academic, New York, 1966.

[24] R. Callender and P. S. Pershan, Phys. Rev. A, 2,672 (1970)

[25] G. Placzek, in "Rayleigh and Raman Scattering", UCRL Trans. No. 526L from: "Handbuch der Radiologie" (E. Marx, ed.), Akademische Verlagsgesellschaft VI 2, p. 205; available from National Technical Information Service, U.S. Dept. of Commerce, Springfield, Va.

[26] L. A. Nafie and W. L. Peticolas, J. Chem. Phys. 57, 3145 (1972).

[27] W. M. McClain, J. Chem. Phys. 55, 2789 (1971).

[28] L. N. Ovander, Opt. Spectry. 9, 302 (1960).

[29] E. B. Wilson, J. C. Decius, and P. C. Cross, "Molecular Vibrations", McGraw-Hill, New York, 1955.

[30] R. G. Gordon, J. Chem. Phys. 43, 1307 (1965).

[31] R. G. Gordon, J. Chem. Phys. 42, 3658 (1965).

[32] N. Davidson, "Statistical Mechanics". McGraw-Hill, New York, 1962.

[33] T. M. Reed and K. E. Gubbins, "Applied Statistical Mechanics", McGraw-Hill, New York, 1973.

[34] A. Abragam, "The Principles of Nuclear Magnetism", Clarendon, Oxford, 1961.

[35] M. C. Wang and G. E. Uhlenbeck, Rev. Mod. Phys. 17, 323 (1945).

[36] J. F. Nye, "Physical Properties of Crystals". Oxford Univ. Press, London, 1957.

[37] A. V. Rakov, Opt. Spectrosc. 7, 128 (1959).

[38] P. Simova and N. Kirov, Advan. Mol. Relaxation Processes 5, 233 (1973).

[39] W. G. Rothschild, G. J. Rosasco and R. C. Livingston, J. Chem. Phys. 62, 1253 (1975).

40 G. W. Gray, K. J. Harrison, J. A. Nash, J. Constant, D. S. Hulme, J. Kirton and E. P. Raynes in "Liquid Crystals and Ordered Fluids" (R. Porter and J. Johnson, eds.), Vol. 2, pp. 617-643. Plenum, New York, 1973.

41 J. L. Janning, Appl. Phys. Lett. 21, 173 (1972).

42 W. Urbach, M. Boix and E. Guyon, Appl. Phys. Lett. 25, 479 (1974).

43 G. D. Dixon, T. P. Brody and W. A. Hester, Appl. Phys. 24, 47 (1974).

44 J. E. Proust, L. Ter-Minassian-Saraga and E. Guyon, Solid State Commun. 11, 1227 (1972).

45 E. A. Wood, "Crystals and Light", Dover, New York, 1977.

46 N. H. Hartshorne and A. Stuart, "Crystals and the Polarising Microscope", American Elsevier, New York, 1970.

47 J. E. Griffiths, J. Chem. Phys. 59, 751 (1973).

48 E. O. Brigham, "The Fast Fourier Transform", Prentice-Hall, Englewood Cliffs, 1974.

49 G. E. Ewing, Acc. Chem. Res. 2, 168 (1969).

50 C. E. Favelukes, A. A. Clifford and B. Crawford, J. Phys. Chem. 72, 962 (1968).

51 T. Fujiyama and B. Crawford, J. Phys. Chem. 73, 4040 (1969).

52 R. P. Young and R. N. Jones, Chem. Rev. 71, 219 (1971).

53 P. Debye, "Polar Molecules". Dover, New York, 1928.

54 W. G. Rothschild, J. Chem. Phys. 65, 455 (1976).

55 K. A. Valiev. Opt. Spectrosc. 11, 253 (1961).

56 T. Tokuhiro and W. G. Rothschild, J. Chem. Phys. 62, 2150 (1975).

57 B. Di Bartolo, "Optical Interactions in Solids". John Wiley, New York, 1968.

58 T. T. Wall, J. Chem. Phys. 51, 113 (1969).

59 S. Bratos and E. Marechal, Phys. Rev. A4, 1078 (1971).

60 S. Bratos, Y. Guissani, and J. C. Leicknam, in "Molecular Motions in Liquids" (J. Lascombe, ed.), p. 187. Reidel, Dordrecht, 1974.

[61] R. Kubo, in "Fluctuations, Relaxation, and Resonance in Magnetic Systems" (D. Ter Haar, ed.). Plenum, New York, 1962.

[62] D. Halliday and R. Resnick, "Physics". John Wiley, New York, 1966.

[63] S. F. Fischer and A. Laubereau, Chem. Phys. Lett. 35, 6 (1975).

[64] J. E. Griffiths, M. Clerc, and P. M. Rentzepis, J. Chem. Phys. 60, 3824 (1974).

[65] W. G. Rothschild, in "Molecular Motions in Liquids" (J. Lascombe, ed.), p. 247. Reidel, Dordrecht, 1974.

[66] J. E. Lydon and C. J. Coakley, J. Phys. (Paris), Colloq. C1-3, 45 (1975).

[67] D. R. Jones, H. C. Andersen, and R. Pecora, Chem. Phys. 9, 339 (1975).

[68] T. T. Wall, J. Chem. Phys. 52, 2792 (1970).

[69] J. P. Heger, Ph.D Thesis, Swiss Federal Institute of Technology. Lausanne, 1975.

[70] B. J. Bulkin, private communication.

[71] A Laubereau, D. von der Linde, and W. Kaiser, Phys. Rev. Lett. 28, 1162 (1972).

[72] J. B. Grun, A. K. McQuillan, and B. P. Stoicheff, Phys. Rev. 180, 61 (1969).

APPENDIX A

INTERPOLATION

This Appendix consists of two parts. In the first, background material will be developed and the justification for the interpolation method of zero filling will be presented for the case of N points zero extended to 2N. The same kind of reasoning is used for zero filling N points to 3N, 4N, etc. In the second part, the placing of the zeros in the data set and the necessary indexing will be delineated.

Part One

The discrete Fourier transform (DFT) of a set of N points is

$$X(n) = \sum_{k=0}^{N-1} x(k) \exp i2\pi \frac{nk}{N}$$

where n = 0,1,2, ... N-1, X(n) = the nth output point, and x(k) = the kth input data point. The four output points of the N = 4 DFT with the above sum expanded are shown in Table 2. Note that the periodic nature of the exponential is taken into account when figuring nk for the values in the Table.

If we look at the same k value part of the expansion for each output point of the N = 4 DFT, we see four vertical columns corresponding

to k = 0,1,2, and 3. Each succeeding member of each column differs from the previous one

$$X(0)=x(0)+x(1)+x(2)+x(3)$$

$$X(1)=x(0)+x(1)\exp i\frac{2\pi}{4}(1)+x(2)\exp i\frac{2\pi}{4}(2)+x(3)\exp i\frac{2\pi}{4}(3)$$

$$X(2)=x(0)+x(1)\exp i\frac{2\pi}{4}(2)+x(2)\exp i\frac{2\pi}{4}(4)+x(3)\exp i\frac{2\pi}{4}(2)$$

$$X(3)=x(0)+x(1)\exp i\frac{2\pi}{4}(3)+x(2)\exp i\frac{2\pi}{4}(2)+x(3)\exp i\frac{2\pi}{4}(1)$$

k=1 column

TABLE 2

by the multiplier of the argument of its exponential being changed by k; see particularly the k=1 column. This change by k is not always apparent as can be seen by looking at the k=3 column. More will be said about this shortly. Note that such a series of output transform points and the corresponding columns for each k value can be set up for a DFT of any number of points.

To understand more clearly what is occurring in each column, especially k=3, the Euler expansion of the exponential is carried out. Thus

$$\exp i\frac{2\pi nk}{N} = \cos\frac{2\pi nk}{N} + i\sin\frac{2\pi nk}{N} .$$

Recalling that the value of the cosine and sine are equal to the projection of a unit radius on the x and y axes respectively, one can draw the following N divided circle to get N such values:

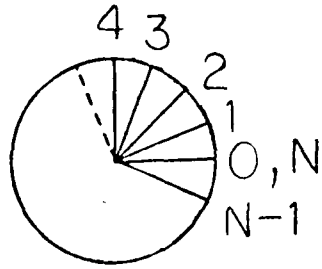

For the N = 4 case, the appropriate unit radius circle would be

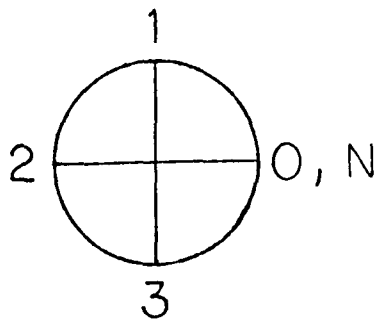

From the above circles we see that the change in the argument, as we go down a column from one member to the next, corresponds to a counter clockwise rotation of the unit radius by k divisions. Thus, for the k=1 column of the N=4 DFT, a rotation of one division around the quartered unit circle above is made at each step. The k=3 column shows, however, an apparent clockwise rotation around the circle. This is an effect common to all the $k \geq N/2$ columns for even N and for $k \geq (N+1)/2$ for all odd N. (From now on, the condition for odd numbers of points will follow the even number condition in parentheses.) The effect results from the fact that the large rotation, (N-a), counterclockwise is identically equal to the small rotation, a, clockwise. For example, going from the second member of the k=3 column, $x(3)\exp i\frac{2\pi}{4}(3)$, to the third member, involves a counter clockwise rotation by three

divisions from radius position 3 to position 2. This is the same as going directly by a clockwise rotation of one division from 3 to 2. If we use + to represent counterclockwise and - to represent clockwise, we have in general

$$+(N-a) = -a.$$

Thus, we have seen from the above background discussion how we can think of the calculation of successive output points of the DFT in terms of columns. Those columns for $0 \leq k < N/2$ $((N+1)/2)$ involve, for calculation of cosine and sine values, counterclockwise rotation by k units around a unit radius circle. Those columns with k such that $N/2$ $((N+1)/2) \leq k < N$ involve a rotation of -a units, where the value of a depends on the column and is related to the large counterclockwise rotation of k units.

The time interval between output points of the DFT is determined by the relation $T = 1/N\Delta f$, where N is the number of points sampled and Δf is the frequency interval between them. For a peak of given frequency range, the time interval is fixed by the above relation since the peak frequency range will equal $N\Delta f$. However, it sometimes would be desirable to examine smaller time intervals than determined by the peak. One cannot sample more points over the same peak range to accomplish this, since the only way to get more points is to decrease the frequency sampling interval, keeping the product, $N\Delta f$, and the time interval, constant. Therefore, an interpolation technique is needed to give additional output points that are placed intermediate in time between the pairs of previously obtained output points for a given set of input points.

A shortening of the time interval can be accomplished if the number of input points can be increased from N to 2N (or 3N, etc.) while keeping Δf constant. The interval would change from $1/N\Delta f$ to $1/2N\Delta f$. By adding N zeros to the N input points such a data expansion can be made. The zeros would have to be placed so that the new output points which are intermediate in time between previously obtained values, follow in the pattern of columns previously mentioned and have an appropriate intermediate value. This will be true for the output points if the following correspondence holds

New Old

$$X(n') = X(n) = \sum_{k=0}^{2N-1} x(k)\,\mathrm{expi}2\pi\frac{n'k}{2N}$$

$$X(n'+1)=\text{interpolated}=\sum_{k=0}^{2N-1} x(k)\,\mathrm{expi}2\pi\frac{(n'+1)k}{2N}$$

$$X(x'+2) = X(n+1) = \sum_{k=0}^{2N-1} x(k)\,\mathrm{expi}2\pi\frac{(n'+2)k}{2N}$$

We note that the proper increment of rotation around the unit radius circle is still maintained between every other point for a given k,

$$\frac{(n'+2)k}{2N} - \frac{n'k}{2N} = \frac{2k}{2N} = \frac{k}{N},$$

where we recall that k/N means rotation by k units around an N divided circle. We also note that a new output point results that is calculated from input data which is multiplied by cosine and sine values intermediate between the previous and next values for a given k since

$$\frac{(n'+1)k}{2N} - \frac{n'k}{2N} = \frac{k}{2N}.$$

Thus, the rotation pattern of the columns seen in the DFT calculation of a series of output points is exploited to give more, though not necessarily new, information.

Part Two

We recall that the DFT calculation requires that each input point have an index k, e.g., x(k). Therefore, the addition of zeros to input data raises the question of which k values are to be associated with them and the original data. The apportionment must be done so that the previously described increments of rotation and the proper clockwise and counterclockwise senses of rotation are retained.

First, let us consider data that originally had k indices such that $0 \leq k < N/2$ ((N+1)/2). Specifically, let us look at one such data point now placed in the zero expanded data set such that the proper correspondence (as mentioned in Part One) holds and its new index is k':

New Old

$X(n') = X(n) =$ ... $x(k')\ \exp i2\pi\frac{n'k'}{2N}$ ...

$X(n'+1) =$ interpolated $=$ ... $x(k')\exp i2\pi\frac{(n'+1)k'}{2N}$ ...

$X(n'+2) = X(n+1) =$ ... $x(k')\exp i2\pi\frac{(n'+2)k'}{2N}$ ...

Looking just at the part that determines rotation around the unit radius circle, we have

$$\frac{n'k'}{2N}$$

$$\frac{(n'+1)k'}{2N} = \frac{n'k'}{2N} + \frac{k'}{2N}$$

$$\frac{(n'+2)k'}{2N} = \frac{n'k'}{2N} + \frac{2k'}{2N}$$

We saw previously that one of the goals of the interpolation was to retain the original increment of rotation between every other output point. Therefore,

$$\frac{2k'}{2N} = \frac{k}{N}$$

where k is the original index of the point under discussion. It is clear that k' = k for all the x(k) with $0 \leq k < N/2$ ((N+1)/2). However, N/2 = 2N/4 ((N+1)/2= (2N+2)/4) in the 2N divided circle and consequently the new indices have the range $0 \leq k' < 2N/4$ ((2N+2)/4). We see that though the new k values, k', are equal to the old k values, they comprise only the first 1/4 k' values (approximately 1/4 for N = odd) of the available 2N ones and since these k' are less than 2N/2 they retain the original counterclockwise sense of rotation. We note that the interpolated points result from the use of cosine and sine values calculated from rotations around the circle of 1/2 of the original increment,

$$\frac{k'}{2N} = \frac{1}{2}\left(\frac{k}{N}\right),$$

and therefore we see that points halfway in time between the original points have had their values adjusted accordingly.

By similar argument, for the data that originally had k values such that N/2 ((N+1)/2) ≤ k < N and involved rotation by -a units we have

$$\frac{n'k'}{2N}$$

$$\frac{(n'+1)k'}{2N} = \frac{n'k'}{2N} + \frac{k'}{2N}$$

$$\frac{(n'+2)k'}{2N} = \frac{n'k'}{2N} + \frac{2k'}{2N}$$

Therefore,

$$\frac{2k'}{2N} = \frac{-a}{N} \quad \text{and} \quad k' = -a$$

However, in this case, it must be clarified how -a relates to the original k values so we can see how the k' relate to them. The connection is clear, -a = + (n-a) and (N-a) = k for N/2 ((N+1)/2 ≤ k < N; therefore,

$$N/2\ ((N+1)/2) \leq N-a < N$$

and by subtracting N throughout

$$-N/2\ ((-N+1)/2) = (N/2)-N(((N+1)/2)-N) \leq -a < 0,$$

where, once again, we think of -a as a clockwise rotation by a units. In the 2N system the above relationship is

$$-2N/4\ ((-2N+2)/4) \leq -a < 0$$

and therefore

$$-2N/4\ ((-2N+2)/4) \leq k' < 0.$$

To this point, we have seen how the connection of -a with the original k values has led to the association of the new values, k', with a clockwise rotation. We can once again take advantage of the connection between clockwise and counterclockwise rotation to establish

$$(3/4)(2N)\ (3/4(2N)+2/4) = 2N-(2N/2)\ ((2N)-(2N/4)+2/4) \leq k' < 2N-0 = 2N.$$

This relation shows that the input data originally associated with $N/2 \leq k < N$ is now indexed with k' values that satisfy

$$3/4(2N)\ ((3/4)(2N)+2/4) \leq k' < 2N,$$

that is, with the last 1/4 (approximately 1/4 for N=odd) of the available 2N k' values.

Since the original data are indexed when expanded to 2N data points by zeros with the first 1/4 and last 1/4 (approximately 1/4 for N=odd) of the available indices, the zeros must be indexed with the middle N indices. Compare, for example, the expanded eight point DFT in Table 3 with the four point DFT given previously.

$$X(o)=x(0)+x(1)\qquad +0+0+0+0+x(6)\qquad +x(7)$$

$$X(1)=x(0)+x(1)\exp i\frac{2\pi}{8}(1)+0+0+0+0+x(6)\exp i\frac{2\pi}{8}(6)+x(7)\exp i\frac{2\pi}{8}(7)$$

$$X(2)=x(0)+x(1)\exp i\frac{2\pi}{8}(2)+0+0+0+0+x(6)\exp i\frac{2\pi}{8}(4)+x(7)\exp i\frac{2\pi}{8}(6)$$

$$X(3)=x(0)+x(1)\exp i\frac{2\pi}{8}(3)+0+0+0+0+x(6)\exp i\frac{2\pi}{8}(2)+x(7)\exp i\frac{2\pi}{8}(5)$$

$$X(4)=x(0)+x(1)\exp i\frac{2\pi}{8}(4)+0+0+0+0+x(6)\exp i\frac{2\pi}{8}(8)+x(7)\exp i\frac{2\pi}{8}(4)$$

$$X(5)=x(0)+x(1)\exp i\frac{2\pi}{8}(5)+0+0+0+0+x(6)\exp i\frac{2\pi}{8}(6)+x(7)\exp i\frac{2\pi}{8}(3)$$

$$X(6)=x(0)+x(1)\exp i\frac{2\pi}{8}(6)+0+0+0+0+x(6)\exp i\frac{2\pi}{8}(4)+x(7)\exp i\frac{2\pi}{8}(2)$$

$$X(7)=x(0)+x(1)\exp i\frac{2\pi}{8}(7)+0+0+0+0+x(6)\exp i\frac{2\pi}{8}(2)+x(7)\exp i\frac{2\pi}{8}(1)$$

TABLE 3

APPENDIX B

THE DFT SYSTEM

Following these few introductory pages, the Discrete Fourier Transform system program listing will be found. The system is written in the Nova Computer assembly language of the Data General Corporation. The system uses a Houston Instruments Digital Plotter. In addition, a Teletype through which the user interacts with the individual programs is required. The interaction consists of the user's keyboard replies to requests for information typed on the teletype printer. A full description of the program, the requests and some typical replies follows.

Each program is called by typing a single letter mnemonic on the teletype keyboard. These mnemonics and the programs they call are as follows:

R	Rotate data
T	Read paper tape
P	Plot, set all parameters
Q	Plot, set only addresses
O	Set minimum = zero
G	Glitch, print addresses and contents
F	Fold data
M	Move data to the right

N Normalize

Z Zero core

D Discrete Fourier transform

L Move data left

A Output ASCII transform results

After the system is loaded into the computer and after each program is executed and is waiting for further instructions, the teletype will print "GOOD! GO AHEAD". If a program is called by mistake or an error is made in a reply, the operator can hit the ESC key on the teletype. The system will return to the GOOD! GO AHEAD waiting state.

The Discrete Fourier Transform (DFT) program is at the heart of the system. A brief description of the algorithm used to calculate it is now given. We saw in the previous appendix how the values of the cosines and sines used in the DFT can be obtained from the projection of a unit radius on x and y axes. We also saw how the first half of the input data could be thought of as forming columns associated with the unit radius rotating in a counterclockwise direction and the second half of the data associated with a clockwise rotation. We can think along these same lines and examine the values of the cosines and sines involved in the calculation of each output point. In other words, we can examine the rows instead of the columns. Each row can be broken up into three or four parts depending on whether the total number of input data points is odd or even. One part will consist solely of the x(0) point and its multiplier, one. If there is an odd number of total points, then the remaining even

number of points can be divided into two equal parts. If there is an even total number, then the remaining odd number of points can be divided into three parts; one part consisting solely of the x(N/2) point and its multiplier, expi2π(Nn/2)/2N, and two remaining equal parts. The two equal parts, for each case, will contain input points with indices indicated as follows:

Odd Total

First part: x(1)-x((N-1)/2) Second part: x((N-1)/2+1)-x(N-1)

Even Total

First part: x(1)-x(N/2-1) Second part: x(N/2+1)-x(N-1)

In either the odd or even total case, the first and second parts bear the same relationship to each other; the cosine and sine values are calculated for each member of the second part, starting with the x(N-1) point and working downward in index, by a clockwise rotation around the unit circle by the same number of divisions as for the counterclockwise rotation used for the calculation of the cosine and sine values of the first part starting with the x(1) point and working upward in indices. This means that the first point of the first part and the last point of the second part will have the same cosine value multiplier and the same sine value multiplier with different signs. The second point of the first part and the next to last point of the second part will have the same cosine multiplier and the same sine multiplier except for sign. This relationship continues for the remaining points. (To see this situation more clearly,

examine the expanded eight point DFT in Table 4.) We are interested only in the real part of the transform, that is, the part calculated only from cosine multipliers. Therefore, for the first and second parts, we can use the same set of cosine values. Since each cosine value is calculated independently as it is needed, this division into two parts saves about one half the cosine computation time.

In practice, the above description is followed closely; the first point, x(0), is stored and the succeeding pairs of points from the first and second parts are multiplied by the appropriate cosine and added after each multiplication to the stored previous values. A counter keeps track of the number of pairs. A test determines if the total number of points is odd or even. In the case of the even total the appropriate multiplication is carried out for the extra point. The result is added to the previously calculated values. This whole process is programmed in a special form of assembly language for use with Data General's "floating point interpreter". Among other virtues (see Chapter Four), this interpreter allows the calculation of accurate cosine values as they are needed and permits their use in non integer arithmetic. A full description of the floating point interpreter is available in the manual supplied by Data General Corporation.

The DFT program is called by typing D on the teletype keyboard. The printer replies with

FOR DATA TO BE TRANSFORMED

BEG ADDR-1

The program is requesting and waiting for the beginning core address

One output point of the summation expanded 8 point DFT

$$X(1)=x(0)+x(1)\exp i\frac{2\pi}{8}(1)+x(2)\exp i\frac{2\pi}{8}(2)+x(3)\exp i\frac{2\pi}{8}(3)+x(4)\exp i\frac{2\pi}{8}(4)+x(5)\exp i\frac{2\pi}{8}(5)+x(6)\exp i\frac{2\pi}{8}(6)+x(7)\exp i\frac{2\pi}{8}(7)$$

TABLE 4

minus one of the data to be transformed. The most convenient number system when dealing directly with minicomputers is the base eight or octal system. Therefore, this reply as well as all others in the system will be an octal number. After the reply is given and carriage return (CR) is hit, the printer will type

FINAL ADDR

The program is waiting for the last core address of the data to be transformed.

After the reply, the printer will type

ZERO EXT? NO(0) 1x(1) 2x(2) ETC

If you wish to add N zeros to the N data points, type 1. To add 2N zeros to the input points, type 2 and so on. To not zero extend the data, just type 0. The purpose of zero extending the input data is discussed in the previous appendix. Zeros are not actually added to the data since they would then become involved in the time consuming and purposeless multiplication by zero. Instead, only their effect on the counter which keeps track of the total number of points is taken into account. Their effect on the cosine argument is automatically taken care of by the adjustment to the total number of points. As a result, the same number of input points, as for the unextended data, is used for the extended data calculation with a large savings of time.

Following the reply to the zero extension request, the teletype will print out

NMB, TRANSFORM PTS OUT

As has been mentioned previously, the DFT produces N output points for N input points. If the data is zero extended to 2N points, the

DFT will output 2N points. Only a relatively small number of the total number of possible output points is needed for the plotting of a meaningful correlation function and a large amount of time would be wasted if all the N or 2N (etc.) output points were calculated. The reply to the above request limits the number of output points to the number desired. Commonly, the reply is $100_{(8)}$ which equals $64_{(10)}$. For $200_{(10)}$ input data points zero extended once to $400_{(10)}$ points, the calculation of the $64_{(10)}$ output points takes approximately seven minutes.

After the reply to the number of output points request is given, the printer types

FOR SING PREC DATA STORED

BEG ADDR-1

The reply should be the beginning address minus one of the locations where the data read in (see later discussion of the read in instruction) is stored. Before computing the DFT, the program takes the single precision raw data, converts it to double precision form and stores it $2000_{(8)}$ locations away from the stored and unchanged single precision data. The program then converts the double precision data that is stored in a maximum $4000_{(8)}$ locations into a floating point form. It is in this form that the data are operated on by the DFT program. The results of the DFT are stored in a maximum $4000_{(8)}$ locations that are $4000_{(8)}$ locations away from the double precision data. The reply to the above request allows the program to take the above data location considerations into account. If, for example, the reply is $7777_{(8)}$, the data allocation would be

loc. $10000_{(8)}$ - - - - - - - - loc. $11777_{(8)}$

single precision data

$2000_{(8)} = 1024_{(10)}$ locations maximum

loc. $12000_{(8)}$ - - - - - - - - loc. $15777_{(8)}$

double precision and floating point data

$4000_{(8)} = 2048_{(10)}$ locations

loc. $16000_{(8)}$ - - - - - - - - loc. 21777

DFT results in floating point form

$4000_{(8)} = 2048_{(10)}$ locations

The general allocation permits a maximum of $2000_{(8)} = 1024_{(10)}$ single precision data points to be transformed. Without zero filling, $2000_{(8)}$ input points will give the complete $2000_{(8)}$ DFT output in the form of floating point numbers (each floating point number requires two storage locations). With zero extension, $2000_{(8)}$ input points will yield only the first $2000_{(8)}$ output points since there is no storage space available to hold the remaining points. To change the storage allocation from $2000_{(8)}$ to another value, ADR (loc. $126_{(8)}$) in the program must be changed.

After the reply, including the carriage return, the program will compute the DFT. On completion of the calculation, the printer will type

NORMALIZE?, 1=YES

Normalization is achieved by dividing, in floating point, every transform resultant point by the value of the first output point since, for the correlation function results, this will be the time = 0 point and

therefore the maximum valued point. The normalization part of the DFT program can be called independently by typing N; this feature is useful if normalized results are desired after unnormalized results have been obtained.

After the normalization request, reply and execution, the message

NMB, TRANSFORM PTS OUT

will be displayed. This calls for the number of points of the DFT result that the operator wishes typed out on the teletype printer. The reply should not be a number of points greater than the number specified to be calculated. (There is no harm in specifying a larger number; the extra values printed will just be meaningless.) The usual procedure is to request for print out the same number as requested to be calculated, though a smaller number can, of course, be printed out. Each point will be written out as a seven digit decimal fraction followed by a positive or negative exponent of ten, e.g., 0.6319451E-01. This part of the program can also be called independently by the letter A in case it is desired to have more or fewer points printed out than first requested.

A description of the various support programs, in their approximate order of use before the DFT is executed, is now given. For each program, typical dialogue is given and explained. Reminder, carriage return must be hit after each reply.

Read Paper Tape (T) is used for reading data into core from punched paper tape,

NMB, DATA PTS, OCTAL

430

LOC FOR STORING DATA

BEG ADDR-1

7777

TTI(1), PTR(2) ?

1

The first reply: Sets the number of points, in base eight, desired to be read from the tape.

Second: Sets the beginning address minus one of the location for the storage of data.

Third: Distinguishes between tape being read in from a teletype reader (TTI) or a high speed reader (PTR).

Plot (P) is used for plotting the data on a Houston Instruments Complot.

AUTO SCALE, 1 = ON

0

MAX PLOT HT=

12

NMB PTS/IN, Y

31

NMB PTS/1N, X

31

PT PLOT, 1=OFF

1

ZERO LINE, 1=ON

0

BEG ADDR-1

7777

FINAL ADDR

10427

The first reply: Replying one (1) will cause the most intense peak to be scaled to fit the maximum plot height; replying zero (0) will plot by dividing the peak intensity according to the points per inch designation where each point represents one unit of intensity.

Second: Sets the maximum plot height; the maximum allowable height is 10 ($12_{(8)}$) inches.

Third: Sets the number of points plotted per inch along the Y axis. To make the setting, one should have an idea of the maximum number of points along the Y axis that will occur in the plot so that the apportionment will allow the intense peaks to fit on scale. For the Houston Instrument Complot plotter, the maximum number of points per inch is $200_{(10)}$. Thus, the maximum peak intensity that can be plotted without using the scale expansion feature is 200 pts/inch x 10 inches = 2,000 points. Remember that each point corresponds to one unit of peak intensity and for a photon counting system, the above limitation means that a peak of a maximum of 2,000 counts per second can be plotted. If autoscale expansion is used, this request for points per inch along the Y axis must be answered, any number will do, though it will be ignored.

Fourth: Sets the number of points per inch along the X axis, where one point corresponds to the intensity at a single wavenumber setting.

Fifth: The reply of 0 will give a plot consisting of only dots with no connecting lines. Replying 1 will give a continuous line plot.

Sixth: If 1 is hit, a baseline of zero is drawn. Replying 0 leaves it out.

Seventh)
Eighth) Sets the location range to be plotted.

Plot (Q) will plot data under conditions set by the previous P plot requests and replies if only the region to be plotted is to be changed.

BEG ADDR-1

10032

FINAL ADDR

10420

First reply)
Second) Sets the location range to be plotted.

Minimum equals zero (Ø) will set the lowest value in a data range to zero and will scale down all the other points by subtracting the lowest value from all the points in the data range. If it is desired to have the lowest value equal one, then the computer console switches should be used to set location 747 to 012044.

BEG ADDR-1

10032

FINAL ADDR

10421

First Reply)
) Sets location range of data.
Second)

Glitch (G) Prints out locations and their contents in octal form.

BEG ADDR-1

10420

FINAL ADDR

10427

First reply)
) Sets the location range of data.
Second)

Fold (F) Will transfer high address data to low addresses symmetrically about an address. This is used to fold the high frequency side of a peak in order to make the whole peak symmetric. Low frequency data are lost.

FOR DATA TO BE FOLDED

BEG ADDR-1

10226

FINAL ADDR

10420

First reply: Sets the beginning location minus one for the data to be folded. For folding about a peak maximum, the reply should be the address of the maximum point.

Second: Sets end of location range.

Note: After performing the folding, the operator must figure out where the low frequency side of the peak now resides. For the above example the following calculation will tell this:

First step: $10420_{(8)}$ $-10226_{(8)}$ $172_{(8)}$

Second step: $10226_{(8)}$ $- 172_{(8)}$ $10034_{(8)}$

The beginning address of the folded peak is $10034_{(8)}$. After the folding of a large number of points, the low frequency side may be located below the starting address of the original data, for example, below $10000_{(8)}$. Therefore, one must choose the data storage areas so that, if this happens, nothing of importance will be overwritten.

Rotate (R) will right circular shift data, assuming high address locations to the left and low to the right, so that the data are in the correct form for the DFT (See Chapter Four).

BEG ADDR-1

10032

FINAL ADDR

10421

FOR POINTS TO BE SHIFTED

BEG ADDR-1

10225

First Reply)
Second) Sets data range of all data involved in the shift.

Third: Sets the beginning address minus one of the high address data that is to be shifted to the lower frequency. Note, the data located in the next address after the address designated in the reply to the third request will be placed, as a result of the rotate operation, in the next address after the address designated in the reply to the first

request. A similar situation exists for the succeeding data and locations. The data previously located in the low addresses will be shifted to high addresses.

Zero (Z) is a miscellaneous program used for setting regions of core to zero.

BEG ADDR-1

10177

FINAL ADDR

10400

First reply)
Second) Sets location range to be zeroed.

Move (M,L) will shift data a number of places to the right (M) or the left (L) overwriting and destroying data contained in the new locations.

FOR PTS TO BE SHIFTED

BEG ADDR-1

10177

FINAL ADDR

10400

NMB, PLACES TO BE SHIFTED

100

First reply)
Second) Sets location range of data to be shifted

Third: Sets the number of places that the data should be shifted either right of left.

Note: This program, like the zero filling one, is a miscellaneous one and is generally not needed.

The following core map shows an outline of the computer location usage. All locations are in octal.

```
27777)
  ↑  )  Data storage
10000)


7777)
  ↑  )  Bootstrap and binary loader for paper tapes
7647)


7577)
  ↑  )  Extended binary floating point interpreter
4100)
       DGC tape # 091-000013-03


4055)
  ↑  )  Writable area for the floating point interpreter
3700)


2464)
  ↑  )  DFT system
0000)
```

Operating Instructions For Computing a DFT

1. Read in data punched on paper tape (T command). Note, the operator must know the number of data points to be read in. This number will have to be provided,in octal form, to the paper tape reading program.

2. Set the minimum value in the spectrum equal to zero (Ø).

3. Plot the spectrum (P or Q). The operator must recall where the data have been stored in core as a result of the T command. In addition, the operator must know the range of points, in octal, to be plotted out.

4. From the plot of the spectrum and the number of points per inch on the X axis that have been plotted, the operator should obtain an approximate idea of the location of the peak maximum.

5. Use the glitch command (G) to examine the region of core around the approximate location of the peak maximum to determine its exact location.

6. Rotate (R) the peak around the location of the peak maximum. Make sure the maximum value point occurs as the first point of the result.

7. Calculate the DFT of the rotated data.

For the $200_{(10)}$ point spectra usually obtained in this thesis work, the above operating instructions usually were applied as follows. The $310_{(8)}$ points were read into the region of core starting at $10000_{(8)}$.

Therefore, the data occupied locations $10000\text{-}10307_{(8)}$. The minimum would then be set equal to zero in the region $10000\text{-}10307_{(8)}$. The plot was obtained using $31_{(8)}$ points per inch along the X axis and the scale expansion feature along the Y axis. The peak maximum was usually located approximately halfway in the data range, loc. $10143_{(8)}$. The locations $10130\text{-}10157_{(8)}$ were examined to obtain the exact address. If, for example, the maximum did occur at $10143_{(8)}$, then the peak was rotated so that the value at $10143_{(8)}$ was at loc. $10000_{(8)}$ with succeeding values in order. The DFT would then be calculated, using zero extension once, of the data in locations $10000\text{-}10307_{(8)}$. The number of transform points printed out was usually $100_{(8)}$.

```
ASM 1 CT0:1 CT1:5/8 STTC/L
PROGRAM IS ABSOLUTE
                        ; DFT
                        ; REVISED 4/9/77
; PREPARED BY KEN BREZINSKY
; STARTING ADDRESS = 413
; THE LOCATIONS OF ALL SUBROUTINES ARE AVAILABLE IN THE TABLE
; BEGINNING AT LOCATION 464
; COMMENTS IN EACH SUBROUTINE POINT OUT IMPORTANT PARTS
; OF THE SUBROUTINE
```

```
---
*       .MAIN

        000000 .LOC 0
00000 000413 CMMD
00001 000413 CMMD
00002 000413 CMMD
00003 000000 0
00004 000000 0
00005 000000 0
00006 000000 0
00007 003700 3700
        000040 .LOC 40
00040 000720 GETC: GETCC
00041 002136 PUTC: PUTC1
00042 000000 0
00043 000000 0
00044 000000 BEGAD: 0
00045 000000 FINAD: 0
00046 000000 NMBER: 0
00047 000664 BBUMP: BUMP
00050 000612 TTEXT: TEXT
00051 000732 CCRL: CRL
00052 000701 NNB: NB
00053 000413 CCMMD: CMMD
00054 000627 DDDIGI: DDIGI
00055 001112 MIN: MINI
00056 001114 MAX: MAXI
00057 001172 SBTRT: SUBME
00060 000671 BBF: BF
00061 000000 TEMP: 0
00062 000000 HOLD: 0
00063 000000 SALVE: 0
00064 000177 TEST: 177
00065 000000 TABLE: 0
00066 000277 MASK: 277
00067 000060 ZERO: 60
00070 000071 NINE: 71
00071 000015 CCR: 15
00072 000012 LFF: 12
00073 000000 TEMP1: 0
00074 000000 HOLD1: 0
00075 000033 EESC: 33
00076 000057 SLH: 57
00077 000712 GETC2: GET
00100 000704 PUTC2 : PUT
00101 000000 OFSET: 0
00102 000000 LSC: 0
00103 000000 YSCAL: 0
00104 000000 NX: 0
00105 000000 CP: 0
00106 000000 PLV: 0
00107 000000 CNTA: 0
00110 000000 CNTB: 0
00111 000000 REM: 0
00112 000000 SAVE: 0
00113 000000 MI: 0
00114 000000 ORIG: 0
00115 000000 RTRN: 0
00116 000000 WC: 0
00117 000000 NP: 0


---
```

```
     .MAIN
00120 000000 ARTRN: 0
00121 000000 BACK: 0
00122 000000 BKA: 0
00123 001141 AMUL: MULTM
00124 001153 ADIV: DIVID
00125 000310 PINCR: 310
00126 002000 ADR: 2000
00127 000003 G1: 3
00130 000005 G2: 5
00131 002054 NNN: N
00132 002113 AAA: A
00133 000001 CDD: 1
00134 000000 NMBER: 0
00135 000000 CNTC: 0
00136 000000 END: 0
              ;THE FOLLOWING ARE FOR F.P. WORK
00137 040420 F2NE: 1.0
00140 000000
00141 040544 PI: 4.2831852                    ;2 PI
00142 103755
00143 000000 NN: 0
00144 000000 0
00145 000000 COSI: 0
00146 000000 0
00147 000000 ARG: 0
00150 000000 0
00151 000000 NU: 0
00152 000000 0
00153 000000 KKK: 0
00154 000000 0
              ;FOLLOWING ARE PERMANENT LOCS
00155 000000 SW1: 0
00156 000000 YINCH: 0
00157 000000 YSL: 0
00160 000000 XSL: 0
00161 000000 PP: 0
00162 000000 ZZ: 0
00163 000000 TEMP2: 0
00164 000000 TEMP3: 0
00165 000000 LC11: 0
00166 177760 M20: -20
              ;END OF PERM. LOC.
00167 002150 TE1: T1-1                ;TEXT POINTERS
00170 002162 TE2: T2-1
00171 002175 TE3: T3-1
00172 002203 TE4: T4-1
00173 002211 TE5: T5-1
00174 002224 TE6: T6-1
00175 002226 TE7: T7-1
00176 002241 TE8: T8-1
00177 002252 TE9: T9-1
00200 002261 TE10: T10-1
00201 002270 TE11: T11-1
00202 002277 TE12: T12-1
00203 002306 TE13: T13-1
00204 002316 TE14: T14-1
00205 002334 TE15: T15-1
00206 002351 TE16: T16-1
00207 002362 TE17: T17-1
```

```
      .MAIN
00210 002374 TE18: T18-1
00211 002407 TE19: T19-1
00212 002417 TE20: T20-1
00213 002427 TE21: T21-1
00214 002444 TE22: T22-1
      000377 .LOC 377
00377 000413 CMMD
```

```
*       .MAIN
        000413 .LOC 413


                ;WAITS CHAR. FROM KEYBOARD
                ;BRANCHES TO SUBROUT.
                ;IF BAD CHAR WAITS


00413 000401 CMMD: 401
00414 020211 LDA 0,TE19
00415 006050 JSR @TTEXT
00416 006051 JSR @CCRL
00417 006077 JSR @GETC2              ;WAIT CHAR.
00420 006100 JSR @PUTC2              ;ECHO
00421 040065 STA 0,TABLE
00422 006051 JSR @CCRL               ;TACK ON CR/LF
00423 020417 TTABL: LDA 0,CCT
00424 040417 STA 0,CT
00425 020417 LDA 0,RRRR
00426 040021 STA 0,21
00427 020416 LDA 0,TTTT
00430 040022 STA 0,22
00431 020065 LDA 0,TABLE
00432 026021 LDA 1,@21
00433 032022 LDA 2,@22
00434 106414 SUB@ 0,1,SZR            ;COMPARE TO TABLE CHAR
00435 000402 JMP .+2
00436 001000 JMP 0,2                 ;BRANCH
00437 014404 DSZ CT
00440 000772 JMP .-6
00441 002053 JMP @CCMMD              ;BAD CHAR GET ANOTHER
00442 000016 CCT: 16
00443 000000 CT: 0
00444 000445 RRRR: RRR-1
00445 000463 TTTT: TT-1
00446 000122 RRR: "R
00447 000124 "T
00450 000103 "C
00451 000120 "P
00452 000117 "O
00453 000107 "G
00454 000106 "F
00455 000115 "M
00456 000116 "N
00457 000132 "Z
00460 000104 "D
00461 000121 "Q
00462 000114 "L
00463 000101 "A
00464 001543 TT: R                   ;ROTATE DATA
00465 000502 T                       ;READ PAPER TAPE
00466 016200 16200                   ;DDT, TEMP UNTIL CASS. ROUT.
00467 001206 P                       ;PLOT SET ALL PARAMETERS
00470 000734 @                       ;MIN=1
00471 001045 G                       ;GLITCH
00472 001023 F                       ;FOLD
00473 000772 M                       ;MOVE DATA RIGHT SHIFT
00474 002054 N                       ;NORMALIZE
```

```
---
        .MAIN
   00475 002102 Z                    ;ZERO CORE
   00476 001600 D                    ;DFT
   00477 001230 Q                    ;PLOT SET ONLY BEGAD AND FINAD
   00500 000753 L                    ;MOVE DATA LEFT SHIFT
   00501 002113 A                    ;OUTPUT ASCII TRANS. RESULTS
```

```
.MAIN

        ;READS PAPER TAPE FROM TELETYPE (TTI)
        ;OR HIGH SPEED READER (PTR)

00502 020167 T: LDA 0,TE1
00503 006047 JSR @BBUMP
00504 050046 STA 2,NMBER
00505 010046 ISZ NMBER
00506 020170 LDA 0,TE2
00507 006050 JSR @TTEXT
00510 006051 JSR @CCRL
00511 020171 LDA 0,TE3
00512 006047 JSR @BBUMP
00513 050044 STA 2,BEGAD
00514 020212 LDA 0,TE20
00515 006047 JSR @BBUMP
00516 151212 MOVR# 2,2,SZC          ;TEST IF TTI OR PTR
00517 000405 JMP .+5
00520 020464 LDA 0,SKPT
00521 024464 LDA 1,NSPT
00522 030464 LDA 2,DIPT
00523 000404 JMP .+4
00524 020463 LDA 0,SKTT
00525 024463 LDA 1,NSTT
00526 030463 LDA 2,DITT
00527 040405 STA 0,.+5
00530 044402 STA 1,.+2
00531 050405 STA 2,.+5
00532 060110 NIOS TTI
00533 000407 JMP KBC
00534 063610 KBST: SKPDN TTI        ;GET CHAR
00535 000777 JMP .-1
00536 060510 DIAS 0,TTI
00537 030064 LDA 2,TEST
00540 143400 AND 2,0
00541 001400 JMP 0,3
00542 004772 KBC: JSR KBST          ;PASS BLANK LEADER
00543 101005 MOV 0,0,SNR
00544 000776 JMP .-2
00545 000401 JMP KBRD               ;IGNORE 1ST CHAR (A)
00546 102440 KBRD: SUBC 0,0         ;READ & STORE
00547 040061 STA 0,TEMP
00550 004764 JSR KBST
00551 004424 JSR KBCK
00552 000776 JMP .-2
00553 024061 LDA 1,TEMP
00554 131120 MOVZL 1,2
00555 151120 MOVZL 2,2
00556 147000 ADD 2,1
00557 125120 MOVZL 1,1
00560 107000 ADD 0,1
00561 044061 STA 1,TEMP
00562 004752 JSR KBST
00563 004412 JSR KBCK
00564 000402 JMP .+2
00565 000766 JMP .-12
```

```
---
        .MAIN
   00566 030061 LDA 2,TEMP
   00567 052044 STA 2,@BEGAD
   00570 010044 ISZ BEGAD
   00571 014046 DSZ NMBER
   00572 000754 JMP KBRD
   00573 062677 ICRST
   00574 006053 JSR @CCMMD
   00575 024067 KBCK: LDA 1,ZERO
   00576 030070 LDA 2,NINE
   00577 142033 ADCZ# 2,0,SNC
   00600 106032 ADCZ# 0,1,SZC
   00601 001400 JMP 0,3
   00602 122400 SUB 1,0
   00603 001401 JMP 1,3
   00604 063612 SKPT: SKPDN PTR
   00605 060112 NSPT: NIOS PTR
   00606 060512 DIPT: DIAS 0,PTR
   00607 063610 SKTT: SKPDN TTI
   00610 060110 NSTT: NIOS TTI
   00611 060510 DITT: DIAS 0,TTI
```

```
;       .MAIN
                ;OUTPUT TEXT AND/OR CARRIAGE RET. AND/OR LF


00612 054063 TEXT: STA 3,SALVE
00613 040021 STA 0,21
00614 024066 LDA 1,MASK
00615 022021 LL: LDA 0,@21
00616 123415 AND# 1,0,SNR
00617 000407 JMP .+7
00620 006100 JSR @PUTC2
00621 101300 MOVS 0,0
00622 123415 AND# 1,0,SNR
00623 000403 JMP .+3
00624 006100 JSR @PUTC2
00625 000770 JMP LL
00626 002063 JMP @SALVE
```

```
---
*       .MAIN


                ;CONVERTS OCTAL INPUT TO BINARY
                ;TESTS IF END OF NUMBER STRING
                ;OUTPUTS CR/LF
                ;MUST HIT CR AFTER INPUT NUMBER STRING


00627 054061 DDIGI: STA 3,TEMP
00630 102440 SUBC 0,0
00631 040074 STA 0,HOLD1
00632 006077 DIGI: JSR @GETC2
00633 024067 LDA 1,ZERO
00634 030070 LDA 2,NINE
00635 142033 ADCZ# 2,0,SNC              ;DIGIT?
00636 106032 ADCZ# 0,1,SZC
00637 000413 JMP CRR                    ;NO, CR?
00640 006100 JSR @PUTC2                 ;YES, ECHO
00641 024067 IN: LDA 1,ZERO
00642 122400 SUB 1,0                    ;STRIP ASCII CODE
00643 024074 LDA 1,HOLD1
00644 125120 MOVZL 1,1                  ;MULT. BY 8
00645 125120 MOVZL 1,1
00646 125120 MOVZL 1,1
00647 107000 ADD 0,1
00650 044074 STA 1,HOLD1                ;ADD IN NEW CHAR. AND STORE
00651 000761 JMP DIGI
00652 024071 CRR: LDA 1,CCR
00653 122414 SUB# 1,0,SZR
00654 000404 JMP KKESC                  ;NOT CR, ESC?
00655 034061 LDA 3,TEMP
00656 030074 LDA 2,HOLD1
00657 000453 JMP CRL                    ;YES, TACK ON CR/LF
00660 024075 KKESC: LDA 1,EESC
00661 122414 SUB# 1,0,SZR
00662 000750 JMP DIGI                   ;NOT CR OR ESC, GET ANOTHER CHAR
00663 002053 JMP @CCMMD                 ;ESCAPE
```

```
---
;       .MAIN


                ;OUTPUTS PARAMETER REQUESTS AND WAITS FOR VALUES

00664 054062 BUMP: STA 3,HOLD
00665 006050 JSR @TTEXT
00666 006051 JSR @CCRL
00667 006054 JSR @DODIGI
00670 002062 JMP @HOLD

                ;GETS AND SETS BEG-1 AND FINAD


00671 054073 BF: STA 3,TEMP1
00672 020171 LDA 0,TE3
00673 006047 JSR @BBUMP
00674 050044 STA 2,BEGAD
00675 020172 LDA 0,TE4
00676 006047 JSR @BBUMP
00677 050045 STA 2,FINAD
00700 002073 JMP @TEMP1

                ;SETS NMBER

00701 020045 NB: LDA 0,FINAD
00702 024044 LDA 1,BEGAD
00703 122400 SUB 1,0
00704 040046 STA 0,NMBER
00705 001400 JMP 0,3


                ;OUTPUT A CHARACTER


00706 063511 OUT: SKPBZ TTO
00707 000777 JMP .-1
00710 061111 DOAS 0,TTO
00711 001400 JMP 0,3

                ;A COMMONLY USED SEGMENT


00712 063610 GET: SKPDN TTI
00713 000777 JMP .-1
00714 060610 DIAC 0,TTI
00715 024064 LDA 1,TEST
00716 123400 AND 1,0
00717 001400 JMP 0,3


---
```

```
;       .MAIN

                ;GET CHAR. FOR FL. PT.


00720 054062 GETCC: STA 3,HOLD
00721 006077 JSR @GETC2
00722 006100 JSR @PUTC2
00723 024071 LDA 1,CCR
00724 106414 SUB# 0,1,SZR
00725 002062 JMP @HOLD
00726 020072 LDA 0,LFF
00727 006100 JSR @PUTC2
00730 020722 LDA 0,CRR
00731 002062 JMP @HOLD

                ;OUTPUT CR/LF


00732 020174 CRL: LDA 0,TES
00733 002050 JMP @TTEXT


                ;SETS LOWEST VALUE = 1


00734 006060 C: JSR @BBF
00735 006052 JSR @NNB
00736 006055 JSR @MIN
00737 034044 LDA 3,BEGAD
00740 054020 STA 3,20
00741 111000 MOV 0,2                    ;RESULTS OF MINI, ADDR. IN AC0
00742 031000 LDA 2,0,2
00743 026020 START: LDA 1,@20
00744 010044 ISZ BEGAD
00745 146400 SUB 2,1
00746 046044 STA 1,@BEGAD
00747 012044 ISZ @BEGAD                 ;+1 TO AVOID ZERO
00750 014046 DSZ NMBER                  ; IF SET MIN = 0 SET 747=401
00751 000772 JMP START
00752 002053 JMP @COMMD
```

```
---
*       .MAIN

                ;PERFORMS A HIGH END MOVE(M)
                ;OR A LOW END MOVE(L)


00753 020175 L: LDA 0,TE7
00754 006050 JSR @TTEXT
00755 006051 JSR @CCRL
00756 006060 JSR @BBF
00757 006052 JSR @NNB
00760 020044 LDA 0,BEGAD
00761 101400 INC 0,0
00762 040106 STA 0,PLW
00763 020213 LDA 0,TE21
00764 006047 JSR @BBUMP
00765 020106 LDA 0,PLW
00766 143400 SUB 2,0
00767 040073 STA 0,TEMP1
00770 126520 SUBZL 1,1
00771 000416 JMP MM
00772 020175 M: LDA 0,TE7
00773 006050 JSR @TTEXT
00774 006051 JSR @CCRL
00775 006060 JSR @BBF
00776 020045 LDA 0,FINAD
00777 040106 STA 0,PLW
01000 006052 JSR @NNB
01001 020213 LDA 0,TE21
01002 006047 JSR @BBUMP
01003 020106 LDA 0,PLW
01004 143000 ADD 2,0
01005 040073 STA 0,TEMP1
01006 126440 SUBZ 1,1
01007 022106 MM: LDA 0,@PLW
01010 042073 STA 0,@TEMP1
01011 125004 MOV 1,1,SZR
01012 000404 JMP .+4
01013 014073 DSZ TEMP1
01014 014106 DSZ PLW
01015 000403 JMP .+3
01016 010073 ISZ TEMP1
01017 010106 ISZ PLW
01020 014046 DSZ NMBER
01021 000746 JMP MM
01022 002053 JMP @CCMMD
```

```
---
;       .MAIN

                ;FOLDS TO GIVE SYMMETRIC PEAK HIGH FREQ TO LOW

01023 020173 F: LDA 0,TES
01024 006050 JSR @TTEXT
01025 006051 JSR @CCRL
01026 006060 JSR @BBF
01027 020044 LDA 0,BEGAD
01030 100400 NEG 0,0
01031 100000 CZM 0,0
01032 040063 STA 0,SALVE
01033 006052 JSR @NNB
01034 030044 LDA 2,BEGAD
01035 034063 LDA 3,SALVE
01036 151400 INC 2,2
01037 021000 LDA 0,0,2
01040 041400 STA 0,0,3
01041 014063 DSZ SALVE
01042 014046 DSZ NMBER
01043 000772 JMP .-6
01044 002053 JMP @CCMMD
```

```
.MAIN

                ;OUTPUTS CONSEQ. ADDR.& CONTENTS

01045 006060 G: JSR @BBF
01046 006052 JSR @NNB
01047 010044 GG: ISZ BEGAD
01050 024044 LDA 1,BEGAD
01051 004411 JSR KK
01052 020076 LDA 0,SLH
01053 006100 JSR @PUTC2
01054 024044 LDA 1,@BEGAD
01055 004405 JSR KK
01056 006051 JSR @CCRL
01057 014046 DSZ NMBER
01060 000767 JMP GG
01061 002053 JMP @CCMMD
01062 054115 KK: STA 3,RTRN
01063 102440 SUBC 0,0
01064 125122 MOVZL 1,1,SZC
01065 101400 INC 0,0
01066 030067 LDA 2,ZERO
01067 143000 ADD 2,0
01070 006100 JSR @PUTC2
01071 020130 LDA 0,G2
01072 040110 STA 0,CNTB
01073 020127 LDA 0,G1
01074 040107 STA 0,CNTA
01075 102440 SUBC 0,0
01076 125122 MOVZL 1,1,SZC
01077 101400 INC 0,0
01100 014107 DSZ CNTA
01101 101121 MOVZL 0,0,SKP
01102 000402 JMP .+2
01103 000773 JMP .-5
01104 030067 LDA 2,ZERO
01105 143000 ADD 2,0
01106 006100 JSR @PUTC2
01107 014110 DSZ CNTB
01110 000763 JMP KK+11
01111 002115 JMP @RTRN
```

```
;       .MAIN

                ;ROUTINES FOLLOWING FIND MINIMUM OR MAXIMUM
                ;POINTS IN AN ARRAY.
                ;
01112 020426          MINI: LDA 0,CON1
01113 101401 INC 0,0,SKP
01114 020424          MAXI: LDA  0,CON1
01115 040414 STA 0,IT
01116 054063 STA 3,SAVE
01117 020046 LDA 0,NMBER
01120 040061 STA 0,TEMP
01121 014061 DSZ TEMP
01122 020044 LDA 0,BEGAD
01123 040022 STA 0,22
01124 101400 INC 0,0
01125 032022 LDA 2,22 @
01126 026022          HARE: LDA 1,@ 22
01127 006057 JSR @SUBTRT
01130 000405 JMP .+5
01131 125112          IT: MOVL@ 1,1,SZC
01132 000403 JMP .+3
01133 133000 ADD 1,2
01134 020022 LDA 0,22
01135 014061 DSZ TEMP
01136 000770 JMP HARE
01137 002063 JMP @ SAVE
01140 125112 CON1: MOVL@ 1,1,SZC
```

```
;       .MAIN


                ;MULTIPLICATION ROUTINE
                ;
01141 102460        MULTM: SUBC 0,0
01142 054074 STA 3,HCLDI
01143 034166 LDA 3,M20
01144 125203 CB99: MOVR 1,1,SNC
01145 101201 MOVR 0,0,SKP
01146 143220 ADDZR 2,0
01147 175404 INC 3,3,SZR
01150 000774 JMP CB99
01151 125260 MOVCR 1,1
01152 002074 JMP @HCLDI
                ;
                ;
                ;
                ;DIVISION ROUTINE
                ;
                ;
01153 102400        DIVID: SUB 0,0
01154 054074 STA 3,HCLDI
01155 142432 SUBZ# 2,0,SZC
01156 000412 JMP CC99
01157 034166 LDA 3,M20
01160 125120 MOVZL 1,1
01161 101100 CC98: MOVL 0,0
01162 142412 SUB# 2,0,SZC
01163 142400 SUB 2,0
01164 125100 MOVL 1,1
01165 175404 INC 3,3,SZR
01166 000773 JMP CC98
01167 176441 SUBC 3,3,SKP
01170 176420 CC99: SUBZ 3,3
01171 002074 JMP @HCLDI


                ;     SUBTRACT ROUTINE.


01172 125112        SUBME: MOVL# 1,1,SZC
01173 000406 JMP BREAD
01174 146400 SUB 2,1
01175 151112 MOVL# 2,2,SZC
01176 125113 MOVL# 1,1,SNC
01177 001401 JMP 1,3
01200 001400 JMP 0,3
01201 146400 BREAD: SUB 2,1
01202 151113 MOVL# 2,2,SNC
01203 125112 MOVL# 1,1,SZC
01204 001401 JMP 1,3
01205 001400 JMP 0,3
```

```
---
;       .MAIN

                ;PLOTTING ROUTINE


01206 020176 P: LDA 0,TE8
01207 006047 JSR @BBUMP
01210 050155 STA 2,SV1
01211 020177 LDA 0,TE9
01212 006047 JSR @BBUMP
01213 050156 STA 2,YINCH
01214 020200 LDA 0,TE10
01215 006047 JSR @BBUMP
01216 050157 STA 2,YSL
01217 020201 LDA 0,TE11
01220 006047 JSR @BBUMP
01221 050160 STA 2,XSL
01222 020202 LDA 0,TE12
01223 006047 JSR @BBUMP
01224 050161 STA 2,PP
01225 020203 LDA 0,TE13
01226 006047 JSR @BBUMP
01227 050162 STA 2,ZZ
01230 006060 Q: JSR @BBF
01231 006052 JSR @NNB
01232 054115       GRAPH: STA 3,RTRN          ;NO PURPOSE
01233 006556 JSR @PD
01234 020044 LDA 0,PEGAD
01235 040073 STA 0,TEMP1
01236 024046 LDA 1,NMBER
01237 044116 STA 1,NC
01240 006055 JSR @MIN
01241 050113 STA 2,M1
01242 151113 MOVL# 2,2,SNC
01243 152400 SUB 2,2
01244 150400 NEG 2,2
01245 050101 STA 2,OFSET
01246 020155 LDA 0,SV1
01247 101004 MOV 0,0,SZR
01250 000411 JMP MAXMIN
01251 030156 LDA 2,YINCH
01252 024157 LDA 1,YSL
01253 006123 JSR @AMUL
01254 131000 MOV 1,2
01255 126000 ADC 1,1
01256 006124 JSR @ADIV
01257 044102 STA 1,LSC
01260 000407 JMP DRAW
01261 006056        MAXMIN: JSR @MAX
01262 024113 LDA 1,M1
01263 132400 SUB 1,2
01264 126000 ADC 1,1
01265 006124 JSR @ADIV
01266 044102 STA 1,LSC
01267 024156         DRAW: LDA 1,YINCH
01270 030125 LDA 2,PINCR
01271 006123 JSR @AMUL
```

```
---
      .MAIN
01272 044103 STA 1,YSCAL
01273 145000 MOV 2,1
01274 030160 LDA 2,XSL
01275 006124 JSR @ADIV
01276 125005 MOV 1,1,SNR
01277 002053 JMP @CCMMD
01300 044104 STA 1,NX
01301 024101 LDA 1,OFSET
01302 030102 LDA 2,LSC
01303 006123 JSR @AMUL
01304 030103 LDA 2,YSCAL
01305 006123 JSR @AMUL
01306 040105 STA 0,CP
01307 040114 STA 0,CRIG
01310 010073 NXPT: ISZ TEMP1
01311 026073 LDA 1,@TEMP1
01312 020101 LDA 0,OFSET
01313 107000 ADD 0,1
01314 030102 LDA 2,LSC
01315 006123 JSR @AMUL
01316 101004 MOV 0,0,SZR
01317 126000 ADC 1,1
01320 030103 LDA 2,YSCAL
01321 006123 JSR @AMUL
01322 040117 STA 0,NP
01323 024105 LDA 1,CP
01324 122400 SUB 1,0
01325 034457 LDA 3,KPY
01326 101112 MOVL# 0,0,SZC
01327 034454 LDA 3,KMY
01330 054106 STA 3,PLW
01331 101112 MOVL# 0,0,SZC
01332 104401 NEG 0,1,SKP
01333 105000 MOV 0,1
01334 020161 LDA 0,PP
01335 101004 MOV 0,0,SZR
01336 000402 JMP CNCTD
01337 006451 JSR @PU
01340 030104       CNCTD: LDA 2,NX
01341 050110 STA 2,CNTB
01342 006124 JSR @ADIV
01343 125005 MOV 1,1,SNR
01344 000452 JMP ZRSLT
01345 030440 LDA 2,KRX
01346 040111 STA 0,REM
01347 020106 LDA 0,PLW
01350 113000       PLOT: ADD 0,2
01351 176000 ADC 3,3
01352 167005 ADD 3,1,SNR
01353 000416 JMP MNR
01354 044107       PLTLP: STA 1,CNTA
01355 063515 SKPBZ PLT
01356 000777 JMP .-1
01357 061115 DCAS 0,PLT
01360 006427 JSR @ESCP
01361 014107 DSZ CNTA
01362 000773 JMP .-5
01363 063515 SKPBZ PLT
01364 000777 JMP .-1
---
```

```
     .MAIN
01365 071115 DCAS 2,PLT
01366 014110 DSZ CNTB
01367 000765 JMP PLTLP
01370 000402 JMP .+2
01371 006421       MNR: JSR @TV
01372 034111       RMDR: LDA 3,REM
01373 175005 MOV 3,3,SNR
01374 000434 JMP PCINT
01375 111000 MOV 0,2
01376 054110 STA 3,CNTB
01377 006413 JSR @TV
01400 000430 JMP PCINT


              ;PLOTTER CONTROL CODE
              ;
              ;
01401 000040 KPU: 40     ;PEN-UP
01402 000020 KPD: 20     ; " -DOWN
01403 000010 KMY: 10     ;MINUS Y
01404 000004 KPY: 4     ;POSITIVE Y
01405 000002 KPX: 2           ;POSITIVE X
01406 000001 KLX: 1           ;MINUS X
01407 001503 ESCP: ESC
01410 001517 PU: PNUP
01411 001522 PD: PNDW
01412 001530 TV: TWOW
              ;
              ;
              ;
              ;
              ;
              ;
01413 030772       XONLY: LDA 2,KPX
01414 006776 JSR @TV
01415 000413 JMP PCINT
01416 101015       ZRSLT: MOV# 0,0,SNR
01417 000774 JMP XONLY
01420 040110 STA 0,CNTB
01421 145000 MOV 2,1
01422 111000 MOV 0,2
01423 006124 JSR @ADIV
01424 040111 STA 0,REM
01425 020760 LDA 0,KPX
01426 030106 LDA 2,PLV
01427 000721 JMP PLOT
01430 024161       PCINT: LDA 1,PP
01431 125005 MOV 1,1,SNR
01432 006757 JSR @PD
01433 020117 LDA 0,NP
01434 040105 STA 0,CP
01435 014116 DSZ NC
01436 000652 JMP NXPT
01437 020161 LDA 0,PP
01440 101005 MOV 0,0,SNR
01441 006747       LEAF: JSR @PU
01442 020117 LDA 0,NP
01443 024114 LDA 1,ZRIG
01444 106400 SUB 0,1
```

```
---
      .MAIN
01445 125005 MOV 1,1,SNR
01446 000410 JMP ZLN
01447 030735 LDA 2,KPY
01450 125113 MOVL# 1,1,SNC
01451 000403 JMP .+3
01452 030731 LDA 2,KMY
01453 124400 NEG 1,1
01454 044110 STA 1,CNTB
01455 006735 JSR @TV
01456 020162       ZLN: LDA 0,ZZ
01457 101005 MOV 0,0,SNR
01460 000415 JMP PADV
01461 020161 LDA 0,PP
01462 101005 MOV 0,0,SNR
01463 006726 JSR @PD
01464 024046 LDA 1,NMBER
01465 030104 LDA 2,NX
01466 006123 JSR @AMUL
01467 044110 STA 1,CNTB
01470 030716 LDA 2,KLX
01471 006721 JSR @TV
01472 044110 STA 1,CNTB
01473 030712 LDA 2,KRX
01474 006716 JSR @TV
01475 006713       PADV: JSR @PU
01476 020125 LDA 0,PINCR
01477 040110 STA 0,CNTB
01500 030705 LDA 2,KRX
01501 006711 JSR @TV
01502 002053 JMP @CCMMD
01503 063610       ESC: SKPDN TTI
01504 001400 JMP 0,3
01505 054120 STA 3,ARTRN
01506 050112 STA 2,SAVE
01507 074510 DIAS 3,TTI
01510 030075 LDA 2,EESC
01511 156405 SUB 2,3,SNR
01512 000403 JMP ABORT
01513 030112 LDA 2,SAVE
01514 002120 JMP @ARTRN
01515 006673       ABORT: JSR @PU
01516 000723 JMP LEAF  ;REPLACE PEN AND ADVANCE
01517 054121       PNUP: STA 3,BACK
01520 034661 LDA 3,KPU
01521 000403 JMP .+3
01522 054121       PNDW: STA 3,BACK
01523 034657 LDA 3,KPD
01524 063515 SKPBZ PLT
01525 000777 JMP .-1
01526 075115 DIAS 3,PLT
01527 002121 JMP @BACK
01530 054122       TVDW: STA 3,BKA
01531 063515       TVA: SKPBZ PLT
01532 000777 JMP .-1
01533 071115 DIAS 2,PLT
01534 006653 JSR @ESCP
01535 014110 DSZ CNTB
01536 000773 JMP TVA
01537 002122 JMP @BKA
```

```
---
      .MAIN
01540 125015          ZFIX: MOV# 1,1,SNR
01541 126520 SUBZL 1,1
01542 001400 JMP 0,3



                    ;ROTATE ARRAY
                    ;USING RIGHT CIRCULAR SHIFT


01543 006060 R: JSR #BBF
01544 050073 STA 2,TEMP1
01545 006052 JSR #NNB
01546 020175 LDA 0,TE7
01547 006050 JSR #TTEXT
01550 006051 JSR #CCRL
01551 020171 LDA 0,TE3
01552 006047 JSR #BBUMP
01553 020073 LDA 0,TEMP1
01554 142400 SUB 2,0
01555 040063 STA 0,SALVE
01556 020046 LDA 0,NMBER
01557 040117 STA 0,NP
01560 034044 LDA 3,BEGAD
01561 175400 INC 3,3
01562 171000 MOV 3,2
01563 014117 DSZ NP
01564 021400 LDA 0,0,3
01565 175400 INC 3,3
01566 025400 LDA 1,0,3
01567 041400 STA 0,0,3
01570 175400 INC 3,3
01571 121000 MOV 1,0
01572 014117 DSZ NP
01573 000773 JMP .-5
01574 045000 STA 1,0,2
01575 014063 DSZ SALVE
01576 000760 JMP .-20
01577 002053 JMP @COMMD


---
```

```
---
;       .MAIN

                ;CLEARS REGION OF CORE
                ;TRANSFERS DATA TO FORM D.P.
                ;CONVERTS TO F.P.
                ;FEEDS INTO DFT

01600 020204 D: LDA 0,TE14
01601 006050 JSR @TTEXT
01602 006051 JSR @CCRL
01603 006060 JSR @BBF
01604 006052 JSR @NNB
01605 020044 LDA 0,BEGAD
01606 040105 STA 0,CP
01607 102440 SUBC 0,0
01610 040151 STA 0,NU
01611 040152 STA 0,NU+1
01612 040153 STA 0,KKK
01613 040154 STA 0,KKK+1
01614 020046 LDA 0,NMBER
01615 040107 STA 0,CNTA
01616 040110 STA 0,CNTB
01617 040111 STA 0,REM
01620 040163 STA 0,TEMP2
01621 105000 MOV 0,1
01622 030133 LDA 2,ODD
01623 147400 AND 2,1
01624 044154 STA 1,KKK+1
01625 125004 MOV 1,1,SZR
01626 000410 JMP .+10
01627 100400 NEG 0,0
01630 100000 COM 0,0
01631 100400 NEG 0,0
01632 100000 COM 0,0
01633 101220 MOVZR 0,0
01634 040134 STA 0,NMBE1
01635 000405 JMP .+5
01636 100400 NEG 0,0
01637 100000 COM 0,0
01640 101220 MOVZR 0,0
01641 040134 STA 0,NMBE1
01642 020214 LDA 0,TE22
01643 006047 JSR @BBUMP
01644 151005 MOV 2,2,SNR
01645 000410 JMP .+10
01646 050135 STA 2,CNTC
01647 020046 LDA 0,NMBER
01650 024046 LDA 1,NMBER
01651 123000 ADD 1,0
01652 014135 DSZ CNTC
01653 000776 JMP .-2
01654 000402 JMP .+2
01655 020046 LDA 0,NMBER
01656 040152 STA 0,NU+1
01657 020210 LDA 0,TE18                ; LEADS TO NMB PTS CALC.
01660 006047 JSR @BBUMP
01661 050112 STA 2,SAVE
01662 020205 LDA 0,TE15

---
```

```
     .MAIN
01663 006050 JSR @TTEXT
01664 006051 JSR @CCRL
01665 020171 LDA 0,TE3
01666 006047 JSR @BHUMP
01667 020126 LDA 0,ADR              ;CHANGE ADR TO CHANGE STOR. ALLOC.
01670 113000 ADD 0,2                ;AC2=BEG AD-1 OF DP&FP
01671 050021 STA 2,21
01672 151400 INC 2,2
01673 155000 MOV 2,3
01674 024046 LDA 1,NMBER
01675 124400 NEG 1,1
01676 124000 COM 1,1
01677 125120 MOVZL 1,1
01700 137000 ADD 1,3
01701 054045 STA 3,FINAD
01702 050044 STA 2,BEGAD
01703 050114 STA 2,CRIG
01704 050122 STA 2,BKA
01705 145000 MOV 2,1
01706 125400 INC 1,1
01707 044117 STA 1,NP
01710 101120 MOVZL 0,0
01711 040115 STA 0,RTRN
01712 113000 ADD 0,2                ;INCR. TO GET LOC. OF RESULTS
01713 050104 STA 2,NX
01714 050164 STA 2,TEMP3
01715 050165 STA 2,LC11
01716 102440 SUBC 0,0               ;CLEAR STORAGE AREA
01717 042021 STA 0,@21
01720 014115 DSZ RTRN
01721 000776 JMP .-2
01722 020105 LDA 0,CP               ;FORM D.P.
01723 030117 LDA 2,NP
01724 040021 STA 0,21
01725 022021 LDA 0,@21
01726 041000 STA 0,0,2
01727 151400 INC 2,2
01730 151400 INC 2,2
01731 014107 DSZ CNTA
01732 000773 JMP .-5
01733 006005 FINI
01734 006004 FETR
01735 064122 FLD3 BKA               ;CONVERT TO F.P.
01736 070116 FST3 NC
01737 062116 FFLO @NC
01740 110000 FIC3
01741 014110 FDSZ CNTB
01742 000774 FJMP .-4
             ;FLOATING POINT DISCRETE FOURIER TRANSFORM
             ;USING COS 2PI N' K/N
             ;N'=INDEX OF OUTPUT PT
             ;K= INDEX OF INPUT PT
             ;N= TOTAL NMB. OF PTS
01743 020137 FLDA 0,FONE
01744 040143 FSTA 0,NN              ;SETS NN=F.P.1
01745 060151 FFLO NN
01746 102400 DDATA: FSUB 0,0        ;DDATA GIVES N'=0 PT & STORES IT
01747 026114 FLDA 1,@CRIG           ;CRIG =ADDR. OF 1ST IN. DATA PT.
01750 010114 FISZ CRIG
```

```
     .MAIN
01751 010114 FISZ CRIG
01752 123000 FADD 1,0
01753 014111 FDSZ REM
01754 000773 FJMP .-5
01755 042104 FSTA 0,@NX              ;NX =L2C. 1ST CUT PT
01756 010104 FISZ NX
01757 010104 FISZ NX
01760 000414 FJMP NIN
01761 052104 DATA: FSTA 2,@NX        ;DATA STORES CUT PTS&INCR.CCS AR
01762 010104 FISZ NX
01763 010104 FISZ NX
01764 020137 FLDA 0,FCNE
01765 024143 FLDA 1,NN
01766 107000 FADD 0,1                ;INCR.N' IN F.P.
01767 044143 FSTA 1,NN
01770 014112 FDSZ SAVE               ;SAVE=N-1
01771 000403 FJMP NIN
01772 100000 FEXT
01773 002131 JMP @NNN                ;EXIT
01774 064134 NIN: FLD3 NMBER
01775 070111 FST3 REM
01776 064044 FLD3 BEGAD
01777 070114 FST3 CRIG
02000 064045 FLD3 FINAD
02001 070136 FST3 END
02002 152400 FSUB 2,2
02003 000432 FJMP CCCS
02004 022114 SU: FLDA 0,@CRIG
02005 024145 FLDA 1,CCSI
02006 120100 FMPY 1,0
02007 113000 FADD 0,2
02010 022136 FLDA 0,@END             ; END CONTAINS FIN. ADDR
02011 120100 FMPY 1,0
02012 113000 FADD 0,2
02013 014111 FDSZ REM
02014 000414 FJMP .+14
02015 060153 EVEN: FFL2 KKK
02016 020153 FLDA 0,KKK
02017 101004 FMOV 0,0,FSZR
02020 000741 FJMP DATA
02021 164060 FCCS 3,1
02022 010114 FISZ CRIG
02023 010114 FISZ CRIG
02024 022114 FLDA 0,@CRIG
02025 120100 FMPY 1,0
02026 113000 FADD 0,2
02027 000732 FJMP DATA
02030 010114 FISZ CRIG
02031 010114 FISZ CRIG
02032 014136 FDSZ END
02033 014136 FDSZ END
02034 000413 FJMP CCS
02035 020143 CCCS: FLDA 0,NN
02036 024141 FLDA 1,PI
02037 120100 FMPY 1,0
02040 024151 FLDA 1,NU
02041 120200 FDIV 1,0               ;FACO=2PIN'/N
02042 040147 FSTA 0,ARG
02043 115000 FMOV 0,3
```

```
      .MAIN
02044 032114 FLDA 2,.ORIG
02045 010114 FISZ ORIG
02046 010114 FISZ ORIG
02047 160060 CCS: FCOS 3,0
02050 040145 FSTA 0,CCSI
02051 020147 FLDA 0,ARG
02052 117000 FADD 0,3                    ;INCR K BY INCR ARG
02053 000731 FJMP SW
```

```
*       .MAIN


                ;DIVIDES ALL FP VALUES IN ARRAY
                ;BY THE 1ST VALUE. RESULTS STORED IN PLACE


02054 020206 N: LDA 0,TE16
02055 006047 JSR @BBUMP
02056 151005 MOV 2,2,SNR
02057 002132 JMP @AAA
02060 020163 LDA 0,TEMP2
02061 101004 MOV 0,0,SZR
02062 000405 JMP .+5
02063 020207 LDA 0,TE17
02064 006050 JSR @TTEXT
02065 006051 JSR @CCRL
02066 002053 JMP @CCMMD
02067 006004 FETR
02070 022164 FLDA 0,@TEMP3
02071 064164 FLDD TEMP3
02072 025400 FLDA 1,0,3
02073 104200 FDIV 0,1
02074 045400 FSTA 1,0,3
02075 110000 FIC3
02076 014163 FDSZ TEMP2
02077 000773 FJMP .-5
02100 100000 FEXT
02101 002132 JMP @AAA


                ;ZERO CORE

02102 006060 Z: JSR @BBF
02103 006052 JSR @NNB
02104 020044 LDA 0,BEGAD
02105 040021 STA 0,21
02106 102440 SUB0 0,0
02107 042021 STA 0,@21
02110 014046 DSZ NMBER
02111 000776 JMP .-2
02112 002053 JMP @CCMMD
```

```
;       .MAIN

                ;CONVERT FLTNG TO ASCII
                ;AND OUTPUTS A NMB. OF PTS

02113 020210 A: LDA 0,TEIB
02114 006047 JSR @4BUMP
02115 050046 STA 2,NMBER
02116 020165 LDA 0,LCII
02117 040062 STA 0,H2LD
02120 006004 FETR
02121 032062 FLDA 2,@H2LD
02122 150000 FFDC 2
02123 010062 FISZ H2LD
02124 010062 FISZ H2LD
02125 014046 FDSZ NMBER
02126 000773 FJMP .-5
02127 100000 FEXT
02130 002053 JMP @CCMMD
```

```
---
*       .MAIN


                ;OUTPUT ASCII AND LF+CR

02131 054415 PUTCC: STA 3,PUTC1+10
02132 063511 SKPBZ TTO
02133 000777 JMP .-1
02134 061111 DOAS 0,TTO
02135 002411 JMP @PUTC1+10
02136 101004 PUTC1: MOV 0,0,SZR       ;ENTER HERE
02137 000772 JMP PUTCC
02140 054407 STA 3,PUTC1+11
02141 020407 LDA 0,CR
02142 004767 JSR PUTCC
02143 034404 LDA 3,PUTC1+11
02144 101300 MOVS 0,0
02145 000764 JMP PUTCC
02146 000000 0
02147 000000 0
02150 005015 CR: 5015
```

```
---
*       .MAIN
                ;TEXT STATEMENTS

                T1: .TXT #NMB,DATA PTS,OCTAL#
02151 046516
02152 026102
02153 040504
02154 040524
02155 050040
02156 051524
02157 047454
02160 052103
02161 046101
02162 000000
                T2: .TXT #LOC FOR STORING DATA#
02163 047514
02164 020103
02165 047506
02166 020122
02167 052123
02170 051117
02171 047111
02172 020107
02173 040504
02174 040524
02175 000000
                T3: .TXT #BEG ADDR-1#
02176 042502
02177 020107
02200 042101
02201 051104
02202 030455
02203 000000
                T4: .TXT #FINAL ADDR#
02204 044506
02205 040516
02206 020114
02207 042101
02210 051104
02211 000000
                T5: .TXT #FOR DATA TO BE FOLDED#
02212 047506
02213 020122
02214 040504
02215 040524
02216 052040
02217 020117
02220 042502
02221 043040
02222 046117
02223 042504
02224 000104
                T6: .TXT #<15><12>#
02225 005015
02226 000000
                T7: .TXT #FOR PTS TO BE SHIFTED#
02227 047506
02230 020122
02231 052120
02232 020123

---
```

```
      .MAIN
02233 047524
02234 041040
02235 020105
02236 044123
02237 043111
02240 042524
02241 000104
                T8: .TXT #AUTO SCALE, I=ON#
02242 052501
02243 047524
02244 051440
02245 040503
02246 042514
02247 020054
02250 036461
02251 047117
02252 000000
                T9: .TXT #MAX PLOT HT=#
02253 040515
02254 020130
02255 046120
02256 052117
02257 044040
02260 036524
02261 000000
                T10: .TXT #NMB PTS/IN,Y#
02262 046516
02263 020102
02264 052120
02265 027523
02266 047111
02267 054454
02270 000000
                T11: .TXT #NMB PTS/IN,X#
02271 046516
02272 020102
02273 052120
02274 027523
02275 047111
02276 054054
02277 000000
                T12: .TXT #PT PLOT,I=OFF#
02300 052120
02301 050040
02302 047514
02303 026124
02304 036461
02305 043117
02306 000106
                T13: .TXT #ZERO LINE,I=ON#
02307 042532
02310 047522
02311 046040
02312 047111
02313 026105
02314 036461
02315 047117
02316 000000
                T14: .TXT #FOR DATA TO BE TRANSFORMED#
```

```
---
      .MAIN
02317 047506
02320 020122
02321 040504
02322 040524
02323 052040
02324 020117
02325 042502
02326 052040
02327 040522
02330 051516
02331 047506
02332 046522
02333 042105
02334 000000
                T15: .TXT @FOR SING PREC DATA STORED@
02335 047506
02336 020122
02337 044523
02340 043516
02341 050040
02342 042522
02343 020103
02344 040504
02345 040524
02346 051440
02347 047524
02350 042522
02351 000104
                T16: .TXT @NORMALIZE?,1=YES@
02352 047516
02353 046522
02354 046101
02355 055111
02356 037505
02357 030454
02360 054475
02361 051505
02362 000000
                T17: .TXT @ALREADY NORMALIZED@
02363 046101
02364 042522
02365 042101
02366 020131
02367 047516
02370 046522
02371 046101
02372 055111
02373 042105
02374 000000
                T18: .TXT @NMB.TRANSFORM PTS OUT@
02375 046516
02376 026102
02377 051124
02400 047101
02401 043123
02402 051117
02403 020115
02404 052120
02405 020123

---
```

```
     .MAIN
02406 052517
02407 000124
                T19: .TXT #GOOD! GO AHEAD#
02410 047507
02411 042117
02412 020041
02413 047507
02414 040440
02415 042510
02416 042101
02417 000000
                T20: .TXT #TTI(1),PTR(2)?#
02420 052124
02421 024111
02422 024461
02423 050054
02424 051124
02425 031050
02426 037451
02427 000000
                T21: .TXT #NMB,PLACES TO BE SHIFTED#
02430 046516
02431 026102
02432 046120
02433 041501
02434 051505
02435 052040
02436 020117
02437 042502
02440 051440
02441 044510
02442 052106
02443 042105
02444 000000
                T22: .TXT #ZERO EXT? NO(0) 1X(1) 2X(2) ETC#
02445 042532
02446 047522
02447 042440
02450 052130
02451 020077
02452 047516
02453 030050
02454 020051
02455 054061
02456 030450
02457 020051
02460 054062
02461 031050
02462 020051
02463 052105
02464 000103
                     .END
```

```
---
          .MAIN
A         002113
AAA       000132
ABORT     001515
ADIV      000124
ADR       000126
AMUL      000123
ARG       000147
ARTRN     000120
BACK      000121
BBF       000060
BBUMP     000047
BEGAD     000044
BF        000671
BKA       000122
BREAD     001201
BUMP      000664
CB99      001144
CC98      001161
CC99      001170
CCMMD     000053
CCOS      002035
CCR       000071
CCRL      000051
CCT       000442
CMMD      000413
CNCTD     001340
CNTA      000107
CNTB      000110
CNTC      000135
CONI      001140
COS       002047
CCSI      000145
CP        000105
CR        002150
CRL       000732
CRR       000652
CT        000443
D         001600
DATA      001761
DDATA     001746
DDDIG     000054
DDIGI     000627
DIGI      000632
DIPT      000606
DITT      000611
DIVID     001153
DRAW      001267
EESC      000075
END       000136
ESC       001503
ESCP      001407
EVEN      002015
F         001023
FINAD     000045
FONE      000137
G         001045
G1        000127
G2        000130
GET       000712
```

```
---
          .MAIN
GETC      000040
GETC2     000077
GETCC     000720
GG        001047
GRAPH     001232
HARE      001126
HCLD      000062
HCLDI     000074
IN        000641
IT        001131
KBC       000542
KBCK      000575
KBRD      000546
KBST      000534
KK        001062
KKESC     000660
KKK       000153
KLX       001406
KMY       001403
KPD       001402
KPU       001401
KPY       001404
KRX       001405
L         000753
LCII      000165
LEAF      001441
LFF       000072
LL        000615
LSC       000102
M         000772
M1        000113
M20       000166
MASK      000066
MAX       000056
MAXI      001114
MAXMI     001261
MIN       000055
MINI      001112
MM        001007
MNR       001371
MULTM     001141
N         002054
NB        000701
NIN       001774
NINE      000070
NMBEI     000134
NMBER     000046
NN        000143
NNB       000052
NNN       000131
NP        000117
NSPT      000605
NSTT      000610
NU        000151
NX        000104
NXPT      001310
@         000734
@DD       000133
@FSET     000101
```

```
---
                .MAIN
ERIG            000114
EUT             000706
P               001206
PADV            001475
PD              001411
PI              000141
PINCR           000125
PLOT            001350
PLTLP           001354
PLV             000106
PNDV            001522
PNUP            001517
POINT           001430
PP              000161
PU              001410
PUTC            000041
PUTC1           002136
PUTC2           000100
PUTCC           002131
Q               001230
R               001543
REM             000111
RMDR            001372
RRR             000446
RRRR            000444
RTRN            000115
SALVE           000063
SAVE            000112
SBTRT           000057
SKPT            000604
SKTT            000607
SLA             000076
START           000743
SU              002004
SUBME           001172
SW1             000155
T               000502
T1              002151
T10             002262
T11             002271
T12             002300
T13             002307
T14             002317
T15             002335
T16             002352
T17             002363
T18             002375
T19             002410
T2              002163
T20             002420
T21             002430
T22             002445
T3              002176
T4              002204
T5              002212
T6              002225
T7              002227
T8              002242
T9              002253
```

	.MAIN
TABLE	000065
TE1	000167
TE10	000200
TE11	000201
TE12	000202
TE13	000203
TE14	000204
TE15	000205
TE16	000206
TE17	000207
TE18	000210
TE19	000211
TE2	000170
TE20	000212
TE21	000213
TE22	000214
TE3	000171
TE4	000172
TE5	000173
TE6	000174
TE7	000175
TE8	000176
TE9	000177
TEMP	000061
TEMP1	000073
TEMP2	000163
TEMP3	000164
TEST	000064
TEXT	000612
TT	000464
TTABL	000423
TTEXT	000050
TTTT	000445
TW	001412
TWA	001531
TWCW	001530
WC	000116
XONLY	001413
XSL	000160
YINCH	000156
YSCAL	000103
YSL	000157
Z	002102
ZERO	000067
ZFIX	001540
ZLN	001456
ZRSLT	001416
ZZ	000162

ASM

Preface to Basic Program Listing

The following Basic program is used to fit a least squares deviation straight line to correlation function data. The program has been tailored for use with the first 25 points, spaced 1.66 picoseconds apart, of DFT results obtained from $200_{(10)}$ points of input data, zero extended once. These 25 points must be typed into the DATA section of the program. The program will compute and print out the logarithm of the 25 points. It then takes the last 13 of these logarithmic values and fits a straight line to them. The ordinate value of the least squares line is printed out for abscissa values of 0,5,10,15,20 which correspond to time values of 2.0,2.5,3.0,3.5 and 4.0 picoseconds respectively.

```
10       DIM X[24]
20      LET X1=-1.66
30      FOR K=12 TO 24
35        LET X1=X1+1.66
40        LET X[K]=X1
50      NEXT K
60      DIM Y[24]
70      FOR K=0 TO 24
80        READ Y[K]
90        LET Y[K]=LOG Y[K]
100        PRINT Y[K]
110     NEXT K
120     LET S0=13
130     LET S1= 0
140     LET S2= 0
150     LET T0= 0
160     LET T1= 0
170     FOR K=12 TO 24
180       LET S1=S1+X[K]
190       LET S2=S2+(X[K]↑2)
200       LET T0=T0+Y[K]
210       LET T1=T1+(X[K]*Y[K])
220     NEXT K
230     LET M=((S0*T1)-S1*T0))/((S0*S2)-(S1↑2))
240     LET B=((S2*T0)-S1*T1))/((S0*S2)-(S1↑2))
250     LET G=-5
260     DIM C[4]
270     DIM D[4]
280     FOR K= 0 TO 4
290       LET G=G+5
300       LET D[K]=G
310       LET C[K]=(M*D[K])+B
320       PRINT D[K],C[K]
330     NEXT K
340     END
400     DATA   1,  .948,  .844,  .772,  .742,  .707,  .645,  .585
410     DATA   .544,  .503,  .45,  .401,  .368,  .339,  .303
420     DATA   .269,  .243,  .219,  .191,  .167,  .151,  .138,  .121
430     DATA   .103,  .092
```